Master Thesis Report

The dynamic behavior of floors in high-rise buildings and their contribution to damping - an analytical model

S. A. van Dijk

Delft University of Technology

TU Delft Delft University of Technology

Challenge the future

Cover photo:
Highrise buildings in Central district Hong Kong Island, a night view: Bank of China Tower, ICBC Building, Chaung Kong Center and Citibank Building (Shutterstock, 2015).

MASTER THESIS REPORT

THE DYNAMIC BEHAVIOR OF FLOORS IN HIGH-RISE BUILDINGS AND THEIR CONTRIBUTION TO DAMPING - AN ANALYTICAL MODEL

by

S. A. van Dijk

in partial fulfillment of the requirements for the degree of

Master of Science

in Civil Engineering,
Structural Engineering with a specialization in Structural Mechanics

at Delft University of Technology,

to be defended publicly on Wednesday July 1st, 2015

Thesis committee:

Chairman:	Prof. Dr. A.V. Metrikine,	TU Delft, Structural Mechanics
Daily supervisor:	MSc. S. Sanchez Gomez,	TU Delft, Structural Mechanics
Supervisor:	Dr. E. Lourens,	TU Delft, Offshore Engineering
Committee member:	Ir. J.M. Houben,	TU Delft, Structural Engineering

PREFACE

After nine months of work, I am proud to present this master thesis report on damping in floors. This study is performed in order toobtain the degree of Master of Sciences in Civil Engineering at Delft University of Technology. The research for my master thesis was carried out in cooperation with the Faculty of Civil Engineering department Structural Mechanics and TNO department Structural Dynamics. My interest in dynamics together with the opportunities given by TU Delft and TNO made that I can look back at a successful period where I have learned more than I could have imagined.

My thesis couldn't be completed without the help of several people. Firstly, I would like to thank my daily supervisor Sergio Sanchez for his guidance throughout the entire process. The many discussions we had not only helped raising my motivation and interest for the study, but they also broadened my view on engineering practice in different disciplines.

Also, I would like to express my gratitude to the chairman of my graduation committee, professor Andrei Metrikine, for his valuable insights and for the guidance during the project. And, I would like to thank Eliz-Mari Lourens for her time and enthusiasm. And Lambert Houben for arranging the ceremonial affairs regarding my graduation.

Large gratitude goes to TNO for facilitating the resources to perform this study. Besides working space, TNO offered me equipment, materials, space, knowledge and guidance for the performance of the experiment. I was given the chance to contribute to two articles which are now published in dutch national magazines, a very nice experience. Also, I would like to thank all people working at TNO Structural Dynamics for the great time I had during my internship and for their interest in my study.

Not only during my graduation, but throughout the many years in Delft my parents, sister, boyfriend, family and friends have supported me. I would like to end with thanking them for this support, making it possible to develop both socially and intellectually from a high-school student to an engineer.

Sara van Dijk
Delft, June 2015

ABSTRACT

The resistance of buildings to static loads is very well defined and regulated in codes compared with the resistance to dynamic loads. However in particular for high-rise buildings the resistance to dynamic loading is of great importance for the design and much less defined. The magnitude of vibrations depends on mass, stiffness and damping properties of the building and on the loading frequency. Damping is the most important factor to reduce the amplitude of vibration at resonance. Whereas stiffness and mass can be determined quite accurately during the design phase of a building for damping it is not yet possible to give an accurate prediction in the design phase. The empirical fomula's developed by Jeary (1986), Tamura (2003, 2012), Lagomarisono (1993) and Davenport and Hill-Carol (1986) based on full-scale measurements in Japan, United States, Italy and Great Brittain show large deviations in the predicted damping values.

Damping in buildings can be assigned to structural damping, aerodynamic damping, intrinsic material damping, radiation damping, damping in non-structural elements and to additional dampers. Damping in floors both comprises intrinsic material damping and structural damping. The Eurocode prescribes damping ratio's of 1% to 2% for buildings categorized in steel buildings, concrete buildings or a combination of both. Full scale measurements in the Netherlands showed a scatter in damping ratio's between 1% and 3.5% and no clear distinction between material types could be made.

Damping is not only dependent on structural properties of all individual components, but also on loading and on response characteristics. Understanding the influence of individual components to damping is key to predict damping in a building accurately. In this research project the focus will be on the contribution of damping in floors to the damping ratio of sender dutch high-rise buildings under wind loading. Here both damping in structural parts, in the connections between the floor and the main structure, and damping in floor-materials are studied.

The goal of this thesis is to describe the damping mechanisms present in floors when buildings are excited by wind load using an simple analytical model. A one-dimensional model is designed, representing the expected behavior of floors in buildings based on the structural lay-out of dutch high-rise buildings. This model consists of an Euler-Bernoulli beam element including material damping following Kelvin-Voight's model and at both boundaries a rational spring, viscous damper and coulomb friction damper representing the structural damping. A solution for the model response is calculated using the Galerkin Approximation Method, where the product of linear modes shapes based on linear boundary conditions and generalized time dependent coordinates approximate the solution, combined with numerical integration following Runge-Kutta. These methods provided accurate solutions.

The model was validated with an experiment. The set-up enclosed two steel columns, hinged connected to the floor, and a concrete bar, clamped between the two steel profiles. Some adjustments on the joint lay-out were made during the experiments. Measured accelerations showed a highly damped system and the decrease of amplitude of vibration was accompanied by a decrease in damping ratio's. Odd modes of the beam coincided with the natural frequencies of the system, with a clear first natural frequency. Strong coupling of higher modes was present at high amplitudes of vibration at the small beginning of the response, but these faded out quickly. Small changes in the natural frequencies of the system with time were detected, but for a founded conclusion further studies are recommended on this subject.

A comparison of the experimental outcome with the analytical one-dimensional model was made and a good fit for the computed response was found. In further studies extension of the model to include a second lateral dimension and torsional modes can be made, or a calibration algorithm can be developed to determine an optimal fit for the damping parameters. Also experiments to study the non-linear material properties of concrete during high amplitude vibrations can be performed in future research to obtain more understanding

the damping mechanisms in floors.

CONTENTS

ABBREVIATIONS AND NOTATIONS

Abbreviations

BC	Boundary conditions
DOF	Degree of freedom
EM	Equation of motion
FFT	Fast Fourrier Transform
FRF	Frequency Response Function
FTF	Fourier transformed function
LHS	Right hand side of the equation
MPi	Acceleration measurement devices
NDOF	Multiple degree of freedom system
nf	Natural frequency
POD	Proper Orthogonal Decomposition
RHS	Right hand side of the equation
SDOF	Single degree of freedom system
SLS	Serviceability Limit State

Notations

β	Function of natural frequency	
δ	Logaritmic decrement	
ϵ	Strain	
η	Loss factor	%
γ	Damping factor	%
κ	Curvature	m^{-2}
μ_i	Friction damping factor	Nms/rad
Ω	External loading frequency	rad/s
ω	Natural frequency	rad/s
$\phi(t)$	Rotation of columns	rad
$\phi_c(t)$	Rotation of columns	rad
$\Phi(t)$	Displacement dependent on t	m
ψ_m	Time dependent part of the solution for mode m	m
ρ	Density	kg/m^3
σ	Stresses	N/m^2
θ	Virtual rotations	rad
φ	Rotation	rad
ζ	Damping ratio	%
A	Cross-sectional area	m^2
A_m	Frequency dependent constant for mode shape	
$a_m(t)$	Time function for the accelerations	m/s^2
B_m	Frequency dependent constant for mode shape	
c	Viscous damping	Ns/m
c_{cr}	Critical damping	
C_{w_m}	Constant for the orthogonality of the modes	
C_m	Frequency dependent constant for mode shape	
$c_{r,i}$	Rotational viscous damper value	Nms/rad
D_m	Frequency dependent constant for mode shape	
E	Young's Modulus or modulus of elasticity	N/m^2
$E*$	Time dependent part modulus of elasticity	N/m^2

EI	Stiffness	Nm^2
F_0	Amplitude of external force	N
F_c	Friction force	N
g	Gravity force	m/s^2
g	Gravity accelerations	
H	Height or vertical coordinate of the position of the concrete beam	m
I	Moment of Inertia	m^4
k	Stiffness	m^{-1}
k_r	Rotational spring stiffness	Nm/rad
L	Beam length	m
M	Mass matrix	kg
m	Mass	kg
m	uncoupled mode	
M	Moment	Nm
M_{ext}	External moment	Nm
N	Normal force	N
n	coupled mode	
q	Distributed load	N/m
q_m	Time dependent part of the solution for mode m	m
$q_m(t)$	Time function for the displacements	m
r_i	Ratational spring stiffness	Nm/rad
t	time variable	s
V	Shear force	N
$v_m(t)$	Time function for the velocities	m/s
$W(x)$	Displacement dependent on x	m
$W(x,\omega)$	Fourrier transform of w(x,t)	m
$w(x,t)$	Vertical deflection	m
w_f	Actual vertical deflection of the floor	m
w_m	Space dependent part of the solution for mode m	m
w_s	Horizontal deflection of the main structure	m
x	Space coordinate, along beam axis	m
y	Vertical space coordinate in beam section	m

1

INTRODUCTION

During the last two centuries, the growth of the world's population caused expanding cities and ever-growing economies. Multiple factors related to economic growth have resulted in a significant increase in demand of floor space for both office and residential buildings within cities. This high demand for floor space challenged engineers to increase heights of newly constructed buildings, something that due to innovations in construction technology and the development of lifts and the fire protection techniques became possible. The application of high-strength materials, like steel in the start of the 20th century, and later on high-strength reinforced or pre-stressed concrete, high-quality steel and composite materials made it possible to build skyscrapers of several hundred meters in height. Nowadays, the symbolic status associated with skyscrapers is the main motivation to challenge engineers in designing skyscrapers with greater heights or more slenderness than ever before. Today, the middle east is leading in the race for highest buildings with the Burj Khalifa over 800 meters in height. Expectations are that in a few years time, the first building will reach the 1000 meter bar. In the Netherlands the building height experience a less rapid growth. The main reasons are the relative soft soil conditions and the population growth in cities which is much smaller than most municipalities. In the Netherlands the highest buildings are located in Rotterdam, with the Maastoren and New Orleans Tower leading with heights just above 150 m.

In contemporary buildings, materials are used in a more efficient way, by eliminating parts of elements which do not contribute to the load bearing capacity or the stability of the structure. Consequently, many innovative structural schemes are developed to increase the strength and stiffness of a building with a minimum of construction materials. The constructive weight per meter in height is strongly reduced, which enables engineers to enhance the height even more. Hence, simultaneously with the height, also the slenderness of buildings changed. Hoederkamp [1] defines slenderness as the ratio of height over width of the lateral load resisting structure at ground level. The use of lighter and stronger structural systems provide not only more interior space per floor, but will also provide smaller required footprints at ground level.

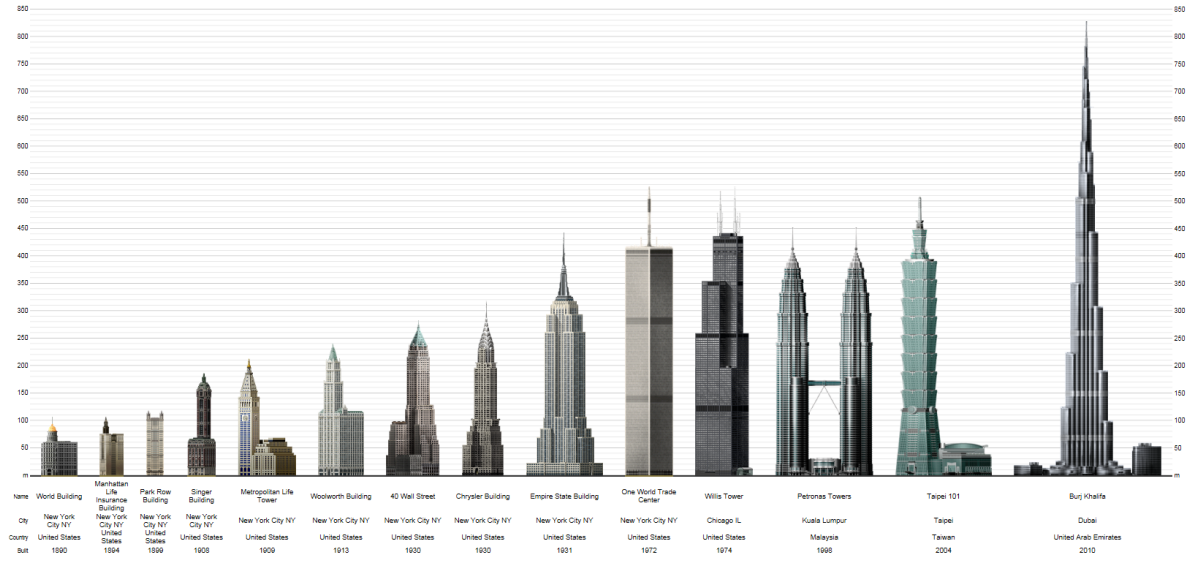

Figure 1.1: Historical timeline of highest buildings in the world [skyscraperpage,2015]

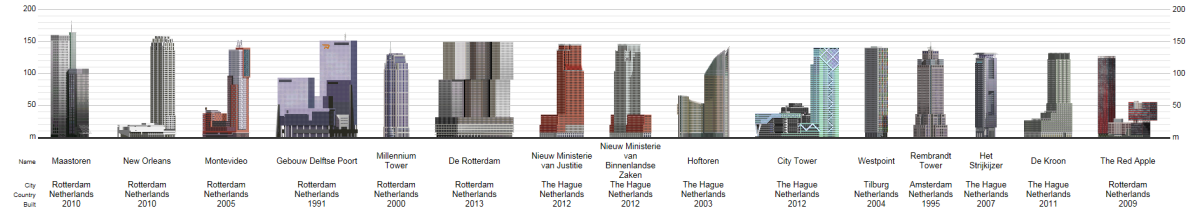

Figure 1.2: Highest ten buildings built in the Netherlands in January 2015 [skyscraperpage,2015]

A high-rise building can be referred to as very tall building, but the height of a building only is not the main factor influencing the stability of a building due to horizontal loading. At ground level, the horizontal forces cause a moment, which is taken up by the main structure. The arm between the outer elements of the main structure has a strong influence on the stresses due to lateral loads at this position. Therefore, it is better to define a highrise building as a building with a slenderness equal of higher than 5 in one of the main directions following Hoenderkamps definition [1]. It should be noted that the slenderness is not generally equal in both horizontal directions in a building, often a strong and weak direction are present with respectively the largest and smallest width. In the Netherlands the height of building is almost linear related to the width, therefore, most dutch buildings taller than 80 to 10 meter can be called highrise buildings [2] and have a slenderness greater than five in one of the directions.

1.1. Problem Statement

Constructing more and more slender buildings results in increasing static and dynamic forces acting on these buildings. The resistance of buildings to static loads is very well defined and regulated in codes compared with the resistance to dynamic loads. But especially for high-rise buildings this resistance to dynamic loading is of great importance for the design. Dynamic loads on buildings comprise three main factors of cause: firstly seismic loading, secondly wind loading and thirdly human-, machine- and sound-induced vibrations. Research related to seismic loading is of increasing importance in the Netherlands as earthquakes in combination with soil resettlement can cause damage and possible failure in structures, particular occurring at existing low-rise buildings in the Northern part of the Netherlands. The third field of cause will induce local vibrations at very high frequencies and is of importance in e.g. the field of acoustics.

For wind-induced dynamic behavior in slender buildings, the comfort of building occupants is often the

most important design criterion [3] in the serviceability limit state, where the criteria for the usability of a structure are set. It is known that in several buildings residents can actually feel movements in days with stormy conditions. Walton et al. showed that in high residental buildings sensations of motion and auditory perception were the most frequently reported cues of building movement [4]. Related research showed that accelerations from levels of 5 mG and larger can be perceived for low frequencies of approximately 0.1 to 1.0 Hz [5]. This dynamic behavior might be experienced as discomfort or even as fear . The duration of exposure and the waveform play an important roles in assessing human perception and their tolerance threshold [6]. High-rise buildings are known to be more sensitive to wind load in comparison to lower buildings or buildings with relatively higher mass. The average hourly wind speed increases with height and causes an increase in magnitude of loading. This increased loading force will result in higher amplitudes of vibration. Moreover, the relation between mass and stiffness determines both the natural frequencies and the amplitude of the response, causing changes in both with increasing building height.

When loading is acting with frequencies very close the the natural frequency of the building resonance occurs, causing an extreme increase in the amplitude of vibration. Damping is the most important factor to reduce the amplitude of vibration at resonance. That is, the level of virations is largely dependent on the structure's total damping. Buildings are in genergal lightly damped structures, experiencing around 1% to 5% of critical damping [7, 8]. Damping has a positive influence on vibrations, hence we would like to design buildings

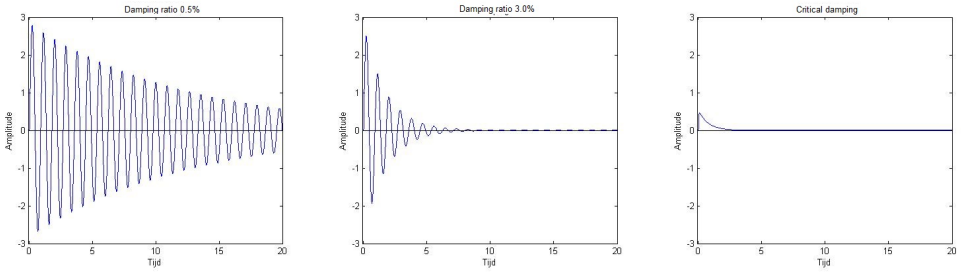

Figure 1.3: The influence of the damping ratio on amplitude of vibration

with enough damping to limit the amplitude of wind-induced vibration. But damping in highrise buildings is a complex phenomenon. Where stiffness and mass can be determined quite accurately during the design phase of a building, particularly by using FEM programs, is it for damping not yet possible to give an accurate prediction in the design phase. In the Eurocode NEN-EN 1991-1-4 damping values for reinforced concrete and steel buildings are proscribed [9]. However, damping is influenced by many properties of the building, it does not only depend on the type of material, but on all structural and non-structural elements present in a building.

Moreover, damping is shown to not only depend on structure properties, but also on loading and response characteristics. In numerous studies since 1977 an increasing relation between amplitude of vibration and the total damping appeared [10]. Also, damping depends on the mode in which the building is vibrating. The dynamic response of a building can be represented by of sum of many harmonic vibrations in different frequencies, each with it's own vibration phase and amplitude. All modes experience different damping values. The first mode, belonging to the lowest natural frequency, has generally the lowest damping and the highest amplitude of vibration.

Identifying damping is very complex, because we are not looking at one damping value which describes the behavior of a building, but at many damping values which change in time. Despite of studies on damping in buildings the last decades, currently no accurate classification for damping exists, which can be used in practice to predict the damping value of a building. Based on full-scale measurements in Japan, United States, Italy and Great Brittain some empirical formulas have been developed by Jeary (1986), Tamura (2003, 2012), Lagomarisono (1993) and Davenport and Hill-Carol (1986). These formulas give a prediction of the damping ratio for a building based on overall building dimensions and construction materials. However, due to the lack of data from full-scale measurements these formulas experience a large scatter with new measurements. Buildings contain many elements and every building is unique which causes large difficulties in classification

of buildings that can be used to predict damping. The main problem is that there exists no model to identify individual damping mechanisms in buildings. Understanding of the influence of individual components to damping is key to predict damping in a building accurately for safe and comfortable building.

1.2. Scope

In this research project the focus will be on the contribution of damping in floors to the damping ratio of buildings. Here both damping in structural parts, in the connections between the floor and the main structure, and damping in floor-materials are studied.

Slender Dutch High-rise buildings under wind loading are studied. The structure of such a building is in the serviceability limit state and encounters medium to heavy wind load, which mainly excites the first mode in the three main directions of the building. In this research, the contribution of damping by a floor to the first global mode of vibration of building is studied. Contribution of other damping mechanisms in the foundation or the facade and the main load bearing and stabilizing structure itself are not taken into consideration.

1.3. Research objective

The main goal of this research is describing the influence of damping mechanisms present in floors with regard to the total damping in a structure. Therefore, firstly, detection of active damping mechanisms is needed. When influences due to changes in these damping mechanisms are known in terms of energy dissipation, the basis is set for a study on damping for different floor and joint characteristics.

Hence, a model is developed which describes the dynamic behavior of a single floor and quantifies the energy dissipation within this floor and it's connections due to excitation of the main structure.

1.4. Research questions

1.4.1. Main question

The research question comprising the research objective can be formulated as follow:

> ***How does the dynamic behavior of floors in slender high-rise buildings in The Netherlands, and especially the energy dissipation in a single floor and its connections to the main structure, contribute to the total damping of the structure?***

In the research question several terms are used which need to be more precisely described.

Dynamic behavior of floors. The entire structure encounters vibrations in three directions: the horizontal x-direction, horizontal y-direction and a torsional direction. The lowest mode in each of the directions is referred to as the first natural mode of the building in respectively the x, y or torsional direction. From measurements on buildings it is concluded that only these first modes contribute significantly to the vibrations of the entire structure. In the excited state, several local vibrations take place in small parts within the structure. Within floors vibrations take place that might not coincide directly with the first global mode, but they are excited due to the overall behavior. Understanding of this dynamic behavior of a floor during wind loading is crucial to evaluate the damping mechanisms present in a floor.

Slender high-rise buildings in The Netherlands. With increasing slenderness the dynamic stability of buildings becomes increasingly important and may even become more important than the static strength and stability of the structure. Higher buildings encounter larger vertical loads which result in the need to increase the overall stiffness to reach the strength level necessary. The mass shows relatively smaller increase compared to the stiffness due to attempts to limit the vertical loads in the structure. From measurements a relation

between the height of a building and the damping ratio is found. A decrease in damping ratio is found for increasing building heights. The dynamic wind load increases with height, which gives a larger dynamic load on higher buildings. In Dutch buildings a clear link with building height and slenderness is found. Due to these reasons, slender high-rise buildings are especially vulnerable to horizontal wind loading effects such as vibrations.

Energy dissipation within in a single floor. It is expected that at least some of the energy dissipation in the structure is due to the dynamic behavior of floors due to excitation of the building due to wind loading. A part is expected to arise from material damping within the floor itself, which is related to stresses and crack lengthening.

Energy dissipation in connections to the main structure. A second contribution to the energy dissipation originates in the structural damping in the joints, where floors are connected with the main load bearing structure. There are several possible damping mechanisms proposed in literature which might reproduce this type of damping.

Total damping of the structure. For design and construction purposes the main demand for this study is understanding of the dynamic response of the total building due to wind loading, because the maximum deflections and accelerations should satisfy the regulations set within the Eurocode. Therefore, understanding whether changes in floor material, lay-out and it's connections will have an significant influence on the total expected damping of the building is one of the main objectives of this study.

1.4.2. Sub-questions

We have formulated the following subquestions:

1. *Has material damping of the floors itself any significant influence on the overall damping of the structure?*

This sub-question anwsers the question whether material damping should be included in a model for damping in floors or that this material damping is small enough when compared to the damping in the joints that it may be neglected in such models.

2. *How can different joint types be represented in a damping mechanism with compatible damping values and damping mechanisms?*

In buildings several types of joints are used for the connection between floor and the main load bearing structure. In the current empirical formulas for damping, no distinction is made between the connection types present in the structure. In reality, it might be expected that different damping values are required when designing a building with solely hinged connections or a building with mainly very stiff connections. In the model the rotational stiffness of connections should the be changeable variables, so the model can study several types of joints that are present within Dutch highrise structures.

3. *What contribution does damping in joints have to the total damping of the structure?*

Next to the sub-question whether material damping has a significant influence, the influence of damping in joints should be studied and compared with the influence of material damping.

4. *Do present non-structural elements, initial stresses and local static loads have a significant influence on the dynamic behavior of floors?*

Multiple possible sub-mechanisms might influence the damping. Among these pretension present in floor slabs influences the stresses and deflections, which are expected to influence both the material damping and the amount of rotations. Also, static loads may influence the behavior of the floor and therewith the damping. And finally, other non-structural elements, present as masses or interface conditions, might be of significant influence on the energy dissipation in floors.

1.5. Report Outline

This report is divided in four parts: the literature study, the database analysis and the model and results part and finally the conclusions and recommendations. Below the content of the parts are shortly summarized.

ch. 2 - 4: Literature Study:

In the Literature Study a general overview on dynamics is provided (ch. 2). Possible solution methods and measurement methods for both linear and nonlinear systems are studied in terms of their applicability in buildings and an overview of plate theory is given. The state of the art of the current prediction models for damping in highrise buildings, referring to both the codes and empirical formula's developed based on full scale measurements are described in (ch. 3). Different existing damping mechanisms are described and discussed in terms of their usability for floors in (ch. 4).

ch. 5: Database analysis:

In the Database analysis twenty Dutch highrise buildings are analyzed on both their structural properties, concerning the structural stability and load transfer flows, and on their general lay-out. The floors are analyzed on material type, dimensions and connections with the main structure. Also a study of the response of a building to various wind loads, including dynamic properties such as stiffness and natural frequencies is presented using both full-scale measurements and literature data.

ch. 6 - 9: Modeling and results:

Methodology:
In the Methodology chapter (ch. 6) both the method for the analytical model and for the experiment are described. First, the analytical model is discussed, elaborating on the choice for the used solution method. In the second part the experimental set-up regarding both equipment and measurements is described. Also the measurement and loading methods are given.

Experimental results:
In this chapter (ch. 7) the data obtained at the experiment are analyzed. Raw experimental data gave horizontal and vertical accelerations at several positions along the beam. These accelerations were used to calculate the corresponding velocities and displacements. The outcomes are then analyzed on present frequencies and modes and the results are presented by deviations on the original test set-up.

1D Model:
This chapter (ch. 8) the analytical model is presented. Both a physical and a mathematical model description are given of the different elements of the model, together with the assumptions made during the model developing process. The derivation of the analytical response, by applying the Galerkin method together with numerical integration is entensively described in the second part of this chapter. The implementation of the solution method and the implementation in matlab and the programming codes are also given in Appendices C and D respectively.

Model Validation: parameter calibration and sensitivity study
In the Model Validation chapter (ch. 9) results from the analytical model are compared with results of the experiment. A sensitivity study is performed for each of the damping parameters and ithe best fitting parameters for both stiffness and damping are presented.

ch. 10 - 11: Conclusions and Recommendations:

This report ends with the conclusions (ch. 10) and recommendations (ch. 11) where the final conclusions are presented and recommendations are given for future research and use of the developed model.

I

Literature Study

2

DYNAMICAL SYSTEMS

There are several options to model a structure for analysis of the dynamic behavior. In this chapter several methods and theories are described for both linear and non-linear systems which can be used to create an analytical model of a floor in a building. Also, solution methods are provided to calculate the dyamical response of those models.

2.1. Modeling dynamical systems

In dynamics, there are two generally accepted methods to determine the equations of motion: using Newton's Second Law or the Euler-Lagrange Equations.

Second Newton's law

Newton's second law states that the rate of change of momentum of a mass equals the force acting on it [11]. Using this equilibrium condition, the equation of motion for any system can be derived by expressing all forces acting on a mass as functions of displacements and rotations. Next, the equation of motion for each possible motion is found by summing up all forces corresponding to a certain motion value, such as a certain displacement or rotation, and setting them equivalent to the rate of change of momentum of a mass of this corresponding degree of freedom, which is the second order time derivative of this degree of freedom

multiplied by the momentum mass.

$$m_1\ddot{x_1} = \sum F\left(x_1, \dot{x_1}, x_1', x_1'', etc\right) \tag{2.1}$$
$$m_2\ddot{x_2} = \sum F\left(x_2, \dot{x_2}, x_2', x_2'', etc\right) \tag{2.2}$$
$$I_1\ddot{\phi_1} = \sum F\left(\phi_1, \dot{\phi_1}, \phi_1', \phi_1'', etc\right) \tag{2.3}$$
$$\text{etc.} \tag{2.4}$$

The Newtonian approach is very well suited for single degree of freedom systems or for systems with infinite degrees of freedom such as a continuous one-dimensional model where those rotations and displacements are a function related to one or multiple space coordinates.

Lagrange Equations

Lagrange Equations are well suited for systems with a finite number of degrees of freedom or for systems with distributed parameters [12]. The basics of the Lagrange Equations of Motion is the derivation of equations from the kinetic energy, the potential energy and the virtual work due to non-conservative forces in the system. The number or equations of motion is equal to the number of degrees of freedom.

Kinetic energy of a generic dynamical system T can be expressed in terms of generalized displacements $(q_1, q_2, ..., q_n)$ and velocities $(\dot{q}_1, \dot{q}_2, ..., \dot{q}_n)$. According to Lagrange, the variation in kinetic energy can be expressed by Equation 2.5. The potential energy V can be expressed in terms of generalized displacements as well, which give the variation of potential energy according to Equation 2.6.

$$\delta T = \sum\left(\frac{\partial T}{\partial q_k}\delta q_k + \frac{\partial T}{\partial \dot{q}_k}\delta \dot{q}_k\right) \tag{2.5}$$

$$\delta V = \sum\left(\frac{\partial V}{\partial q_k}\delta q_k\right) \tag{2.6}$$

Using d'Alemberts principle, which states that the virtual work performed by effective forces through infinite small virtual displacements compatible with the system constraints is zero [12], yields Equation 2.7.

$$\sum (F_i - m_i\ddot{r}_i)\cdot\delta r_i = 0 \tag{2.7}$$

The virtual work can be described as a part done by non-conservative forces and a part as work by conservative forces, the kinetic energy. The virtual work of the non-conservative forces can be described in the non-conservative forces Q_k and generalized displacements.

$$\overline{\delta W}_{nc} = \sum_{k=1}^{n} Q_k\delta q_k \tag{2.8}$$

The Lagrange equations can be derived from the equations above. Assuming that every virtual generalized displacement δ_k is zero gives the Lagrange equations according to Jia [11]:

$$\frac{d}{dt}\left(\frac{\partial T}{\partial \dot{q}_k}\right) - \frac{\partial T}{\partial q_k} + \frac{\partial V}{\partial q_k} = Q_k \tag{2.9}$$

For damped systems an additional term in the left hand side is present, containing the dissipation function D:

$$\frac{d}{dt}\left(\frac{\partial T}{\partial \dot{q}_k}\right) - \frac{\partial T}{\partial q_k} + \frac{\partial V}{\partial q_k} + \frac{\partial D}{\partial \dot{q}_k} = Q_k \tag{2.10}$$

For systems with conservative forces, where multiple degrees of freedom are of interest, the Lagrangian equation of motion can be very effective. However for systems with nonlinear damping or damping dependent on position and time, the work between two points can not be separated from the taken path. For systems including friction mechanisms, producing non-conservative damping, the Lagrange method is not very suit-

able. Also for systems with infinitely many degrees of freedom, giving infinitely many equations, the Newton law based approach is more suitable.

2.1.1. Model types and degrees of freedom

Single Degree of Freedom System (SDOF)

A single degree of freedom system is a simple model describing the dynamical behavior of a system with damping and experiencing an external force using a single degree of freedom.

A single degree of freedom system with a linear spring and dash-pot is described by Equation 2.11. x is the only degree of freedom and can represent any motion direction. $F(t)$ is the external force applied on the system and can occur as any function of t, c and k are respectively the viscous damping value and the spring stiffness. The solution of this problem is x as an function of time $x(t)$.

$$m\ddot{x} + c\dot{x} + kx = F(t) \tag{2.11}$$

The response to this system for free vibration has in general a sinusoidal form

$$x(t) = e^{-nt} X \sin(\omega_n t + \phi) \quad \text{where} \quad \omega_n = \sqrt{k/m} \quad \text{and} \quad c/m = 2n \tag{2.12}$$

ω_n is called the natural frequency of the system. Without any external loading, the system will always vibrate in the natural frequency, because for vibrating in this frequency the least amount of energy is needed. The magnitude of amplitude of the response is dependent on the loading frequency relative to the natural frequency. Very high amplitudes are found when the frequency of the load is equal to the natural frequency of the system. This occurrence is called resonance and should be prevented from happening.

$$|H(\omega)| = \frac{\left|U_{steadystate}\right|}{|U_{static}|} = \frac{1}{\sqrt{(1-\frac{\omega^2}{\omega_n^2})^2 + \frac{4n^2}{\omega_n^2}\frac{\omega^2}{\omega_n^2}}} \tag{2.13}$$

Multiple Degrees of Freedom Systems (NDOF)

A system can be modeled as with a finite number of degrees of freedom with N masses which are connected to each other and to the surrounding with springs and dash-pots. The general description of such a system is:

$$\mathbf{M}\ddot{x} + \mathbf{C}\dot{x} + \mathbf{K}x = \underline{F}(t) \tag{2.14}$$

When the system is uncoupled, each degree of freedom has its independent equation of motion which can be solved as SDOF individually. For larger N or in the case of dependent matrices, such a method can be very time consuming. Note that as soon as one spring or other element has an influence on more than one degree of freedom, the system is coupled and the equations of motion can not all be solved individually.

The responses of the MDOF system for free vibration can be represented by a sum of harmonic responses:

$$\underline{x}(t) = \sum \underline{\hat{x}_i} \sin(\omega_i t + \varphi_i) \tag{2.15}$$

A system with N degrees of freedom vibrates in N natural frequencies (ω_i) and in N principle modes of vibration ($\underline{\hat{x}_i} \sin(\omega_i t + \varphi_i)$). The mode at the lowest natural frequency is called the fundamental mode of vibration. The response can be written as a sum of harmonic functions in the natural frequencies. The number of functions should be equal to the number of natural frequencies and the amount of degrees of freedom.

$$\underline{x}(t) = \sum_{}^{N} \underline{\hat{x}_i} u_i(t)) = \mathbf{E}\underline{u}(t) \tag{2.16}$$

In mechanical systems or systems consisting out of multiple bodies, masses or other elements related to each other and for system with several well distinctive mode of vibrations NDOF systems are very useful.

Continuous Systems (CS)

One-dimensional structures with distributed mass, stiffness and loading such as flexural beams, strings or columns can very well be represented by continuous models, where infinite degrees of freedom distributed on a space domain x. The function which describes the motion is now dependent on both space and time: $w(x,t)$. This has as result that the equations of motions become partial differential equations.

The equations of motion of 1D continuous systems in general have the format of Equation 2.17 [13], where a second order derivative in time is present together with a second or fourth order space derivative, dependent on the situation.

$$\frac{\partial^2 w}{\partial t^2} = c^2 \frac{\partial^2 w}{\partial x^2} + Q \tag{2.17}$$

In a continuous system the deflection of the response, w, is dependent on both x and t. Therefore, besides initial conditions, also space conditions, called boundary conditions, are needed to fully describe the problem. There are infinite number of degrees of freedom and therefore infinite number of modes in which the system can vibrate.

2.2. Solution methods for Linear Systems

Several methods are developed to solve dynamical systems. Among the analytical methods two type of methods are reflected on. Firstly, the use of mode shapes and natural frequencies and secondly, the used of the frequency domain.

2.2.1. Natural frequencies and mode shapes

In most methods the calculation of the dynamic response is based on the use of eigenfrequencies and mode shapes to represent the behavior of a system. These eigenfrequencies and mode shapes are determined by the structure material properties, the general geometry and support conditions. The number of natural frequencies depend on the number of degrees of freedom in the system.

The essence of Modal Analysis is the assumption that the responds can be represented as a summation of eigenvectors or mode shapes multiplied by an unknown time function [13]. For free vibrations the eigenfrequencies at which the structure will resonate are determined. Damping is hereby not taken into account and is assumed to not have an influence of the natural frequencies. For each natural frequency, an accompanying eigenvector $\underline{\hat{x}}$ or mode can be determined.

$$\mathbf{M}\ddot{u} + +\mathbf{K}u = 0\,, \qquad \det(-\omega_i \mathbf{M} + \mathbf{K}) = 0 \quad \Rightarrow \omega_i = ... \tag{2.18}$$

$$(-\omega_i \mathbf{M} + \mathbf{K})\,\underline{\hat{x}} = 0 \quad \Rightarrow \mathbf{E} = \left[\underline{\hat{x}}_1 \underline{\hat{x}}_2 ...\right] \tag{2.19}$$

The solution to the homogeneous, forced or damped system is found in the form of a summation of the eigenfrequencies and the modes. Using the orthogonality properties of the eigenvectors, the modal mass and modal stiffness of the system are derived giving uncoupled equations where a solution can be determined for each mode individually.

There are some restrictions to this method, modal analysis is strongly linked to the linearity properties of the system due to its basic assumption of a summation of modes. For a system with damping, the Modal Damping can be computed using the eigenvectors. However, the Modal damping is not generally uncoupled for all modes. Eigenvectors are not orthogonal with respect to the damping. For complex modal analysis, equal damping ratio for all principal modes of vibrations is assumed. This deviates from reality where increasing or decreasing damping ratios for higher natural frequencies are possible [13]. Rayleigh damping uses a proportional modal damping matrix related to the modal stiffness and modal mass matrix to describe the damping in all modes [14].

When following the Classical Method or Method of Separation of Variables for continuous systems, the equation of motion gives the eigenfrequency by assuming the deflection of for example the beam at position x and time t is $z(x,t) = X(x)\Phi(t)$ and substitute this in the equation of motion.

$$EI\frac{d^4z}{dx^4} + \mu\frac{d^2z}{dt^2} = 0 \tag{2.20}$$

$$\Rightarrow EI\frac{d^4X}{dx^4}\Phi(t) + \mu\frac{d^2\Phi}{dt^2}X(x) = 0 \tag{2.21}$$

$$\frac{EI\frac{d^4X}{dx^4}}{\mu X(x)} = \frac{\frac{d^2\Phi}{dt^2}}{\Phi(t)} = \text{constant} = \omega^2 \tag{2.22}$$

A solution for $X(x)$ is expressed in the form of a trigonometric function can be found by solving the left equation. This solution is only dependent on x and can therefore be called the space solution. The space solution is representing the mode shape, by determining A_i for each natural frequency with use of the boundary conditions.

$$X(x) = A_1 sin(\kappa x) + A_2 cos(\kappa x) + A_3 sin(i\kappa x) + A_4 cos(i\kappa x) \tag{2.23}$$

Where κ is related to the natural frequencies of the system ω:

$$\omega_i = \sqrt{\kappa^4\frac{EI}{\mu}} \tag{2.24}$$

The natural frequency for a beam is dependent on support conditions and the beam stiffness properties [11].

Equivalent system analysis uses only information on one specific fundamental natural frequency, a system or structure is idealized as a discrete SDOF system. Instead of the general stiffness of the beam, an equivalent stiffness and an equivalent mass are used in the calculations. This equivalent stiffness k_{eq} or mass m_{eq}corresponds with the degree of freedom used in the simplified model. For systems where damping is present, also a equivalent damping value is needed. Where for stiffness and mass general excepted methods exist, is finding the equivalent damping much more complicated. According to Jia, the equivalent damping can be found using kinetic and potential energy formulations [11].

$$\omega_n = \sqrt{\frac{k_{eq}}{m_{eq}}} \tag{2.25}$$

$$T_{kin} = \frac{1}{2}m_{eq}\dot{x}(t)^2 \tag{2.26}$$

$$V_{pot} = \frac{1}{2}k_{eq}x(t)^2 \tag{2.27}$$

$$E = -\int_{x_1}^{x_2} c_{eq}x(t)\,dx \tag{2.28}$$

This method is very often used in practice, because a SDOF system is mathematically the most simple system to handle. Therefore, is several codes formulations are based on those types of models for a wide range of applications.

2.2.2. Solving in frequency domain

When the response is determined in the time domain a solution is found in the form of one or multiple functions dependent on time and space. For simple systems with a few natural frequencies or a load very close to one of the natural frequencies, a solution in the time domain is easily obtained. In reality, the response signal contains a variety of frequencies. A simpler approach is then solving the system in the frequency domain. Fourier Transform or Transformations to the Laplace Domain are generally accepted methods to transform a system out of the time domain and back. Both techniques for transforms mentioned below are based on the linear superposition principle. Therefore for some systems, such as nonlinear systems, an exact solution to

the equation of motion can not be derived using those techniques, a solution has to be found with numerical approximations when solving in the time domain[15].

2.3. Non linear systems

For a linear problem the response is proportional to the load and excitations to which it is subjected [11]. Therefore, a study of a linear system can be performed using linear differential equations for which a general solution is found.

In the real world purely proportional systems do not occur [11] and linear models are solely approximations of the reality. With avoiding more complex analysis, in most mathematical models the combined damping effect is assumed to be in the form of equivalent viscous damping, as an approximation for the actual damping, with linear equations [11, 16].

Nonlinearity can occur in four ways in a system according to Keulen [17]:

- *Geometrical non-linearities*
  Here a non-linear relation between displacements, deformations and forces exists, such as buckling or second order effects due to initial incontinuities.

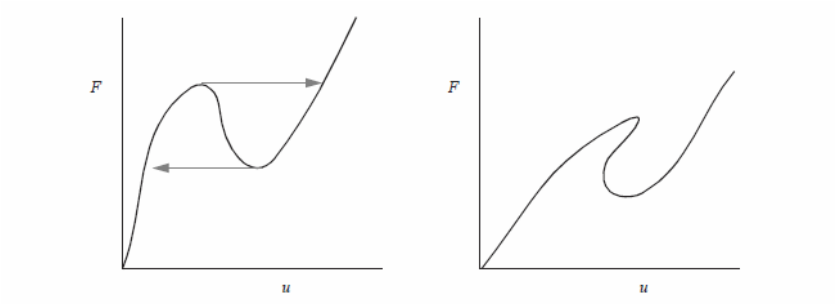

Figure 2.1: Non-linear behavior due to geometrical non-linearities in the force-displacement diagram [17]

- *Physical non-linearities*
  Nonlinear material behavior belongs to the physical non-linearity. When the material stress–strain relationship remains linearly elastic, the change of stiffness is insignificant and the system behaves linear. However, when the stress-strain relationship changes, this brings a change in stiffness and can lead to significantly larger deformations [11]. Events such as yielding of materials, creep, relaxation of stresses and cracking of materials fall under this category of nonlinear behavior.

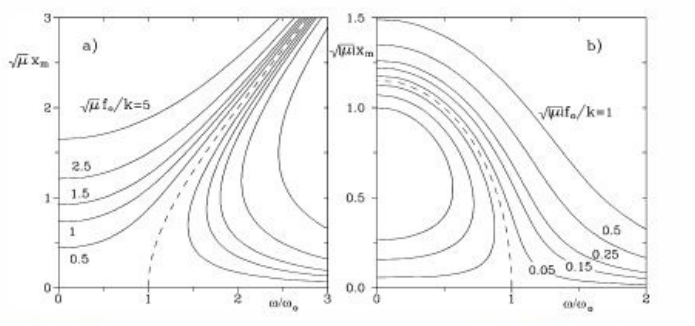

Figure 2.2: Hardening and softening as effects of nonlinearities [15]

- *Non-linearities in the boundary conditions*
  The system itself is linear, but due to non-linearities in the boundaries the response is nonlinear. An

example for such a boundary condition is friction.

- *Interaction with the environment*
  Nonlinear effects due to interaction of the construction with the environment. For problems within the construction of buildings, this type of non-linearity does not occur. For systems where a part of the solid reacts with the environment and causes properties regarding to stiffness, mass or damping to change, this type of non-linearity might be decisive.

Properties of nonlinear systems produce complex responses where large variations in amplitude and frequency occur due to small changes loading. The properties of a nonlinear system can be listed as follows [18]:

- Multiple steady state solutions are possible as response to the same input. Some might be stable, other unstable.
- Discontinuities and significant changes in the response of the system occur when a forcing parameter is slowly varied. This is called the jump phenomena.
- Responses at other frequencies than the forcing frequency occur.
- Internal resonances occur. Different parts of the system vibrate at different frequencies with steady amplitudes.
- Without explicit external periodic forcing self sustained oscillations occur.
- Chaotic vibrations occur. Which are unstable complex irregular motions that are very sensitive to initial conditions.

Also it is observed that for most nonlinear systems , the sequence of loading effects the response of the system. This load sequence effect can be associated with changes of the global or local stiffness due to plastic behavior, geometrical non-linearities or changes in the support conditions due to the reaction of the system on earlier loads [19].

For all nonlinear systems the main property of a linear system, the superposition principle which holds that the summation of responses to individual forces is equal to the total responds to the forces combined, is not applicable. In linear systems the response of a system is proportional to the load and excitation, where in a nonlinear system the stiffness or load are dependent on the deformation resulting in the need to update the modes in each time step. Nonlinear systems are therefore difficult to analyze both analytically and numerically. Especially for systems with more degrees of freedom, with increasing the importance of non-linearity, solving the system becomes computationally more difficult. For a nonlinear problem the number of possible outcomes is undetermined and therefore no general solution exists. With the consequence that large uncertainties remain when a solution is found.

Weakly and strongly nonlinear systems

When a system is weakly nonlinear the system is either weakly nonlinear in itself or it operates in conditions, for example with small amplitudes, which prevent the nonlinear nature of the system to significantly effect the response [15]. Weakly nonlinear systems can be described using approximations and methods based on the linear solutions. Strong nonlinear systems, however, can not be solved analytically. The response of a nonlinear system is far from harmonic and can only be computed when numerically approximated and validated with physical experiments.

2.4. Methods for nonlinear systems

Like linear systems can be described by sets of linear differential equations (DE's), so can nonlinear systems be described by sets of nonlinear DE's. However, there is no generally applicable method to solve nonlinear DE's. There are different methods and techniques developed which can be used to study the responds of nonlinear systems. However, all methods provide an approximate solution for the nonlinear system. An

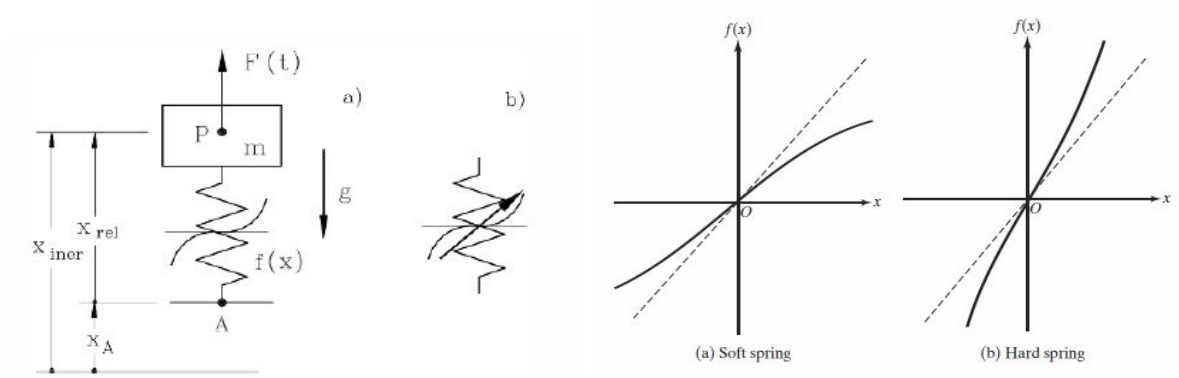

(a) Conservative nonlinear SDOF system with nonlinear spring (b) Hardening and softening effect in nonlinear spring

Figure 2.3: Hardening and softening effect in nonlinear spring force-displacement diagram[15]

exact solution can only be derived for a small selection of nonlinear systems which are described with simple second-order differential equations [20]. Mainly due to the extended use of finite element methods is the direct time integration combined with decent integration methods for reaching equilibrium within each time increment the most used method to obtaining nonlinear responses in civil engineering practice [11]. In this section are besides the direct time integration methods some of the analytical approximate methods listed which can be used to solve weakly nonlinear systems.

The methods for studying the response of nonlinear differential equations can be subdivided into [18]:

1. Basic analytical methods
   Direct integration method
   Linearization of nonlinear system
2. Heuristic techniques
   Galerkin Method
   Harmonic Balance method
3. Asymptotic techniques
   Ritz averaging method
   Methods of averaging and multiple scales
4. Numerical methods
   Direct numerical integration
   Iterative solution methods
   Incremental solution methods

Below a short description on the usability of all methods is given. The Galerkin Method and the Direct Numerical Integration method are used in this thesis, those methods are described more extensively. In Appendix B the other methods are described.

2.4.1. Basic Analytical methods

The simple analytical methods are only valid for a small selection of dynamical systems which meet specific requirements. Only weak nonlinear system and systems containing uncoupled damping and a low order derivatives can be solved analytically by those methods.

2.4.2. Heuristic Techniques

With heuristic methods the solution is approximated with a periodic solution. The approximated solution is convergent with adding additional terms to the periodical solution [18]. However, the accuracy of a given

number of terms within the periodic solution is unknown. These heuristic methods are therefore restricted to periodic solutions and the instability of the solution should taken into account.

Galerkin method

The Galerkin Method is a widely used method for finding approximate solutions to partial differential equations [21]. The Galerkin method is a method to approximate the solution with a sum of periodic function which consists of the product of the eigenfunction of the linear system and generalized time-dependent coordinates. The equations are projected on the linear space [22]. The problem is described with linear boundary conditions and an equation of motion where all nonlinear forces due to both internal and external effects are present.

The Galerkin continuous projection consists of two steps:

1. The first step is to give an approximation to the solution in the form of the sum of a product of a basis function and an unknown time coefficient. The base functions are determined by the linear space.

$$v(x,t) = \sum_{n=1}^{\infty} v_n(x,t) = \sum_{n=1}^{\infty} p_n(x) q_n(t) \tag{2.29}$$

2. The second step is to substitute the approximated function into the differential equation. Hereby a residual term $r(t)$ is obtained which contains all nonlinear contributions. The other term contains the orthogonal projector to the linear space

$$v(x,t) = \sum_{n=1}^{\infty} p_n(x) q_n(t) + res \tag{2.30}$$

After the projection, the unknown coefficients can be found. By using the orthogonality property of the linear modes a set of N nonlinear equations and N unknown time dependent coordinates is obtained. By making the residual orthogonal to the assumed basis functions, the residual contributes to the set of N nonlinear equations by coupling of the nonlinear equations.

Mahmoodi [23] used the method of multiple scales together with the Galerkin projection on visco-elastic continuous beams with linear boundary conditions and found accurate results compared with experiments. Pesheck has used the method to model many coupled normal modes and showed that a wide variety of forms of non-linearities at the boundaries are allowed within the solution procedure with little additional analytic work. Also the method significant promise for the development and understanding of reduced-order models for nonlinear systems according to Pesheck [24].

Kalashnikova used the Galerkin projection for continuous nonlinear equations with nonlinear boundary conditions. As the boundary conditions of the discretized system are not in general inherited by the reduced order model obtained after the projection, they should be implemented separately in the reduced order model [25]. Hereby the penalty method is used where the entire boundary value problem is rewritten in a single equation that is valid on both solid and boundary.

In finite elements the Bubnov-Galerkin method is used to find the best solution to a given collection of functions by taking the weak form of the governing equation which is multiplied by a weight function from the same finite dimensional space, dependent on the spatial boundaries due to Dirichlet boundary conditions, and integrating over the space [26], which is in principle equal to the method described above applied to a discrete problem. Several other variations on the Galerkin method exist for specific areas of practice, such as Petrov-Galerkin method where the weight functions come from a different space than the trial functions [26] or other nonlinear Galerkin Methods for Navier-Stokes equations [27], which are often used at fluid dynamics.

Harmonic Balance method

The technique of Harmonic Balance (HBM) is a specialized application of the Galerkin method to find periodic solutions in vibration problems. In harmonic balance, there is a periodic solution with a convergent

Fourier series representation we wish to approximate [18]. All harmonics of the motion must then be so called balanced by substitution in the equation of motion and finding a set of nonlinear equations for the amplitudes of the various harmonics. HBM is based on finding linearized coefficients which depend on both the frequency and the amplitude of oscillations [28]. Not all harmonics can be balanced because for some harmonics the number of unknowns is larger than the number of equations [15]. Usually only a few harmonic terms are used to approximate the solutions. According to Genta, the harmonic balance technique is very good in the case of hardening or mildly nonlinear systems with softening and small amplitudes [15].

2.4.3. Asymptotic Techniques

Asymptotic techniques depend on some parameter in the problem being very small or very large. The solution is sought for the limit where this very small parameter goes towards zero or the large parameter goes to infinity [18]. Methods such as the method of multiple scales [29] and averaging [30] is used in combination with the Galerkin method to study the weakness of nonlinear terms in the slow time scale.

2.4.4. Numerical methods

As mentioned above are numerical methods the most used methods in engineering practice, both direct integration of the equation of motion and numerical integration after several transformation steps. However, in nonlinear dynamics it is difficult to determine the quality of the found solution based on solely numerical simulations [18]. An analytical or theoretical study of simplified nonlinear systems is an essential contribution to all-numerical studies of large nonlinear systems.

Direct integration method

The response is obtained by integrating the equation of motion directly. Solutions to the system contain time histories and therefore a deterministic function for the excitations is needed to determine the amplitude at each time step [11]. The state of the system at time $t + \Delta t$ is computed from the known conditions at state t based on integration scheme's. The interval length should be small enough to eliminate large errors, but large enough to reduce the calculation effort.

Within the direct integration methods a distinction is made between implicit integration methods and explicit methods. Explicit methods are conditionally stable where implicit scheme's are unconditionally stable. Explicit methods are stable when the time step is smaller than the critical time step. With the need for a small time step, explicit methods are not suitable for long duration events. At implicit methods, the accuracy of the response is not guaranteed and the calculation time at each step is longer than for explicit methods. Explicit methods are often used for systems with large deformations or non-linearities, where implicit methods are used for linear systems with long duration events [11].

There are many integration schemes developed for initial value problems with ordinary differential equations. The most simple scheme is the Euler method. Closely related are the Trapezoidal method and the midpoint-method. They are easy to implement, but have a small maximum accuracy and are therefore not suited for nonlinear systems.

The implicit Euler method is described with:

$$y_{n+1} = y_n + h \cdot f(t_n, y_n) \tag{2.31}$$

Taylor methods look for higher order approximations following the Taylor polynomial approximation. However for computing higher order approximations, higher order derivatives of the true solution are needed which makes the method very time-consuming [31]

Runge-Kutta methods, and especially higher order RK-methods, provide a more accurate accuracy within reasonable computation time. The fourth-order Runge-Kutta method having a truncation error of $O(h^4)$ is

one of the most widely used methods for solving differential equations [32] due to the relatively high accuracy compared with the calculation effort.

Runge-Kutta Method:

$$y_{n+1} = y_n + \frac{h}{6}(k_1 + 2\cot k_2 + 2 \cdot k_3 + k_4) \tag{2.32}$$

$$k_1 = f(t_n, y_n) \tag{2.33}$$

$$k_2 = f(t_n + h/2, y_n + k1 \cdot h/2) \tag{2.34}$$

$$k_3 = f(t_n + h/2, y_n + k2 \cdot h/2) \tag{2.35}$$

$$k_4 = f(t_n + h, y_n + k3 \cdot h) \tag{2.36}$$

In Figure B.1 the Runge-Kutta method is compared with the Euler method for a simple first order differential equation.

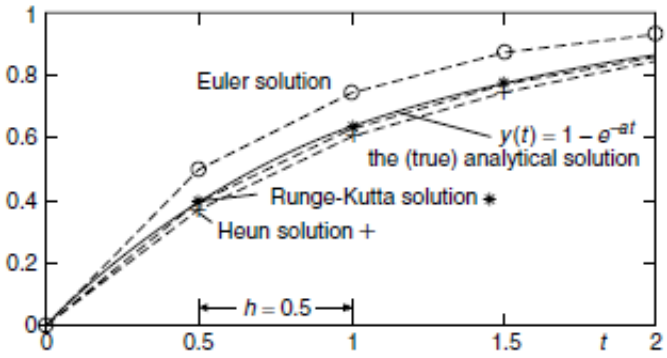

Figure 2.4: Comparison numerical integration schemes [32]

Multi-step methods use solution values at several previous nodes to compute the numerical solution. Adams-Bashforth methods and Adams-Moulton methods are the most used multiple-step methods [31]. They can cope with stiff differential equations, but the accuracy relative to computations time is low.

Below, the frequently used numerical methods from Matlab are compared. For non-stiff differential equations on a small time span, the 4/5th order Runge-Kutta is the best fitting method. This method is used to find the response of the model. This implementation can be found in Appendix D.

Solver	**name**	**implicit-explicit**	**solver type**	**accuracy order**	**Problem type**	**Computation time / When to Use**
ode45	4/5thorder runge kutta	explicit	one-step	Medium	Nonstiff	Medium/ Most of the time. This should be the first solver you try.
ode23	2/3thorder runge kutta	explicit	one-step	Low	Nonstiff	Medium - low /For problems with crude error tolerances or for solving moderately stiff problems.
ode113	Adams-Bashforth-Moulton PECE solver	explicit	multi-step	Low to high	Nonstiff	High For problems with stringent error tolerances or for solving computationally intensive problems.
ode15s	Backwords differential equation (BDE) solver	implicit	multi-step	Low to medium	Stiff	Medium - Low / If ode45 is slow because the problem is stiff.

ode23s	2nd order Rosenbrock formule		one-step	Low	Stiff	Low / If using crude error tolerances to solve stiff systems and the mass matrix is constant.
ode23t	trapezoidal rule		one-step	Low	Moderately Stiff	Low / For moderately stiff problems if you need a solution without numerical damping.
ode23tb	combination RK and trapezoidal rule and BDE	implicit	multi-step	Low	Stiff	Medium / If using crude error tolerances to solve stiff systems. [31–34]

Table 2.1: Comparison numerical integration schemes

2.5. Plate Dynamics

"A plate is a solid body bounded by two surfaces, where the distance between the two surfaces, the thickness, is assumed to be small compared to the lateral dimensions" [21]. Plates can be modeled as two-dimensional systems with material properties in two lateral directions. While for most cases at beams flexural and torsional are considered uncoupled, flexural and twisting behavior of plates can not be uncoupled [11].

Besides plates a second type of two-dimensional structures are membranes. Membranes are considered as perfectly thin plate or lamina that are subjected to tension. Any resistance to shear or bending forces are neglected and at membrane only in-plane stretching or tensile forces contribute to deformations [21] and therefore they are not applicable to floors.

There are two well known theories for plates: the classical plate theory, also called the Kirchoff plate theory, and the Reissner-Mindlin plate theory [11]. The classical theory is mostly-used for thin plates and does not take into account any shear deformation. Plates are considered as thin when the ratio of its thickness to the smaller lateral dimension is smaller than 1/20 [21]. For thick plates, shear deformations play a significant role in the overall deformations and the RM theory gives a better approximation. The Reissner-Mindlin theory is an extension to the Timoshenko beam theory and takes besides shear deformation also rotary inertia into account. Several other plate theories exist which take shear into account by Levi, Reissner, Hencky, Mindlin and Kromm [35]. Also, higher order shear plate theories are developed. They can be used for modeling the buckling behavior of plates or other higher order effects. However, deriving exact results of those higher order theories is impossible, numerical approximations are necessary [35].

For floors the length-thickness ratio is usually below this 1/20 ratio and they have significant flexural stiffness. Therefore, floor slabs can be considered as thin plates which follow the Kirchoff Plate Theory where transverse deformation to the mid-plane are studied.

2.5.1. Kirchoff Plate Theory or Classical Plate Theory

The Kirchoff Plate Theory is an extension to the Euler Bernoulli Beam theory in two directions and therefore follows the assumptions of the Euler-Bernoulli beam theory [21]:

1. The thickness of the plate is small compared to its lateral dimensions
2. The middle plane of the plate does not undergo in-plane deformation.
3. The displacement components of the mid-surface of the plate are small compared to the thickness of the plate.
4. The influence of transverse shear deformation is neglected and plane sections remain normal to the mid-surface after deformation.
5. The transverse normal strain ϵ_{zz} under transverse loading can be neglected.

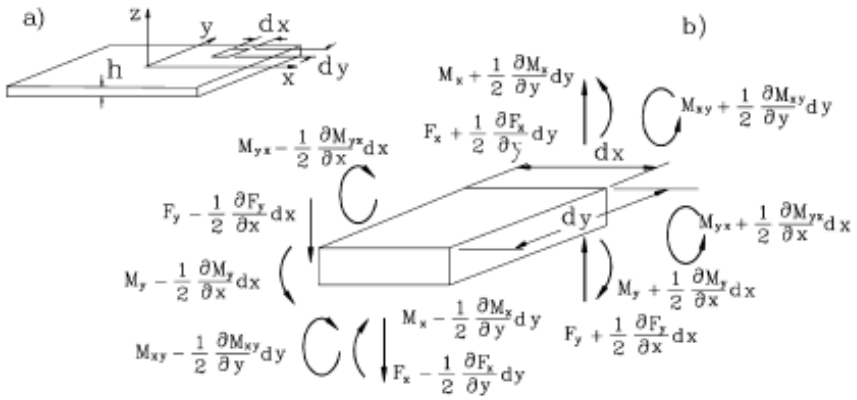

Figure 2.5: Reference system plate forces and moments Kirchoff Plate Theory [20]

When the mid-plane is not stretched, strains are only related to bending and twisting. Because the transverse shear is neglected plane stress can be assumed where no stresses in normal direction on the surface area are present. For an isotropic elastic thin plate with plane stress, the relation between stresses σ and strains ϵ is the described with the following [36]

$$\sigma = \begin{Bmatrix} \sigma_x \\ \sigma_y \\ \sigma_{xy} \end{Bmatrix} = \frac{E}{1-\nu^2} \begin{bmatrix} 1 & \nu & 0 \\ \nu & 1 & 0 \\ 0 & 0 & \frac{1-\nu}{2} \end{bmatrix} \begin{Bmatrix} \epsilon_x \\ \epsilon_y \\ \gamma_{xy} \end{Bmatrix} = \mathbf{H}\epsilon \tag{2.37}$$

The moment-curvature relation can be obtained by integrating the equation above.

$$M_x = -D\left(\frac{\partial^2 w}{\partial y^2} + \nu\frac{\partial^2 w}{\partial x^2}\right) \tag{2.38}$$

$$M_y = -D\left(\frac{\partial^2 w}{\partial x^2} + \nu\frac{\partial^2 w}{\partial y^2}\right) \tag{2.39}$$

$$M_{xy} = -(1-\nu)D\frac{\partial^2 w}{\partial x \partial y} \tag{2.40}$$

From the torsional and vertical equilibrium can respectively the relation between shear force resultants and moment and the equation of motion been derived, see Figure 2.5.

$$D\nabla^4 w + \rho h\ddot{w} = f(x,y,t) \qquad \text{where} \qquad D = \frac{Eh^3}{12(1-\nu^2)} \qquad \text{and} \qquad \nabla^2 w = \frac{\partial^2 w}{\partial x^2} + \frac{\partial^2 w}{\partial y^2} \tag{2.41}$$

For simply supported rectangular plates this gives natural frequencies following [21]:

$$\omega_{ik} = \pi^2\sqrt{\frac{D}{\rho h}}\left[\left(\frac{i}{a}\right)^2 + \left(\frac{k}{b}\right)^2\right] = \pi^2\sqrt{\frac{Eh^2}{12\rho\left(1-\nu^2\right)}}\left[\left(\frac{i}{a}\right)^2 + \left(\frac{k}{b}\right)^2\right] \tag{2.42}$$

where a and b represent the plate dimensions and i and k the modes in respectively x and y direction.

Several solutions are presented in literature for certain dimensions and supports [14]. It should be noted that the classical thin plate theory overestimates the plate frequencies since the plate flexibility and inertia are underestimated because the effects of transverse shear and rotary inertia terms are neglected [37]. This error increases with an increasing thickness of the plate.

For simply supported rectangular plates the Kirchoff plate theory gives eigenmodes in the form of:

$$W(x,y) = A\sin(\alpha x)\ sin(\gamma y) \qquad \text{where} \qquad \alpha_i = \frac{i\pi}{a} \qquad \text{and} \qquad \gamma_k = \frac{k\pi}{b} \qquad i,k = 1,2,...,\infty \tag{2.43}$$

For orthogonal plates, the fundamental mode shapes resemble in each direction the corresponding mode shape calculated with the Euler-Bernoulli beam theory [16]. But besides the flexural stiffness, mass and boundary conditions, also the lateral contraction coefficient influences the natural frequency. Several mode shapes are shown in Figure 2.6

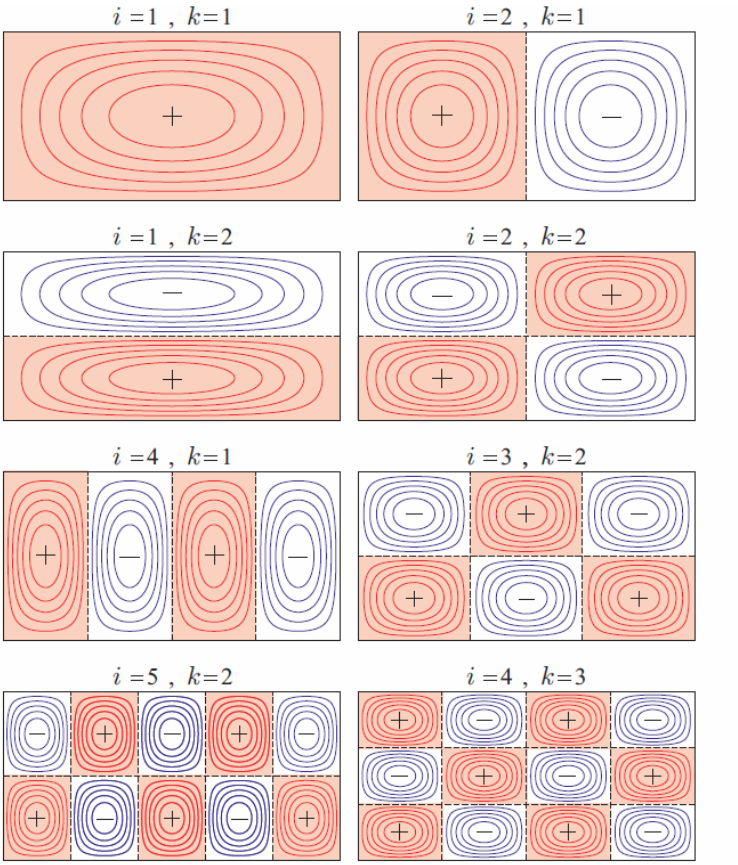

Figure 2.6: Mode shapes of a rectangular plate [36]

2.5.2. Reissner-Mindlin theory

The Reissner-Mindlin theory is the most-used theory for thick plates. As stated above in the Mindlin plate theory shear deformations are considered. A constant shear stress distribution through the thickness is assumed . It is assumed that any line originally normal to the plate median surface will remain straight during deformation, but not generally normal to the median surface [37]. For Mindlin's theory only for simply supported rectangular plates or two-sides simply supported plates exact solutions are possible. In several studies numerical solutions for the first order Mindlin plate theory are used to approximate problems [38].

The equations of motion of the Mindlin theory are the following, derived from Figure 2.7 [21]:

$$k^2 Gh\left(\nabla^2 w + \frac{\partial \phi_x}{\partial x} + \frac{\partial \phi_y}{\partial y}\right) + f(x,y,t) = \rho h \frac{\partial^2 w}{\partial t^2} \tag{2.44}$$

$$\frac{D}{2}\left[(1-\nu)\nabla^2 \phi_x + (1+\nu)\frac{\partial}{\partial x}\left(\frac{\partial \phi_x}{\partial x} + \frac{\partial \phi_y}{\partial y}\right)\right] - k^2 Gh\left(\phi_x + \frac{\partial w}{\partial x}\right) = \frac{\rho h^3}{12}\frac{\partial^2 \phi_x}{\partial t^2} \tag{2.45}$$

$$\frac{D}{2}\left[(1-\nu)\nabla^2 \phi_y + (1+\nu)\frac{\partial}{\partial y}\left(\frac{\partial \phi_x}{\partial x} + \frac{\partial \phi_y}{\partial y}\right)\right] - k^2 Gh\left(\phi_y + \frac{\partial w}{\partial y}\right) = \frac{\rho h^3}{12}\frac{\partial^2 \phi_y}{\partial t^2} \tag{2.46}$$

Solutions have to be sought for both w, ϕ_x and ϕ_y.

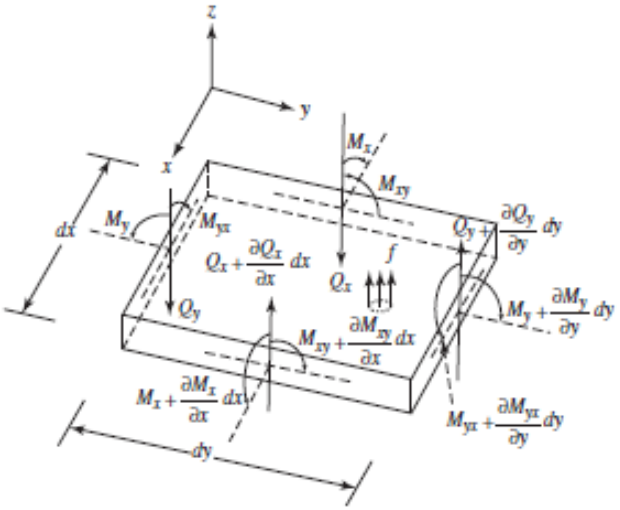

Figure 2.7: Reference system plate forces and moments for Reissner-Mindlin theory [20]

2.5.3. Plates as one-directional or SDOF systems

For orthotropic plates where stiffness of the weak direction deformation has relatively little effect on the frequency and fundamental modes, studying the fundamental shape in the strong direction only can be sufficient according to Falati [16]. Especially for one-way spanning slabs the strong direction is governing. Two-way spanning slabs exhibit more isotropic behavior, no exact solutions of their mode shapes and natural frequencies have been obtained by studying the governing direction [16].

In guidelines for the acceptable accelerations of floors due to human induced vibrations, the floor slab is studied as an equivalent single degree of freedom model, where natural frequencies are determined using formula's based on the Kirchoff plate theory [39]. The natural frequency is dependent on supports and length-width ratio by introducing a value for α.

$$f = \frac{\alpha}{L^2}\sqrt{\frac{Et^3}{12\mu(1-\nu^2)}} \tag{2.47}$$

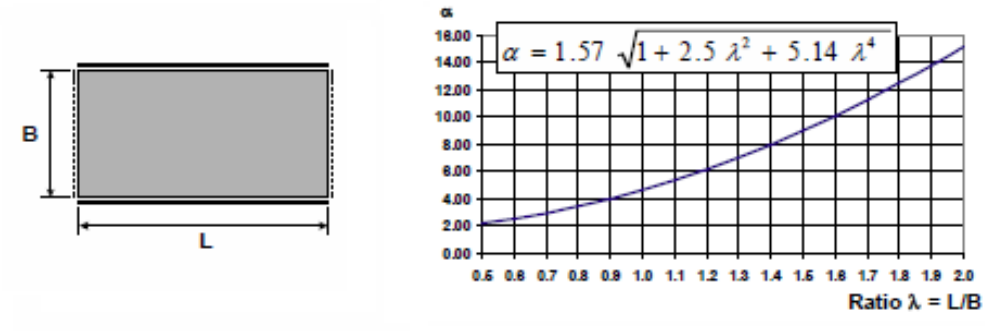

Figure 2.8: Relation between natural frequency and floor length and width dimensions [39]

When both lateral direction are assumed to contribute to the dynamic behavior, the natural frequency is calculated for both directions the resulting decisive natural frequency of the total system is calculated using Dunkerley's method in a summation of the natural frequency of the individual parts. As can be seen, the lowest of the component mode frequencies will be dominant for the frequency of the total system.

$$\frac{1}{f_0^2} = \frac{1}{f_{01}^2} + \frac{1}{f_{02}^2} + \frac{1}{f_{03}^2} \tag{2.48}$$

The equivalent mass is then determined as a percentage of the total mass of the floor and is calculated by an integral on the first mode shape of the floor over the both horizontal directions on the floor multiplied by the averaged distributed mass. For floors clamped at two sides and simply supported at the other two sides, the modal mass is set as $M_{equivalend} = 0.20 M_{tot}$ [39].

3

STATE OF THE ART - DAMPING IN HIGH-RISE BUILDINGS

In this chapter methods to prescribe damping values to buildings in the design stage are presented. The Eurocode is compared with the important damping predictors based on empirical studies. This chapter finishes with a disquisition of damping mechanisms in buildings.

3.1. Prediction of damping

As stated before, damping in a building is a complex process. Determining the damping value for a structure is particularly difficult because the factors of influence are not completely known. Building properties such as dimensions and geometry of building are showed to relate the quantity of damping [10]. Hart and Vasudevia found a correlation between the main building material and the damping value. This can be assigned to the differences in material properties, but is more likely mainly caused by differences in building lay-out for each of those materials. For other building properties such as the stability system, floor height, connection types or partition walls, the influences are still unknown.

Moreover, an documented increase of damping with the vibrational amplitude in different studies show that the traditional concept of equivalent viscous damping, where a linear relation of damping with the velocity is assumed, can only be used at a small range of low amplitudes where the damping can be considered as constant according to the predictors discussed in this chapter. At larger amplitudes the change of damping with amplitude should be taken in account [40]. Also some other effects, such as relaxation of steel with time and the presence of cracks in concrete might influence the damping of a structure.

3.1.1. Eurocode

In the Eurocode the wind load is taken into account as a static load [9]. A dynamical multiplication factor is used to calculate the additional dynamic effect for the ultimate limit state. In the Eurocode a building is anathematized per natural frequency as a SDOF system. All contributions to the total vibration amplitude are summed together [41]. The assumption is made that the structures possesses linear elastic behavior and classical normal modes. Usually only the first natural frequency in different directions are important for calculation the dynamic response.

According to EN 1991-1-4 the dynamic structural properties for each model are given by:

- natural frequency
- modal shape
- equivalent mass
- logarithmic decrement of damping

The fundamental dynamic properties are roughly evaluated using simplified semi-empirical or empirical equations, provided they are adequately proved [9]. The first natural frequency in the weak direction of a building is the most important for the response of a building and is empirically given by a function of the height of a building for buildings below 200 meter in height [41] and for multi-storey buildings with a height larger than 50m [9].

$$n_1 = \frac{46}{h} \qquad \text{in}[Hz] \tag{3.1}$$

where h is the height of the structure in m.

The fundamental flexural mode $\varphi_1(z)$ of buildings is given by an empirical equation, based on differences of the shear contribution to the mode with respect to the bending contribution. The following equation is given in the Eurocode:

$$\Phi_1(z) = \left(\frac{z}{h}\right)^{\zeta} \tag{3.2}$$

where ζ is 0.6 for slender frame structures with non load-sharing walling or cladding and 1.0 for buildings with a central core plus peripheral columns or larger columns plus shear bracing and 1.5 for slender cantilever buildings and buildings supported by central reinforced concrete cores.

The equivalent mass per unit length of the fundamental mode is given by a function dependent on the flexural mode shape and the characteristic mass per unit length:

$$m_e = \frac{\int_0^h m(x)\Phi_1^2(x)dx}{\int_0^h \Phi_1^2(x)dx} \tag{3.3}$$

The logarithmic decrement of damping is estimated by the summation of the structural damping δ_s, the aerodynamic damping δ_a and the additional damping due to tuned mass dampers and other special devices δ_d.

$$\delta = \delta_s + \delta_a + \delta_d \tag{3.4}$$

Approximated values for the structural damping, δ_s, are given for the first fundamental mode, dependent on construction material and construction type, see Figure 3.1.

Structural type	structural damping, δ_s
reinforced concrete buildings	0,10
steel buildings	0,05
mixed structures concrete + steel	0,08
reinforced concrete towers and chimneys	0,03

Figure 3.1: Logaritmic decrement according to EN-1991-1-4 [9]

These values for damping are not normative values, they are approximate terms using simplified analytical and semi-empirical equations [7, 8]. Most structural engineers use those values, because appropriate damping values are still unknown. Uncertain is also distribution and the change of resulting in smaller damping values causing structural and comfort problems.

3.1.2. Current damping predictors

Multiple studies attempted to predict the damping value of a particular tall building. Problems occurred due to paucity of measurements of actual building and with processing the obtained data [10]. The first real predictors for damping in a building that were developed are based on the the Equivalent viscous damping concept, which was mentioned by Jacobsen in 1930. The value for those equivalent viscous damping values, ζ_s, depend on some basic conditions of the structure. This type of model estimation is still adopted in the codes, as described in the previous section, where a specific damping value is given to different type of structures independent on the magnitude of vibration. There is a big variation around 40-70% in the actual measured damping values for buildings [42]. For the estimated predicted damping values similar deviations arise, both smaller and larger than predicted. The current generation of damping predictors are based on full-scale mea-

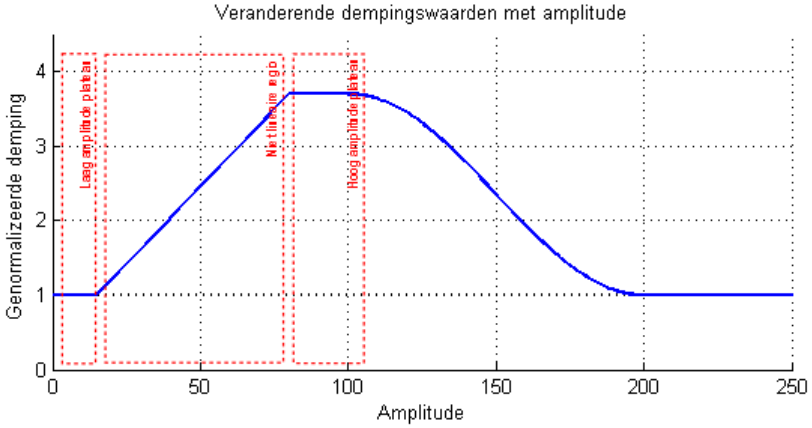

Figure 3.2: Schematical representation of the development of damping with amplitude.

surements on buildings. They are amplitude dependent, in contradiction to the older generation of damping predictors where the concept of viscous damping is mainly represented in the formulas. In early studies, in 1977, Wyatt detected a relation between the measured damping value and the amplitudes. Between end of the 80's and 2000 four formula's were developed and adopted based on databases of full scale measurements in Japan, Italy and Great-Britain by Jeary (in 1986), Davenport and Hill-Carol (in 1986), Lagamarisino (in 1993) and Tamura et al. (in 2000) as described is Appendix A. The four full-scale measurements have a large scatter of damping values within each database and each database varies strongly from the other databases. This dissimilarity is caused by the differences in soil, building methods and codes between those databases on which the formula's are based, which explains the non-similarity among them. Also, the buildings experience very different loading scenario's, where in Japan Earthquake loads are very common, in Britain damping in building is determined for wind influences. As a result, also the constants in the new empirical formula's, which are determined based on those measurements, have a large dissimilarities between the different formula's. When applying all four formula's on a building, four different outcomes for the damping emerge.

Although all formula's would yield significantly different outcomes when calculating the damping value of a building, each can be written in the same format, depending on a low value and an amplitude dependent value:

$$\zeta_s(X) = \zeta_b + \zeta_c(X) \leq \zeta_{s,max} \tag{3.5}$$

$$\zeta_c(X) = \alpha X^a \tag{3.6}$$

Where $\zeta_s(X)$ is the amplitude-dependent structural damping ratio for a given building. ζ_b is a certain con-

stant baseline damping ratio , $\zeta_c(X)$ the amplitude-dependent component and $\zeta_{s,max}$ is the upper limit for the structural damping. All constants, ζ_b, α and a, are related to different building properties. In Figure 3.3 the parameters for the four most known empirical formula's are placed side by side [42]. Those formula's

Reference	Baseline damping ratio	Amplitude coefficient	Amplitude exponent	Maximum damping ratio
Jeary (1986)	$\zeta_b = 0.01 f \approx \frac{0.46}{H}$	$\alpha = \frac{10\sqrt{\delta\gamma 2}}{H}$	$a = 1$	$\zeta_{s,\max} = 6 \times 10^{-5} H + 0.013$[b]
Davenport and Hill-Carroll (1986)	$\zeta_b = 0$	$\alpha = \frac{\alpha_1}{H^{\alpha_2}}$	$a = \alpha_2$	(None specified)[c]
Lagomarsino (1993)	$\zeta_b = \beta_1 f + \beta_2 / f$	$\alpha = \frac{\beta_3}{\Delta H}$	$a = 1$	(None specified)
Tamura et al. (2000, 2012)	$\zeta_b = \gamma_1 f + \gamma_2 \approx \frac{\gamma_4}{H} + \gamma_2$	$\alpha = \frac{\gamma_5}{H}$	$a = 1$	$\zeta_{s,\max} = \gamma_1 f + \gamma_2 + 2 \times 10^{-5} \gamma_3$[d]

Figure 3.3: Parameters of different damping predictors: (f) natural frequency, (H) building height, (D) horizontal building dimension, (α_i) parameters dependent upon number of storeys and primary construction material, (β_i) and (γ_i) parameters depending on primary construction material [42]

to predict damping are only valid at lower amplitudes. In 2013 Aquino and Tamura studied the damping at higher amplitudes. They found a decrease in damping with amplitude for high amplitudes after reaching one or multiple top damping values. According to Aquino et al. the critical amplitude level is of the order around a drift ratio of 10^{-5} to 10^{-4}. This maximum value is also called the critical tip drift ratio for the amplitude. For building excited on wind loads such amplitudes have not been measured yet, here the maximum drift ratio's measured are below 10^{-4} [42].

A second property of those predictor formula's is that they only describe damping in the first natural mode in the weakest horizontal direction. When studying the dynamic response of buildings, usually the three first natural modes corresponding with the three main directions in which the building vibrates are taken into account. However, all modes from both the two horizontal displacement directions, in the weak and strong directions, of the building and a torsional displacement direction can have influence in the response of a building. And in all three directions wind excites multiple vibration modes in different frequencies. But for wind loading only the first natural frequencies of each direction will contribute to the response. This phenomenon has two main reasons. Firstly, because of the low wind frequencies, only the first natural frequency of the building will have a significant influence on the amplitude with which the building vibrates. And secondly, the damping in each mode is correlated to the frequency in which the mode vibrates. For higher frequencies, higher damping values are found and a relatively smaller contribution to the amplitude.

Thirdly, the formula's by Jeary, Lagomarisino and Tamura are based on a small selection of the global building properties. The height of the building, the footprint and global structural building material are used when determining the natural frequency and the damping expected for a building.

From measurement at buildings in Japan and Great-Brittain is found that the damping value depends on the amplitude of vibration. This effect is taken into account in those formula's. This causes the damping ratio to be described by a constant lower boundary damping ratio and a amplitude dependent component. Together they give the expected damping ratio for a building for a certain range of predefined vibration amplitudes. In the formula's Jeary and Tamura also an upper limit maximum is present for the damping.

In 2013 a study to the damping ratio for high amplitudes is done by Tamura and Aquino et al. In earlier observations Tamura observed a stop of the increase of damping at larger amplitudes and after a certain critical amplitude level a decrease in damping is visible [42]. This decrease shows around 10^{-4} of the tip drift ratio. The function of decay and the magnitude is unknown, due to the lack of full-scale measurements close to the elastic limits of the main load bearing structure. A framework is proposed by Tamura based on slip-slip mechanisms as an extend to current damping estimators. Nevertheless, no solid conclusions are based on the development of damping for high amplitudes.

Although those formula's are the best available predictors at the moment, they exclude many building characteristics, such as the soil-structure interaction and the effect of non-structural elements. Also all predictors use different constants when determining damping and give different damping ratio's when applied to dutch buildings.

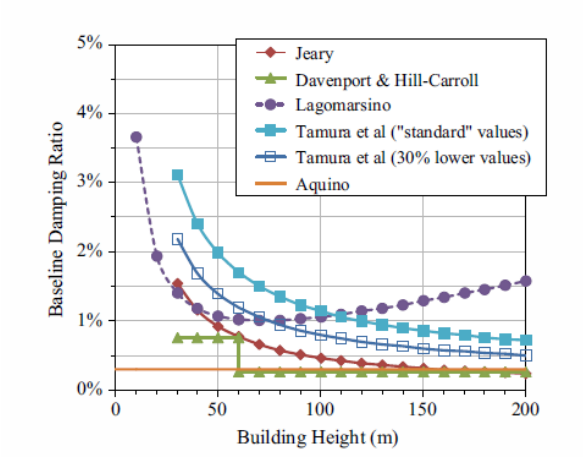

Figure 3.4: Zero amplitude value by empirical formula's based on building height [42]

3.2. Damping mechanisms in buildings and floors

A building is a complex structure and the influence of different damping mechanisms is still unknown, largely because the nonlinear nature of damping and the large variety of contributing damping processes [43]. Following Davenport and Lagomarsino [44], these processes can be categorized as: intrinsic material damping, structural damping, foundation damping, aerodynamic damping and additional damping. In Figure 3.5 the damping mechanisms are summarized. For floors both material damping and structural damping have to be considered.

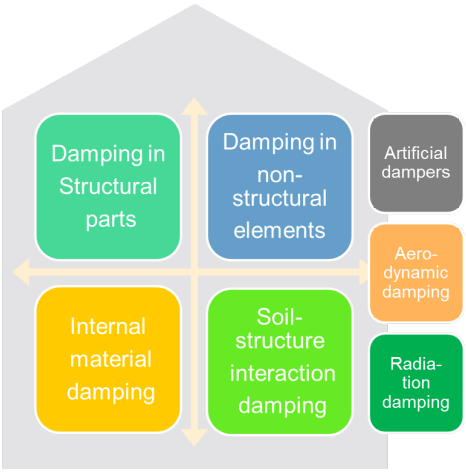

Figure 3.5: Classification of damping mechanisms in buildings [7, 8]

3.2.1. Radiation Damping

Radiation damping is the energy radiated into surrounding medium [45]. At the supports, through the foundation towards the soil, radiation damping is expected to have a significant influence. For floors radiation damping is not of importance.

3.2.2. Aerodynamic Damping

With aerodynamic damping energy radiates through waves from the mechanical system to the surroundings [14]. Energy is then removed from the system and drawn into the surrounding air flow. Aerodynamic damping

is dependent on both the velocity of the surrounding air flows as on the velocity of the system itself. At floors in buildings the relative airflow is very low and therefore aerodynamic damping is assumed to not have any significant influence.

3.2.3. Intrinsic material Damping

"Material damping is energy dissipation by deformation in a medium into irreversible inter-crystal heat flux"[45]. As stated in the section above, intrinsic material damping can both contain damping due to deformations dependent on the stress values or due to micro-slipping within the material inter-crystals. In Section 4.4 more information can be found on material damping.

3.2.4. Structural Damping in structural elements

With structural Damping is referred to friction forces due to macro-slipping at interfaces between both structural and non-structural elements.In Section 4.3 more information can be found on structural damping.

3.2.5. Damping in non-structural elements

Based on full scale measurements Devin et al. concluded that the level of measured damping under forced vibrations varies as the structure evolves to completion. The highest damping values were measured after completion of the building including non-structural elements [43]. In Figure 3.6 the values for the damping ratios for three stages of the building are shown.

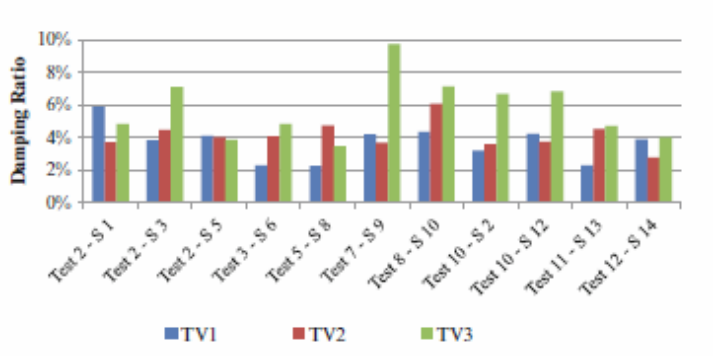

Figure 3.6: Damping ratio for different stages of construction: erection of the main load bearing structure (TV1), main facade elements connected (TV2) and the completed building (TV3) [43]

3.2.6. Active and Passive artificial Dampers

Added artificial dampers can be present in highrise buildings. The can either conduct damping with or without external energy and control [45].

4

DAMPING

In this third chapter of the literature study the damping phenomenon is described. The three main types of damping are described and damping mechanisms in joints and materials are studied.

4.1. What is damping?

The amount of movement in the dynamic response of any structure is mainly determined by the amount of energy present in the system. Damping is defined as a complex mechanism that causes dissipation of energy in the system. Mechanisms that causes dissipation of energy from the system are called damping mechanisms.

> *Damping is the energy dissipating property of materials and members undergoing time dependent deformations and or displacements.*

Gaul —1999 [45]

Where the amount of energy initially present in a system depends on the energy introduced by external loadings, the initial conditions and the initial state of the structure. Damping is solely responsible for the decrease of energy and therefore for decays in the vibration amplitudes.

> *Damping is a practical measure of the efficiency of a system in dissipating the energy that it acquires, in its attempt to return to quiescent conditions.*

Jeary —1986 [40]

The energy loss is either dissipated within the system or transmitted away by radiation [45]. When the energy is dissipated within the system, the energy from vibrations within the structure is converted into heat. Damping can be categorized as either inherent damping, which occurs naturally within the structure or its environment, or external damping through installed apparatus such as an active or passive added damper [11]. In this thesis only inherent damping is discussed. Also, only internal damping is discussed which is defined as damping inside the defined system boundaries [45].

4.2. Damping mechanisms

There are many proposed damping mechanisms in literature that function as a model for the removal of energy. Since damping is a unknown factor in the field of dynamics, any mechanism where damping forces occur in opposite direction of motion can represent damping. Within damping models, a distinction can be made between linear and non-linear damping models. In this chapter different damping models are discussed which are derived from either viscous damping, friction damping or the hysteric damping principle.

4.2.1. Viscous damping

In Figure 4.1b the vibrations of a system with viscous damping are shown and in Figure 4.1b the symbolic representation of a viscous damper. It is the most widely used damping mechanism. This type of damping is analogous to the damping produced by the motion of fluids [46]. Viscous damping is characterized as linear damping, where the damping forces are linearly proportional to the velocity and working in the opposite direction of motion. Viscous damping can be mathematically described rather straightforward, often leading to analytically solvable equations of motions and exact solutions for the dynamics. For that reason, when possible, structural applications are often approximated with viscous damping, mostly in combination with a single degree of freedom system or with several modes and viscous modal damping.

The damping force in a viscous damping mechanism is described with:

$$F_c = c\,\dot{x}(t) \tag{4.1}$$

The damping coefficient c determines the amount of damping and whether the system is critically damped. When the damping coefficient is positive and the structure is statically stable, the system is also dynamically stable because the amplitude decreases due to the positive damping and the structure returns at least asymptotically to the equilibrium position [15].

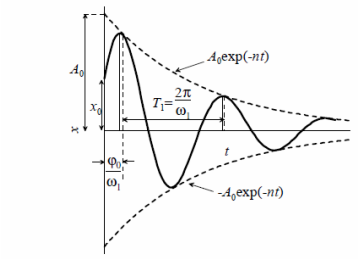

(a) Responds to viscous damping [47]

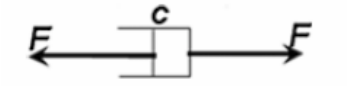

(b) Symbolic epresentation of viscous damping [11]

Figure 4.1: Viscous damping representation

The work done by the damping forces is equal to the dissipated energy and can be described in relation to the velocity for a linear viscous system:

$$W = F_d\,\dot{x} = -c\dot{x}^2 \tag{4.2}$$

When the structure vibrates, the energy dissipation per cycle is proportional to the frequency and to the square of the amplitude of the motion. For a system vibrating in a higher frequency, not only more energy is dissipated per cycle, but also more cycles occur within the same time span. Thus the total dissipated energy

within this time span increases with the frequency.

$$e_d = \int_0^T W dt \quad = -cx_0^2\omega^2 \int_0^{2\pi} \sin^2(\omega t) dt \quad = -\pi c x_0^2 \omega \tag{4.3}$$

Viscous damping is often described in terms of the damping ratio ζ, which is defined as the ratio between the damping constant c and the critical damping $2m\omega_n$. The critical damping is the lower boundary for damping when the structure not longer vibrates with an oscillating movement. Most structures, among which building structures, are strongly underdamped when damping in the system is modeled as viscous damping, which means that the damping constant is much smaller then the critical damping and the structure vibrates in an oscillating motion.

$$\zeta = \frac{c}{2m\omega_n} \tag{4.4}$$

4.2.2. Friction damping

Friction damping mechanisms are often discrete and nonlinear damping mechanisms. Friction is the tangential reaction force between two surfaces in contact or can be described as the resistance to motion during rolling of sliding of a body in tangential contact with an other body [28]. According to Coulomb the damping force is a constant force in opposite direction of the relative velocity and independent on either the magnitude of velocity or displacement, but multiple other damping mechanisms were developed where displacements or limit values influence the magnitude of the friction damping force. In Figure 4.2a and 4.2b respectively the ideal dry friction mechanism and the decay of a SDOF system to pure damping are shown.

$$F = F_v \text{sign}(v) = \begin{cases} +F_v & \text{for } x > 0 \\ -F_v & \text{for } x < 0 \end{cases} \qquad \text{where} F_v = \mu N \tag{4.5}$$

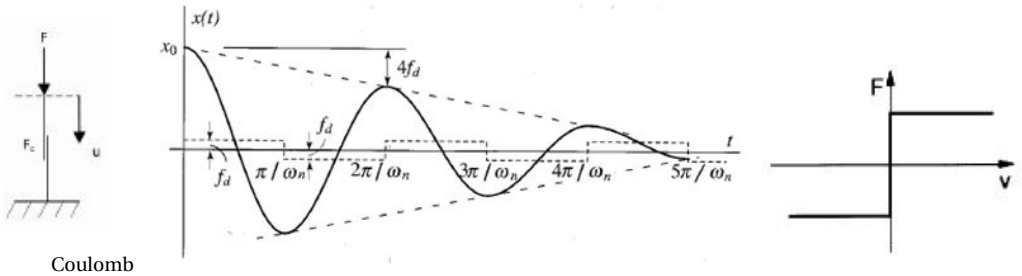

(a) Coulomb damping mechanism [48]

(b) Linear decay in response signal due to coulomb damping [12]

(c) Force-velocity diagram of friction damping [12]

Figure 4.2: Friction damping representation

4.2.3. Damping with hysteric loops or Structural Damping

Hysteric damping is defined as internal damping or energy losses per cycle proportional to the displacement [15]. In 1952 Ungar and Kerwin [49] defined damping for slightly damped systems with mass-less visco-elastic springs as the ratio of the dissipated energy per cycle and the instantaneous total energy. The maximum instantaneous energy was determined by the storing energy in the spring at maximum deflection, which gives the connection between damping, force and deflection that is the basis for hysteric damping today.

Especially damping in materials is often described with hysteresis loops. When loading and unloading of materials or structures occurs in a very short time frame a hysteresis loop can be drawn in a force-displacement diagram or in a stress-strain diagram. The area of the loop represents the amount of energy needed to deform the material and the work done by the damping force in one cycle.

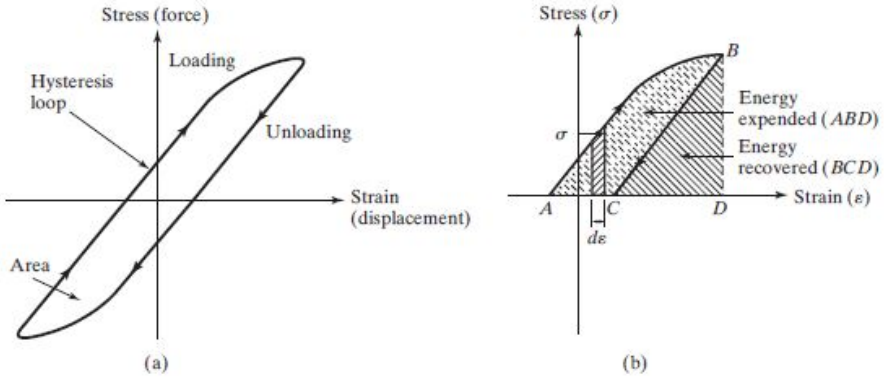

Figure 4.3: Hysteresis loop for elasto-plastic materials [20]

In Figure 4.3 the hysteresis loop for elasto-plastic materials is shown. For linear damping the hysteresis loop is an ellipse, see Figure 4.4 a. For nonlinear damping, see Figure 4.4 b, the hysteresis loop is peaked [50]. Hysteresis refers to a system that exhibits path or rate dependent memory. The friction principle is very suitable to be expressed in hysteresis, because friction is strongly path-dependent, similar for stress-dependent material damping.

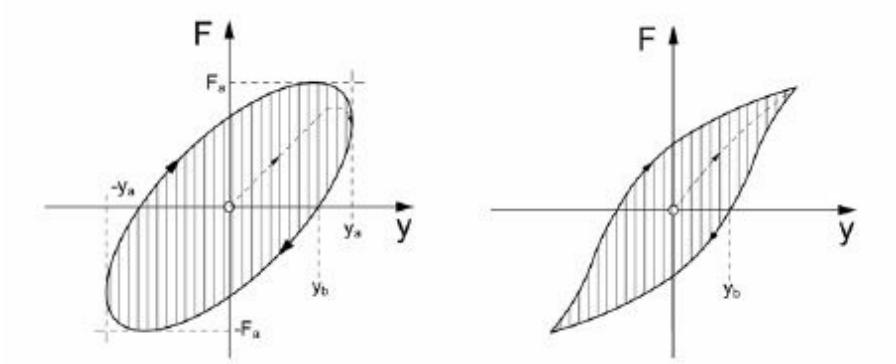

Figure 4.4: Hysteresis loop for linear damping (left) and nonlinear damping (right) [50]

4.3. Damping in joints

For structures made of steel or concrete, the material damping is rather small [11], around respectively 0.4 and 0.9 %. In reality much higher damping values are found for these structures. Therefore, there must be other sources of damping that significantly influence the dynamic behavior. The damping generated by structural joints is typically such a type of damping, which is called structural damping, or slip damping [11]. Friction damping mechanisms are found to be frequently the dominant damping mechanisms in assembled structures [51].

Slip damping arises from the boundary shear effects at joints between distinguishable parts or at mating surfaces [11]. Slip damping can have contributions from a variety of damping mechanisms; there can be viscous damping, but also Coulomb friction or a combination.

Friction in joints at element level is often referred to as slip or macro-slip, because energy dissipation is produced during slide of the surface. There are two types of slip described in literature. Firstly Macro slip, which is slip over the entire contact surface of the joint, there is relative motion over the contact area between two

surfaces. The second, Micro-slip, occurs locally, at smaller scale, within materials due to crack formation or inter-layer sliding. Within a joint micro-slipping can be present due non-uniformly distributed stresses, due to local deformations or cracks. The force-displacement diagram of macro slip and micro slip is given in Figure 4.5.

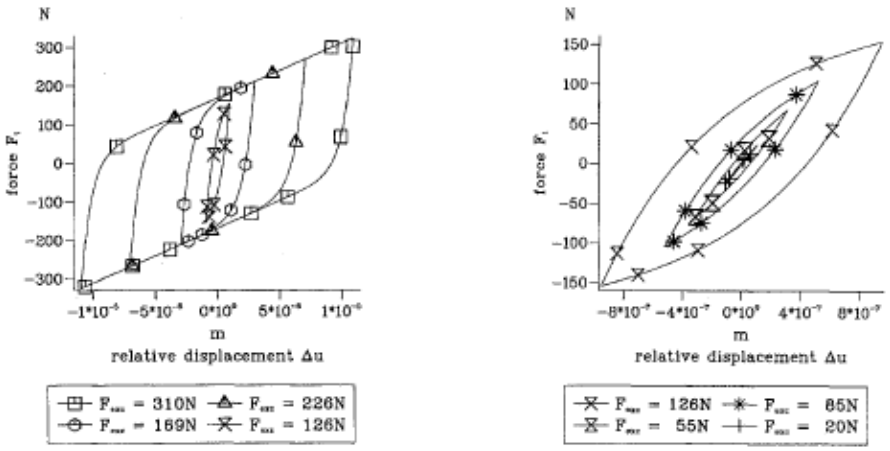

Figure 4.5: Macrolip (left) and microslip (right) represented in hysteresis graphs [52]

A large number of studies of friction exists in the fields of aerospace, mechanical or structural applications. However, for none of these application areas a generic model of friction has been agreed upon. For structures, Abolmaali performed numerous experiment to determine the total energy dissipation capacity for joints. Different hysteresis graphs are found for different joint types and failure mechanisms. No clear relation was found between individual hysteresis parameters and the measure of energy dissipation. However, based on the hysteresis shapes it may be concluded that different friction damping mechanisms were excited for the different compositions, but also during loading. The parameters that influence the damping mechanisms appear to change during the experiments.

> *The dynamic friction is a collection of many complex mechanical, chemical and dynamical phenomena enwinded in a mosaic whose features cannot be grasped through isolated simple experiments.*

Oden —1985 [53]

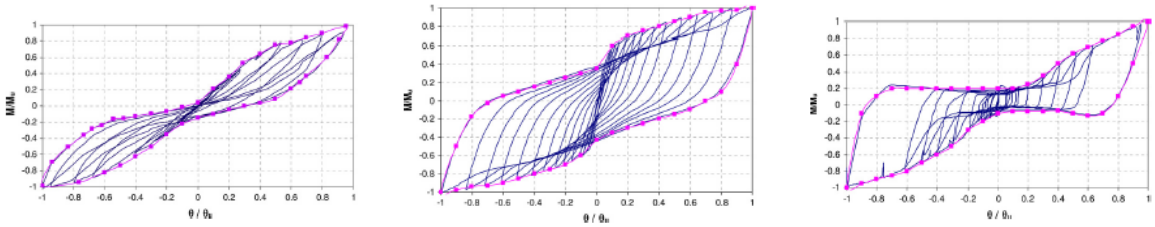

Figure 4.6: Hysteresis loops for several bolted joints loaded until failure [54]

Optimal combination of friction parameters

Damping decreases the amplitude of dynamic vibrations in a structure, so an optimal combination of parameters should give the maximum damping. However, a small deviation from this optimum may lead to a significant damping reduction. Also, the optimum condition may result in serious corrosion due to wear [11].

For example, allowing more relative motion with optimum interface pressure and geometry might increase the damping, it also coincides with reduced stiffness and increased corrosion of joint surfaces, which leads to unknown change of behavior over time.

4.3.1. Parameterizing friction

In numerous studies parameters that influence the friction force are found. However, the direct relation between the joint properties and the friction force remains uncertain. According to Astr*ö*m a relation with the normal force acting on a surface due to tensile stresses in bolts and the friction force is shown to have a significant contribution to the friction [55]. According to Olssen et al. the magnitude of the friction force depends also, besides the relative displacement and velocity of the bodies, on many different mechanisms: the contact geometry and topology of both surfaces, properties of the bulk and surface materials and the presence of lubrication [56].

The significance of the influence of each parameter varies per case due to usage tolerances or manufacturing processes [57]. Therefore, the parameters can not be modeled accurately without taking uncertainties into account. Several studies have been carried out on random variability in parameters. Those studies, however, go beyond the focus of this thesis.

In next paragraphs, several parameters present in friction models are studied.

Contact surface

No surface is perfectly flat, any surface of contacts shows irregularities concerning geometry and material properties [58]. On microscopic scale several deviations from the plane are visible, called asperities, defining the geometry of the surface. Depending on the type of material and the method of production of the surface the height of the peak, the average slope and the space between them vary [53].

The stiffness of the surface is found to be proportional to the roughness and the deformations of the asperities. Oden concludes that only for very small loads at very polished surfaces, deformation of the asperities is elastic, for other cases deformations of asperities are plastic. For concrete materials in construction, the surface is less polished and the material is less stiff, thus non-elastic deformations of asperities should be assumed.

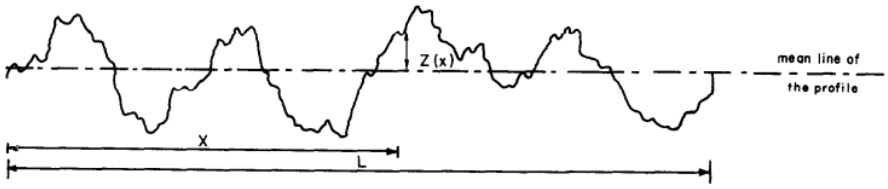

Figure 4.7: Geometry of a material surface [53]

According to Andresson dry contacts have a higher static friction than dynamic or sliding friction. During slip, the surface properties change due to local deformations and cracks, resulting in a non-constant friction force due to the surface properties.

Material properties

Between different materials differences in surface roughness, fabrication method and stiffness are of influence on the friction. Concrete is shown to have lower stiffness properties and a less smooth surface than steel. Due to the brittle behavior local non-linear deformations are caused by crack formation rather than plastic deform. Further, the fabrication is less controlled and concrete is affected strongly by creep, resulting in larger uncertainties than for steel materials. Due to both characteristics an higher energy dissipation is

expected in concrete than for steel. However, the set-up of joints in concrete materials is very different and a clear comparison can not be made.

Contact area and geometry

The area of contact and therewith the geometry of the structure elements has a large influence on the amount of friction. The effective area where damping forces due to stiction and slipping are present changes during vibrations. Furthermore, this can have an effect on the normal force. Whiteman modeled this effect with a displacement dependent friction force [59]. The damping was found to depend strongly on the amplitude of vibration.

Normal force

Higher clamping pressure causes greater penetration of asperities [57], followed by larger bruto contact area and larger friction. We can say that in principle, the friction force in a joint arises from shearing and torsional forces between the parts and is governed by the tension in the bolt and the friction coefficient [57]. Normal pressure and tangential stresses are coupled [58]. Without any clamping pressure, no load transmittance due to friction and no friction damping is activated. For high normal forces, the pressure at the joint surfaces is high, causing little slip. Low pressure causes large slip, but under low pressure the shear due to friction is small. The maximum energy dissipation is in between these limits. Beards found in experiments that by controlling inter-facial slip an optimum clamping force exists for the maximum energy dissipation [57].

The stress distribution over the interface surface is not uniformly distributed. The normal force due to clamping at the bolt decreases with distance away from the bolt hole, causing a decrease in frictional stress. According to Ibrahim, at those lower stress regions, micro-slip develops first [57]. For tangential load which is not large enough for full slip of the joint, some local slip occurs in the lower pressure stress regions.

Also, the stresses change in time, both due to relative motion between the surfaces and due to change in stresses within the material. Creep and relaxation are important in static analysis, but also influence the dynamic behavior. Relaxation is the decrease of stresses present in a material with time. With relaxation the pressure on the joint surfaces decreases, causing in general an decrease in friction. Also, a decrease of the joint stiffness has large consequences for the system, such as reduced natural frequencies. Due to the complex nature, relaxation of bolts adds additional uncertainty to the joints parameters.

4.3.2. Application of friction-based models at joints

Two broad classes of friction-based models can be distinguished: the constitutive contact models and phenomenological contact models. The first type are models based on a local approach of the problem, based on contact mechanics and relations between displacements, stresses and forces within the friction contact areas. Phenomenological contact models represent the friction force as a function of the relative displacement [57]. These models are based on experimental observations and global relations between the tangential force, the relative displacements and the normal force. The latter type, phenomenological models, is less complex and more often used in applications [58] .

Following Andersson [60] friction models can be categorized in five categories:

- Friction models for transient sliding under dry, boundary and mixed lubrication conditions.
- Friction models for micro-displacements of engineering surfaces subjected to transient sliding
- Friction models often used in the simulation and control of technical systems
- Combined friction models that represent physical behaviors fairly well but are also suitable for use in simulating systems.
- Friction models that take into account the stochastic nature of interacting surface asperities.

Within all categories constitutive and phenomenological models have been developed. For civil structure,

only the first two categories are important and phenomenological models are preferred. The best choice for a friction model depends on type of contact, running conditions and the behavior of interest and changes per situation.

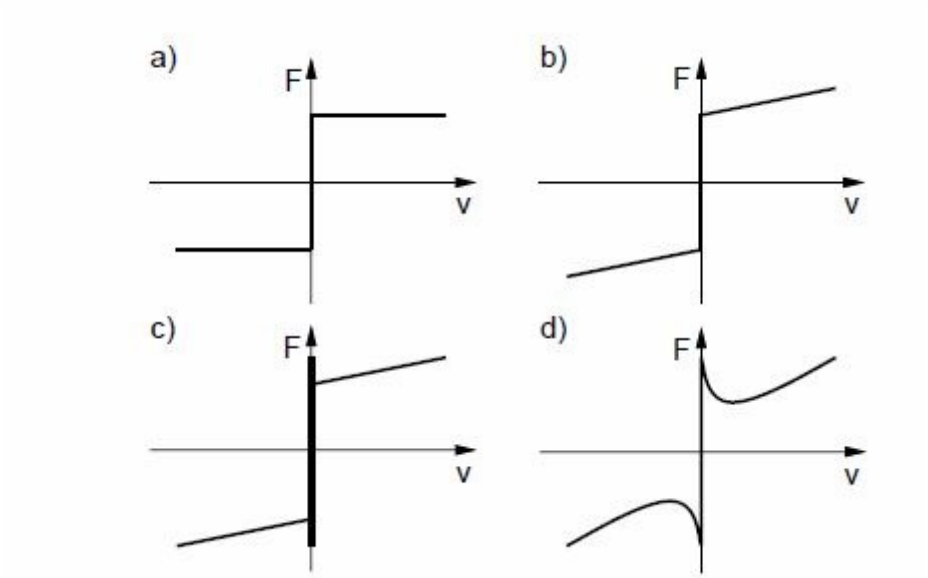

Figure 4.8: Force-Velocity diagram for a) Coulomb Friction, b) Coulomb Friction with viscous damping, c) Stiction plus Coulomb Friction with viscous damping [61]

Below, a selection of friction models used in connections in given.

The most basic friction model is the pure coulomb damping mechanism which gives a constant damping force is, of which the magnitude is related to the normal force and a friction coefficient, and the direction of the force is opposite to the motion of the body [46]. In Figure 4.2a the friction mechanism is presented.

- *Pure coulomb friction model*

  A constant friction force which depends on friction coefficient μ and normal force N. The friction force for pure Coulomb friction can be represented by the piecewise function below. This formulation does not specify the friction force for zero velocity. It may be zero or has any force from between $-F_v$ to F_v. With the stick-slip principle a zero-velocity friction value is taken into account.

$$F = F_v \text{sign}(v) = \begin{cases} +F_v & \text{for } x > 0 \\ -F_v & \text{for } x < 0 \end{cases} \qquad \text{where} F_v = \mu N \tag{4.6}$$

  The pure Coulomb friction model is often used do describe friction in mechanical contacts for both dry contacts and mixed lubrication contacts, such as with the Extended Greenwood model, where a constant normal force is present on the surfaces [62].

- *Whiteman Model*

  Whiteman studied a displacement dependent normal force and therefore friction force. He found that an optimal displacement-normal force relation exists to optimize the damping [59] .

Several effects have been described in literature for the development of the friction force with increasing velocities. In Figure 4.8 the development of the friction force with velocity is shown for four effects that are often present within more detailed friction models. Figure 4.8 a shows the pure coulomb model, which is described above with a constant friction force.

- *Viscous coulomb friction model*

  In Figure 4.8 b coulomb friction with viscous damping is shown, where the damping force increases with increasing amplitude linearly related with velocity of vibration.

$$F = F_v|v|^a sign(v) \tag{4.7}$$

  An advantage compared with pure coulomb damping is that the friction force at zero sliding is defined [60].

- *Bristle Model*

  As the surfaces move relative to each other the strain in the bond increases and the bristles act as springs giving rise to a friction force

$$F = \sum_{i=1}^{N} \sigma_0(x_i - b_i) \tag{4.8}$$

Figure 4.8 c shows the stiction effect. With stick-slip a large static friction damping value is present, causing zero displacement due to sticking. When the friction force reaches a certain level, the system reaches the slip stage with a constant or an increased damping with an increase in relative motion. Hereby, the static damping force is higher than the dynamic damping force at small relative velocities [63]. This static force depends on the tangential stiffness between the bodies in contact, corresponding with local elastic deformations at the surface.

- *Pure stiction Model*

  For the stiction model and static force is described at zero velocity.

$$f(x) = \begin{cases} F_e & \text{if } v = 0 \quad \text{and} |F_e| < F_s \\ F_s sgn(F_e) & \text{if } v = 0 \quad \text{and} |F_e| \geq F_s \end{cases} \tag{4.9}$$

- *Dahl model*

  Based on the stress-strain curve. Subjected to stress the friction force increases gradually until rupture. Friction force is a function of the displacement and the sign of the velocity. It is rate independent. [56]

$$\frac{dF}{dx} = \sigma(1 - \frac{F}{F_c} sign(v))^\alpha \frac{dF}{dt} = \frac{dF}{dx}\frac{dx}{dt} = \frac{dF}{dx} v = \sigma(1 - \frac{F}{F_c} sign(v))^\alpha v \tag{4.10}$$

In figure 4.8 d the stribeck effect is shown. A nonlinear negative dependency between the friction force and small relative velocities was found in experiments. For higher velocities a linear relation between friction value and velocity is present where friction increases with time.

- *Stribeck friction model*

$$F = (F_c + (F_s - F_c) exp^{-(|v|/v_s)^i)}) \text{sign}(v) + k_v v \tag{4.11}$$

- *Dankowicz friction model*

  A variant on the Dahl model.

$$\dot{z} = \dot{x}\left(1 - \frac{z}{\delta}\text{sign}(\dot{x})\right) \tag{4.12}$$

$$F = \frac{F_{max}}{\delta} z \tag{4.13}$$

- *Lugre Model*

  An extension of the Dahl Model with a velocity dependent friction contribution. When a tangential force is applied the bristles will deflect like springs. If the deflection is sufficiently large the bristles start to slip. The average bristle deflection for a steady state motion is determined by the velocity. It is lower at low velocities, which implies that the steady state deflection decreases with increasing velocity. This models the phenomenon that the surfaces are pushed apart by the lubricant, and models the Stribeck effect [56]. The LuGre model is inherently rate dependent. The LuGre model is described by:

$$\dot{z} = \dot{x}\left(1 - \frac{z}{\delta}\text{sign}(\dot{x})\right) \tag{4.14}$$

$$g(v) = \frac{1}{\sigma_0}(F_c + (F_s - F_c)exp^{-(|v|/v_s)^2)}) \tag{4.15}$$

$$F = \sigma_0 z + \sigma_1 \dot{z} + k_v \dot{x} \tag{4.16}$$

  Where v is the velocity between the two surfaces in contact, z the internal friction state or b̈ristle deflectionänd F the predicted friction force which has an damping value associated with micro-displacement (σ_1), a general form for the memory less velocity dependent term ($f(v)$) which can be seen as an viscous damping part $f(v) = \sigma_2 v$. The function $g(v)$ describes the Stribeck effect.
  Badila [61] studied the Lugre Model for a steel frame. The parameters with a large influence on the decay of the response were the friction force and viscous damping of the bristles.

4.4. Material Damping

In materials a distinction can be made between elastic and non-elastic materials. An elastic material is a material that does not dissipate energy during deformation. After removing the load, the material deforms back to its initial shape. The potential energy stored in the material is sequentially transformed into kinetic energy. Hooke describes the relation between strain, ϵ, and stresses, σ, with the Modulus of Elasticity, E, [15] in Hooke's law, Equation 4.17.

$$\sigma = E\epsilon \tag{4.17}$$

The stress-strain relation is linear for ideal elastic material and can be described by a constant Modulus of Elasticity. A structural element made of such a material can therefore be modeled as a linear spring. In reality, without any source of external energy, no real system maintains an undiminished amplitude of vibration. Also, in reality no material is ideal elastic. The Modulus of Elasticity in Hooke's Law changes in time, depending on the strain magnitude or loading speed. This time dependent change can represent relaxation or fatigue effects in materials is often referred to as softening and hardening properties of materials. In Figure 2.2 (Chapter 2) changes in the Modulus of Elasticity are shown, as the changing relation between loading and strain. The load speed dependency of the Modulus of Elasticity is referred to as the non-linear Modulus of Elasticity

Non-elastic deformations are deformations that are not reversible by removing the load. They can occur simultaneously with elastic deformations. Hereby, the potential energy of the material before and after loading and unloading is changed, because during the loading cycle energy is dissipated from the system. This type of energy dissipation in materials per cycle is called material damping [50]. Material damping can be defined as the conversion of vibration energy, in the form of kinetic and strain energy, of a vibrating system consisting of a volume of solid matter into heat [64]. The amount of energy dissipated is influenced by a variety of properties of the material:

1. local defects and impurities
2. the microscopic composition
3. macroscopic composition
4. geometry

Also numerous external factors influence the material damping:

1. type of stress
2. stress amplitude
3. stress variation
4. number of cycles
5. environmental influences: temperature
6. other

For construction materials different damping factors have been determined in literature [11],[14],[15],[46],[12]. These values can be used when modeling material damping as equivalent viscous damping in the system. The values for construction materials are very small. Only a few percentages of critical damping are reached in the materials with the highest damping values. However, this does not imply that that material damping can be neglected as contributors of damping in buildings. Also, the error of those proposed damping values can differ strongly per material, because extensive testing of construction elements for damping such as for mass or stiffness are not performed routinely. Also, concrete, steel and composite materials react differently to stresses and therefore they can have other damping mechanisms which are decisive. For concrete for example the cracking stage of the material has proven to have a strong influence on the amount of damping present [46].

material	material damping
Steel	0.004
reinforced concrete	0.009
pre-stressed concrete	0.009
pine wood	0.021
beech wood	0.025
natural rubber	0.03
clay	0.02 – 0.05

Figure 4.9: Values for material damping for different materials where damping is described with damping ratio $\zeta = c/2\sqrt{(km)}$ [14]

Material damping can be described with two different types of units according to Harris [64]:

1. the energy dissipated per cycle in a structural element or test specimen
2. the ratio of the dissipated energy per cycle to a reference strain energy or elastic energy

The total damping energy dissipated by the entire specimen per cycle is calculated by integration of specific damping energy throughout the material volume.

$$D_t = \int_{V_o} D\mathrm{d}V = \int_0^{\sigma_d} D\frac{\mathrm{d}V}{\mathrm{d}\sigma}\mathrm{d}\sigma \tag{4.18}$$

In an harmonic vibrating system different stress amplitudes are present in the material, depending on the location in the structure. Among others the type of loading and the shape of a structure have influence in the stress distribution. Therefore, calculating the total dissipated energy per cycle is very complicated, since maximum stress amplitude, geometry, distribution of the internal stresses, all play a role [14]. The relation between material damping and stress is often defined by the following equation in literature 4.19 [50].

$$D = J \cdot \left(\frac{\sigma}{\sigma_e}\right)^n \tag{4.19}$$

For which J and n are constants that are defined in literature for different materials. This relation between damping and stress is valuable in the lower stress region, before plastic deformation takes the uphand. Defined by Harris [64], the lower stress region comprises up to 70 percent of the fatigue strength at $2 \cdot 10^7$ cycles. In Figure 4.10 This exponential correlation for different materials is shown.

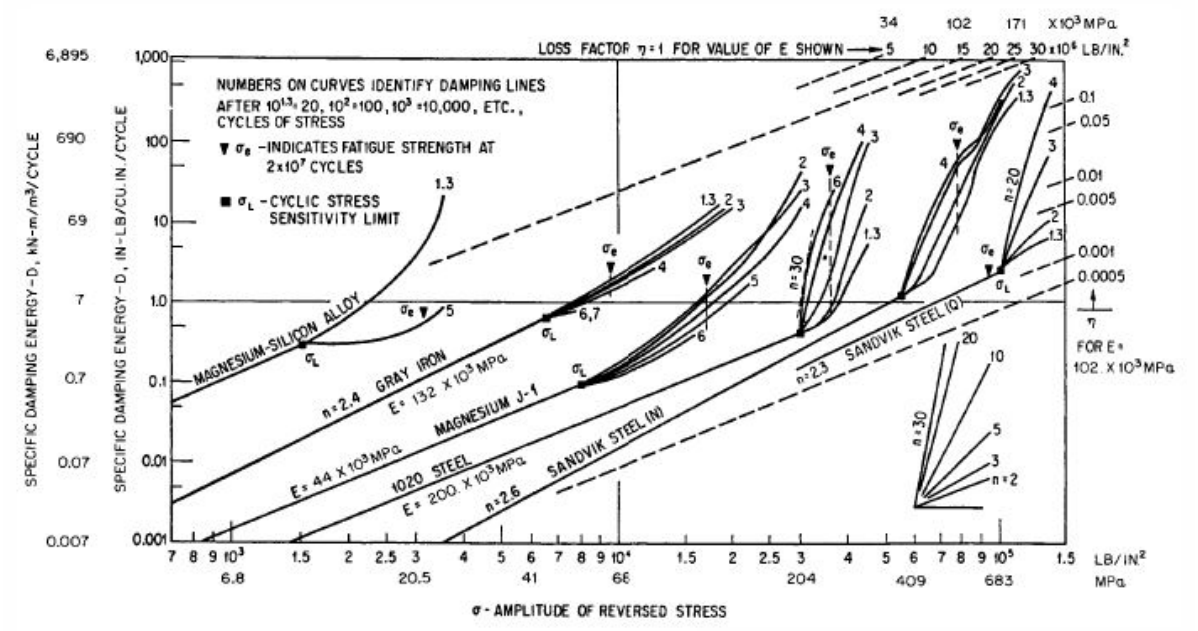

Figure 4.10: The relation between damping energy and stress [64]

4.4.0.1. Types of Material Damping

There are two main types of material damping: rate-dependent material damping and rate-independent material damping. Because of the stress related characteristics, material damping is often represented by hysteresis loops, with dynamic hysteresis and static hysteresis for respectively rate-dependent and rate-independent damping.

Rate-dependent material damping

Rate-dependent materials have stress-strain laws which can be described by a differential equation containing stress, strain, and time derivatives of stress or strain [64]. For rate-dependent materials the rate of loading influences the response. The ideal rate-dependent materials behave visco-elastic. They encounter linear damping. However, other types of materials with rate-dependent damping exist, they are described with non-linear relations to damping. Particularly at high stress levels those non-linearities have a significant influence on the damping. Also, when the dynamic behavior of a material is strongly dependent on temperature and frequency, a representation by a visco-elastic material is not accurate. In reality, no purely visco-elastic model can describe material damping in all stages of loading.

A second distinction among rate-dependent materials can be made between recoverable and non-recoverable materials or a combination of both. Anelastic mechanisms describe a recoverable, rate dependent mechanism. Pure visco-elastic materials fall within the second category and are non-recoverable.

For visco-elastic materials the rate of loading influences the response. The strain will obtain larger amplitudes, when the stress varies slowly in comparison with a fast fluctuating stress change with the same peak value. Visco-elastic materials are therefore per definition very sensible to creep contributions. High polymers, Metals at elevated temperatures, Glasses, rubbers and plastics are often modeled as visco-elastic materials when they are within the small strain region.

An anelastic material does not encounter a permanent set over time. Internal friction can cause such rate-dependent damping, where after unloading the strain will reduce to zero and negative creep occurs. Here the quantity of damping is independent on the stress amplitude, but dependent on frequency and temperature [65].

Rate-independent material damping

Rate-independent damping is damping which does not depend on the rate of loading or the frequency of loading, but does depend on the magnitude of loading and on time histories. Plastic strain falls under rate-independent damping. Rate-independent material damping is always accompanied by irreversible deformations. Hereby, a time dependency of the quantity of damping is present.

4.4.1. Mathematical representation of material damping

Linear damping models

Linear damping models are most used to represent material damping. Linear models have sufficient accuracy for the low-stress regime, according to Bert [66]. In addition, linear analyses are computationally much more economical. Linear models for material are therefore frequently used and studied. The simplest linear models for the behavior of a solid material are single-parameter models. They are not very appropriate to represent the behavior of most real materials.

- Idealized spring
  The idealized spring exhibits a restoring force proportional to the displacement, thus no damping
- Idealized dashpot
  The idealized dashpot produces a force linearly proportional to the velocity

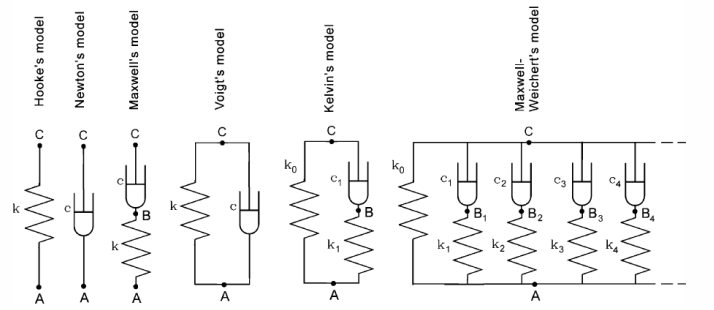

Figure 4.11: One- and two-parameter models representing material damping [15]

Two-parameter models are more representative for some cases and not very mathematical difficult to calculate. Those models are very often used in practice.

- Maxwell model
  The Maxwell model comprises a spring and dashpot in mechanical series. The model is a good approximation for a visco-elastic liquid. However, internal stresses and afterworking cannot been provided with this model.
- Kelvin-Voigt model
  The Kelvin-Voigt model comprises a spring in parallel with a dashpot. It is a good approximation for a visco-elastic solid, because internal stresses and afterworking. However, there is no elastic response during application or release of loading, the creep rate approaches zero for long durations of loading and there is no permanent set irrespective of the loading history. The energy dissipated per cycle is frequency-dependent.
- Kimball-Lovell
  In the Kimball-Lovell model the energy dissipation per cycle was independent of the frequency, but dependent on the square of displacement.

Also,three-parameter models and four-parameter models are developed. These models are complex and the use is restricted.

- Standard Linear solid or Simple Anelastic Model

- Kelvin Chain
- Generalized Maxwell model
- Biot Model

Nonlinear damping models

The nonlinear material models are weakly nonlinear. The most used model represents the dissipated energy per unit volume per cycle as being proportional to the stress of a power a such as in Equation 4.19.

4.4.2. Material properties and damping

Concrete and steel have very different structural properties. Therefore, their damping properties differ also. The fundamental physical mechanisms that determine the damping in metals are thermo-elasticity on both macro and micro scale, grain boundary viscosity, point-defect relaxations, eddy-current effects, stress-induced ordering and electronic effects [66]. For non-metallic materials the physical micro-mechanisms are less known. Composites are build up from connected parts with different properties, often polymers for which numerous research to damping is performed. Here, besides internal damping, also damping at the interfaces of the individual part is present.

4.4.2.1. Steel

Steel material has generally two stages of behavior: elastic and plastic behavior, mainly dependent on the magnitude of loading. At both stages very different damping mechanisms and quantities are valid. For the lower strain region, steel can be represented by a material with visco-elastic damping.

Kelvin-Voigt has presented a model which is based on viscous damping that can represent this type damping mechanism quite accurately. The stess-strain relation of the classical Kelvin-Voigt model for visco-elastic material is the following [29]

$$\sigma = Ee + C\dot{e} \tag{4.20}$$

The modulus of elasticity includes a linear and a linear damped part. For higher stresses reaching 0.35% of

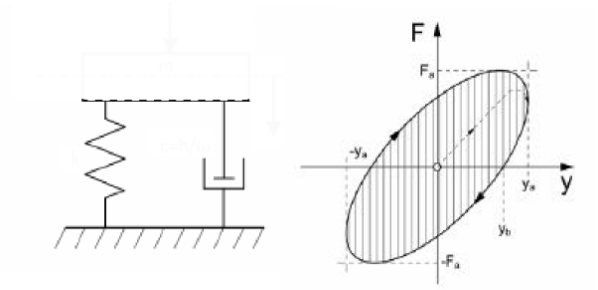

Figure 4.12: The Kelvin-Voigt model for visco-elastic material damping [48]

the maximum strain, plastic strain has to be taken into account and history dependency has to be combined with rate dependent material behavior.

4.4.2.2. Concrete

When no cracks occur in an ordinary or prestressed concrete structure, material damping can be modeled as pure viscous damping. Chowdhurry showed that damping ratios increased significantly when the specimens were damaged or cracked [46]. Machrenholtz and Bachmann proposed that damping in the cracked stage in reinforced concrete elements occurs due to two kinds of energy dissipation mechanisms [67]:

- nearly pure viscous damping in concrete elements in uncracked compression
- nearly pure friction damping due to friction between concrete and reinforcing steel in the cracked tension zone.

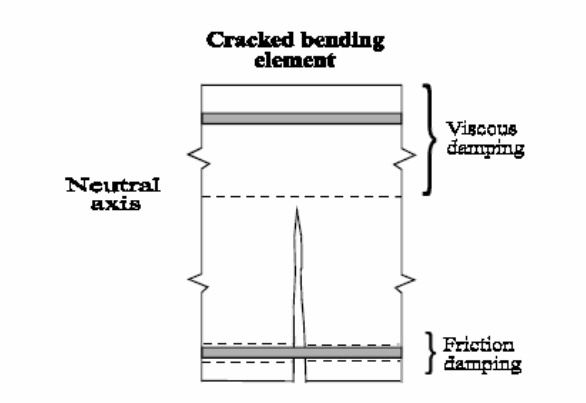

Figure 4.13: Damping mechanisms in a concrete element [46]

Equivalent damping of a cracked beam results from the simple sum, in terms of energy, of the both damping mechanisms. This equivalent damping ratio increases during the crack formation stage due to the development of new cracks, but with further increase of stresses the damping ratio decreases rapidly. In Figure 4.14a the change in damping during different stages of cracking of the material is represented. In the crack formation stage a rapid increase in damping is visible as soon as crack formation starte, and damping decreases again with further stress increase.

In a concrete elements viscous damping is present in the uncracked part of the element. In the cracked part friction damping is present corresponding with highly localized energy dissipation [68]. A combined model of those mechanisms should be looked at for further research, but determination of damping coefficients will be a difficult task. For the cracked stage Frachetti et al. proposed a combined model with non-linear damping and viscous damping [67]. However, the decay of amplitudes at high stresses does not match experimental values.

Concrete elements include always steel reinforcement in current structural applications. Damping in concrete is meant with damping before yielding of the reinforcement. Damping in reinforcement is mainly related to the stress intensity, for in bending excited elements such as floors due displacements due to moments, and to cracks and crack occurring mechanisms.

Material	ξ
Reinforced concrete	
- small stress intensity (uncracked)	0.007 - 0.010
- medium stress intensity (fully cracked)	0.010 - 0.040
- high stress intensity (fully cracked but no yielding of reinforcement)	0.005 - 0.008
Prestressed concrete (uncracked)	0.004 - 0.007
Partially prestressed concrete (slightly cracked)	0.008 - 0.012
Composite	0.002 - 0.003
Steel	0.001 - 0.002

(a) Material damping according to Chowdhurry in damping ratio [46]

material	material damping
Steel	0.004
reinforced concrete	0.009
pre-stressed concrete	0.009
pine wood	0.021
beech wood	0.025
natural rubber	0.03
clay	0.02 – 0.05

(b) Material damping according to Spijkers in damping ratio [14]

Material	Damping of the critical (%)
Reinforced concrete	0.5 (uncracked)–3 (cracked)
Steel	0.05–0.4
Cast iron	0.15–1.5
Pure aluminum	0.001–0.1
Dural aluminum alloy	0.02–0.05
Manganese copper alloy	2.5–5
Lead	0.4–0.7
Natural rubber	5–15
Hard rubber	50
Glass	0.03–0.1
Wood	0.25–0.5

(c) Material damping according to Jia [11] in percentage of damping ratio

Figure 4.14: Damping ratio's for concrete according to literature

According to Chowdhurry, multiple properties of a concrete beam influence the measured damping. The modulus of elasticity, compressive strength and steel ratio have a direct influence. Also other properties, such as the moisture content or time can change the damping. Due to molecular properties of concrete, concrete has a sensitivity to moisture content, causing dry concrete to have lower damping ratios [46]. The damping ratio increases with aging, due to a combination of changes to the concrete properties. Also, the

amplitude of vibration or the dynamic strain has a large effect on the damping. A linear variation between logarithmic decrement and amplitude of vibration was found [46]. According to Falati a small increase in natural frequency is observed in measurements due to prestressing of concrete beams [16]. Due to the presence of compresses stresses, a larger part or the entire cross-section remains uncracked which increases the stiffness. This also caused changes in crack formation and crack opening, causing higher or lower damping values.

4.4.2.3. Composites

Different energy dissipation mechanisms are involved with the damping in composite materials. Each mechanism is dependent on parameters like frequency, amplitude and environmental conditions. Most important mechanisms occurring in composite materials are [65]:

- Visco-elastic behavior of fiber materials
- Thermo-elastic damping due to cyclic heat flow from stress regions
- Coulomb frictions in unbounded regions and between interfaces
- Energy dissipation in cracks and delaminations

Damping thus depends on the constituent layer properties as well as layer orientations and interlaminar effects. Interleaving visco-elastic layers then increases the damping of structures, because additional stresses and friction forces will occur between the layers [69].

Viscous damping is the dominant mechanism, for undamaged composites vibrating at small amplitudes. For larger vibrations, the interlaminar damping has a larger contribution and these effects should be taken into account. Different analytical models are developed for the overall material damping in composite materials and layered structures based on the strain energy present in different parts of the material.

The damping capacity is determined as the ratio between the change in strain energy and the maximum strain energy:

$$\varphi = \frac{\Delta U}{U} \tag{4.21}$$

Where the strain energy is written as a summation of individual strain components:

$$U = \frac{1}{2}\int\int\int \sigma^T \epsilon dV \tag{4.22}$$

$$= U_{11} + U_{22} + U33 + U_{12} + U_{13} + U_{23} \tag{4.23}$$

$$U_{ij} = \frac{1}{2}\int\int\int \sigma_{ij}\epsilon_{ij} dV \tag{4.24}$$

And the dissipated energy is written with a specific loss factor η_{ij}

$$\Delta U = \Delta U_{11} + \Delta U_{22} + \Delta U33 + \Delta U_{12} + \Delta U_{13} + \Delta U_{23} \tag{4.25}$$

$$\Delta U_{ij} = 2\pi\eta_{ij}\int\int\int \frac{1}{2}\sigma_{ij}\epsilon_{ij} dV \tag{4.26}$$

With the Strain Energy Method, the amount of dissipated energy as equivalent viscous damping is expressed in terms of strain, stress and loss factors [70].

$$\xi_{mat} = \frac{1}{2}\frac{\eta_{11}U_{11} + \eta_{22}U_{22} + \eta_{33}U_{33} + \eta_{12}U_{12} + \eta_{13}U_{13} + \eta_{23}U_{23}}{U_{11} + U_{22} + U_{33} + U_{12} + U_{13} + U_{23}} \tag{4.27}$$

II

Database Analysis

5

DATABASE ANALYSIS

In this chapter the findings from the database analysis are summarized. For fifteen Dutch Buildings, the damping ratio during wind loading is determined from full-scale measurements. Their structural design and floor layout are analyzed.

5.1. Full-scale measurements

TNO has applied full-scale measurements between 1970 and 2014 on fifteen buildings in the Netherlands ([71], [72] , [73], [74], [75]). Those buildings were built between 1968 and 2013 with heights ranging from 30 to 120 meter. The overall structure of those buildings were very different. Also large cantilevers, large open spaces and other discontinuities in structures design were present. This made classification and comparison of the buildings with respect to the measured damping values very difficult. Besides the variety in building characteristics, also the wind load on the buildings encountered a strong variation in mean wind load, turbulence intensity and main wind direction. Most measurements have been taken at stormy conditions with winds around 6-8 Bf, but in small time frames of around one to six hours.

During those measurements the eigenfrequencies and the modal damping ratios were determined from the measurements. For most measurements a low-pass filter was used on the measured accelerations, transformed into the frequency domain, and the half-power bandwidth method [10, 11] was used to determine the damping. Hereby, only the first natural frequency was considered providing damping ratio's for the three main directions of a building: horizontal in weak direction, horizontal in strong direction and torsion around the vertical axis. The damping ratio ζ was determined as the ratio between the measured damping c_1 and the critical damping c_{cr}.

	Height [m]	Footprint [m^2]	Material	Lay-out stability
Nissan gebouw	54	1200	steel	rigid frames
HGB gebouw	26	1320	concrete	shear walls
CIG gebouw	22	260	steel	braced frames
Hago gebouw	30	484	concrete	walls and rigid frames
La Fenetre	60	1080	steel	tube and braced frames with outriggers
Winston Ch. toren	80	1166	concrete	tube in tube
Montevideo	147		concrete	tube and bundled tubes
Hoftoren	142		concrete	core
Kennedytoren	82,8	778	steel	bundled tubes
Erasmus MC	104	2607	concrete	tube in tube
EWI TU Delft	90	1458	steel + concrete	shear walls
Bouwes Palace	61	513	concrete	core
Nederlandse Bank	58	785	concrete	core
Oval building	94	130	concrete	core
Graventower	30	484	concrete	core

Table 5.1: Overview buildings measured by TNO between 1970 and 2005

In Table 5.1 the overal properties of the buildings are listed together with the measured eigenfrequencies and damping values in Table 5.2. The given masses were determined by van den Berg [2] and van Kooten [73]. From literature some limit values for the damping factor for buildings are given as 0.5% for the lower limit damping ratio for steel constructions and 1.0% for the bottom limit damping ratio for steel constructions [71]. Compared with the values from measurements, these bottom values were by far not reached. Compared with the damping values following the Eurocode, 0.01 (1%) for steel constructions and 0.02 (2%) for concrete constructions, both much higher damping values and lower damping values were found in practice. Also, multiple steel structures appeared to have higher damping values than some of the concrete structures, contradicting the classification in the Eurocode.

Name	Slenderness		Mass [10^3 kg/ m]	Natural frequency [Hz]			Damping [%]		
	x	y		x	y	ϕ	x	y	ϕ
Nissan gebouw	3.6		349	0.60			3.10		
HGB gebouw	2.2			1.30			2.60		
CIG gebouw	1.7			2.10			2.80		
Hago gebouw	1.4		114	0.60			3.10		
La Fenetre	5.8	1.2	290	1.13	1.60	1.60	3.60	1.80	2.20
Winston Ch. toren	3.2	1.6	250	0.55	0.79	0.78	1.70	1.40	1.40
Montevideo	5.4	5.4	413	0.50	0.42	1.06	1.10	1.00	1.50
Hoftoren	4.7	2.8		0.40	0.60	1.10	1.90	1.30	0.80
Kennedytoren	5.8	2.3	176	0.72	0.45	0.79	2.00	1.80	3.10
Erasmus MC	3.2	1.4	798	0.48	0.50	1.54	2.10	3.60	
EWI TU Delft	5.1	1.1	267	0.44	0.68	3.10	1.50	2.20	
Bouwes Palace			203	0.96	0.88	1.28	1.80	1.60	
Nederlandse Bank	3.5		190	0.63	1.07	1.25	1.60	2.70	
Oval Building				0.41	0.58	0.82			
Graventower	4.5		114	1.6	1.6	1.1	3.6	2.0	2.2

Table 5.2: Measured first natural frequencies and damping values. x and y are the main horizontal directions and ϕ corresponds with the torsional mode.

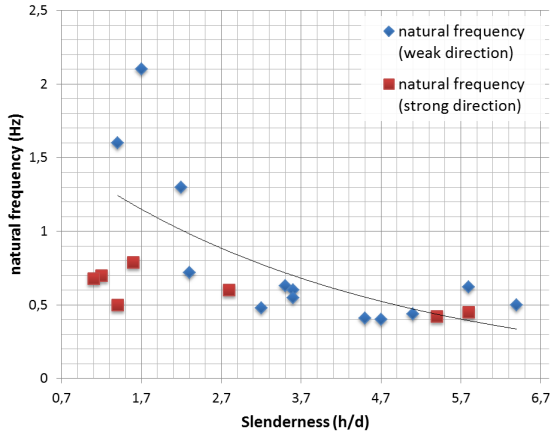

(a) Natural frequency of Dutch buildings versus the slenderness

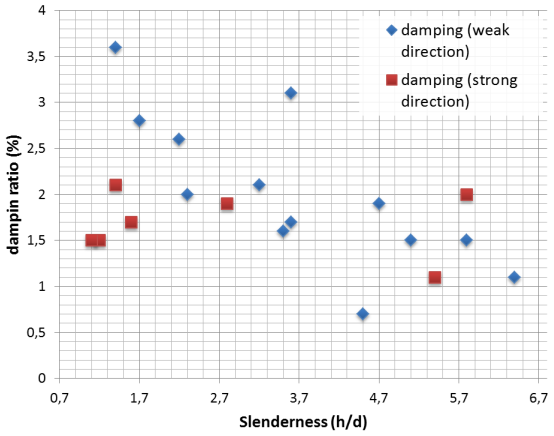

(b) Damping ratio of Dutch buildings versus the slenderness

Figure 5.1: Relation slenderness and damping ratio for Dutch Buildings

From the 15 buildings measured, only five buildings had a slenderness above 4.5 in one or multiple directions. In Figure 5.1a it can be seen that buildings with high slenderness, above 4.5, tends to have low natural frequencies, around 0.5 Hz. But the scatter in damping ratios for those slender buildings is still large, as can be seen in Figure 5.1b. This low correlation between the natural frequency and the damping ratio can be seen clearly in Figure 5.2b. However, all damping predictors have formulated a relation between those two factors.

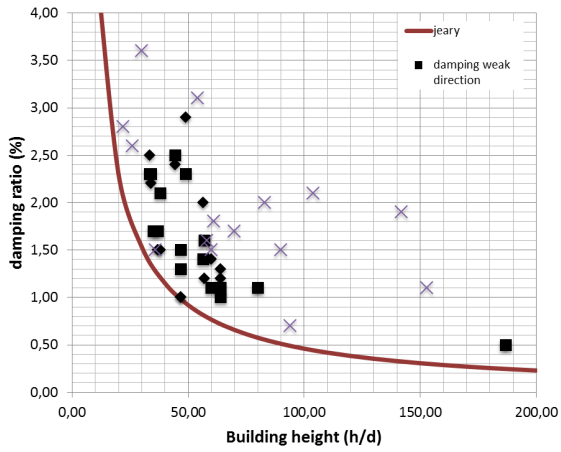

(a) Damping ratio of Dutch and Great-Britain buildings compared with the lower bound plateau by Jeary

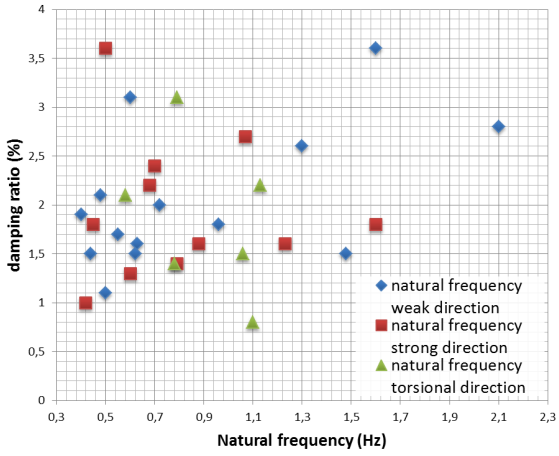

(b) Relation damping ratio and natural frequency

Figure 5.2: Relation damping ratio and building height for Great-Britain buildings and the relation between natural frequency and damping ratio

This can be explained by the many varied mechanisms that influence the damping ratio. Also, the wind conditions during the measurements were not identical. This influences the damping ratio, which changes with amplitude of vibration, but does not affect the measured natural frequency. Comparing the measured damping values with the lower boundary for the damping ratio as stated by Jeary as a function of building heigth, show that all measured damping ratios in Dutch buildings as well as buildings in Great Brittain are above this boundary, Figure 5.2a

5.2. Building lay-out

5.2.1. Structural lay-out

According to Hoenderkamp the main building types with respect to the stabilizing members can be distinguished as rigid frames, shear walls, tube structures, tube-in-tube structures, braced frames or mega-braced frames [1]. For structures with stability elements in the center of the building, all horizontal loads are transported from the facades through the floors to one or multiple cores in the center of the building. For the braced tube type, the horizontal loads are taken up by diagonal members in the facade directly. The tube-tube or wall-frames combination is a combination of both, where the horizontal loads are partly taken up by the core and partly by the outer diagonals. Shear walls are not often present in tall slender buildings, because for this type massive walls are applied, which take up the horizontal forces in their longitudinal direction. In Figure 5.3 the different types for the stability are shown.

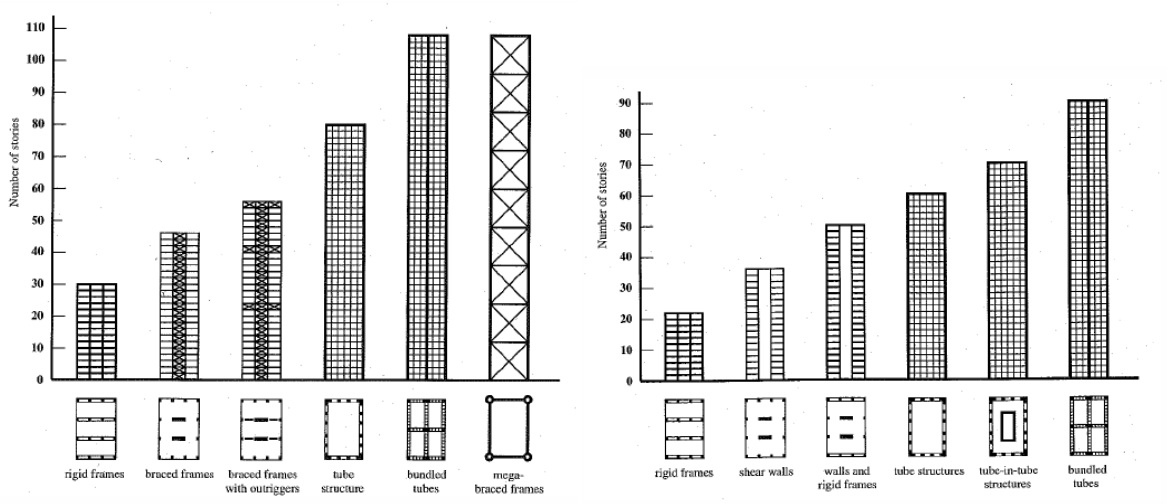

(a) Types of lateral stability systems for steel structures

(b) Types of lateral stability systems for concrete structures

Figure 5.3: Types of lateral stability systems present in the Netherlands [1]

According to Van der Berg [2] two groups can be distinghuised for the overal deformation due to the horizontal stabilizing structure of buildings: deformation due to cantilever bending and deformation due to frame action. In the first group deformations originate from axial deformations within construction elements. Most structural stabilizing system fall within this group: shear walls, core structures, braced frames and tybe structures. For the second group shear deformations and flexure bending of frame members define the overall deformation, mainly present in rigid frames. Most slender structure are covered by the first group and experience deformations due to cantilever bending.

5.2.2. Floor material and lay-out

The Research Rationalisatie Bouw, the Research Foundation of Building in the Netherlands listed the available floor types in the Netherlands in 2007 [76]. Below, the floor types are shortly described.

Hollow core floor: "Kanaalplaatvloer" The hollow core floor system was developed as an prefabricated alternative for the solid concrete floor, where the hollow cores give a reduction of weight. A plate is typically 1,2 m in width and contains pretensioned steel bars in the longitudal direction. Several variations of hollow core floors exist such as the wing floor, where the hollow core slab is mounted on a wide slab floor providing 600 mm wide wings, that make these floor very suitable for concealing cables and pipes [77].

Wide slab flooring: "Breedplaatvloer" Breedplaatvloeren are partly precast concrete floor slabs. It consists out of thin prefabricated concrete floor slabs with pretensioning or lattice girders providing strength

for handling the plates. After mounting the plates and providing additional reinforcement a concrete top layer is poured on the thin plates. Variations on the standard wide slab floors make weight reduction, such as with a Polyplaatvloer, longer spans and two-directional spanning possible. The Bubbledeckvloer uses two-directional reinforcement and weight reductions due to plastic bolls, giving self-supporting floors with spans up to 15 meter. Airdeck is a similar variation of the wide slab floor.

Rib floors: "Ribbenvloer" A rib floor is a self-supporting systemfloor of prefabricated elements, which are given ribs in the longitudal direaction or both directions, the Frame Floor, for additional strength.

Solid concrete slabs: "Massive plaatvloer" Solid concrete slabs are pretensioned self-supporting floors. Solid slabs can both be used as prefabricated plates or as casted in situ. They have a higher weight than the conventional hollow core slabs, providing good acoustic isolation.

Steel-concrete floors: "Staal-betonvloeren" These floors consist out of steel plates, usually of a ribbed or tapered form, on which concrete is casted in situ. Additional reinforcement is placed upon the steel plates and a mould are place on the ends of the plates. The OP-deck floor uses ribbed steel plates, covered with isolation at the bottom side, and topped with reinforcement following the rib direction. Resulting in one-directional spanning of the floor slabs. The Infra+ floor uses a concrete slab in which several steel profiles are casted. With this floor no concrete top layer is casted and the hollow space which is used for pipes and cables is closed with a simple deck plate [77], a similar floor is the Slimline floor [78].

Steel floors: "Stalen vloersystemen" For other steel floor systems, steel itself together with timber or other materials replace the function of concrete in the floors. These floors are one-directional and not self-supporting. They are based on a structure of steel beams.

Timber floors Solid timber floors are not self-supporting floors. They can be used for structures with relative low loading. Timber system floors, such as the Flex Floor [77], are low-weight floors consisting of timber beams and plates filled up with isolation material. Vibration properties of these floors are high.

(a) Hollow Core slab

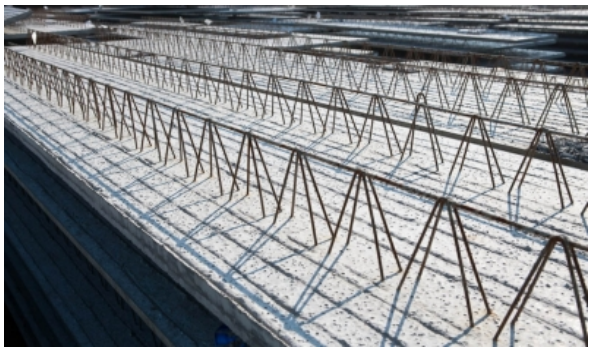

(b) Wide Slab Floor

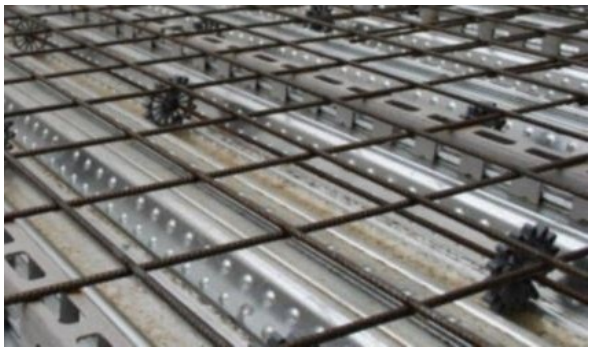

(c) Steel-concrete Floor

(d) Rib Floor

Figure 5.4: Types of floor systems in the Netherlands

According to Hoenders the following four floor types were present in Dutch Buildings with a steel structure above 70m in 2007: Hollow core slab, Steel-concrete floor, Wide slab floor, Casted concrete and Infra+ plates [1]. In Table 5.3 the floors present in the measured buildings are shown.

Building name	Floor type	QTY	Connection	Floor material	Spanning direction
Nissan gebouw	Hollow core slabs	11	simpl. sup.	concrete	single
HGB gebouw	TT-plates	10		concrete	single
CIG gebouw	Hollow core slabs	6		concrete	single
Hago gebouw	Prefabricated concrete	10		concrete	single
La Fenetre	Infra+ slabs	17		steel + concrete	single
Winston Ch. toren	Concrete casted in situ		stiff	concrete	single
Montevideo	Prefabricated concrete	43		concrete	single
Hoftoren	Concrete casted in situ			concrete	single
Kennedytoren	Steel-concrete floor	22	weak	steel + concrete	single
Erasmus MC	Prefabricated concrete			concrete	single
EWI TU Delft	Prefabricated concrete			concrete	single
Bouwes Palace	Unknown			concrete	single
Nederlandse Bank	TT elementen			concrete	single
Oval building	Bubbledeck floors			concrete	multiple

Table 5.3: Floor characteristics of measured buildings

5.2.3. Connections Floor and MLBS

Except for self-supporting floors, floors are placed on floor beams which are connected to the columns and which carry the load to the MLBS. Side beams are present to generate additional support at the side of the floor plate, providing stiffness to the structure. Most floors above have a single spanning direction and contain those floor beams, externally or integrated in the floor system. The floor beams are in general very stiff connected to the MLBS with continuous reinforcement or with a stiff bolted connection. For internal floor beams the connection between plate and beams is very stiff as well. But in general, the connection between the floor beams and the floor plates is less stiff. Concrete plates are often simply supported by the floor beams. An additional top layer of concrete provides some rotational stiffness resulting in a connection that is neither a hinge nor a fully clamped joint.

III

Modeling and Results

6

METHODOLOGY

In this chapter the method for the analytical model and experiment are described. In the first part the solution method for the analytical model is discussed. In the second part details regarding the experimental set-up are given.

An analytical model is designed representing a typical floor with a single spanning direction present in the standard structural type of a highrise building in the Netherlands. Therefore, findings from the Database analysis form the effective basis of the model. Simple existing damping mechanisms from literature are implemented to simulate the damping. With lab experiments the model is validated and damping parameters of the model are determined. Both the model and the experiment study the behavior of a floor represented by an one-dimensional floor beam, where only the first natural mode of the building in one single direction is considered.

6.1. Analytical model

Based on the outcomes of the Literature Study and the Database analysis a choice for a structural system and a floor type is made which is representative for most of the analyzed buildings. Next, a model is designed which represents the floor and its connections being a schematization of the real building structure. This model as shown in Figure 6.1 consists of an Euler-Bernoulli beam element including material damping following Kelvin-Voight's model and at both boundaries a rational spring, viscous damper and coulomb friction damper. A extended description of this model and its elements can be found in Chapter 8.

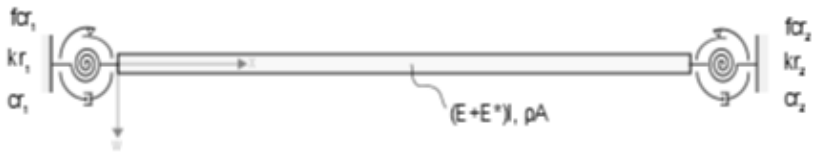

Figure 6.1: Used 1D continuous model

6.1.1. Calculation methods

For finding the dynamic response due to loading a combination of analytical hand-calculations and a numerical calculations was used. Hereby, two calculation methods were followed in an attempt to find responses for different combinations of model parameters. The second method, the method regarding Galerkin, was shown to have accurate results and was used for the comparison with experimental outcomes.

- *Solving in Frequency Domain with Fourier Transform.* Applying Fourier Transform on the equation of motion and boundary conditions provided a transfer function for the response. Initial conditions were introduced following the relation between Laplace and Fourier for first and second time derivatives present in the equation of motion. The input loading transformed to the frequency domain, together with the transfer function provided the actual response in time domain. Inverse FFT provided the response in time. However, several difficulties arose. In general, nonlinear forces such as friction damping could not be taken into account using the Fourier transform. Studying the model in several intervals with continuous friction forces was possible, but at the transitional points between the intervals the solution was inaccurate while those contain valuable information for the response. Also, boundary conditions which were time dependent, such as the column rotations provided large difficulties. In Figure 6.2b this calculation method is described. In Appendix F a further study in the Frequency domain is given.
- *Extended modal analysis with Galerkin Approximation Method.* With the second method first, the natural frequencies and orthogonal mode shapes were determined without taking into account any effects due to damping. Next, the damping components were taken into account and their contribution to the responds was modeled as coupled equations. Fixed rotations were the driving forces of the system. The response function was determined using numerical integration in Matlab following the integration scheme of Runge-Kutta. In Figure 6.2a the followed solution method is shown. In Chapter 8 this method is extensively described.

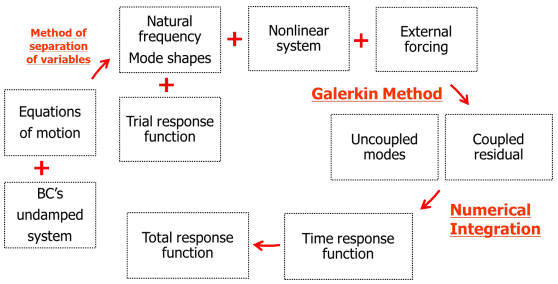

(a) Method Extended modal analysis with Galerkin Approximation

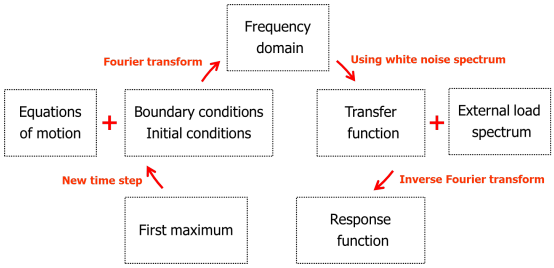

(b) Method solving in Frequency Domain with Fourrier Transform

Figure 6.2: Calculation Methods

6.2. Experiment

For the validation of the Analytical model an experiment is performed. It is important to note that the experimental design aims to represent the properties of the analytical model; and thus does not represent an actual building structure. Below the experimental set-up and information the measurements and tests is provided.

6.2.1. Experimental set-up

The general set-up is shown in Figure 6.3. The set-up encloses two steel columns, a concrete bar and several steel profiles for the connections.

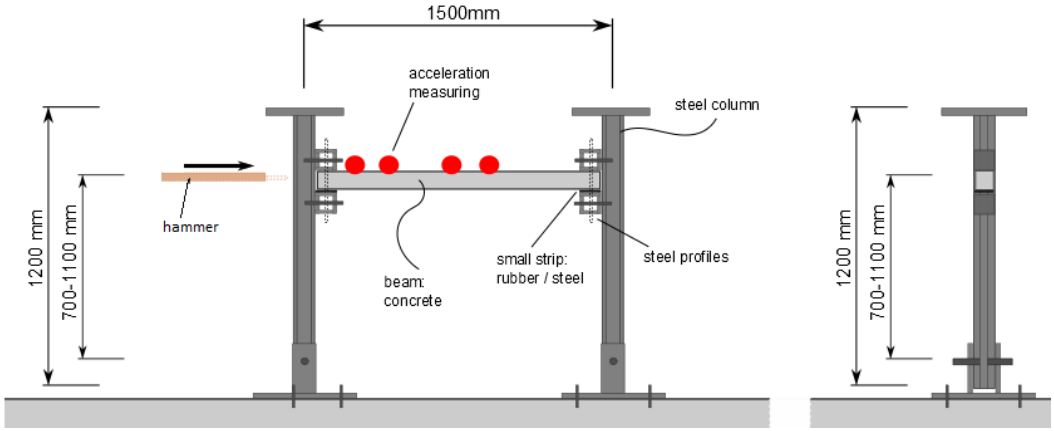

Figure 6.3: The experimental set-up. Left, front view. Right, side view.

The steel columns are hinged connected to the floor, which represents an infinite stiff medium. The concrete bar is clamped to the column with use of two angle profiles. Those angular profiles are stiffly bolted to the columns. A vertical pretensioned pin at both sides of the concrete beam, clamps the beam between the two steel profiles. Some adjustments on the properties of the connection were made by adding a cork layer between the concrete beam and steel profiles. Also, adjustments to the pretension forces in the connection were made, changing the rotational stiffness of the connection. The first test set-up, as referred to in this thesis did not include additional highly damped material or loosening of the bolts.

	Device	**Amount**	**Practice**
1	Hammer	1	Free excitation structure
2	Hydraulic excitation device	1	Forced excitation structure
3	Acceleration measurement devices	3	Measuring accelerations in beam and colums
4	Load cell	1	Measuring static deflections

Table 6.1: Used devices for experiment

	Materials	**Amount**	**Properties**		
1	Concrete beam	1	100*100*1150 mm	medium stiff	30 kg
2	Steel columns	2	150*150*1200 mm	very stiff	
3	Steel profiles at connections	4	100*100*8 mm	S355	
4	Bottom end plate columns	2	1000*1000*20 mm	very stiff	

Table 6.2: Materials used for performing experiment

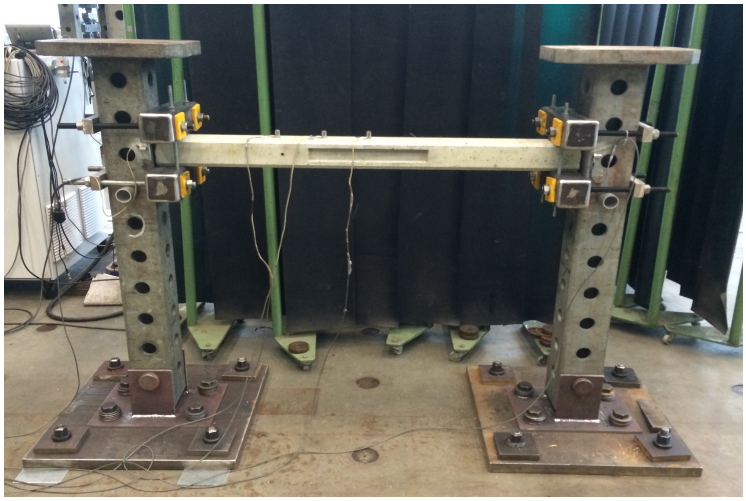

(a) Experimental set-up front view

(b) Experimental set-up bird view

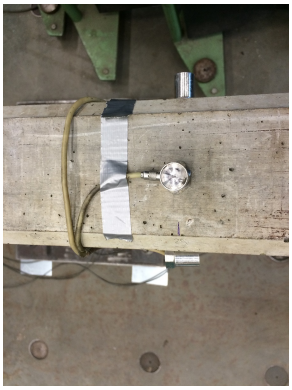

(c) Measurement devices

(d) Column-beam connection

(e) Position loading with impact hammer

(f) Hinged bottom column connection

Figure 6.4: Experimental set-up

6.2.1.1. Loading

A pulse load is used to excite the structure, applied to the left column at 90 cm height as can be seen in Figure 6.4e. The pulse is given by an impact hammer ICP including a load cell that measures the force at the contact area. In red in Figure 6.5 the exact loading forces, measured by the load cell are shown. The hammer is only a fraction of a second in contact with the structure. It should then be noted that some additional forces were measured in the contact area of the hammer without actual contact with the structure. This occurred due to small movements of the hammer and relative movements of its internal mass. In blue, the representative loading profile is shown, there the loading force is only given a value else than zero on a very short time frame.

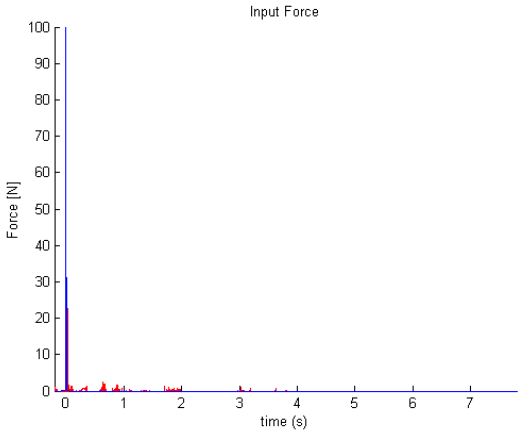

Figure 6.5: Input force

6.2.2. Measurements

The accelerations are measured using LMS software and Scadas III acceleration measurement devices. Two reference devices are placed at both columns at height of the beam, measuring the horizontal accelerations. Three additional devices were placed at different positions on the beam. The locations of these devices were changed for several series of tests. In Appendix G an overview of the used positions per test is given. The devices on the beam mainly measured vertical directions. However, some additional tests have been carried out, to examine the relation between the horizontal displacements in the beam and column. In Figure 6.6 possible positions for the acceleration devices are shown, the red dot represents an acceleration device at 1/4 of the span length.

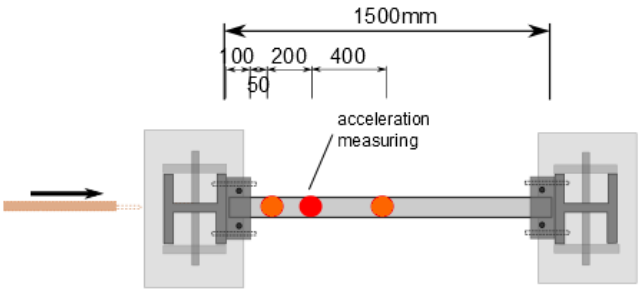

Figure 6.6: Possible locations of the accelerometers in experimental set-up on 1/8th 1/4th and 1/2 of the span length

7

EXPERIMENT

In this chapter the data obtained in the experiment is analyzed. Experimental data contain horizontal and vertical accelerations at several positions along the beam. These accelerations were used to calculate the corresponding velocities and displacements. A numerical integration scheme based on the trapezoidal rule [32] was used in Matlab, see Appendix G . A 1-500 Hz bandpass filter was used and the offset of the signal was removed to obtain a clean signal.

7.0.3. Natural frequencies

The measured accelerations and the measured forces were transformed to the frequency domain to detect the natural frequencies of the system from the peaks in the frequency response function. The frequency response functions and natural frequencies were studied at different locations on the beam to detect the accompanying modes.

Figure 7.1a showed the unfiltered acceleration signal, measured at 1/4 th of the beam. Here, the first peak was visible at 13.5 Hz. This peak is not clearly present in signals measured at the center of the beam, as shown in Figure 7.1b, pointing towards a knot position at the center of the beam of the accompanying mode.

Around 180-210 Hz several high peaks were present within a small frequency range. These peaks represented modes that were strongly correlated with each other, these corresponding modes exchanged energy causing unclear peaks. This phenomenon is also called modal interaction [18]. In the horizontal accelerations measured in the columns no coupling of modes was present. Two clear first peaks occured at 13 Hz and 180 Hz, as can be seen in Figure 7.1c.

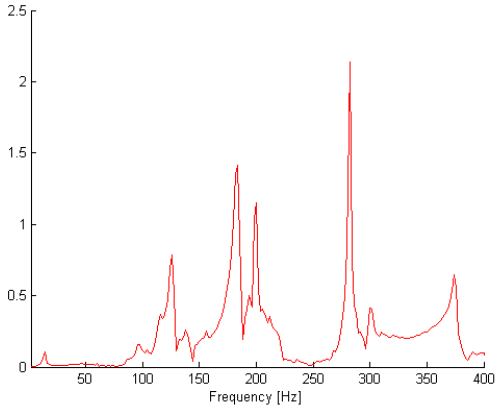

(a) Frequency response function for vertical accelerations around 1/4 the of the beam

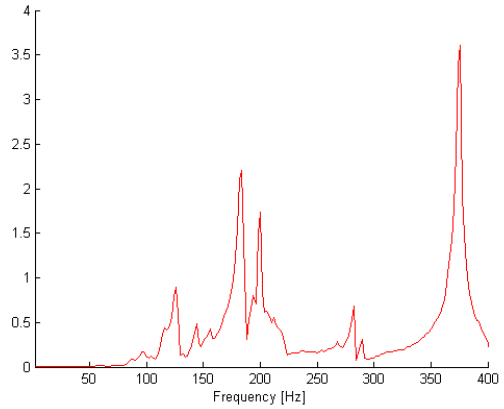

(b) Frequency response function for vertical accelerations at the center of the beam

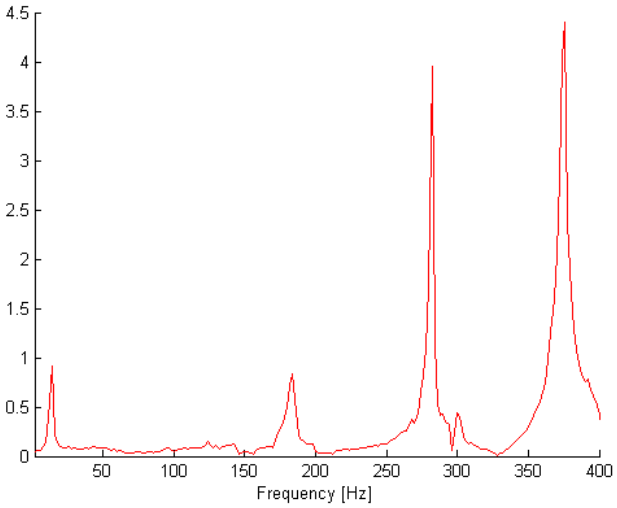

(c) Frequency response function for horizontal accelerations in the column at height of the beam

Figure 7.1: Frequency response function for unfiltered accelerations for first test set-up, not including a layer of highly damped material at joint interface or loosened bolts

At 380 Hz a large peak was measured at all locations. Also at 280 Hz a clear and large peak was present. Those high frequency peaks were, however, not expected, because high frequencies usually experience high damping values causing smaller peaks than lower natural frequencies. In the experiment the structure is exited with an impuls load containing a wide range of frequencies, thus these peaks were not extra enchanted by the external load. The used sampling frequency was 4096Hz, which should be accurate for frequencies until 400-1000 Hz. In the measurement devices that were recording horizontal accelerations in the columns, these peaks were also measured, eliminating high peaks due to local vibrations of the concrete beam. The used accelerometers are commonly used in this frequency range and their own natural frequency is designed to not have an influence in this range. However the combination of glue, the accelerometer an the concrete and steel surface can give combined local vibrations that vibrate in respectively 280 Hz and 380 Hz.

Due to discontinuities in the measured signal at the start and end of the signal, noise in the form of high peaks could be present in the final signal after applying Fast Fourier Transform [79]. When introducing a window in the time signal, giving an exponential decay of amplitude close to both the start and end of the signal, these high peaks disappeared. In Figure 7.2 the frequency response of this processed signal using a Hamming window is shown. But, due to the application of a window, information in the beginning of the signal is lost. In our case, especially at the beginning high frequencies were present which were strongly damped and could not be omitted. Thus it is very likely that the peaks disappeared because they are only present in the strongly reduced vibrations at the first milliseconds of the signal. Not only high frequencies, but all amplitudes in Figure 7.2 are strongly reduced, because most vibration took place at very beginning of the signal.

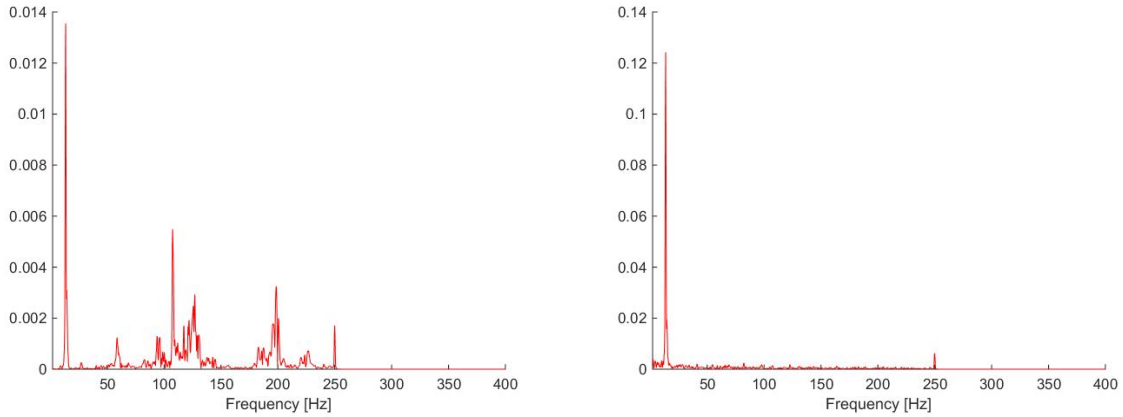

(a) Frequency response function for vertical accelerations around 1/4 the of the beam

(b) Frequency response function for horizontal accelerations in the column at height of the beam

Figure 7.2: Frequency response function for unfiltered accelerations for first test set-up using a Hamming window with fast Fourier transform, causing a lost of high frequency vibrations

In Figure 7.3 the measured time signal of the first test set-up is compared with a 13.5 Hz sine function. A slight change in the natural frequencies seemed to exist in the form of a decrease of the natural frequencies with time. This indicated a decrease in stiffness properties of the system.

Several time intervals were studied individually. The Fast Fourier Transform was applied and the magnitude and location of the peaks were determined. In Figure 7.3b it can be seen that high frequencies were only present in the signal at the start of the vibrations. The high peaks between 100 Hz and 200 Hz were reduced significantly within the first 0.2 s. However, some small peaks were still present. Coupling of modes, however, is not strongly present at these smaller amplitudes. Due to this appearing amplitude dependency, these high coupled peaks might indicate a relation with cracking of the concrete, related with high local energy dissipation and reduction of the local stiffness of the beam.

The position of the peaks above 50 Hz changed in different time intervals, while the first peaks remained close to 13.5 Hz. The exact position of the lower peaks changed slightly during several time-intervals. However, due to the short length of the system compared with the sampling frequency the accuracy of 0.5 Hz in the frequency domain could only be obtained using at least 1.5 s of the time signal, which is too large to show a clear difference in natural frequencies, because of short time of vibration. On intervals of 0.7 s a fluctuation between 13 Hz and 14 Hz was found for the first test set-up. For the test with loosened bolts and added highly damped material at the joint interface a decrease from 11 Hz to 9 Hz was detectable at time intervals of 0.7 s.

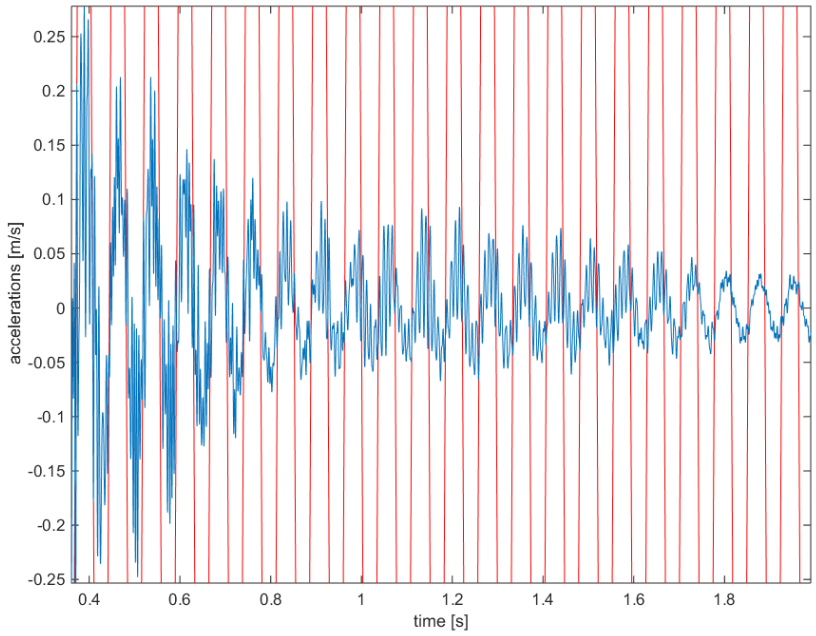

(a) Comparison signal and sine function with 13.5 Hz frequency

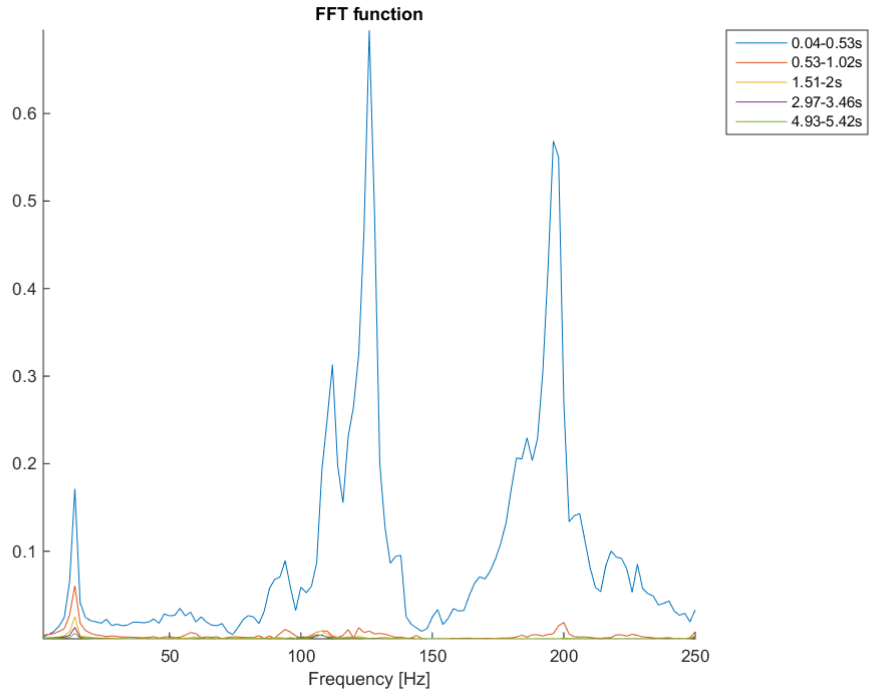

(b) Frequency response function for unfiltered accelerations on different time intervals

Figure 7.3: Changes in natural frequency in time for first test set-up for vertical accelerations around 1/4 the of the beam

7.0.4. Modes

From comparing the horizontal accelerations measured at the two columns during several tests it could be concluded that both columns vibrated in phase. After removing frequencies above 125 Hz with a bandpass filter from the test signal, to obtain a clear signal of the lower frequencies, it could be seen that the measured horizontal accelerations at both columns at the height of the beam, accelerometers MP1 and MP2, had minimums and maximums occurring simultaneously. This can be seen in Figure 7.4. The amplitude of vibration, however, was not of the same size. The column at which the structure is excited experienced higher accelerations, velocities and deflections, which could have been caused by horizontal slip in both joints.

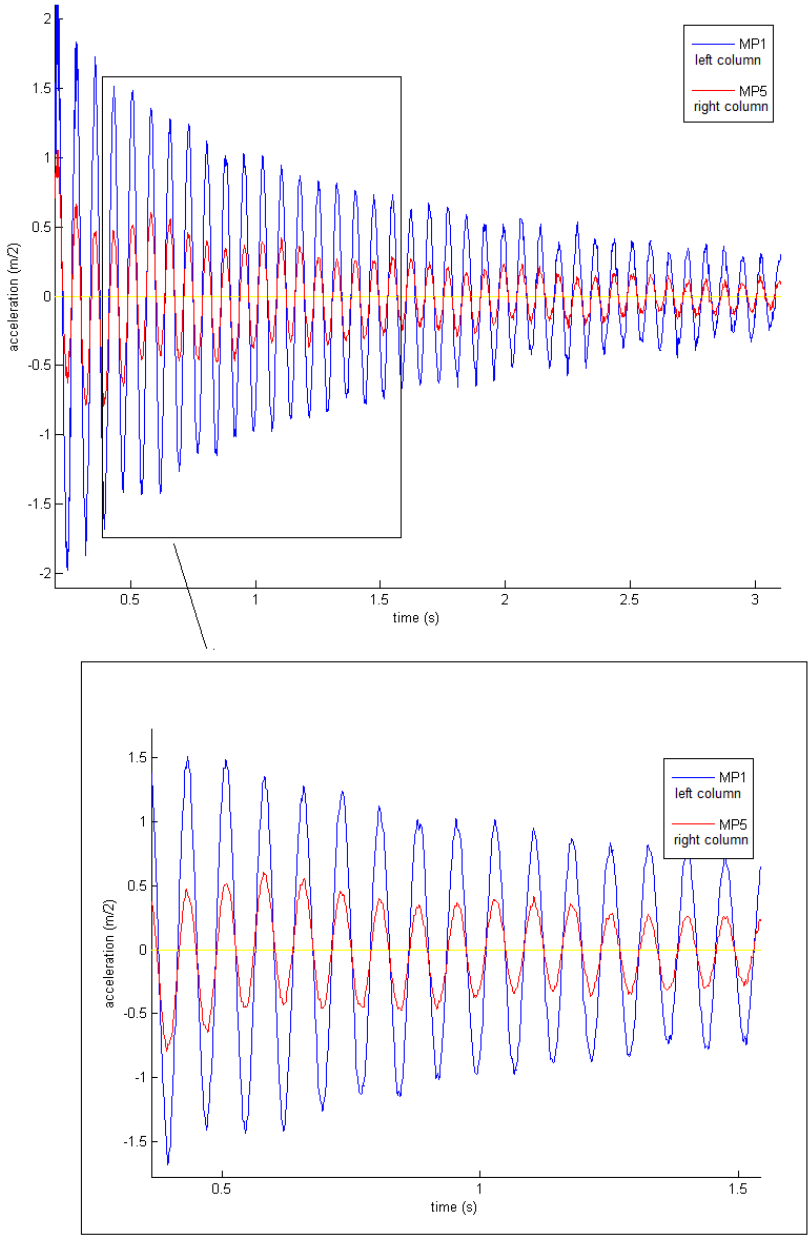

Figure 7.4: Horizontal accelerations at the columns for first test set-up, using a bandpass filter from 2 to 200 Hz to remove high-frequency noise

From measurements of the accelerations positioned at 1/4 th and 3/4 th of the beam, respectively at 290

mm from the left connection (MP3) and at 290 mm from the right connection (MP4), it could be seen that at the first noticeable frequency accelerometers MP3 and MP4 measured vibrations in anti-phase, see Figure 7.5. The frequency referred to is 13,5 Hz, giving around 6.7 periods in 0.5 s. It thus can be concluded that the corresponding mode in the concrete beam has the shape of an odd mode, which is equal to the second expected natural frequency of the beam.

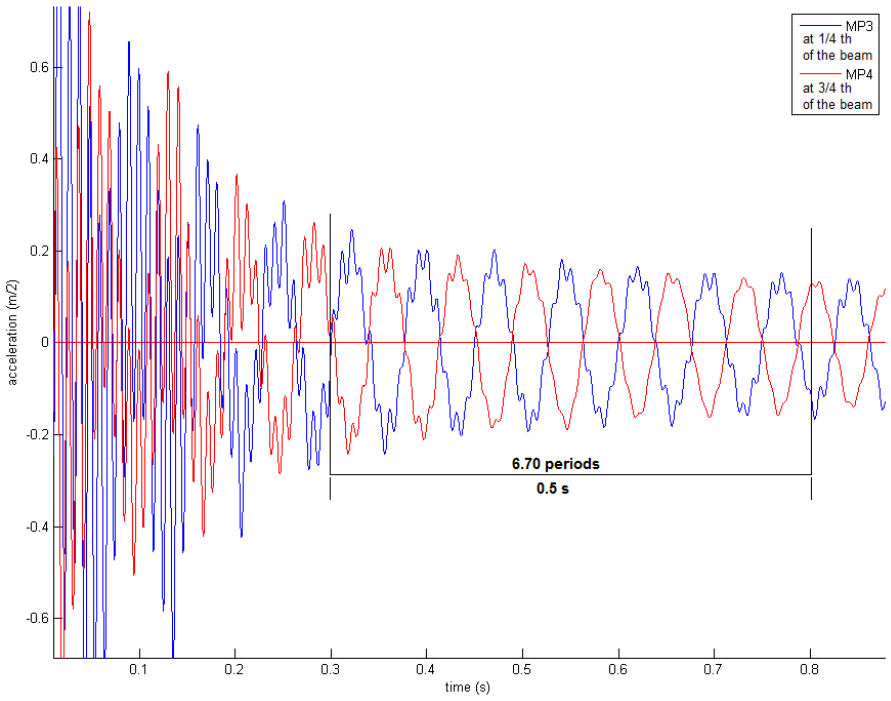

Figure 7.5: Comparing vertical accelerations on 1/4th of the beam (MP3) with accelerations on 3/4th of the beam (MP4)

7.0.5. Damping

The structure is strongly damped. Within eight seconds the amplitude of the lowest frequency was reduced to 1% of the maximum amplitude measured, higher frequencies damped out sooner. Still the system is under-critical damped. Further it could be noticed that at different amplitudes of vibration and different damping values were present, both within one single test and between two test with different maximum amplitudes. Within a signal higher exponential decays were found within the first part of the response. This might be caused by the modal interaction with higher modes. In Figure 7.6 the decay in amplitude for the low frequencies in the response signal is shown. It can be seen clearly that an exponential fit with a greater logarithmic decrement matched the first 0.5 second compared with a fitting curve for the end of the signal.

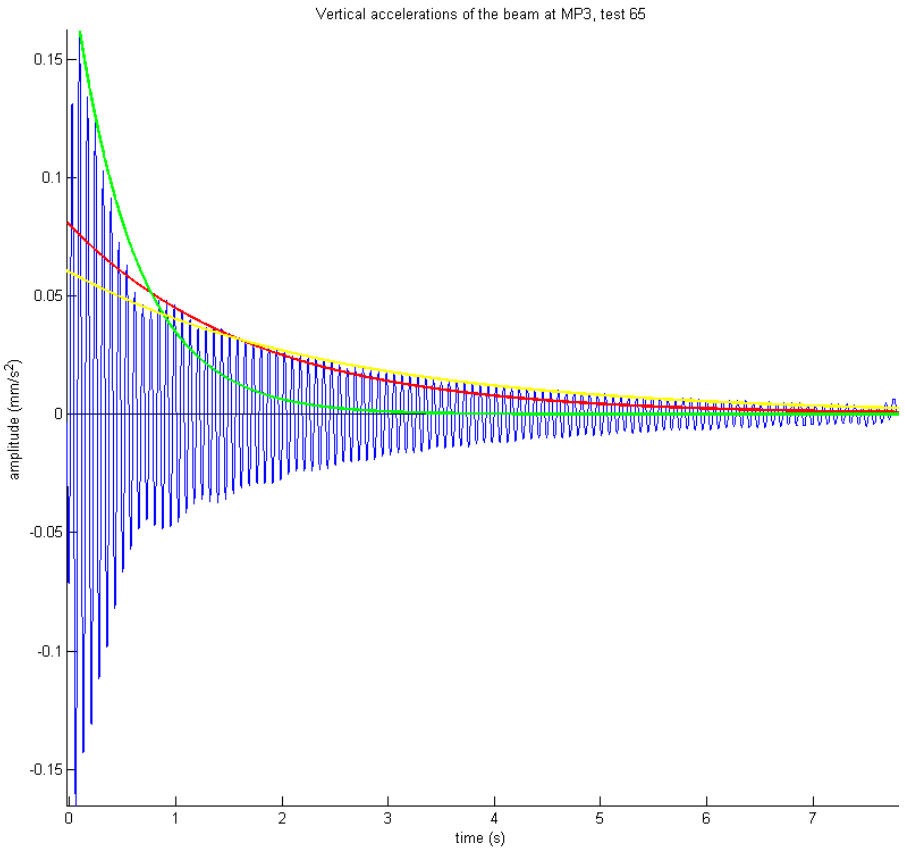

Figure 7.6: Comparing experimental signal with several exponential decays

This damping behavior can be explained by assuming that different damping mechanisms are decisive at different amplitudes. Coulomb friction only depends on the direction of velocity and is constant for several magnitudes of velocity, where viscous damping and material damping decrease with decreasing amplitudes.

In several tests with different force magnitudes a similar change in decay occured during the oscillations. In all experiments a stronger exponential decay in the first oscillations then in subsequent oscillations was found.This change in decay occured at all tests around a fixed amplitude, around 0.4 m/s^2 for the 13.5Hz mode.

Before this turning point various decays and damping ratios were present at tests with different starting amplitudes, Figure 7.7a and 7.7b. For the principal mode an average damping ratio between 0.11 and 0.13 was found for the first part of the response at different tests. Due to the nonlinear behavior of the system no clear difference in damping values for these responses could be distinguished.

In Figure 7.7b some small vibrations are present which were not present in the unfiltered signal. These small vibrations are obtained at the inverse fourier transform.

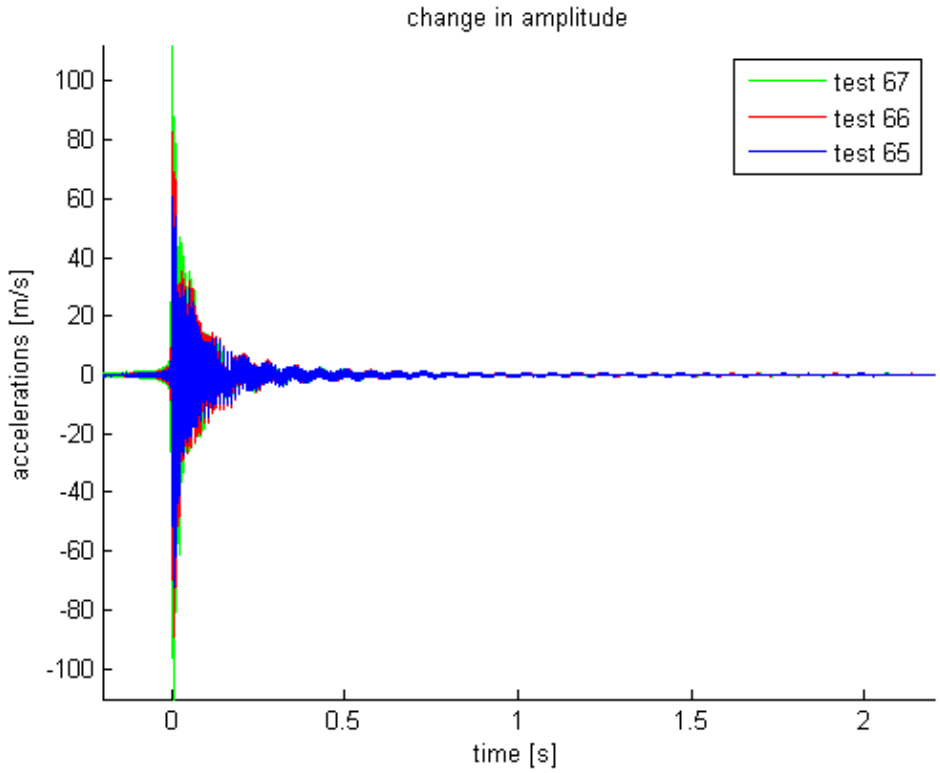

(a) Changes in magnitude of excitation

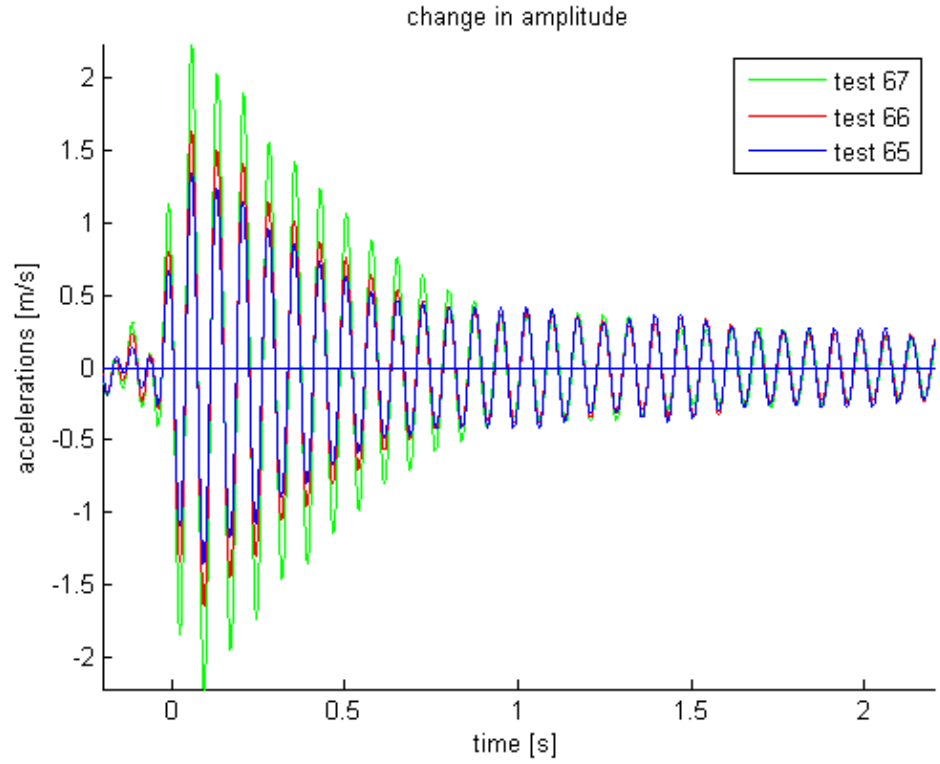

(b) Changes in magnitude of excitation, using a bandpass filter between 2 and 20 Hz to separate the first mode

Figure 7.7: Comparing accelerations at 1/4 th of the beam of the response signal for different loading magnitudes

Changes to test set-up

It can be noticed that adding a layer of highly damped material at the interface of both connections causes changes in the dynamic response of the beam. A shift in natural frequencies (Figure 7.8c) was detectable, which could be ascribed to the increase of the rotational capacity of the joints and the decrease in rotational stiffness. Also, the system encountered higher damping values, as can be seen in Figures 7.8a end 7.8b. This increase in damping ratio results from a decrease of critical damping due to the stiffness and an increase of amplitudes of vibrations where velocity and displacement dependent damping mechanisms cause higher energy dissipation.

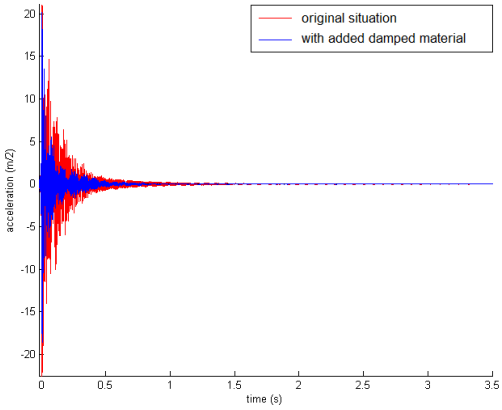

(a) Influence additional strong damping material in the joints

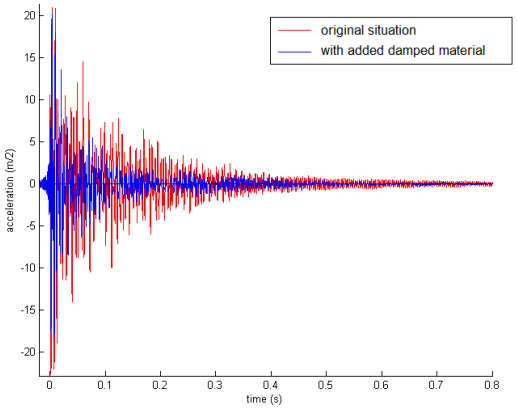

(b) Influence additional strong damping material in the joints, first part of the signal

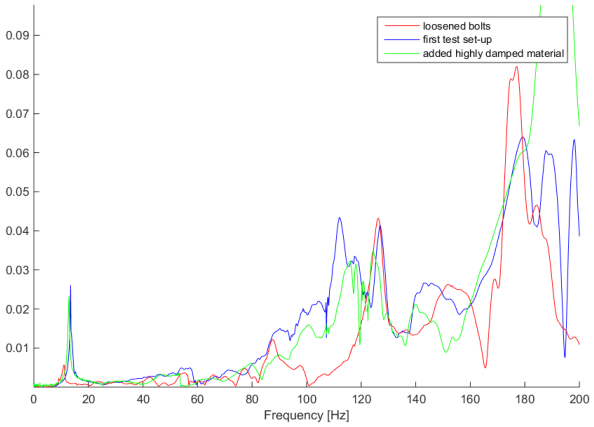

(c) Influence additional strong damping material in the joints, frequency response

Figure 7.8: Influence adding highlydamped material at the joint interfaces

Loosening the bolts had a large impact on the stiffness of the joints and therefore also on the magnitude of vibration. This agreed well with the designed analytical model where the quantity of rotational stiffness influences the vibrations present in the concrete beam. A change to smaller frequencies is visible in Figure 7.8c. When an equal maximum amplitude of vibration occurred for the two cases, higher damping was found for the case with loosened bolts. Also, larger maximum amplitudes of vibrations were present in the loosened situation for equal forces bringing larger damping values.

8

1D Model and Solutions Methods

In this chapter a description of the 1D model can be found. The derivation of the model is described from physical and mathematical starting point in the first part of this chapter. In the second part, the used solution methods are described.

8.1. Physical description model

Due to the common use of single span floors in buildings and decisive stiffness characteristics in the spanning direction, we modeled the floor as one-dimensional model. The floor was modeled assuming that the building behaves in the serviceability limit state with small deformations and where the structure is in the crack stabilizing stage, meaning that cracks are present, but no new cracks are created. Cracks can open and close following the rotations and the deformations during vibrations, but nonlinear material damping due to crack formation is not present in the structure.

The floor is supported by partly clamped connections, containing some rotational capacity and rotational stiffness. When the main load bearing structure is vibrating, moments are induced on the floor at the supports related to the rotation of the main structure and related to the rotational capacity of the joints. It is assumed that all only the first mode has significant influence on the introducing moments. Due to the local deformations in the joints, viscous damping is expected to be present in these joints depending on the rate of change of the deformations or the time derivative of the relative rotations of the main structure and the floor. Due to these relative rotations also relative moment at the contact interfaces occurs and friction forces are expected to be present at the joints.

Assumption 1: The floor and its connections are in the crack stabilizing stage

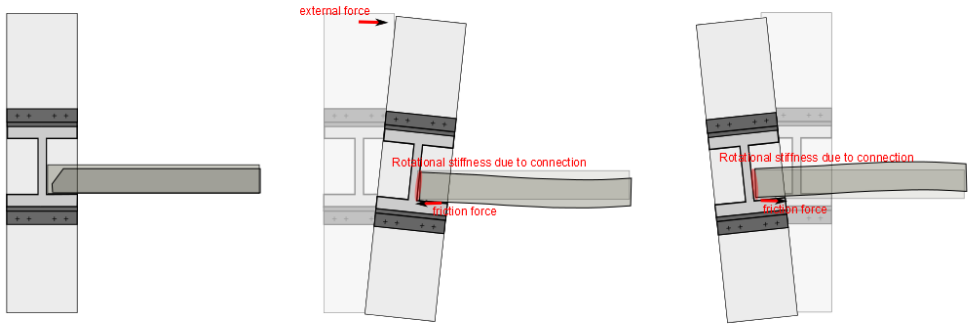

Figure 8.1: Physical representation of actual forces present in the column-to-floor connections

According to literature, nonlinear damping is present in wind-induced vibrating buildings. An amplitude dependency of the damping ratio is found. In this model, no amplitude dependent damping is present within the materials, all nonlinear behavior originates at the boundaries.

The floor is described with a continuous one-dimensional model as shown in Figure 8.2. The equation of motion is derived following the Euler Bernoulli Beam theory. The Euler-Bernoulli beam theory has similar assumptions as the classical plate theory or Kirchhoff theory for plates and is based on smalll deflections with thin plates. These assumptions are summed in this paragraph. For less slender beams, having a height width ratio greater than 5, the theory is not valid and Timoshenko theory or Reissner-Mindlin plate theory gives a better approximation of the problem.

Assumption 2: The influence of transverse shear deformation is neglected.

In this thesis thin plates and slender beams are studied neglecting shear deformations, because for floors the width is commonly less than one-fifth of the predominant lateral dimensions. This implies that plane sections normal to the mid-surface before deformation remain normal to the mid-surface even after deformation and that the mid-plane does not undergoes elongation or shortening.

Assumption 3: The middle plane of the plate or beam does not undergo in-plane deformation.

Assumption 4: Plane sections normal to the mid-surface before deformation remain normal to the mid-surface after deformation

This assumption implies that the transverse shear strains, ϵ_{xz} and ϵ_{yz}, are negligible, where z denotes the thickness direction. Rotations are caused by internal moments and all deflections are related to these moments as well. All internal shear forces can be derived from the internal moments and there are no deflections due to shear. The transverse normal stress σ_{zz} is small and hence can be neglected compared to the other components of stress.

Assumption 5: The transverse normal strain ϵ_{zz} under transverse loading can be neglected.

In nonlinear vibrations of elastic beams, mainly non-linearities in inertia and stiffness count to the non-linearities, while material damping non-linearities are negligible [29]. Therefore, the material damping is chosen as for a visco-elastic beam with the Kelvin-Voigt model implemented. For this type of linear material damping the damping mechanism is based on material behavior in which the Modulus of Elasticity is dependent on the change rate of the strain at a point in the structure [23].

Assumption 7: The material damping present in the beam is linearly depending on the rate of strain.

For calculation purposes it is assumed that the material damping is present at all positions within the beam element, except for the interfaces at the joints.

Assumption 8: Material damping is present within the entire beam, except at the boundaries.

At the boundaries three elements describe the forces within the joints where the floor is connected to the main structure. Firstly, a rotational spring element is present simulating the rotational stiffness of the joint. Secondly, a viscous dashpot is present at the boundaries, representing the linear damping in the joints due to small deformations. Finally, two coulomb damping mechanisms are present imitating friction damping present at the connections. In Figure 8.2 an overview of the model is given.

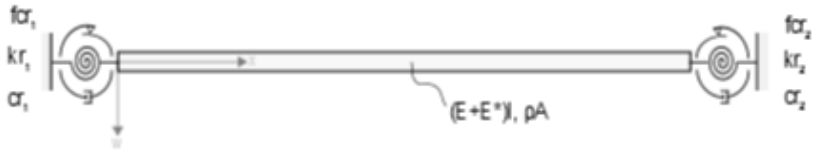

Figure 8.2: Analytical 1D model

Due to the wind loading, the total building is excited. Mainly the building's first modes in all three directions contribute to the vibration. The floor is excited by the rotations of the main structure at the height of the floors due to this wind load. The total displacements in the floor are described with w. These displacements are built up from relative displacements of the floor in relation with the entire structure, w_r, and with the rotations which are imposed by rotations of the entire structure, w_ϕ. The relation of the relative displacements to the overall displacements in described with:

$$w = w_r + w_\phi \tag{8.1}$$

At the boundaries the damping mechanisms and the rotational springs depend on the relative displacements of the floor with respect to the entire structure.

8.2. Mathematical model description

8.2.1. Equation of motion

The equation of motion describes the equilibrium of the beam. For the model the theory of Euler-Bernoulli for beams is used, which assumes deformations in the beam are caused by bending of the beam. Any contributions to the deformation due to shear of plane sections are neglected. Due to the fact that the entire structure will not reach the ultimate limit state and only very small deformations are expected to occur in the beam, we assume that only small deflections are present in the structure.

Assumption 9: Only small deflections are present in the structure.

For small deflections θ the following kinematic relations between deflection, rotation and curvature can be described by Equation 8.2 and 8.3 [80], by using the approximation that ds is a straight line and using $\sin\theta \approx \tan\theta \approx \theta$ and $\cos\theta \approx 1$ valid for small deformations.

$$\frac{\partial w}{\partial x} = \theta \tag{8.2}$$

$$\frac{\partial^2 w}{\partial x^2} = \kappa = \frac{\partial \theta}{\partial x} \tag{8.3}$$

The assumption of Euler-Bernoulli states that the strain changes linear with the height of the beam:

$$\epsilon(z) = y \cdot \kappa \tag{8.4}$$

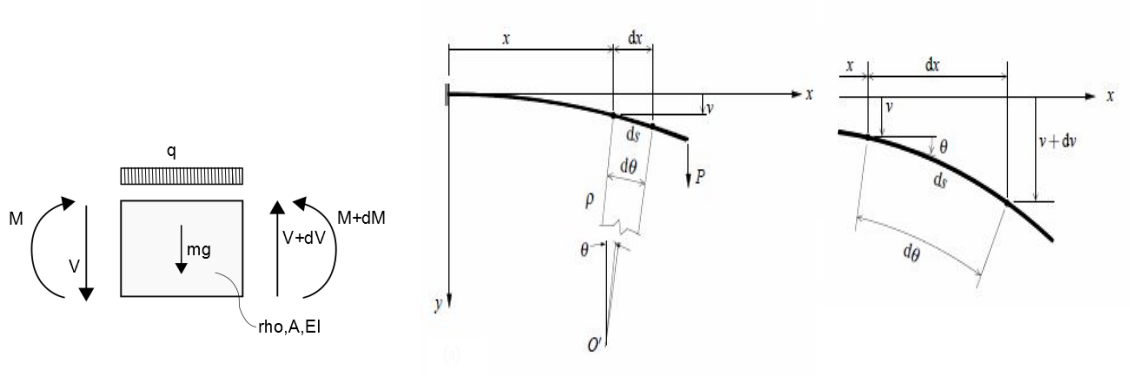

(a) Beam segment with length dx, including all internal and external working forces (b) Beam deformation and axis definition

Figure 8.3: Static relations of an Euler Bernoulli beam element

The bending moment can be expressed in terms of deflections by using Hooke's law $\sigma(z) = E\epsilon(z)$ and the equations above:

$$M = \int dM = \int \sigma_x y dA = \int E\epsilon y dA \tag{8.5}$$

$$= E\left(\int y^2 \partial A\right)\kappa \tag{8.6}$$

$$= -EI\frac{\partial^2 w}{\partial x^2} \tag{8.7}$$

Using Figure 8.3b the relation between shear force and bending moment can be determined from the static momentum equilibrium. When dx approaches an infinite small segment, any products of differentials will be discarded from the equation and a relation between moment and shear force can be found.

$$-M + M + dM - V dx + \frac{1}{2}\left((q - \phi Ag\right) dx^2 = 0 \tag{8.8}$$

$$\Rightarrow V = \frac{\partial M}{\partial x} \tag{8.9}$$

Using Newton's second law in the vertical direction for a infinite small segment gives the basis for the equation of motion. Inserting the expressions above into the equation provides the equation of motion in the form that will be used in further calculations.

$$\rho A dx \cdot a = \sum F_y \tag{8.10}$$

$$\rho A dx \cdot \frac{\partial^2 w}{\partial t^2} = q(x,t) \cdot dx + F_z + V - V - dV \tag{8.11}$$

$$\rho A\frac{\partial^2 w}{\partial t^2} = q(x,t) + \rho A(x)g - \frac{dV}{dx} \tag{8.12}$$

$$\Rightarrow \rho A\frac{\partial^2 w}{\partial t^2} + \frac{\partial^2}{\partial x^2}\left(EI\frac{\partial^2 w}{\partial x^2}\right) = q(x,t) + \rho A(x)g \tag{8.13}$$

The own weight only influences the static deformations for damped structures and can be neglected in this dynamic study. Also, no further loading in vertical direction is present on the structure. Then, only the inertial mass is important.

$$\rho A\frac{\partial^2 w}{\partial t^2} + \frac{\partial^2}{\partial x^2}\left(EI\frac{\partial^2 w}{\partial x^2}\right) = 0 \tag{8.14}$$

Material damping

Material damping is based on the implemented Kelvin-Voigt model for internal stresses, simulating the visco-elastic behavior. The stress within the material is dependent on the change rate of strain with a Dynamic Modulus of Elasticity $E*$:

$$\sigma = E\epsilon + E^* \frac{d\epsilon}{dt} \tag{8.15}$$

The relation between moments and displacements becomes now:

$$M = \int dM = \int \sigma_x y dA = \int \left(E\epsilon + E^* \frac{d\epsilon}{dt} \right) y dA \tag{8.16}$$

$$= \int E\epsilon y dA + \int E^* \frac{d\epsilon}{dt} y dA \tag{8.17}$$

$$= E + \left(\int y^2 \partial A \right) \kappa + E^* \left(\int y^2 dA \right) \dot{\kappa} \tag{8.18}$$

$$= \left(E + E^* \frac{\partial}{\partial t} \right) I \frac{\partial^2 w}{\partial x^2} \tag{8.19}$$

This makes the equation of motion including damping:

$$\rho A \frac{\partial^2 w}{\partial t^2} + EI \frac{\partial^4 w}{\partial x^4} + E^* I \frac{\partial}{\partial t} \frac{\partial^4 w}{\partial x^4} = 0 \tag{8.20}$$

8.2.2. Boundary conditions

The boundary conditions fullfill requirements for the boundaries of the model. Those requirements can contain static properties, like restricted and fixed displacements or rotations, or dynamic demands, in the form of moments and shear forces. Boundary conditions follow from static equilibrium or dynamic equilibrium at the boundaries. For fixed rotations or deformations the static equilibrium for the corresponding degree of freedom is used. For the second type of boundary conditions, either the torque equilibrium or the vertical force equilibrium provides the boundary condition. For a fourth order space derivative in the equation of motion at a model with two boundaries also four boundary conditions have to be set, two at each boundary: a static and dynamic BC.

Three elements are present in the model at the boundaries: a rotational spring, a viscous damper providing a torque damping force and a coulomb friction element providing a torque damping force as shown in Figure 8.2. The internal moment at any time of the beam is described by Equation 8.7:

$$M_{internal} = -\left(E + E^* \frac{\partial}{\partial t} \right) I \frac{\partial^2 w}{\partial x^2} \tag{8.21}$$

And the dynamic boundary condition is given by the torque moment equilibrium at $x = 0$:

$$M_{internal} = -M_{spring} - M_{dashpot} - M_{friction} \tag{8.22}$$

$$\Longrightarrow \qquad \left(E + E^* \frac{\partial}{\partial t} \right) I \frac{\partial^2 w}{\partial x^2} = M_{spring} + M_{dashpot} + M_{friction} \tag{8.23}$$

At the boundaries, the forces present due to deformations at the spring and the presence of dashpots and friction devices, are dependent on the relative rotations between floor and main structure.

$$M_{spring} = kr_i \cdot \varphi_{rel} = kr_i \left(\frac{\partial w}{\partial x} - \frac{\partial w_\phi}{\partial x} \right) \tag{8.24}$$

$$M_{dashpot} = cr_i \cdot \dot{\varphi}_{rel} = cr_i \left(\frac{\partial^2 w}{\partial t \partial x} - \frac{\partial^2 w_\phi}{\partial x \partial t} \right) \tag{8.25}$$

$$M_{friction} = F_c \cdot sgn(\dot{\varphi}_{rel}) = F_c sgn\left(\frac{\partial^2 w}{\partial t \partial x} - \frac{\partial^2 w_\phi}{\partial x \partial t}\right) \tag{8.26}$$

Inserting in the left dynamic boundary condition gives:

$$(1) \qquad \left(E + E^* \frac{\partial}{\partial t}\right) I \frac{\partial^2 w}{\partial x^2}|_{x=0} = kr_1 \left(\frac{\partial w}{\partial x} - \frac{\partial w_\phi}{\partial x}\right)|_{x=0} + cr_1 \left(\frac{\partial^2 w}{\partial t \partial x} - \frac{\partial^2 w_\phi}{\partial x \partial t}\right)|_{x=0} + \mu_1 sgn\left(\frac{\partial^2 w}{\partial t \partial x} - \frac{\partial^2 w_\phi}{\partial x \partial t}\right)_{x=0} \tag{8.27}$$

For the left boundary of the model the kinematic boundary condition is based on fixed displacements:

$$(2) \qquad w(0) = 0 \tag{8.28}$$

For the right boundary of the model the kinematic boundary condition is written as:

$$(3) \qquad w(L) = 0 \tag{8.29}$$

And the dynamic boundary condition is given by the torque moment equilibrium at $x = L$:

$$(4) \qquad \left(E + E^* \frac{\partial}{\partial t}\right) I \frac{\partial^2 w}{\partial x^2}|_{x=L} = -kr_2 \left(\frac{\partial w}{\partial x} - \frac{\partial w_\phi}{\partial x}\right)|_{x=L} - cr_2 \left(\frac{\partial^2 w}{\partial t \partial x} - \frac{\partial^2 w_\phi}{\partial x \partial t}\right)|_{x=L} - \mu_2 sgn\left(\frac{\partial^2 w}{\partial t \partial x} - \frac{\partial^2 w_\phi}{\partial x \partial t}\right)_{x=L} \tag{8.30}$$

It is assumed that both sides of the floor act in phase and with equal amplitude. The rotations of the column at height of the floor are also referred to with $\varphi_c(t)$.

The equation of motion and the four boundary conditions are summarized below:

8.2.3. Summary EM and BC

$$\rho A \frac{\partial^2 w}{\partial t^2} + EI \frac{\partial^4 w}{\partial x^4} + E^* I \frac{\partial}{\partial t} \frac{\partial^4 w}{\partial x^4} = 0 \tag{8.31}$$

$$(1) \qquad w(0) = 0 \tag{8.32}$$

$$(2) \qquad \left(E + E^* \frac{\partial}{\partial t}\right) I \frac{\partial^2 w}{\partial x^2}|_{x=0} = kr_1 \left(\frac{\partial w}{\partial x} - \varphi_c(t)\right)|_{x=0} + cr_1 \left(\frac{\partial^2 w}{\partial t \partial x} - \dot{\varphi}_c(t)\right)|_{x=0} + \mu_1 sgn\left(\frac{\partial^2 w}{\partial t \partial x} - \dot{\varphi}_c(t)\right)_{x=0} \tag{8.33}$$

$$(3) \qquad w(L) = 0 \tag{8.34}$$

$$(4) \qquad \left(E + E^* \frac{\partial}{\partial t}\right) I \frac{\partial^2 w}{\partial x^2}|_{x=0} = -kr_2 \left(\frac{\partial w}{\partial x} - \varphi_c(t)\right)|_{x=L} - cr_2 \left(\frac{\partial^2 w}{\partial t \partial x} - \dot{\varphi}_c(t)\right)|_{x=L} - \mu_2 sgn\left(\frac{\partial^2 w}{\partial t \partial x} - \dot{\varphi}_c(t)\right)_{x=L} \tag{8.35}$$

$$\tag{8.36}$$

Where the dynamic modulus of elasticity is described with:

$$\begin{cases} E* = E* & \text{for} \quad x \neq 0 \wedge x \neq L \\ E* = 0 & \text{for} \quad x = 0 \wedge x = L \end{cases} \tag{8.37}$$

8.2.4. External loads

The wind load can be introduced in the model in two different manners. The first manner, sets initial conditions such as initial displacements and velocities at the boundary. This gives a free vibration problem. For the second manner an external moment in introduced at the boundaries.

External Impulse Force

The impulse force on the column is introduced in the floor beam as a moment. The relation between the impulse force and the moment at the connections is determined using statical calculations. In Figure 8.4 the relation between the external Impulse Force and the Internal moment is shown.

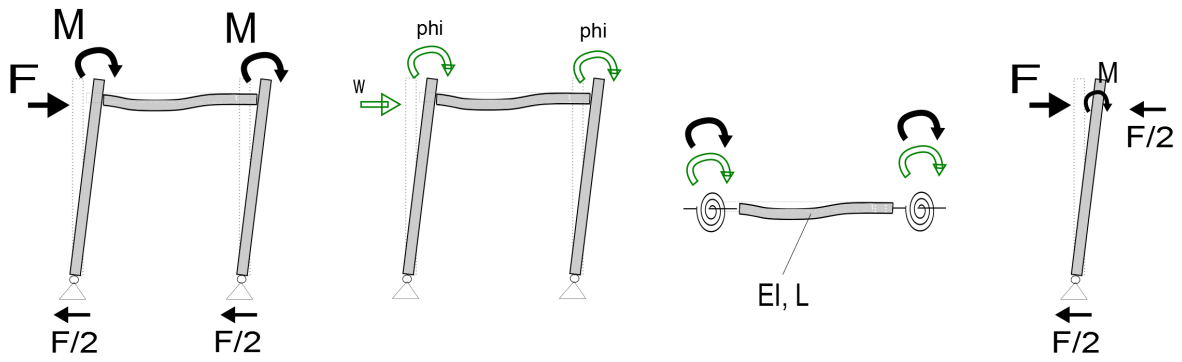

Figure 8.4: Overview on load mechanisms and static loads, among which the internal moment M, due to an external force F.

The two columns are assumed as very stiff compared to the beam and the influence of rotational capacity for heavy loading at a very short time span at the connection is neglected. A mechanism occurs where the floor shows deformations due to internal moments introduced the connection. The relation between the rotation at the connections and the introduced moment results from deformations of the floor beam, is given with:

$$\phi = \frac{L}{6EI} M \tag{8.38}$$

This relation is obtained, using statical equilibrium equations following Euler Bernoulli, as

$$EIw'''' = 0 \tag{8.39}$$

$$w(0) = 0, \qquad -EIw''(0) = M \tag{8.40}$$

$$w(L) = 0, \qquad -EIw''(L) = -M \tag{8.41}$$

$$\rightarrow \quad w'(x) = \frac{1}{EI}\left(1/3M\frac{x^3}{L} - 1/2Mx^2 + 1/6M\right) \quad \rightarrow \quad w'(0) = \frac{L}{6EI}M \quad = \quad \phi \tag{8.42}$$

The relation between rotation at the connection and the amplitude of excitation at F, between H as the height of the floor with respect to the hinge and F the amplitude of excitation

$$\phi = \frac{F}{H} \tag{8.43}$$

This gives the amplitude of the internal moment M at the connection with respect to the amplitude of excitation F.

$$M(t) = F(t) \cdot \frac{6EI}{HL} \tag{8.44}$$

An impulse can be described with:

$$F(t) = \delta(t)F_0 \tag{8.45}$$

Giving for the internal moment:

$$M_{ext}(t) = \delta(t)F_0 \cdot \frac{6EI}{HL} \tag{8.46}$$

Such an external moment can be used for calculations in the frequency domain, however the magnitude of this external load is very hard to measure experimentally.

Fixed Displacements and Rotations

The second option is using fixed displacements and rotations. These displacements can directly be determined from measurements, but they bring another difficulty with them. The displacements can only be determined for the entire dynamic deformation and not for single modes. When using initial displacement to study free vibrations with a mode approximation, an initial displacement should be given to each of the modes.

The statical deformation due to horizontal loading on the building causes the floor to deform in a shape which is most similar to the second mode shape. Assigning the initial deformation to the second mode gives an approximation for the initial conditions, however other modes should also be given an initial value.

8.3. Solutions

8.3.1. Extended Modal Analysis - Natural frequency and natural mode shape determination

For the determination of the linear mode shapes and the natural frequencies, no damping contributions or external forces are taken into account. The equation of motion that describes the behaviour of the beam for the first model is stated as follow.

$$\rho A \frac{\partial^2 w}{\partial t^2} + \left(E + E * \frac{\partial}{\partial t} \right) I \frac{\partial^4 w}{\partial x^4} = 0 \tag{8.47}$$

Because of the assumption that material damping is present at all positions of the beam, except at both boundaries where the other damping mechanisms are decisive, the boundary conditions are stated as:

$$EI \frac{\partial^2 w}{\partial x^2}|_{x=0} = kr_1 \frac{\partial w}{\partial x}|_{x=0} \tag{8.48}$$

$$w(0) = 0 \tag{8.49}$$

$$EI \frac{\partial^2 w}{\partial x^2}|_{x=L} = -kr_2 \frac{\partial w}{\partial x}|_{x=L} \tag{8.50}$$

$$w(L) = 0 \tag{8.51}$$

We are searching for the linear mode shape, so all damping contributions are removed from the system, remaining the following equation of motion:

$$\rho A \frac{\partial^2 w}{\partial t^2} + EI \frac{\partial^4 w}{\partial x^4} = 0 \tag{8.52}$$

The method of separation of variables is used for solving this homogeneous equation of motion. A trial solution is used, containing both a space related and a time related part:

$$w(x,t) = W(x)\,\Psi(t) \tag{8.53}$$

Where $\Psi(t) = \sum \hat{\Psi} exp(i\omega t)$

Using substituting of the trial solution into the equation of motion, a time independent equation of motion can be derived which describes together with the boundary conditions the modes of vibration.

$$-\rho A W(x)\,\omega^2 \Psi(t) + EI \frac{\partial^4 W(x)}{\partial x^4} \Psi(t) = 0 \tag{8.54}$$

$$EI \frac{\partial^4 W(x)}{\partial x^4} - \rho A \omega^2 W(x) = 0 \qquad \text{for all t} \tag{8.55}$$

$$\frac{\partial^4 W(x)}{\partial x^4} - \beta^4 W(x) = 0 \qquad \text{for all t} \tag{8.56}$$

where $\beta^4 = \frac{\rho A \omega^2}{EI}$.

The normal modes are assumed to be of the form:

$$W(x) = \sum_{}^{4} C_k exp(\lambda_k x) \tag{8.57}$$

Inserting in Equation C.17 gives the roots of the lambda's in the assumed solution.

$$\lambda_1 = \beta, \lambda_2 = -\beta, \lambda_3 = i\beta, \lambda_4 = -i\beta \tag{8.58}$$

$$W(x) = C_1 exp(\beta x) + C_2 exp(-\beta x) + C_3 exp(i\beta x) + C_4 exp(-i\beta x) \tag{8.59}$$

$$W(x) = A\cosh(\beta x) + B\sinh(\beta x) + C\cos(\beta x) + D\sin(\beta x) \tag{8.60}$$

For finding the modes the boundary conditions of C.2-C.5 should be met.

$$EI\frac{d^2W}{dx^2}|_{x=0} = kr_1\frac{dW}{dx}|_{x=0} \tag{8.61}$$

$$W(0) = 0 \tag{8.62}$$

$$EI\frac{d^2W}{dx^2}|_{x=L} = -kr_2\frac{dW}{dx}|_{x=L} \tag{8.63}$$

$$W(L) = 0 \tag{8.64}$$

Substitution of C.21,C.22 and C.23 in the Boundary Conditions gives a system of equations, which can be written in the form of a matrix of coefficients:

$$\begin{bmatrix} EI\beta^2 & -kr_1\beta & -EI\beta^2 & -kr_1\beta \\ 1 & 0 & 1 & 0 \\ EI\beta^2\cosh(\beta L) + kr_2\beta\sinh(\beta L) & EI\beta^2\sinh(\beta L) + kr_2\beta\cosh(\beta L) & -EI\beta^2\cos(\beta L) - kr_2\beta\sin(\beta L) & -EI\beta^2\sin(\beta L) + kr_2\beta\cos(\beta L) \\ \cosh(\beta L) & \sinh(\beta L) & \cos(\beta L) & \sin(\beta L) \end{bmatrix} \begin{bmatrix} A \\ B \\ C \\ D \end{bmatrix} = 0 \tag{8.65}$$

8.3.1.1. Natural frequencies

The determinant of this matrix gives an equation dependent on β. Non-trivial solutions only exist when the determinant of the matrix above is equal to zero. So, only for specific β's there exist non-trivial solutions. These β's contain the natural frequencies of the system.

$$\begin{aligned} \text{Determinant} = {} & \cos(\beta L)^2\beta^2 kr_1 kr_2 - 2(EI)^2\sinh(\beta L)\sin(\beta L)\beta^4 \\ & - EI\sinh(\beta L)\cos(\beta L)\beta^3 kr_2 - EI\cosh(\beta L)\sin(\beta L)\beta^3 kr_2 \\ & - 2EI^2\sinh(\beta L)\sin(\beta L)\beta^4 + 2EI\sinh(\beta L)\cos(\beta L)\beta^3 kr_1 \\ & - EI\sinh(\beta L)\cos(\beta L)\beta^3 kr_2 - 2EI\cosh(\beta L)\sin(\beta L)\beta^3 kr_1 \\ & - EI\cosh(\beta L)\sin(\beta L)\beta^3 kr_2 + \sinh(\beta L)^2\beta^2 kr_1 kr_2 \\ & - \cosh(\beta L)^2\beta^2 kr_1 kr_2 - \sin(\beta L)^2\beta^2 kr_1 kr_2 = 0 \end{aligned}$$

The determinant equation is solved using a script in Matlab 2013a, as shown Appendix D .

8.3.1.2. Validate Natural Frequencies and compare with literature

In Table 8.1 the derived natural frequencies are checked for the case using $r_1 = r_2 = 0$ with the values found in literature [14] stating:

$$\omega_n^2 = \frac{EI}{\rho A}\left(\frac{n\pi}{l}\right)^4 \qquad \text{with} \qquad (n = 1,2,\cdots\infty) \tag{8.66}$$

	nf model	**nf literature**	**difference**
1st nf	9,8696044	9,8696044	0
2nd nf	39,478417	39,478418	0
3rd nf	88,826439	88,826440	-1,4210854e-14
4th nf	157,91367	157,91367	2,8421709e-14
5th nf	246,74011	246,74011	2,8421709e-14

Table 8.1: Natural Frequencies comparison with literature [rad/s]

Only very small errors of the order 10^{-14} occur. Given the accuracy of Matlab identical results as described in literature are found. For various spring stiffnesses, the natural frequencies are shown in Tables 8.2 and 8.3.

For the first case the natural frequencies tend to go to a limit value, which should correspond to the natural frequencies of the fully clamped beam. The second case also tends to a maximum value, which matches the clamped-simply supported beam frequency [14, p.80].

	r1=r2=0	r1=r2=1	r1=r2=1e3	r1=r2=1e10	r1=r2=1e100	Literature
1st nf	9,8696044	17,2695452	22,2844714	22,3732854	22,3732854	22,4
2nd nf	39,4784176	49,9601489	61,4287831	61,6728228	61,6728229	61,7
3rd nf	88,8264396	101,3178956	120,4264620	120,9033917	120,9033917	121,0
4th nf	157,9136704	171,7479411	199,0735094	199,8594480	199,8594481	200,0
5th nf	246,7401100	261,5268391	297,3851232	298,5555351	298,5555352	298,0

Table 8.2: Relation natural frequencies with spring stiffnessess both boundaries [rad/s]

	r1=r2=0	r1=1, r2=0	r1=1e3, r2=0	r1=1e10, r2=0	r1=1e100, r2=0	Literature
1st nf	9,8696044	10,7144016	15,3875359	15,4182057	15,4182057	15,4
2nd nf	39,47841764	40,3985500	49,8657822	49,9648620	49,9648620	50,0
3rd nf	88,8264396	89,7730108	104,0416193	104,247696	104,2476965	104,0
4th nf	157,9136704	158,8735949	177,9184236	178,2697295	178,2697295	178,0
5th nf	246,7401100	247,7080659	271,4965642	272,0309712	272,0309713	272,0

Table 8.3: Relation natural frequencies with spring stiffness single boundary [rad/s]

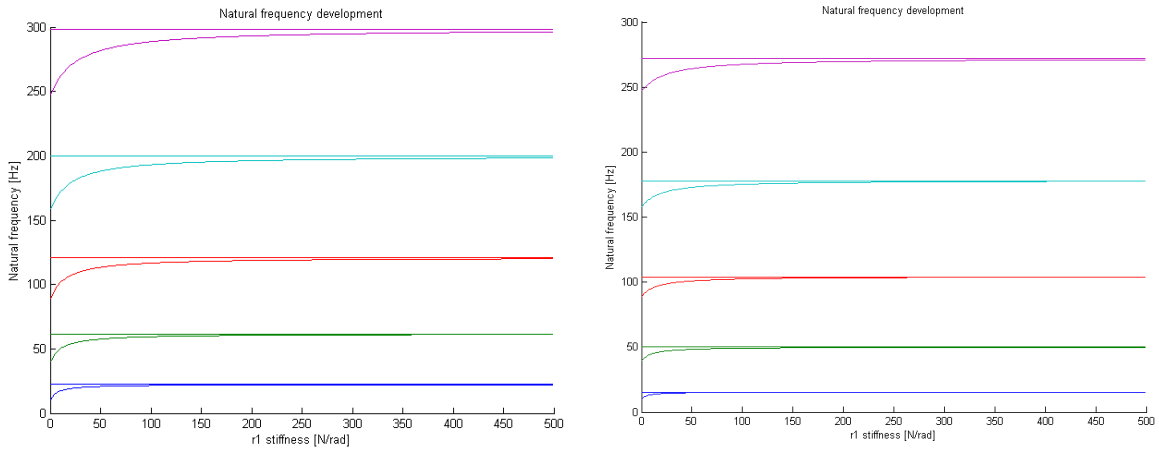

(a) rotational springs at both sides

(b) one rotational spring and one side simply supported

Figure 8.5: Change of natural frequencies with increasing rotational spring stiffnessess compared with the limit value from literature

8.3.1.3. Mode shapes

For each β a corresponding space solution exists, which can be determined by solving the unknown constants A, B, C and D which depend on the boundary conditions and the natural frequency. There are infinitely many solutions for these constants, because each solution can be multiplied by any constant. When a non-zero value is valid for constant D, this constant is set to 1 and all other constants are replaced by a ratio over D.

$$D(\beta) = 1 \tag{8.67}$$

$$\begin{bmatrix} EI\beta^2 & -kr_1\beta & -EI\beta^2 & -kr_1\beta \\ 1 & 0 & 1 & 0 \\ EI\beta^2\cosh(\beta L) + kr_2\beta\sinh(\beta L) & EI\beta^2\sinh(\beta L) + kr_2\beta\cosh(\beta L) & -EI\beta^2\cos(\beta L) - kr_2\beta\sin(\beta L) & -EI\beta^2\sin(\beta L) + kr_2\beta\cos(\beta L) \\ \cosh(\beta L) & \sinh(\beta L) & \cos(\beta L) & \sin(\beta L) \end{bmatrix} \begin{bmatrix} A/D \\ B/D \\ C/D \\ D/D \end{bmatrix} = 0 \tag{8.68}$$

$$\Longrightarrow \begin{bmatrix} EI\beta^2 & -kr_1\beta & -EI\beta^2 \\ 1 & 0 & 1 \\ EI\beta^2\cosh(\beta L) + kr_2\beta\sinh(\beta L) & EI\beta^2\sinh(\beta L) + kr_2\beta\cosh(\beta L) & -EI\beta^2\cos(\beta L) - kr_2\beta\sin(\beta L) \end{bmatrix} \begin{bmatrix} A/D \\ B/D \\ C/D \end{bmatrix} = \begin{bmatrix} +kr_1\beta \\ 0 \\ +EI\beta^2\sin(\beta L) \\ -kr_2\beta\cos(\beta L) \end{bmatrix} \tag{8.69}$$

For each value β now a value for the unknown constants A,B and C can be determined and the mode shape for each natural frequency is determined.

$$\begin{bmatrix} A(\beta) \\ B(\beta) \\ C(\beta) \end{bmatrix} = \begin{bmatrix} EI\beta^2 & -kr_1\beta & -EI\beta^2 \\ 1 & 0 & 1 \\ EI\beta^2\cosh(\beta L) + kr_2\beta\sinh(\beta L) & EI\beta^2\sinh(\beta L) + kr_2\beta\cosh(\beta L) & -EI\beta^2\cos(\beta L) - kr_2\beta\sin(\beta L) \end{bmatrix}^{-1} \begin{bmatrix} +kr_1\beta \\ 0 \\ +EI\beta^2\sin(\beta L) \\ -kr_2\beta\cos(\beta L) \end{bmatrix} \tag{8.70}$$

Using Maple, the following functions describe how A,B,C and D depend on β.

$$\begin{aligned} A(\beta) = {} & (EI\sinh(\beta L)\beta + \cosh(\beta L)kr_2)kr_1/(2EI^2\sinh(\beta L)\beta^2 + EI\cosh(\beta L)\beta kr_1 \\ & + 2EI\cosh(\beta L)\beta kr_2 + EI\cos(\beta L)\beta kr_1 + \sinh(\beta L)kr_1kr_2 + \sin(\beta L)kr_1kr_2) + kr_1(EI\beta^2\sin(\beta L) \\ & - kr_2\beta\cos(\beta L))/(\beta(2EI^2\sinh(\beta L)\beta^2 + EI\cosh(\beta L)\beta kr_1 + 2EI\cosh(\beta L)\beta kr_2 + EI\cos(\beta L)\beta kr_1 \\ & + \sinh(\beta L)kr_1kr_2 + \sin(\beta L)kr_1kr_2)) \end{aligned} \tag{8.71}$$

$$\begin{aligned} B(\beta) = {} & -(EI\cosh(\beta L)\beta + EI\cos(\beta L)\beta + \sinh(\beta L)kr_2 + \sin(\beta L)kr_2)kr_1/(2EI^2\sinh(\beta L)\beta^2 \\ & + EI\cosh(\beta L)\beta kr_1 + 2EI\cosh(\beta L)\beta kr_2 + EI\cos(\beta L)\beta kr_1 + \sinh(\beta L)kr_1kr_2 \\ & + \sin(\beta L)kr_1kr_2) + 2EI(EI\beta^2\sin(\beta L) - kr_2\beta\cos(\beta L))/(2EI^2\sinh(\beta L)\beta^2 \\ & + EI\cosh(\beta L)\beta kr_1 + 2EI\cosh(\beta L)\beta kr_2 + EI\cos(\beta L)\beta kr_1 + \sinh(\beta L)kr_1kr_2 + \sin(\beta L)kr_1kr_2) \end{aligned} \tag{8.72}$$

$$\begin{aligned} C(\beta) = {} & -(EI\sinh(\beta L)\beta + \cosh(\beta L)kr_2)kr_1/(2EI^2\sinh(\beta L)\beta^2 + EI\cosh(\beta L)\beta kr_1 + 2EI\cosh(\beta L)\beta kr_2 \\ & + EI\cos(\beta L)\beta kr_1 + \sinh(\beta L)kr_1kr_2 + \sin(\beta L)kr_1kr_2) - kr_1(EI\beta^2\sin(\beta L) \\ & - kr_2\beta\cos(\beta L))/(\beta(2EI^2\sinh(\beta L)\beta^2 + EI\cosh(\beta L)\beta kr_1 + 2EI\cosh(\beta L)\beta kr_2 + EI\cos(\beta L)\beta kr_1 \\ & + \sinh(\beta L)kr_1kr_2 + \sin(\beta L)kr_1kr_2)) \end{aligned} \tag{8.73}$$

$$D(\beta) = 1 \tag{8.74}$$

This makes the mode shape:

$$w_n(x) = A_n \cosh(\beta_n x) + B_n \sinh(\beta_n x) + C_n \cos(\beta_n x) + D_n \sin(\beta_n x) \tag{8.75}$$

With derivatives:

$$\frac{dw_n}{dx} = \beta_n \left(A_n \sinh(\beta_n x) + B_n \cosh(\beta_n x) - C_n \sin(\beta_n x) + D_n \cos(\beta_n x) \right) \tag{8.76}$$

$$\frac{d^2 w_n}{dx^2} = \beta_n^2 \left(A_n \cosh(\beta_n x) + B_n \sinh(\beta_n x) - C_n \cos(\beta_n x) - D_n \sin(\beta_n x) \right) \tag{8.77}$$

$$\frac{d^3 w_n}{dx^3} = \beta_n^3 \left(A_n \sinh(\beta_n x) + B_n \cosh(\beta_n x) + C_n \sin(\beta_n x) - D_n \cos(\beta_n x) \right) \tag{8.78}$$

$$\frac{d^4 w_n}{dx^4} = \beta_n^4 \left(A_n \cosh(\beta_n x) + B_n \sinh(\beta_n x) + C_n \cos(\beta_n x) + D_n \sin(\beta_n x) \right) = \beta_n^4 w_n(x) \tag{8.79}$$

In Matlab these constants are determined for all natural frequencies. In Figures 8.6a to 8.6a the first five mode shapes are plotted for different values for the rotational stiffnesses at the boundaries.

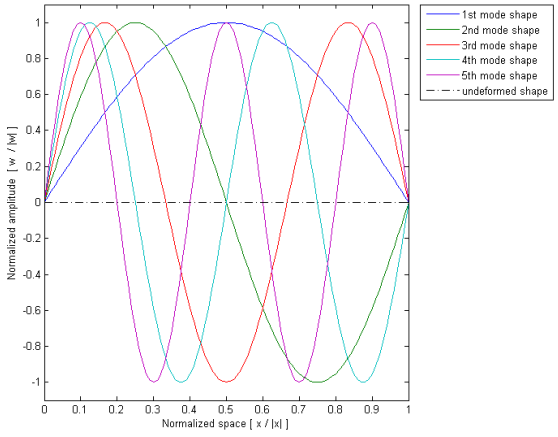

(a) no spring stiffness

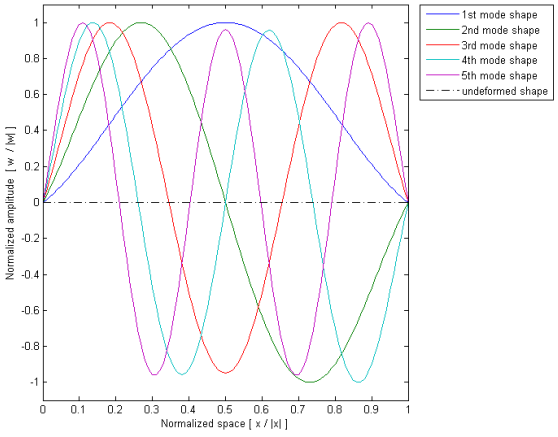

(b) small spring stiffnesses

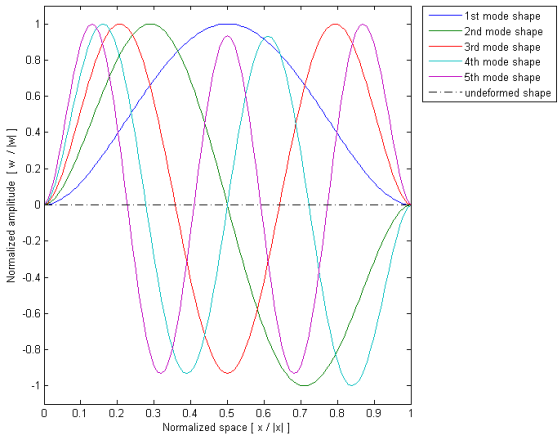

(c) large spring stiffness

Figure 8.6: Mode shapes with changing spring stiffnesses at both supports

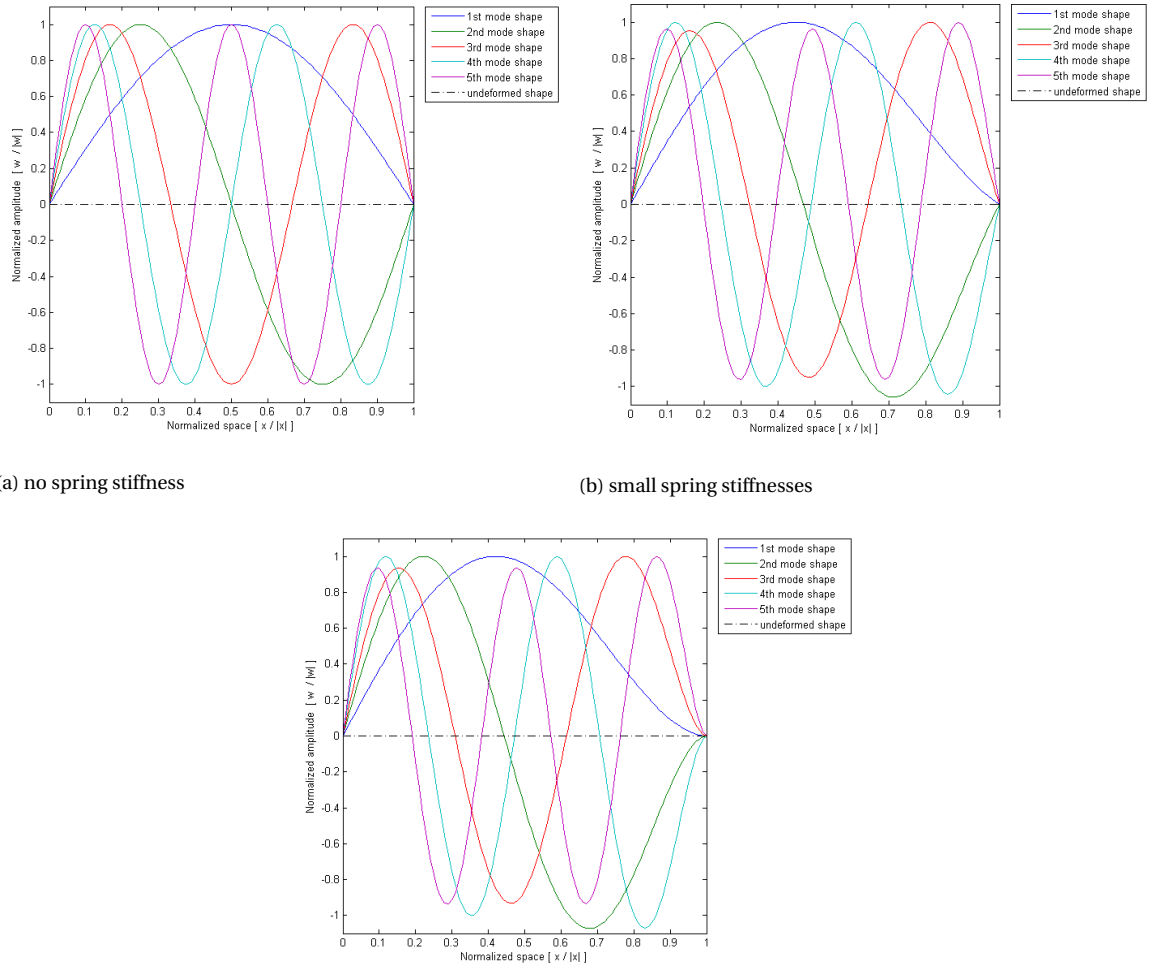

(a) no spring stiffness

(b) small spring stiffnesses

(c) large spring stiffness

Figure 8.7: Mode shapes with changing spring stiffnesses at the right support and simply supported at the left boundary

8.3.2. Extended Modal Analysis - Galerkin approximation for nonlinear part

Now we search for a solution to the system including nonlinearities and damping. The equation of motion and the boundary conditions are the following:

$$\rho A\frac{\partial^2 w}{\partial t^2}+\left(E+E*\frac{\partial}{\partial t}\right)I\frac{\partial^4 w}{\partial x^4}=0 \tag{8.80}$$

(1) $$w(0)=0 \tag{8.81}$$

(2) $$EI\frac{\partial^2 w}{\partial x^2}|_{x=0}=kr_1\left(\frac{\partial w}{\partial x}|_{x=0}-\varphi_c(t)\right)+cr_1\left(\frac{\partial^2 w}{\partial t\partial x}|_{x=0}-\dot{\varphi}_c(t)\right)+\mu_1 sgn\left(\frac{\partial^2 w}{\partial t\partial x}|_{x=0}-\dot{\varphi}_c(t)\right) \tag{8.82}$$

(3) $$w(L)=0 \tag{8.83}$$

(4) $$EI\frac{\partial^2 w}{\partial x^2}|_{x=L}=-kr_2\left(\frac{\partial w}{\partial x}|_{x=L}-\varphi_c(t)\right)-cr_2\left(\frac{\partial^2 w}{\partial t\partial x}|_{x=L}-\dot{\varphi}_c(t)\right)-\mu_2 sgn\left(\frac{\partial^2 w}{\partial t\partial x}|_{x=L}-\dot{\varphi}_c(t)\right) \tag{8.84}$$

Here $\varphi(t)$ and $\dot{\varphi}(t)$ are the rotations of the MLBS.

For implementing the Galerkin approximation, the part of the boundary conditions which is not satisfied by the natural mode shapes is introduced in the equation of motion. This part contains all forces concerning damping and ϕ_c. Boundary conditions (1) and (3) and the rotational springs are already met by the linear mode shapes:

$$w_n(x)=A_n\cosh(\beta_n x)+B_n\sinh(\beta_n x)+C_n\cos(\beta_n x)+D_n\sin(\beta_n x) \tag{8.85}$$

Rewriting the equation of motion gives:

$$\begin{aligned}\rho A\frac{\partial^2 w}{\partial t^2}+EI\frac{\partial^4 w}{\partial x^4}+E^*I\frac{\partial}{\partial t}\frac{\partial^4 w}{\partial x^4}&\\ =\delta'(x)\left\{cr_1\left(\frac{\partial^2 w}{\partial t\partial x}-\dot{\varphi}_c(t)\right)+\mu_1 sgn\left(\frac{\partial^2 w_f}{\partial t\partial x}-\dot{\varphi}_c(t)\right)+kr_1\left(-\varphi_c(t)\right)\right\}&\\ -\delta'(x-L)\left\{-cr_2\left(\frac{\partial^2 w}{\partial t\partial x}-\dot{\varphi}_c(t)\right)-\mu_2 sgn\left(\frac{\partial^2 w_f}{\partial t\partial x}-\dot{\varphi}_c(t)\right)-kr_2\left(-\varphi_c(t)\right)\right\}&\end{aligned} \tag{8.86}$$

Following the Galerkin Method, the trial solution is described by Equation 8.88, consisting of a summation of the product of a time related part and the mode shapes of the linear problem [29].

$$w(x,t)=\sum_{n=1}^{\infty}\psi_n(t)\,w_n(x) \tag{8.87}$$

Inserting in the equation of motion and solving the equation of motion will give a approximated solution containing a part with uncoupled modes and a residual, which is including the nonlinear part of the solution ([30], [24]).

$$w(x,t)=\sum_{m=1}^{\infty}\psi_m(t)\,w_m(x)+\text{res} \tag{8.88}$$

LHS

Substituting the trial solution into the equation of motion and using the relation between $w_n(x)$ and $w_n''''(x)$ gives for the left hand side of Equation 8.86 :

$$\text{LHS} = \rho A \frac{\partial^2 w}{\partial t^2} + EI \frac{\partial^4 w}{\partial x^4} + E^* I \frac{\partial}{\partial t} \frac{\partial^4 w}{\partial x^4} \tag{8.89}$$

$$= \rho A \sum_{n=1}^{\infty} \ddot{\psi}_n(t) w_n(x) + EI \sum_{n=1}^{\infty} \psi_n(t) w_n''''(x) + E^* I \sum_{n=1}^{\infty} \dot{\psi}_n(t) w_n''''(x) \tag{8.90}$$

$$= \rho A \sum_{n=1}^{\infty} \ddot{\psi}_n(t) w_n(x) + EI \sum_{n=1}^{\infty} \psi_n(t) \beta_n^4 w_n(x) + E^* I \sum_{n=1}^{\infty} \dot{\psi}_n(t) \beta_n^4 w_n(x) \tag{8.91}$$

$$= \rho A \sum_{n=1}^{\infty} \ddot{\psi}_n(t) w_n(x) + EI \beta_n^4 \sum_{n=1}^{\infty} \psi_n(t) w_n(x) + E^* I \beta_n^4 \sum_{n=1}^{\infty} \dot{\psi}_n(t) w_n(x) \tag{8.92}$$

The Galerkin's projection is obtained by multiplication of the equation of motion with a base function $w_m(x)$ which fit the non-damped linear boundary conditions, the mode shapes, and then by integration over the length of the beam [81]. Using the orthogonality conditions of the mode shapes, which gives that $\int w_n(x) w_m(x) dx = 0$ for $n \neq m$ [14], the modes can be uncoupled.

$$\int_0^L \text{LHS} w_m^2(x) dx = \int_0^L \left(\rho A \sum_{n=1}^{\infty} \ddot{\psi}_n(t) w_n(x) \right) w_m(x) dx + \int_0^L \left(EI \beta_n^4 \sum_{n=1}^{\infty} \psi_n(t) w_n(x) \right) w_m(x) dx + \int_0^L \left(E^* I \beta_n^4 \sum_{n=1}^{\infty} \dot{\psi}_n(t) w_n(x) \right) w_m(x) dx \tag{8.93}$$

$$= \rho A \ddot{\psi}_m(t) \int_0^L w_m^2(x) dx + EI \beta_m^4 \psi_m(t) \int_0^L w_m^2(x) dx + E^* I \beta_m^4 \dot{\psi}_m(t) \int_0^L w_m^2(x) dx \tag{8.94}$$

where $\int_0^L w_m^2(x) dx$ is defined as:

$$\int_0^L w_m^2(x) dx = \int_0^L \left(A_m \cosh(\beta_m x) + B_m \sinh(\beta_m x) + C_m \cos(\beta_m x) + D_m \sin(\beta_m x) \right)^2 dx \tag{8.95}$$

$$\begin{aligned}
&= \frac{1}{8} \frac{1}{\beta_m} (-4 A_m \exp^{2\beta_m L} B_m + 2 A_m \exp^{4\beta_m L} B_m \\
&+ 8 A_m D_m \exp^{2\beta_m L} - 8 B_m C_m \exp^{2\beta_m L} + 8 C_m D_m \exp^{2\beta_m L} + B_m^2 \exp^{4\beta_m L} \\
&+ A_m^2 \exp^{4\beta_m L} + 4 A_m C_m \exp^{3\beta_m L} \cos(\beta_m L) + 4 A_m C_m \exp^{3\beta_m L} \sin(\beta_m L) \\
&- 4 A_m C_m \exp^{\beta_m L} \cos(\beta_m L) + 4 A_m C_m \exp^{\beta_m L} \sin(\beta_m L) - 4 A_m D_m \exp^{\beta_m L} \cos(\beta_m L) \\
&- 4 A_m D_m \exp^{\beta_m L} \sin(\beta_m L) + 4 B_m C_m \exp^{\beta_m L} \cos(\beta_m L) - 4 B_m C_m \exp^{\beta_m L} \sin(\beta_m L) \\
&+ 4 B_m D_m \exp^{\beta_m L} \cos(\beta_m L) + 4 B_m D_m \exp^{\beta_m L} \sin(\beta_m L) - 4 A_m D_m \exp^{3\beta_m L} \cos(\beta_m L) \\
&+ 4 A_m D_m \exp^{3\beta_m L} \sin(\beta_m L) - 4 B_m^2 \beta_m L \exp^{2\beta_m L} + 4 B_m C_m \exp^{3\beta_m L} \cos(\beta_m L) \\
&+ 4 B_m C_m \exp^{3\beta_m L} \sin(\beta_m L) - 4 B_m D_m \exp^{3\beta_m L} \cos(\beta_m L) + 4 B_m D_m \exp^{3\beta_m L} \sin(\beta_m L) \\
&+ 4 C_m^2 L \exp^{2\beta_m L} \beta_m + 4 C_m^2 \exp^{2\beta_m L} \cos(\beta_m L) \sin(\beta_m L) - 8 C_m D_m \cos(\beta_m L)^2 \exp^{2\beta_m L} \\
&+ 4 D_m^2 L \exp^{2\beta_m L} \beta_m - 4 D_m^2 \exp^{2\beta_m L} \cos(\beta_m L) \sin(\beta_m L) + 4 A_m^2 \beta_m L \exp^{2\beta_m L} \\
&+ 2 A_m B_m - A_m^2 - B_m^2) \exp^{-2\beta_m L}
\end{aligned} \tag{8.96}$$

$$\int_0^L w_m^2(x) dx = C_{w_m} \tag{8.97}$$

which gives a constant. As can be seen, all terms in the LHS contain fully uncoupled modes.

RHS

Exactly the same are taken for the right hand side. Substituting the general solution into the equation of motion and expressing the approximate solution in linear mode shapes gives for the right hand side of Equation 8.86 :

$$\begin{aligned}\text{RHS} = \delta'(x)&\left\{cr_1\left(\frac{\partial^2 w}{\partial t\partial x}-\dot{\varphi}_c(t)\right)+\mu_1 sgn\left(\frac{\partial^2 w_f}{\partial t\partial x}-\dot{\varphi}_c(t)\right)+kr_1\left(-\varphi_c(t)\right)\right\}\\ &-\delta'(x-L)\left\{-cr_2\left(\frac{\partial^2 w}{\partial t\partial x}-\dot{\varphi}_c(t)\right)-\mu_2 sgn\left(\frac{\partial^2 w_f}{\partial t\partial x}-\dot{\varphi}_c(t)\right)-kr_2\left(-\varphi_c(t)\right)\right\} \quad (8.98)\\ =\delta'(x)&\left\{M_{BC,l}\left(\frac{\partial^2 w}{\partial t\partial x},\dot{\varphi}_c(t),\varphi_c(t)\right)\right\}-\delta'(x-L)\left\{M_{BC,r}\left(\frac{\partial^2 w}{\partial t\partial x},\dot{\varphi}_c(t),\varphi_c(t)\right)\right\} \quad (8.99)\\ =\delta'(x)&\left\{M_{BC,l}\left(\sum_{n=1}^{\infty}\dot{\psi}_n(t)w_n'(x),\dot{\varphi}_c(t),\varphi_c(t)\right)\right\}-\delta'(x-L)\left\{M_{BC,r}\left(\sum_{n=1}^{\infty}\dot{\psi}_n(t)w_n'(x),\dot{\varphi}_c(t),\varphi_c(t)\right)\right\} \quad (8.100)\end{aligned}$$

Where

$$M_{BC,l}\left(\frac{\partial^2 w(x,t)}{\partial t\partial x},\dot{\varphi}_c(t),\varphi_c(t)\right)=cr_1\left(\frac{\partial^2 w(x,t)}{\partial t\partial x}-\dot{\varphi}_c(t)\right)+\mu_1 sgn\left(\frac{\partial^2 w(x,t)}{\partial t\partial x}-\dot{\varphi}_c(t)\right)+kr_1\left(-\varphi_c(t)\right) \quad (8.101)$$

$$M_{BC,r}\left(\frac{\partial^2 w(x,t)}{\partial t\partial x},\dot{\varphi}_c(t),\varphi_c(t)\right)=-cr_2\left(\frac{\partial^2 w(x,t)}{\partial t\partial x}-\dot{\varphi}_c(t)\right)-\mu_2 sgn\left(\frac{\partial^2 w(x,t)}{\partial t\partial x}-\dot{\varphi}_c(t)\right)-kr_2\left(-\varphi_c(t)\right) \quad (8.102)$$

Multiplication with me mode shapes $w_m(x)$ and integration over the length of the beam gives the right hand side of Galerkin's projection.

$$\begin{aligned}\int_0^L \text{RHS}\,w_m(x)dx=&\int_0^L\delta'(x)\left\{M_{BC,l}\left(\sum_{n=1}^{\infty}\dot{\psi}_n(t)w_n'(x),\dot{\varphi}_c(t),\varphi_c(t)\right)\right\}w_m(x)dx\\ &-\int_0^L\delta'(x-L)\left\{M_{BC,r}\left(\sum_{n=1}^{\infty}\dot{\psi}_n(t)w_n'(x),\dot{\varphi}_c(t),\varphi_c(t)\right)\right\}w_m(x)dx \quad (8.103)\end{aligned}$$

Using partial integration removes the derivative of the Delta Dirac function and gives us the following form of the equation:

$$\begin{aligned}\int_0^L\delta'(x-a)f(x)w_m(x)dx&=\left[f(x)w_m(x)\delta(x-a)\right]_0^L-\int_0^L\delta(x-a)\frac{d}{dx}\left(f(x)w_m(x)\right)dx \quad (8.104)\\ &=\left[f(x)w_m(x)\delta(x-a)\right]_0^L-\int_0^L\delta(x-a)\left(f'(x)w_m(x)+f(x)w_m'(x)\right)dx \quad (8.105)\end{aligned}$$

Because $w_m(x)=0$ for $x=0$ and $x=L$, the first term falls out of the equation leaving

$$\int_0^L\delta'(x-a)f(x)w_m(x)dx=-\int_0^L\delta(x-a)\left(f'(x)w_m(x)+f(x)w_m'(x)\right)dx \quad (8.106)$$

using the properties of the Delta-Dirac function

$$\int_{-\infty}^{\infty}\delta(x-a)g(x)=f'(a)w_m(a)+f(a)w_m'(a) \quad (8.107)$$

and because of the boundary conditions the first term falls out of the equation, leaving

$$\int_0^L\delta'(x-a)f(x)w_m(x)dx=-f(a)w_m'(a) \quad (8.108)$$

Now, using this relation in Equation 8.103 gives:

$$\begin{aligned}
&\int_0^L \text{RHS} w_m(x)dx \\
&= \int_0^L \delta'(x)\left\{M_{BC,l}\left(\sum_{n=1}^{\infty}\dot{\psi}_n(t)w_n'(x),\dot{\varphi}_c(t),\varphi_c(t)\right)\right\}w_m(x)dx \\
&\qquad - \int_0^L \delta'(x-L)\left\{M_{BC,r}\left(\sum_{n=1}^{\infty}\dot{\psi}_n(t)w_n'(x),\dot{\varphi}_c(t),\varphi_c(t)\right)\right\}w_m(x)dx \qquad (8.109)\\
&= -M_{BC,l}\left(\sum_{n=1}^{\infty}\dot{\psi}_n(t)w_n'(0),\dot{\varphi}_c(t),\varphi_c(t)\right)w_m'(0) + M_{BC,r}\left(\sum_{n=1}^{\infty}\dot{\psi}_n(t)w_n'(L),\dot{\varphi}_c(t),\varphi_c(t)\right)w_m'(L) \qquad (8.110)\\
&= -cr_1\left(\sum_{n=1}^{\infty}\dot{\psi}_n(t)w_n'(0)-\dot{\varphi}_c(t)\right)w_m'(0) - \mu_1 sgn\left(\sum_{n=1}^{\infty}\dot{\psi}_n(t)w_n'(0)-\dot{\varphi}_c(t)\right)w_m'(0) \\
&\qquad - kr_1\left(-\varphi_c(t)\right)w_m'(0) - cr_2\left(\sum_{n=1}^{\infty}\dot{\psi}_n(t)w_n'(L)-\dot{\varphi}_c(t)\right)w_m'(L) \\
&\qquad - \mu_2 sgn\left(\sum_{n=1}^{\infty}\dot{\psi}_n(t)w_n'(L)-\dot{\varphi}_c(t)\right)w_m'(L) - kr_2\left(-\varphi_c(t)\right)w_m'(L) \qquad (8.111)
\end{aligned}$$

LHS and RHS combined

The LHS is after the multiplication with a base function and integration over the beam length transformed into uncoupled terms independent of x, the right hand side, however, is still coupled and x-dependent with two Delta Dirac functions present. The complete equation becomes:

$$\begin{aligned}
&\rho A\ddot{\psi}_m(t)\int_0^L w_m^2(x)dx + EI\beta_m^4\psi_m(t)\int_0^L w_m^2(x)dx + E^*I\beta_m^4\dot{\psi}_m(t)\int_0^L w_m^2(x)dx \\
&\qquad = -cr_1\left(\sum_{n=1}^{\infty}\dot{\psi}_n(t)w_n'(0)-\dot{\varphi}_c(t)\right)w_m'(0) - \mu_1 sgn\left(\sum_{n=1}^{\infty}\dot{\psi}_n(t)w_n'(0)-\dot{\varphi}_c(t)\right)w_m'(0) \\
&\qquad\qquad - kr_1\left(-\varphi_c(t)\right)w_m'(0) - cr_2\left(\sum_{n=1}^{\infty}\dot{\psi}_n(t)w_n'(L)-\dot{\varphi}_c(t)\right)w_m'(L) \\
&\qquad\qquad - \mu_2 sgn\left(\sum_{n=1}^{\infty}\dot{\psi}_n(t)w_n'(L)-\dot{\varphi}_c(t)\right)w_m'(L) - kr_2\left(-\varphi_c(t)\right)w_m'(L) \qquad (8.112)
\end{aligned}$$

Shortened to:

$$\begin{aligned}
&\rho A\ddot{\psi}_m(t)C_{w_m} + EI\beta_m^4\psi_m(t)C_{w_m} + E^*I\beta_m^4\dot{\psi}_m(t)C_{w_m} \\
&\qquad = -cr_1\left(\sum_{n=1}^{\infty}\dot{\psi}_n(t)w_n'(0)-\dot{\varphi}_c(t)\right)w_m'(0) - \mu_1 sgn\left(\sum_{n=1}^{\infty}\dot{\psi}_n(t)w_n'(0)-\dot{\varphi}_c(t)\right)w_m'(0) \\
&\qquad\qquad - kr_1\left(-\varphi_c(t)\right)w_m'(0) - cr_2\left(\sum_{n=1}^{\infty}\dot{\psi}_n(t)w_n'(L)-\dot{\varphi}_c(t)\right)w_m'(L) \\
&\qquad\qquad - \mu_2 sgn\left(\sum_{n=1}^{\infty}\dot{\psi}_n(t)w_n'(L)-\dot{\varphi}_c(t)\right)w_m'(L) - kr_2\left(-\varphi_c(t)\right)w_m'(L) \qquad (8.113)
\end{aligned}$$

For solving it numerically, first the highest order derivative, ψ_n, is factored out. Resulting is Equation 8.115, which can be solved numerically.

$$\begin{aligned}\ddot{\psi}_m(t) = &- \frac{cr_1\left(\sum_{n=1}^{\infty}\dot{\psi}_n(t)\,w_n'(0) - \dot{\varphi}_c(t)\right)w_m'(0)}{C_{w_m}\rho A} - \frac{\mu_1 sgn\left(\sum_{n=1}^{\infty}\dot{\psi}_n(t)\,w_n'(0) - \dot{\varphi}_c(t)\right)w_m'(0)}{C_{w_m}\rho A} \\ &- \frac{kr_1\left(-\varphi_c(t)\right)w_m'(0)}{C_{w_m}\rho A} - \frac{cr_2\left(\sum_{n=1}^{\infty}\dot{\psi}_n(t)\,w_n'(L) - \dot{\varphi}_c(t)\right)w_m'(L)}{C_{w_m}\rho A} \\ &- \frac{\mu_2 sgn\left(\sum_{n=1}^{\infty}\dot{\psi}_n(t)\,w_n'(L) - \dot{\varphi}_c(t)\right)w_m'(L)}{C_{w_m}\rho A} - \frac{kr_2\left(-\varphi_c(t)\right)w_m'(L)}{C_{w_m}\rho A} \\ &- \frac{EI}{\rho A}\beta_m^4\psi_m(t) - \frac{E^*I}{\rho A}\beta_m^4\dot{\psi}_m(t) \end{aligned} \tag{8.114}$$

$$\begin{aligned}\ddot{\psi}_m(t) = &- \frac{cr_1\left(\sum_{n=1}^{\infty}\dot{\psi}_n(t)\,w_n'(0) - \dot{\varphi}_c(t)\right)w_m'(0)}{C_{w_m}\rho A} - \frac{\mu_1 sgn\left(\sum_{n=1}^{\infty}\dot{\psi}_n(t)\,w_n'(0) - \dot{\varphi}_c(t)\right)w_m'(0)}{C_{w_m}\rho A} \\ &- \frac{kr_1\left(-\varphi_c(t)\right)w_m'(0)}{C_{w_m}\rho A} - \frac{cr_2\left(\sum_{n=1}^{\infty}\dot{\psi}_n(t)\,w_n'(L) - \dot{\varphi}_c(t)\right)w_m'(L)}{C_{w_m}\rho A} \\ &- \frac{\mu_2 sgn\left(\sum_{n=1}^{\infty}\dot{\psi}_n(t)\,w_n'(L) - \dot{\varphi}_c(t)\right)w_m'(L)}{C_{w_m}\rho A} - \frac{kr_2\left(-\varphi_c(t)\right)w_m'(L)}{C_{w_m}\rho A} \\ &- \omega_m^2\psi_m(t) - \frac{E^*I}{EI}\omega_m^2\dot{\psi}_m(t) \end{aligned} \tag{8.115}$$

Summary analytical equations

$$w(x,t) = \sum_{n=1}^{\infty} \psi_n(t)\, w_n(x) \tag{8.116}$$

$$\begin{aligned}\ddot{\psi}_m(t) = &- \frac{cr_1\left(\sum_{n=1}^{\infty}\dot{\psi}_n(t)\,w_n'(0) - \dot{\varphi}_c(t)\right)w_m'(0)}{C_{w_m}\rho A} - \frac{\mu_1 sgn\left(\sum_{n=1}^{\infty}\dot{\psi}_n(t)\,w_n'(0) - \dot{\varphi}_c(t)\right)w_m'(0)}{C_{w_m}\rho A} \\ &- \frac{kr_1\left(-\varphi_c(t)\right)w_m'(0)}{C_{w_m}\rho A} - \frac{cr_2\left(\sum_{n=1}^{\infty}\dot{\psi}_n(t)\,w_n'(L) - \dot{\varphi}_c(t)\right)w_m'(L)}{C_{w_m}\rho A} \\ &- \frac{\mu_2 sgn\left(\sum_{n=1}^{\infty}\dot{\psi}_n(t)\,w_n'(L) - \dot{\varphi}_c(t)\right)w_m'(L)}{C_{w_m}\rho A} - \frac{kr_2\left(-\varphi_c(t)\right)w_m'(L)}{C_{w_m}\rho A} \\ &- \omega_m^2\psi_m(t) - \frac{E^*I}{EI}\omega_m^2\dot{\psi}_m(t)\end{aligned} \tag{8.117}$$

where

$$C_{w_m} = \int_0^L w_m^2(x)\,dx \tag{8.118}$$

and

$$w_i(x) = A_i\cosh(\beta_i x) + B_i\sinh(\beta_i x) + C_i\cos(\beta_i x) + D_i\sin(\beta_i x) \tag{8.119}$$

$$w_i'(x) = A_i\beta_i\sinh(\beta_i x) + B_i\beta_i\cosh(\beta_i x) - C_i\beta_i\sin(\beta_i x) + D_i\beta_i\cos(\beta_i x) \tag{8.120}$$

with

$$\begin{aligned}A_i = &(EI\sinh(\beta_i L)\beta_i + \cosh(\beta_i L)kr_2)kr_1/(2EI^2\sinh(\beta_i L)\beta_i^2 + EI\cosh(\beta_i L)\beta_i kr_1 \\ &+2EI\cosh(\beta_i L)\beta_i kr_2 + EI\cos(\beta_i L)\beta_i kr_1 + \sinh(\beta_i L)kr_1kr_2 + \sin(\beta_i L)kr_1kr_2) \\ &+kr_1(EI\beta_i^2\sin(\beta_i L) - kr_2\beta_i\cos(\beta_i L))/(\beta_i(2EI^2\sinh(\beta_i L)\beta_i^2 + EI\cosh(\beta_i L)\beta_i kr_1 \\ &+2EI\cosh(\beta_i L)\beta_i kr_2 + EI\cos(\beta_i L)\beta_i kr_1 + \sinh(\beta_i L)kr_1kr_2 + \sin(\beta_i L)kr_1kr_2))\end{aligned} \tag{8.121}$$

$$\begin{aligned}B_i = &-(EI\cosh(\beta_i L)\beta_i + EI\cos(\beta_i L)\beta_i + \sinh(\beta_i L)kr_2 \\ &+\sin(\beta_i L)kr_2)kr_1/(2EI^2\sinh(\beta_i L)\beta_i^2 + EI\cosh(\beta_i L)\beta_i kr_1 + 2EI\cosh(\beta_i L)\beta_i kr_2 \\ &+EI\cos(\beta_i L)\beta_i kr_1 + \sinh(\beta_i L)kr_1kr_2 + \sin(\beta_i L)kr_1kr_2) + 2EI(EI\beta_i^2\sin(\beta_i L) \\ &-kr_2\beta_i\cos(\beta_i L))/(2EI^2\sinh(\beta_i L)\beta_i^2 + EI\cosh(\beta_i L)\beta_i kr_1 + 2EI\cosh(\beta_i L)\beta_i kr_2 \\ &+EI\cos(\beta_i L)\beta_i kr_1 + \sinh(\beta_i L)kr_1kr_2 + \sin(\beta_i L)kr_1kr_2)\end{aligned} \tag{8.122}$$

$$\begin{aligned}C_i = &-(EI\sinh(\beta_i L)\beta_i + \cosh(\beta_i L)kr_2)kr_1/(2EI^2\sinh(\beta_i L)\beta_i^2 + EI\cosh(\beta_i L)\beta_i kr_1 \\ &+2EI\cosh(\beta_i L)\beta_i kr_2 + EI\cos(\beta_i L)\beta_i kr_1 + \sinh(\beta_i L)kr_1kr_2 + \sin(\beta_i L)kr_1kr_2) \\ &-kr_1(EI\beta_i^2\sin(\beta_i L) - kr_2\beta_i\cos(\beta_i L))/(\beta_i(2EI^2\sinh(\beta_i L)\beta_i^2 + EI\cosh(\beta_i L)\beta_i kr_1 \\ &+2EI\cosh(\beta_i L)\beta_i kr_2 + EI\cos(\beta_i L)\beta_i kr_1 + \sinh(\beta_i L)kr_1kr_2 + \sin(\beta_i L)kr_1kr_2))\end{aligned} \tag{8.123}$$

$$D_i = 1 \tag{8.124}$$

and

$$\beta_i^4 = \frac{\rho A\omega_i^2}{EI} \tag{8.125}$$

a function of the natural frequency

8.3.3. Extended Modal Analysis - Numerical integration

For solving the time function numerically using the Runge-Kutta integration scheme, first the second order derivative is transformed into a set of coupled first order equations. Introducing two new parameters, $q_m(t)$ and $p_m(t)$.

$$\begin{cases} q_m(t) = \psi_m(t) \\ v_m(t) = \dot{\psi}_m(t) \end{cases} \tag{8.126}$$

$$\begin{cases} \dot{q_m}(t) = \dot{\psi}_m(t) \\ \dot{v_m}(t) = \ddot{\psi}_m(t) \end{cases} \tag{8.127}$$

Using the variables as determined in Section C.2 gives for each mode the following set of equations that can be solved numerically.

$$\begin{cases} \dot{q_m}(t) = v_m \\ \dot{v_m}(t) = -\dfrac{cr_1\left(\sum_{n=1}^{\infty} v_n(t)\,w_n'(0) - \dot{\varphi}_c(t)\right)w_m'(0)}{C_{w_m}\rho A} - \dfrac{\mu_1 sgn\left(\sum_{n=1}^{\infty} v_n(t)\,w_n'(0) - \dot{\varphi}_c(t)\right)w_m'(0)}{C_{w_m}\rho A} \\ \qquad - \dfrac{kr_1\left(-\varphi_c(t)\right)w_m'(0)}{C_{w_m}\rho A} - \dfrac{cr_2\left(\sum_{n=1}^{\infty} v_n(t)\,w_n'(L) - \dot{\varphi}_c(t)\right)w_m'(L)}{C_{w_m}\rho A} \\ \qquad - \dfrac{\mu_2 sgn\left(\sum_{n=1}^{\infty} v_n(t)\,w_n'(L) - \dot{\varphi}_c(t)\right)w_m'(L)}{C_{w_m}\rho A} - \dfrac{kr_2\left(-\varphi_c(t)\right)w_m'(L)}{C_{w_m}\rho A} \\ \qquad - \omega_m^2 q_m(t) - \dfrac{E^* I}{EI}\omega_m^2 v_m(t) \end{cases}$$

For the one-mode approximation, $m = 1$ and $n = 1$,, where only one uncoupled mode and also only one coupled mode is taken into account for the calculation of $\varphi(t)$, this gives two coupled equations. This is a coarse approximation of the first mode, because many uncoupled modes should be taken into account for an accurate approximation for the first mode. The actual response is now the product of the solution for $\varphi_1(t)$ and $w_1(x)$.

$$\begin{cases} \dot{q_1}(t) = v_1 \\ \dot{v_1}(t) = -\dfrac{cr_1\left(v_1(t)\,w_1'(0) - \dot{\varphi}_c(t)\right)w_1'(0)}{C_{w_1}\rho A} - \dfrac{\mu_1 sgn\left(v_1(t)\,w_1'(0) - \dot{\varphi}_c(t)\right)w_1'(0)}{C_{w_1}\rho A} \\ \qquad - \dfrac{kr_1\left(-\varphi_c(t)\right)w_1'(0)}{C_{w_1}\rho A} - \dfrac{cr_2\left(v_1(t)\,w_1'(L) - \dot{\varphi}_c(t)\right)w_1'(L)}{C_{w_1}\rho A} \\ \qquad - \dfrac{\mu_2 sgn\left(v_1(t)\,w_1'(L) - \dot{\varphi}_c(t)\right)w_1'(L)}{C_{w_1}\rho A} - \dfrac{kr_2\left(-\varphi_c(t)\right)w_1'(L)}{C_{w_1}\rho A} \\ \qquad - \omega_1^2 q_1(t) - \dfrac{E^* I}{EI}\omega_1^2 v_1(t) \end{cases}$$

8.3.3.1. Multiple (M) mode approximation

For the N-mode approximation, $2M$ coupled equations are obtained when calculating $\varphi_m(t)$. At each mode m, the corresponding uncoupled mode is representing the linear part. For the nonlinear part all coupled modes N should be taken into account.

$$
\begin{cases}
\dot{q}_1(t) = v_1 \\
\dot{v}_1(t) = -\dfrac{cr_1\left(\sum_{n=1}^{N} v_n(t)\,w_n'(0) - \dot{\varphi}_c(t)\right)w_m'(0)}{C_{w_m}\rho A} - \dfrac{\mu_1 sgn\left(\sum_{n=1}^{N} v_n(t)\,w_n'(0) - \dot{\varphi}_c(t)\right)w_m'(0)}{C_{w_m}\rho A} \\
\qquad - \dfrac{kr_1\left(-\varphi_c(t)\right)w_m'(0)}{C_{w_m}\rho A} - \dfrac{cr_2\left(\sum_{n=1}^{N} v_n(t)\,w_n'(L) - \dot{\varphi}_c(t)\right)w_m'(L)}{C_{w_m}\rho A} \\
\qquad - \dfrac{\mu_2 sgn\left(\sum_{n=1}^{N} v_n(t)\,w_n'(L) - \dot{\varphi}_c(t)\right)w_m'(L)}{C_{w_m}\rho A} - \dfrac{kr_2\left(-\varphi_c(t)\right)w_m'(L)}{C_{w_m}\rho A} \\
\qquad - \omega_1^2 q_1(t) - \dfrac{E^* I}{EI}\omega_1^2 v_1(t) \\
\dot{q}_2(t) = v_2 \\
\dot{v}_2(t) = -\dfrac{cr_1\left(\sum_{n=1}^{N} v_n(t)\,w_n'(0) - \dot{\varphi}_c(t)\right)w_m'(0)}{C_{w_m}\rho A} - \dfrac{\mu_1 sgn\left(\sum_{n=1}^{N} v_n(t)\,w_n'(0) - \dot{\varphi}_c(t)\right)w_m'(0)}{C_{w_m}\rho A} \\
\qquad - \dfrac{kr_1\left(-\varphi_c(t)\right)w_n'(0)}{C_{w_m}\rho A} - \dfrac{cr_2\left(\sum_{n=1}^{N} v_n(t)\,w_m'(L) - \dot{\varphi}_c(t)\right)w_m'(L)}{C_{w_m}\rho A} \\
\qquad - \dfrac{\mu_2 sgn\left(\sum_{n=1}^{N} v_n(t)\,w_n'(L) - \dot{\varphi}_c(t)\right)w_m'(L)}{C_{w_m}\rho A} - \dfrac{kr_2\left(-\varphi_c(t)\right)w_m'(L)}{C_{w_m}\rho A} \\
\qquad - \omega_2^2 q_2(t) - \dfrac{E^* I}{EI}\omega_2^2 v_2(t) \\
\quad \vdots \\
\dot{q_m}(t) = v_m \\
\dot{v_m}(t) = -\dfrac{cr_1\left(\sum_{n=1}^{N} v_n(t)\,w_n'(0) - \dot{\varphi}_c(t)\right)w_m'(0)}{C_{w_m}\rho A} - \dfrac{\mu_1 sgn\left(\sum_{n=1}^{N} v_n(t)\,w_n'(0) - \dot{\varphi}_c(t)\right)w_m'(0)}{C_{w_m}\rho A} \\
\qquad - \dfrac{kr_1\left(-\varphi_c(t)\right)w_m'(0)}{C_{w_m}\rho A} - \dfrac{cr_2\left(\sum_{n=1}^{N} v_n(t)\,w_n'(L) - \dot{\varphi}_c(t)\right)w_m'(L)}{C_{w_m}\rho A} \\
\qquad - \dfrac{\mu_2 sgn\left(\sum_{n=1}^{N} v_n(t)\,w_n'(L) - \dot{\varphi}_c(t)\right)w_m'(L)}{C_{w_m}\rho A} - \dfrac{kr_2\left(-\varphi_c(t)\right)w_m'(L)}{C_{w_m}\rho A} \\
\qquad - \omega_m^2 q_m(t) - \dfrac{E^* I}{EI}\omega_m^2 v_m(t)
\end{cases}
$$

The actual response of the system is given with:

$$w(x,t) = \sum_{i=1}^{M} \psi_i(t)\,w_i(x) \tag{8.128}$$

for an approximation with M modes.

8.3.4. Convergence of additional modes

The amount of n coupled contributions present in the modes m and the amount of uncoupled modes m present in the actual response should be determined. At the numerical integration the number of linear modes that are calculated should be equal or larger than the number of coupled modes as can be seen by Equation 8.128, because those non-linear contributions are based on the modes. And thus at least $m = n$ modes should be calculated for n non-linear contributions.

The final solution is described with a simple summation from the obtained output for each mode after the numerical integration:

$$w(x,t) = \sum_{i=1}^{M} \psi_i(t)\, w_i(x) \tag{8.129}$$

Here, M indicates the number of m modes that are taken into account in the final solution. The computational effort is therefore much larger for increasing the non-linear contribution, then for adding an additional mode to the final solution. Therefore, the number of linear modes m and non-linear mode contributions n that is taken into account is equal.

The number of non-linear and linear modes that are taken into account when modeling is determined by looking at the convergence of the error by adding more modes to the final solution. The rate of convergence depends on several factors. Firstly, the type of external loading and the initial conditions of the system. When the loading frequency changes, the contributions of frequencies close to the loading frequency changes. Secondly, the position at the beam for which the convergence of additional modes is studied has an influence. Positions close to knots of modes, encounter smaller contributions from those modes.

The rate of convergence in our case is studied for the response at one-fourth of the beam, the position which experienced the largest amplitudes and the position where the model outcome is compared with the experimental response. The difference in total area of the fft of the response at 1/4 th og the beam , based on the addition of a Nth mode is determined. At the sixt mode the error is reduced to 99 % of the initial error comparing the first and second mode and at the 10th mode 99.5 %. At very high modes, above mode number 15, the error was found to fluctuate and no accurate prediction of the real error could be given. This fluctuation was probably related to a numerical error for calculating the natural frequencies and modes. The 6th mode coincides with a frequency around 104 Hz and the 10th mode with a frequency of 285.3 Hz.

9

MODEL VALIDATION: PARAMETER CALIBRATION AND SENSITIVITY STUDY

In this chapter the outcome of the analytical model and it's implementation in Matlab2013a is studied and validated with the experiment. The chapter consists out of three parts. In the first part assumptions for the parameters are searched based on literature, experimental measurements and studies on reference model. In the second part the sensitivity of each damping parameter is studied with regard to the presented 1D model. In the third part a set of parameters is presented which compares the modeled outcome with the experimental results.

9.1. First assumptions for model parameters

The length of the beam between the two connections, L, was measured as 1150 mm. The inertial mass, ρA, is equal to the weight per meter of the beam. From measurements it was found that the concrete beam of length 1340.0 mm had a weight of 27.5 kg with an accuracy of 0.1 kg. The measured mass gave a ρA of 20.5 kg/m. A was measured as 0.0098 m^2, resulting in a density of $\rho = 2000$ kg/m^2, which is around 20% less than normal construction concrete of 2400 kg/m^2. The concrete was thus of lower quality than standard construction concrete.

Assumptions for stiffness

The beam stiffness was calculated from static deflections obtained during the built-up of the experiment for the simply supported and connected situation. After applying a load of 130 kg distributed over the middle

290 mm of a simply supported beam, a deflection of 0.210 mm was measured. For the connected situation deflections of 0.084 mm and 0.120 mm were measured in setup Test A and setup Test B respectively. With

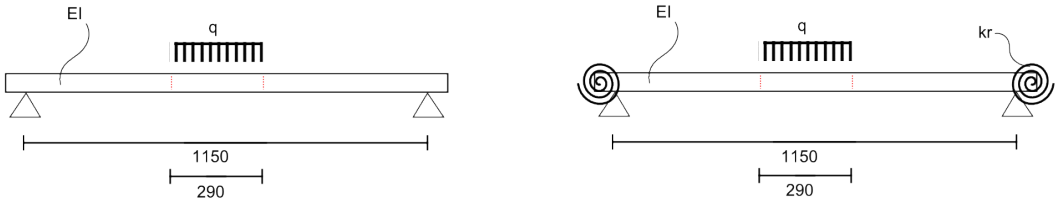

(a) Reference EB model, simply supported

(b) Reference EB model with two rotational springs

Figure 9.1: models for stiffness calculation

simple static calculations the beam stiffness belonging to the measured value was determined at 184.8 Nm^2, using a simply supported Euler Bernoulli beam reference model, see Figure H.1a. For the calculation of the spring stiffnesses, a reference model with two equally stiff rotational springs at the two boundaries was used as shown in Figure H.1b. For Test A the stiffness was determined at 1215.4 Nm/rad and for Test B at 417.3 Nm/rad. For full calculations see Appendix H.

From the values set above, the natural frequencies of the system were calculated, see Table 9.1. These frequencies differed from the frequencies observed in the experimental test. As described in Table 9.3, the first strongly excited natural frequency found was 13.5 Hz. This frequency corresponded with the second mode of the floor. A parameter fitting script starting at the calculated values above, was used to find values for k_r and EI that would reproduce a second natural frequency corresponding with the second natural frequency found from the test measurements. After several calibrations new estimates for the stiffness were found: $kr_i = 574.4$ and $EI = 110.6$.

	Test A	**Test B**
1st	6.07	4.95
2nd	17.90	16.14
3rd	36.67	34.49
4th	62.54	60.08
5rd	95.60	92.94
6th	135.88	133.08
7th	183.42	180.51
8th	238.23	235.23
9th	300.30	297.25
10th	369.67	366.55

Table 9.1: Calculated natural frequencies for first assumptions for EI and kr based on statical calculations

	Test A	**Test B**
1st	4.49	4.02
2nd	13.50	12.75
3rd	27.92	26.99
4th	47.86	46.82
5rd	73.38	72.6
6th	104.51	103.34
7th	141.26	140.05
8th	183.64	182.40
9th	231.66	230.38
10th	285.31	284.01

Table 9.2: Calculated natural frequencies after several calibrations for EI and kr

	Test A	**Test B**
1st	?	?
2nd	13.5	12.75
3rd	?	?
4th	48.8	53.6
5rd	?	?
6th	94.5	122.4
7th	113?	?
8th	176.9	193
9th	?	?
10th	281.2	279

Table 9.3: Determined natural frequencies from FRF acceleration functions during experiment

Assumptions for column rotations

The rotations of the column, $\phi(t)$, were calculated from the measured accelerations at the left column. A bandpass-filter was used to remove frequencies above 1000 Hz and below 3 Hz to limit noise within the measurements and to preventing errors from numerical integration. From the measured accelerations, the associated velocities and positions were obtained using a trapezoidal integration scheme using a time step equal to the sampling frequency of 4096 Hz. These displacements were transferred into rotations by using the relation for small angles:

$$x = l_x \cdot \theta \qquad \longleftrightarrow \qquad \theta = x/l_x = x/0.9m \tag{9.1}$$

Assumption for material damping

In literature several values for concrete material damping are given. Falati found for reinforced concrete without post-tensioning a damping ratio as 0.9% based on lab experiments [16], Chowdhurry gave a damping ratio range of 0.007 to 0.010 for uncracked reinforced concrete with small stress intensity [46], Jia stated 0.5% of critical damping for uncracked concrete [11] and Spijkers gave a damping ratio of 0.009 for reinforced concrete. Average this gives a damping ratio of 0.8-0.9 % for uncracked reinforced concrete

The equivalent damping ratio was determined with the logarithmic decrement method [43] for a reference model with simple supports and varying E^*. A relation between the found damping ratio and the material damping is shown in Figure 9.2a. A linear increase of the damping ratio was found for increasing material damping. The steepness differed per mode, for higher modes a larger increase with material damping was found. An $E*$ around $1.68 * 10^4$ approximated the 0.009 damping ratio in literature for the first mode. However, for the second mode, which was decisive for the final outcome, this value for $E*$ resulted in a much higher damping ratio, namely 0.035. A frequency independent relation between damping ratio and material damping E^* was obtained by dividing the damping ratio by the squared frequency of the corresponding mode, Figure 9.2b.

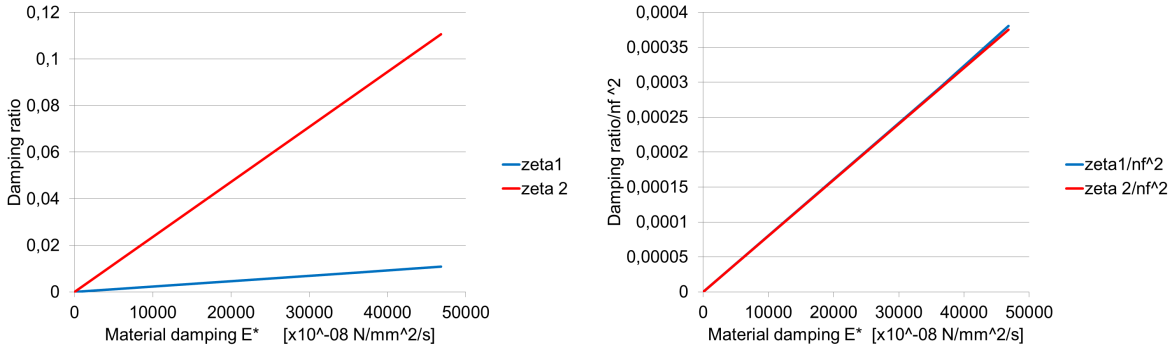

(a) Frequency dependent increase of damping ratio for increasing material damping

(b) Frequency independent increase of damping ratio for increasing material damping

Figure 9.2: Relation material damping and damping ratio for simply supported beam

In the measured signal from the experiment, no general damping ratio can be determined due to the non-linear behavior of the damping. When applying the logarithmic decrement method, a damping ratio of 0.02 was obtained on the first 0.5 seconds. For a short epoch at the start higher values of damping were observed. We concluded that other damping mechanisms are present, which have a significant influence on damping at higher amplitudes.

Assumptions for boundary damping mechanisms

Based on the assumption of a symmetric system, for μ and c_r equally large damping values were assumed at both boundaries. For several values of c_r and μ the damping ratio was calculated using the logarithmic decrement method, for a simply supported beam and for a beam with two springs at the boundaries.

Unlike for material damping, no comparable damping ratios were found in Literature for reference models. As a result the obtained damping ratio could not be compared with literature and no first estimate for μ and c_r could be made.

9.2. Sensitivity study

In this section the influence of different values for E^*, c_r and μ on the accelerations and displacements both in free vibrations and in forced vibrations was studied. For this, the analytical solution implemented in Matlab

was used.

9.2.1. Influence E^*

Material damping gave an exponentially shaped decay for the free vibration response. Mostly the high modes were found to be influenced by material damping, as a result high modes damp out fast compared with lower modes.

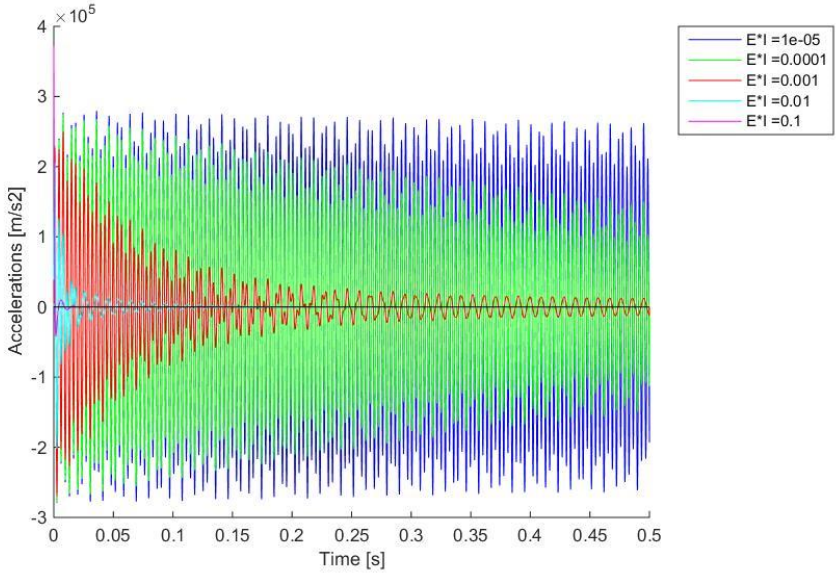

Figure 9.3: Accelerations at 1/4 th of the beam showing the influence of material damping for free vibrations, $\mu M = 0$, $c_r = 0$

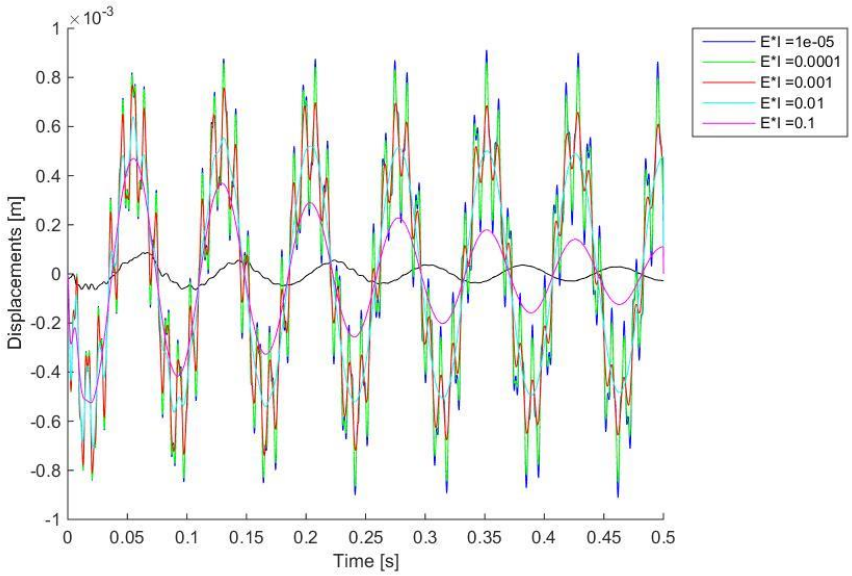

Figure 9.4: Displacements at 1/4 th of the beam showing the influence of material damping for free vibrations, $\mu M = 0$, $c_r = 0$

No coupling of modes was found, which is expected for linear material damping and can be seen from Equation 8.117 as no coupled contributions are present related to the material damping E^*.

When viscous damping at the boundaries or friction damping at the boundaries, was strongly present in the

system, material damping had also a significant influence on the decay. However, in practice, the possibility to change the intrinsic material damping in construction members by replacing materials is small. The influence of material damping on the total damping of the structure could be changed by changing the beam stiffness within the system, because material damping was found to be directly related to the present stresses in the structure.

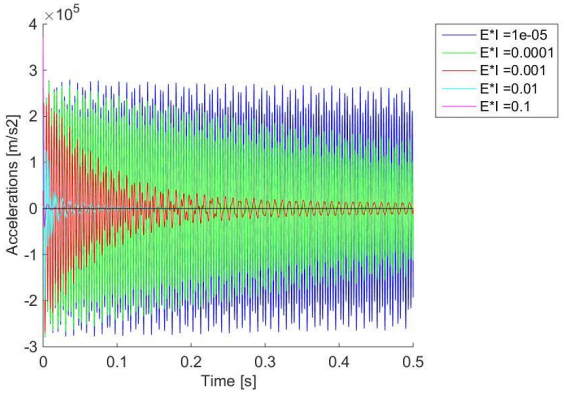

(a) Accelerations for changing material damping, $\mu M = 0$, $c_r = 0$

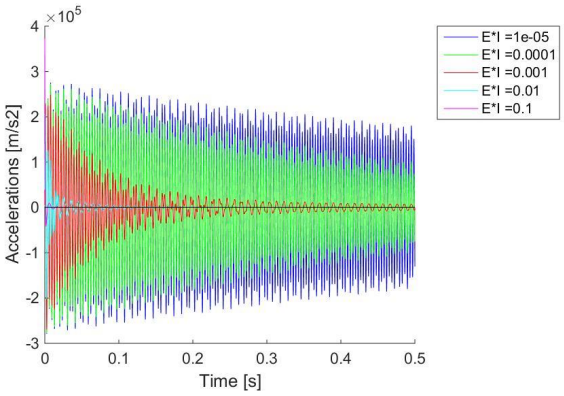

(b) Accelerations for changing material damping with high viscous damping, , $\mu M = 0$, $c_r = 100$

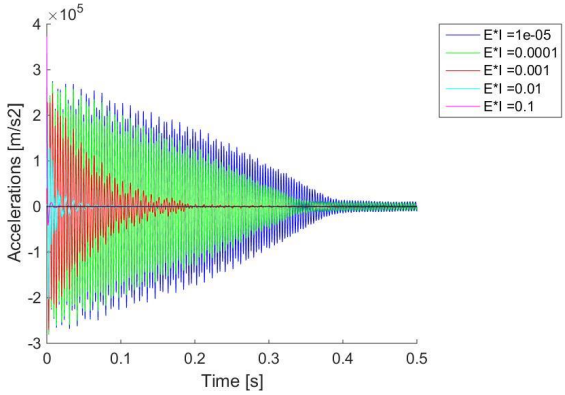

(c) Accelerations for changing material damping with high friction damping, , $\mu M = 100$, $c_r = 0$

Figure 9.5: Accelerations 1/4 th of the beam showing the influence of material damping for forced vibrations

Small changes in the material damping resulted to large changes to the number of modes present in the system simulating the experimental measurements.

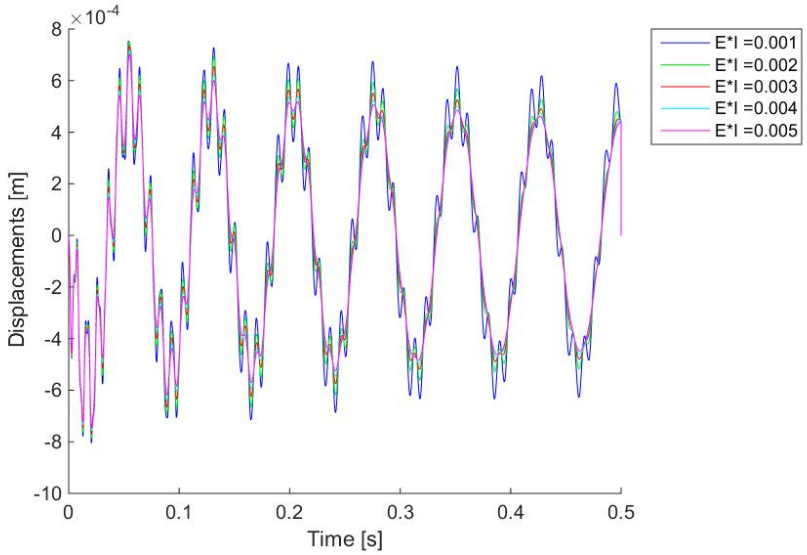

Figure 9.6: Accelerations at 1/4 th of the beam showing the influence of small changes in material damping for forced vibrations, $\mu M = 2$, $c_r = 100$

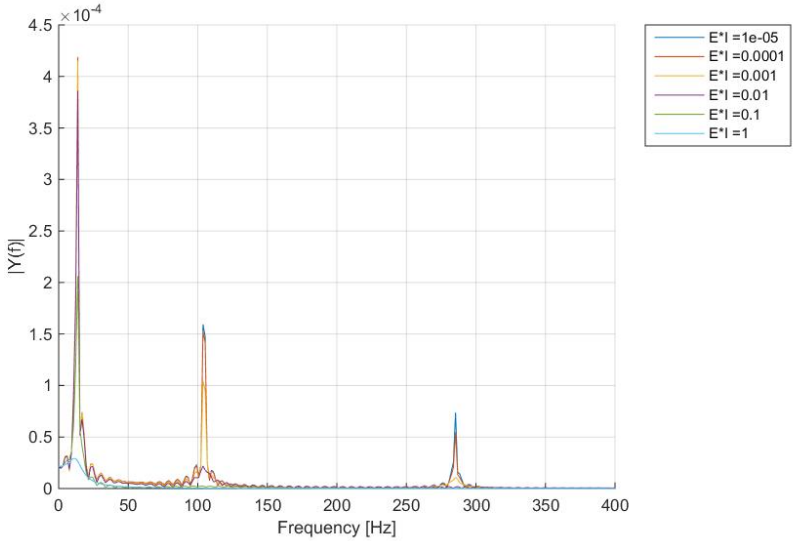

Figure 9.7: FFT plot for accelerations at 1/4 th of the beam showing the influence of small changes in material damping for forced vibration, $\mu M = 2$, $c_r = 100$

Small changes in the material damping did not resulted in changes to the frequencies of excitation. The natural frequencies were also studied for a wide range of material damping. A small change in the natural frequency was found for high material damping.

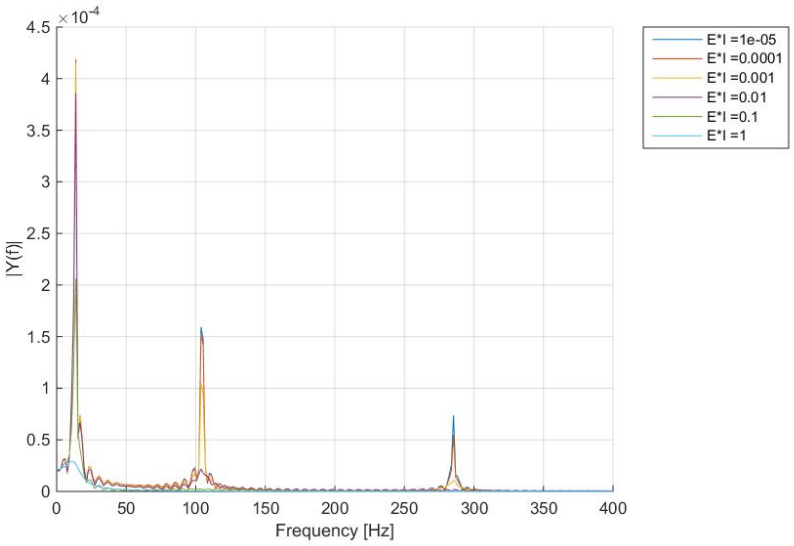

Figure 9.8: FFT plot for accelerations at 1/4 th of the beam showing the influence of changes in material damping for free vibration, $\mu M = 0$, $c_r = 0$

9.2.2. Influence c_r

The influence of viscous damping at the boundary on the excited frequencies, as shown below, was better visible compared with changes in the natural frequency for increasing material damping, shown above. However, only for high damping values a shift of the peak was detectable.

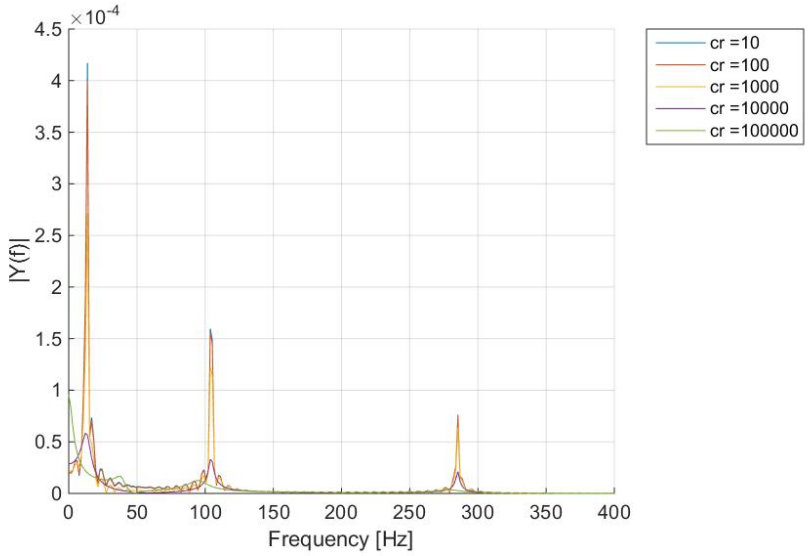

Figure 9.9: FFT plot for accelerations at 1/4 th of the beam showing the influence of changes in viscous damping at the boundaries for free vibration, $E^* I = 0$, $\mu M = 0$

Viscous damping gave a clear exponential decay, provoking that larger energy dissipation at high amplitudes of vibration. Several modes were excited in the response of the model and all modes encountered equally large damping.

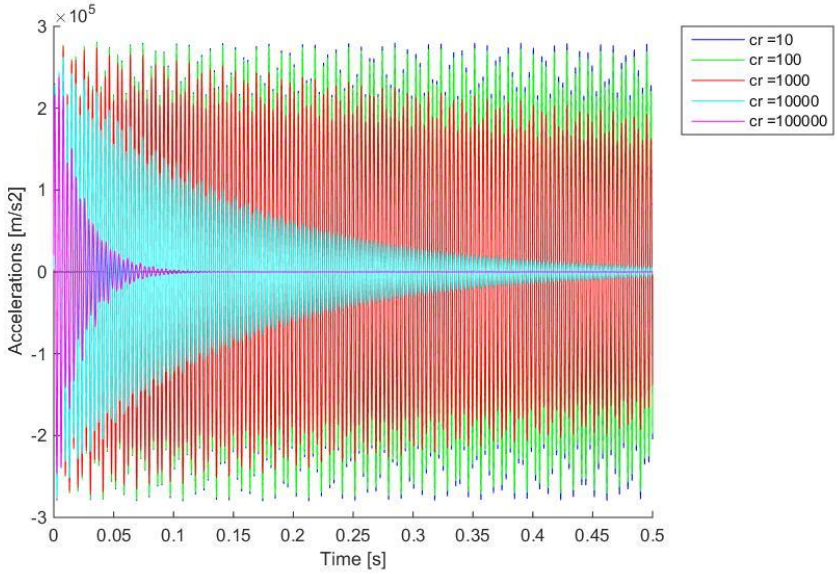

Figure 9.10: Accelerations at 1/4 th of the beam showing the influence of viscous damping at the boundaries for free vibrations, $E^* I = 0$, $\mu M = 0$

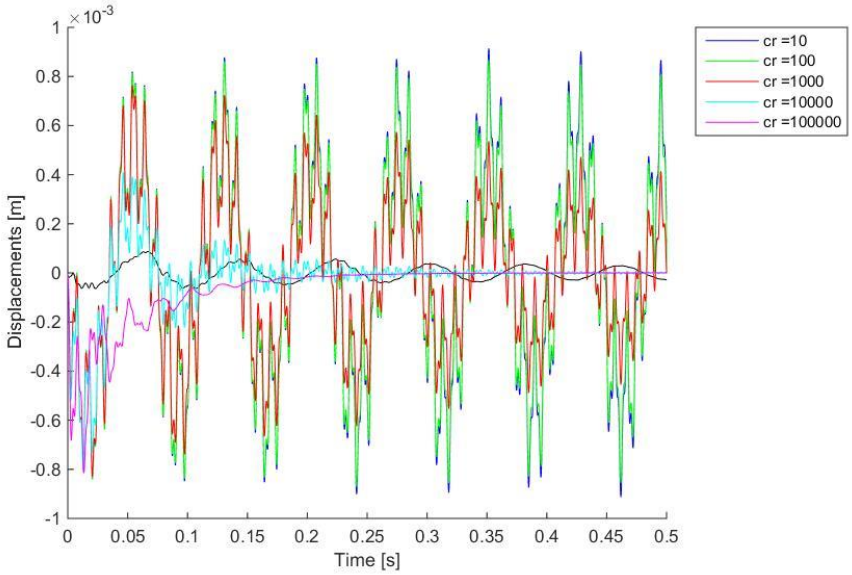

Figure 9.11: Displacements at 1/4 th of the beam showing the influence of viscous damping at the boundaries for free vibrations, $E^* I = 0$, $\mu M = 0$

When damping in the system was highly determined by friction in the boundaries, the influence of viscous damping was limited. For high material damping, the viscous damping had very small influence. For high friction damping there was found a influence by viscous damping when the viscous damping was larger than the friction.

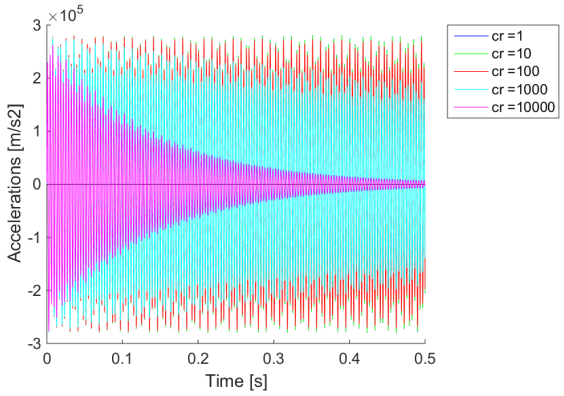

(a) Accelerations for changing viscous damping at the boundaries, $E^*I = 0$, $\mu M = 0$

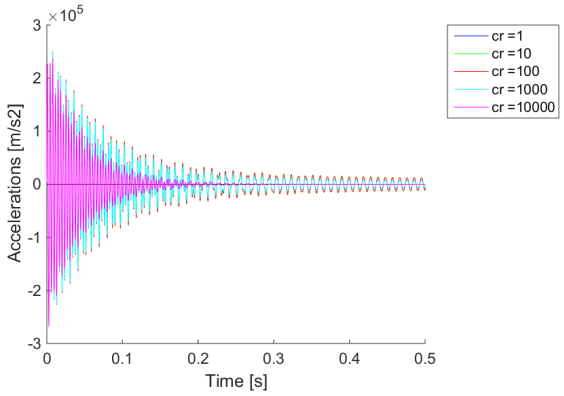

(b) Accelerations for changing viscous damping at the boundaries with high material damping, $E^*I = 0.001$, $\mu M = 0$

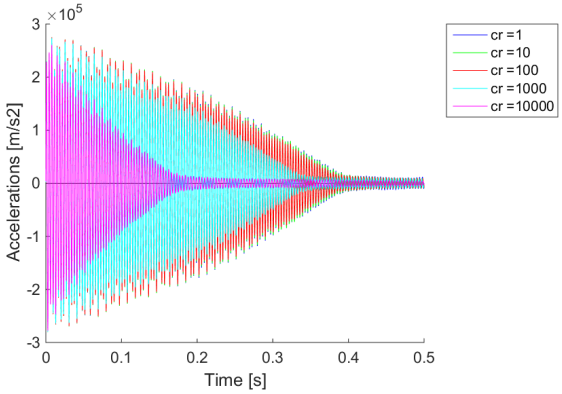

(c) Accelerations for changing viscous damping at the boundaries with high friction damping, $E^*I = 0$, $\mu M = 100$

Figure 9.12: Accelerations at 1/4 th of the beam showing the influence of viscous damping at the boundaries for forced vibrations

Small changes in the viscous damping parameters at the boundary of the system were shown to not have any significant influence to the damped system or in changes in the natural frequency.

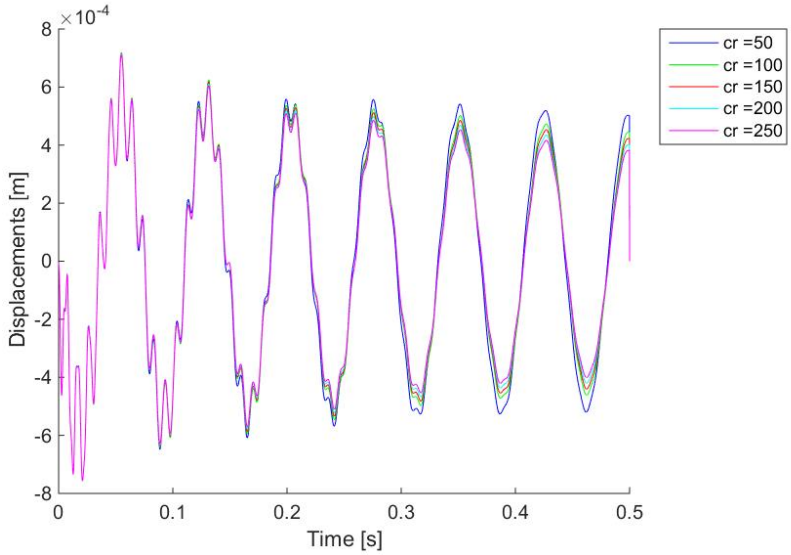

Figure 9.13: Accelerations at 1/4 th of the beam showing the influence of small changes in material damping, $E^*I = 0.004$, $\mu M = 2$

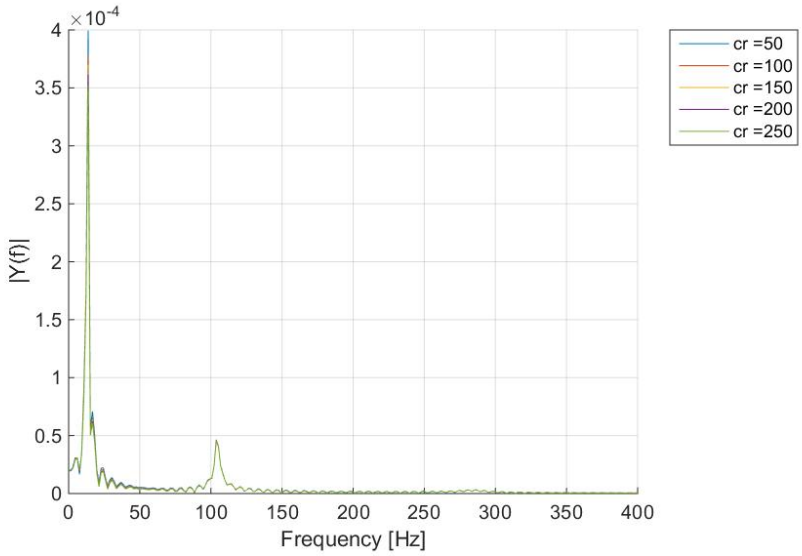

Figure 9.14: FFT plot for accelerations at 1/4 th of the beam showing the influence of small changes in material damping, $E^*I = 0.004$, $\mu M = 2$

9.2.3. Influence μ

For mu a linear decay in the response was visible. Also a turning point was present, where the decay changed. In the free vibration situation a steady state situation develops where vibrations remain in the system due to the friction. In the forced vibration situation a similar turning point was present, after this turning point is reached, the decrease in amplitude stopped.

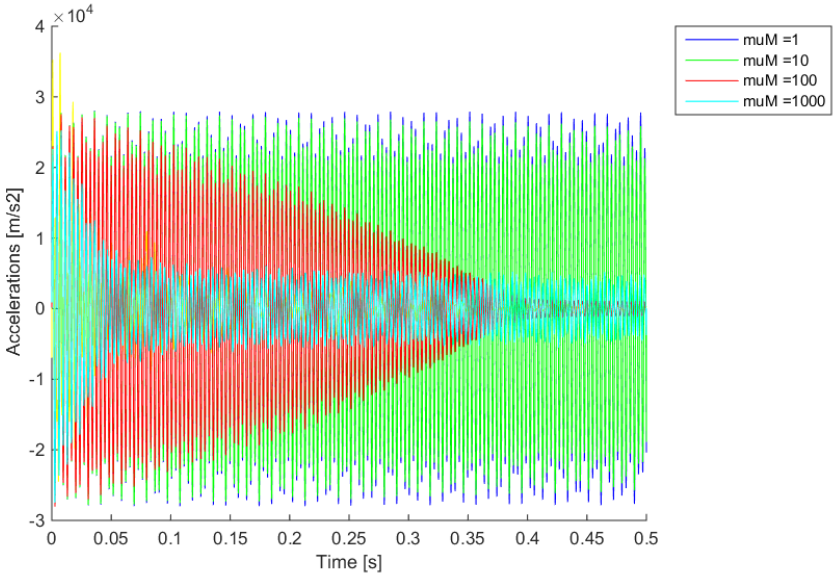

Figure 9.15: Accelerations at 1/4 th of the beam showing the influence of friction damping at the boundaries for free vibrations, $E^* I = 0$, $c_r = 0$

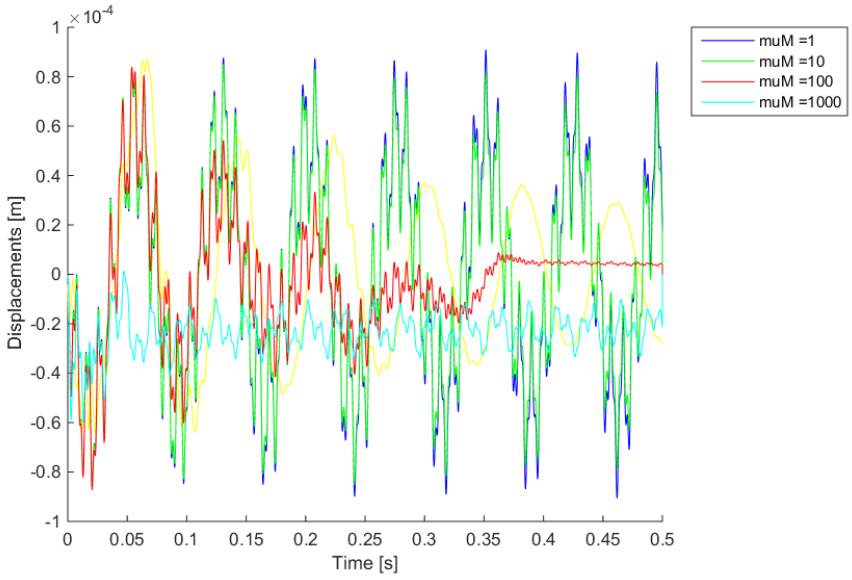

Figure 9.16: Displacements at 1/4 th of the beam showing the influence of friction damping at the boundaries for free vibrations, $E^* I = 0$, $c_r = 0$

The changes in frequency were found to be rather large for larger values of friction damping, as can be seen below

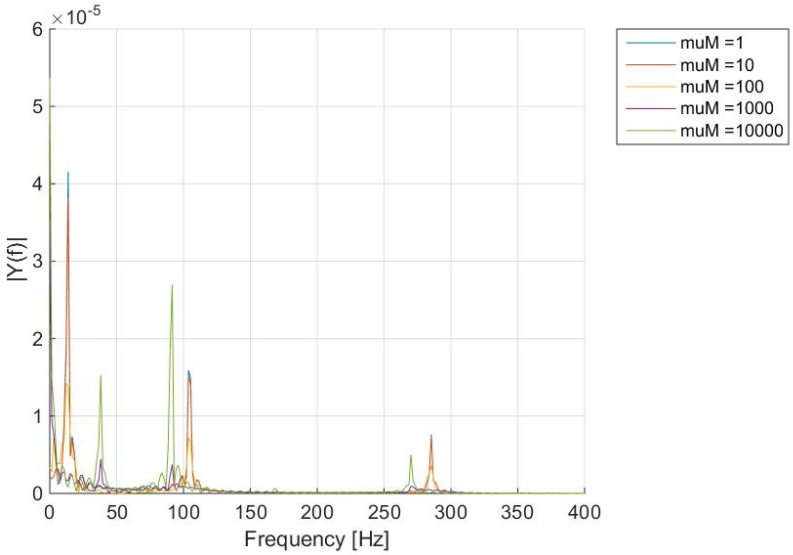

Figure 9.17: FFT plot for accelerations at 1/4 th of the beam showing the influence of friction damping at the boundaries for free vibrations, $E^* I = 0$, $c_r = 0$

Friction was found to have an influence when viscous damping is strongly present in the system. For equal damping values, friction was the dominant mechanism. When material damping was strongly present, friction damping was found to have a smaller influence.

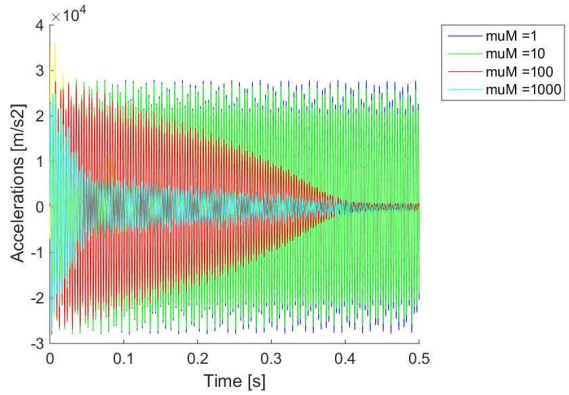

(a) Accelerations for changing friction damping at the boundaries, $E^*I = 0$, $c_r = 0$

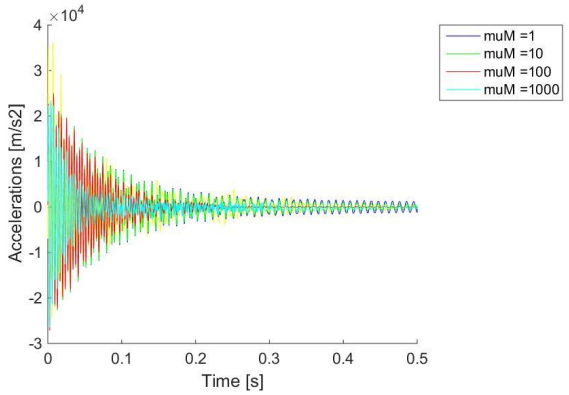

(b) Accelerations for changing friction damping at the boundaries, $E^*I = 0.001$, $c_r = 0$

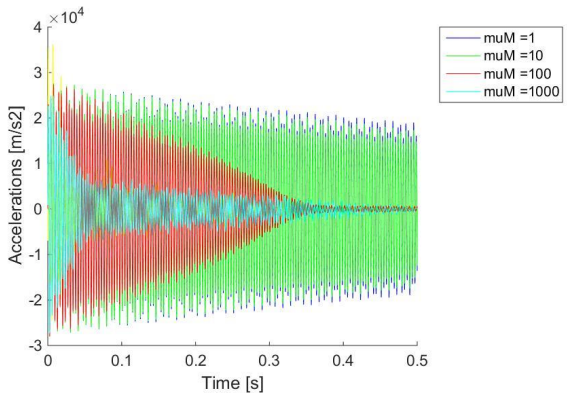

(c) Accelerations for changing friction damping at the boundaries, $E^*I = 0$, $c_r = 1000$

Figure 9.18: Accelerations at 1/4 th of the beam showing the influence of friction damping at the boundaries for forced vibrations

Small changes in the friction damping parameters at the boundary of the system introduced significantly more damping compared with changes to viscous damping at the boundaries.

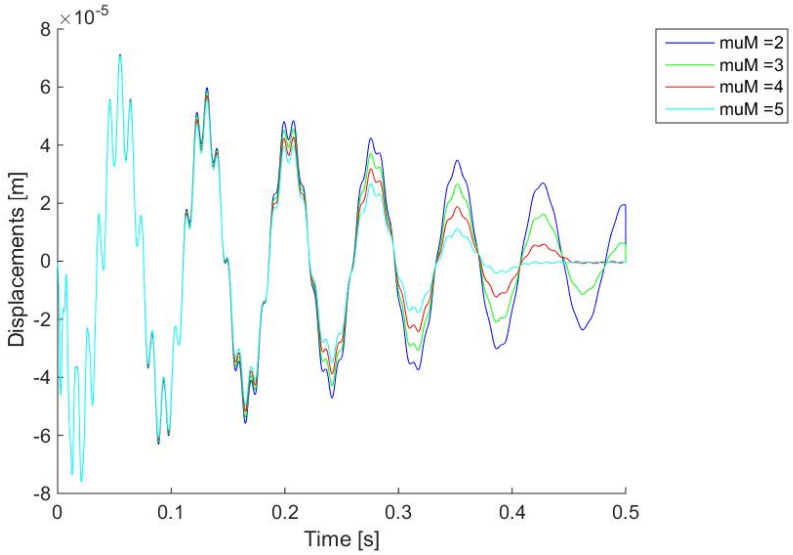

Figure 9.19: Accelerations at 1/4 th of the beam showing the influence of small changes in friction damping at the boundaries for forced vibrations, $E^* I = 0.04$, $c_r = 2$

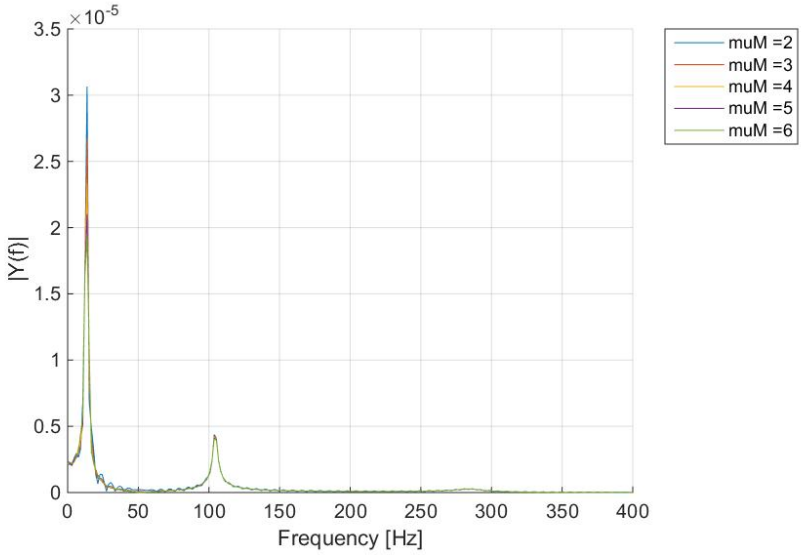

Figure 9.20: FFT plot for accelerations at 1/4 th of the beam showing the influence of small changes in friction damping at the boundaries for forced vibrations, $E^* I = 0.04$, $c_r = 2$

9.2.4. Influence stiffness system and other parameters

Mass and dimensions had an influence on the modes and natural frequencies. However, those values were fixed in this study. The stiffness of the system had a very large influence on the decay of amplitudes as shown in Figures 9.21a to 9.22b. The beam stiffness had the largest influence in natural frequency and indirectly on the damping. For the linear mode shapes, as determined in Section 8.3.1, an equal relation with the natural frequency was detected.

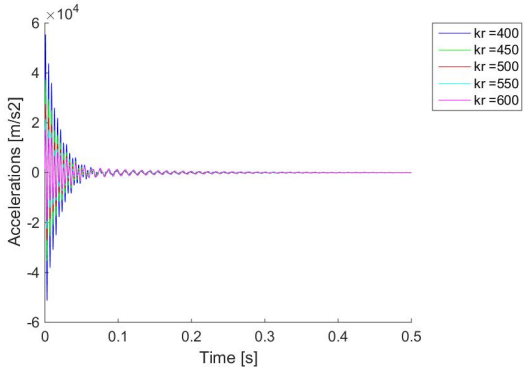

(a) Accelerations at 1/4 th of the beam showing the influence of beam stiffness for forced vibrations, $E^*I = 0.004$, $c_r = 100$, $\mu M = 2$

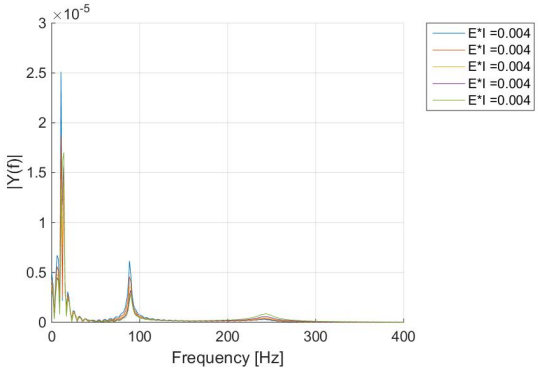

(b) FFT plot of accelerations at 1/4 th of the beam showing the influence of beam stiffness for forced vibrations, $E^*I = 0.004$, $c_r = 100$, $\mu M = 2$

Figure 9.21: Influence beam stiffness for forced vibrations

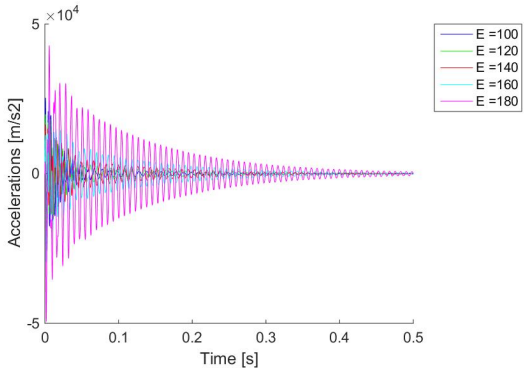

(a) Accelerations at 1/4 th of the beam showing the influence of spring stiffness for forced vibrations, $E^*I = 0.004$, $c_r = 100$, $\mu M = 2$

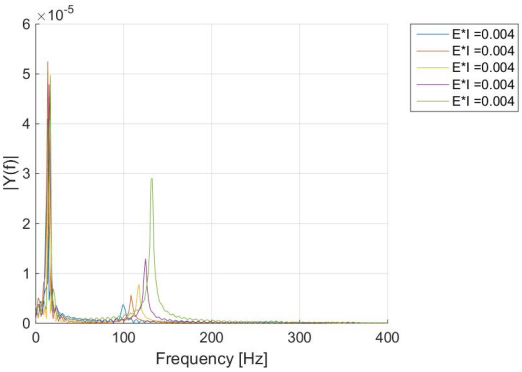

(b) FFT plot for accelerations at 1/4 th of the beam showing the influence of spring stiffness for forced vibrations, $E^*I = 0.004$, $c_r = 100$, $\mu M = 2$

Figure 9.22: Influence spring stiffness at the boundaries for forced vibrations

9.3. Final results

The test set-up that was compared with the model outcome is the normal test-set up, comprising the set-up without added damped material or loosened bolts. The stiffness properties of the joints in this set-up are expected to encounter smaller changes during the experiment.

The analytical model takes ten modes into account for the determination of the response. The experimental data was processes using a bandpass filter eliminating frequencies above 500 Hz. Several combinations of damping parameters were found to fit the response of the in Matlab implemented analytical problem accurately with the obtained signal from the experiment. After several calibration a best fit was found with the following damping parameters and other model parameters:

E^*I	0.004	N/mm^{2}s
c_r	100	Nm/(rad/s)
μM	2	Nm/(rad/s)

ρ	2	kg/m^2
A	0.0098	m^2
L	1.15	m
EI	110.6	Nm^2
kr	574.4	Nm/rad

Table 9.4: Model parameters

Material damping was found to have a significant influence on the damping. The material damping determines the numbers of modes present in the system, where due to friction and viscous damping energy was shared between several modes. The viscous damping parameter at the boundary was found to be higher than the friction damping parameter.

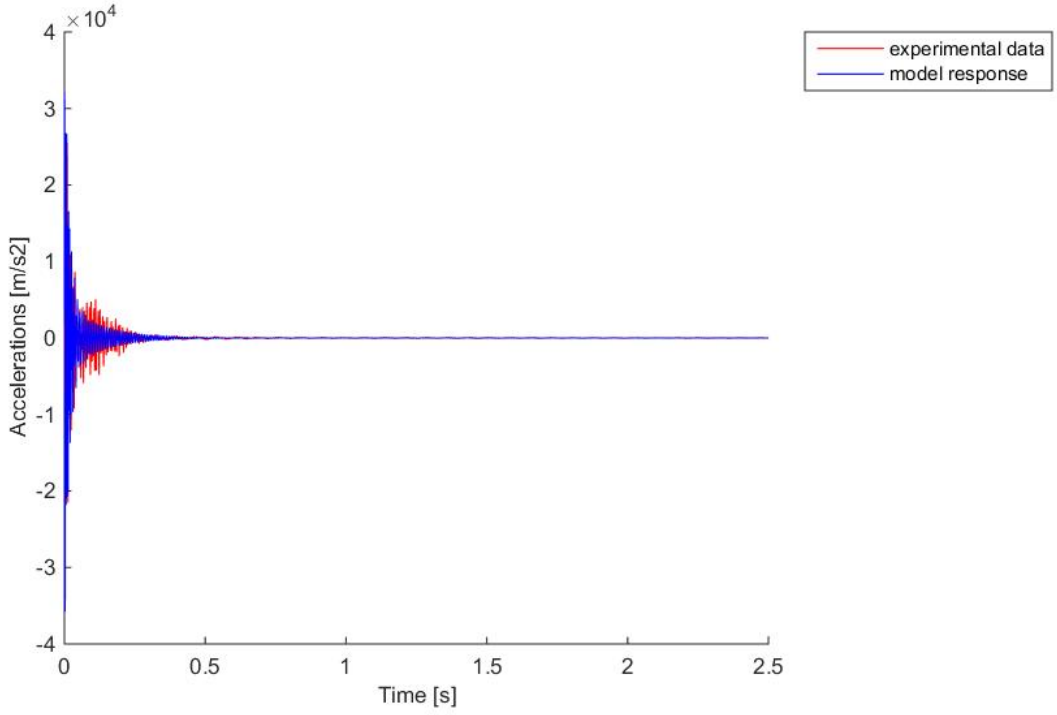

Figure 9.23: Accelerations at 1/4 th of the beam compared with measured accelerations

A good fit was found for the first part of the signal, however, beating of the amplitude was measured in the experiment, which was not present in the modeled response, as can be seen in Figure 9.23 and 9.24. A vibrational mode was excited and measured that did not exist in the model. The excited frequencies in the first part also had a good match in first epoch, but around the beat higher frequencies are measured in the experiment. Following Figure 9.26 a large quantity of high frequencies was present, but these, according to Chapter 7, these higher frequencies were only present in the very beginning of the signal and thus can not influence the beating. Maybe, changes to the stiffness of beam and connections influences the beating phenomenon by changes in the natural frequency of the system.

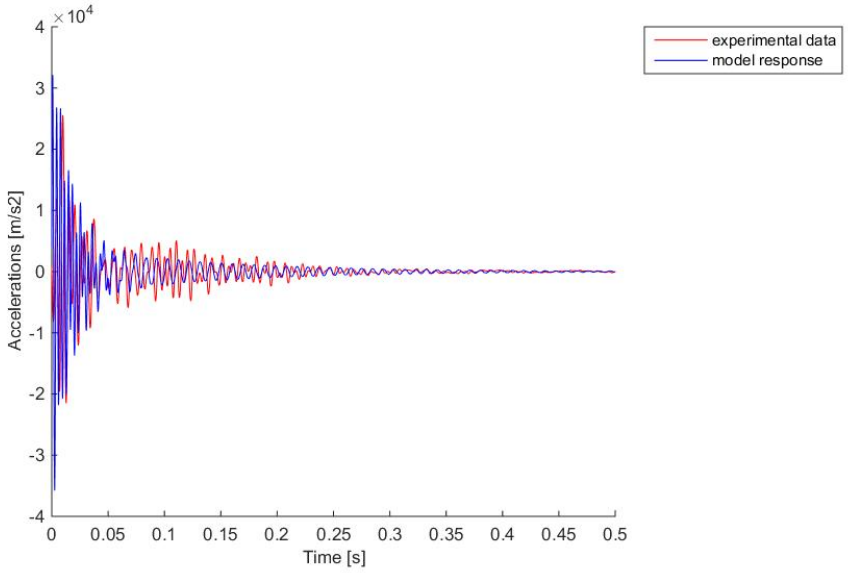

Figure 9.24: Accelerations at 1/4 th of the beam compared with measured accelerations

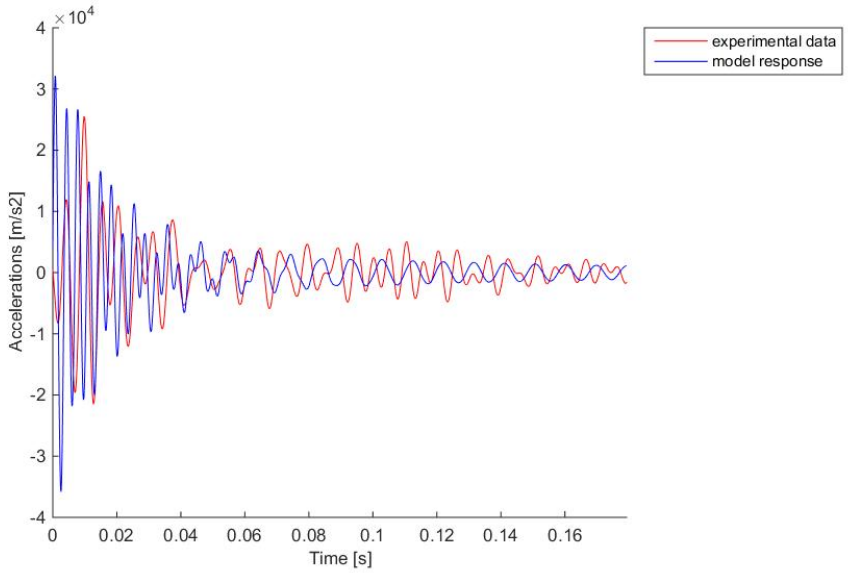

Figure 9.25: Accelerations at 1/4 th of the beam compared with measured accelerations

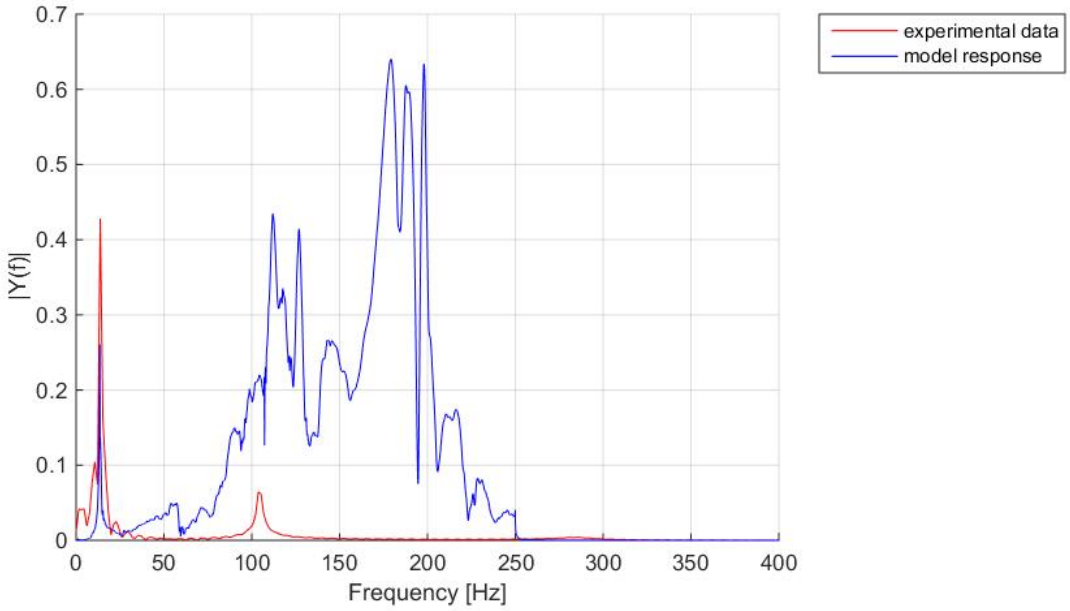

Figure 9.26: FFT plot of the accelerations at 1/4 th of the beam compared with measured accelerations

The modeled response has also a strong coherence with calculated displacements from the measurements, Figure 9.27. Both the amplitude, number of modes and natural frequency show similarities. The frequency transform of the modeled response had strong coherence with the frequency transform of calculated displacements from the measurements, Figure 9.28. The modeled natural frequency, however, showed a mismatch after 0.25 s compared with the experimental data. The model does not allow changes in natural frequency for fixed stiffness and damping parameters, thus the change in frequency in time had to be present during the experiment.

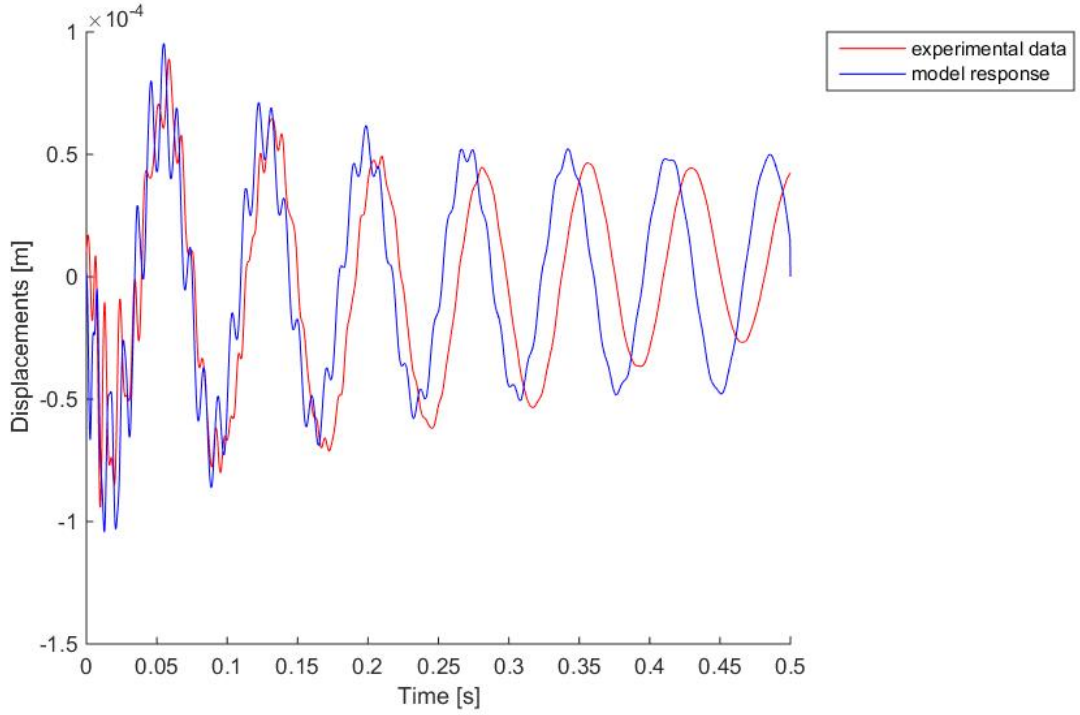

Figure 9.27: Displacements at 1/4 th of the beam compared with displacements calculated from measured accelerations

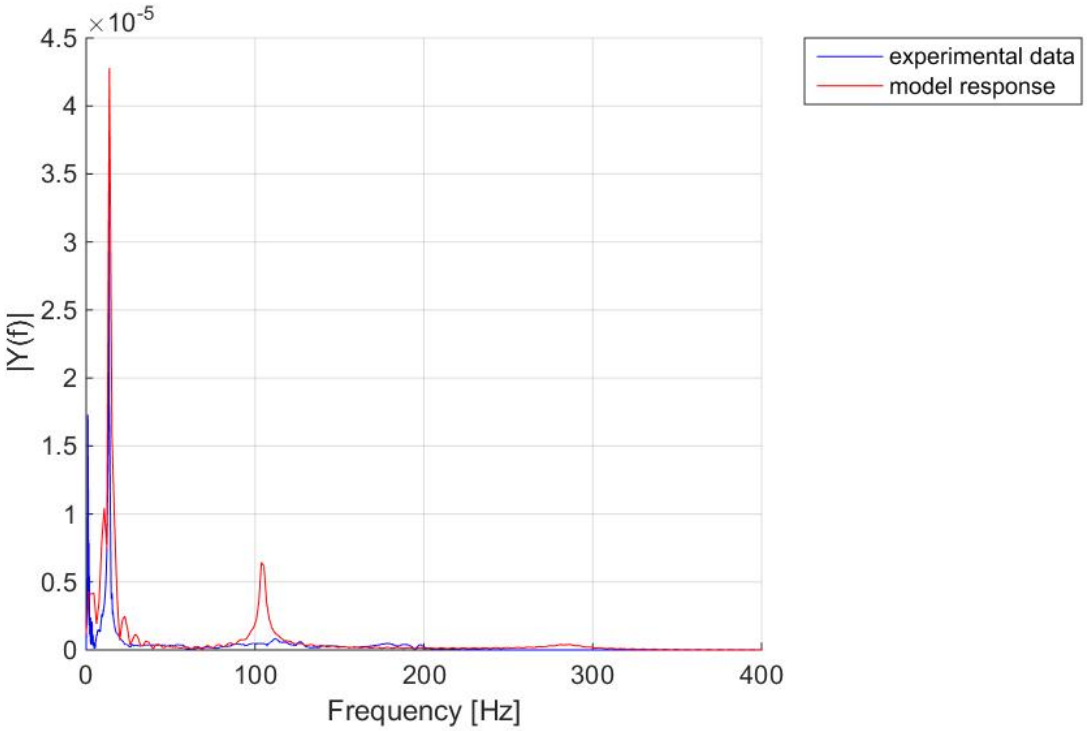

Figure 9.28: FFT plot of the displacements at 1/4 th of the beam compared with measured accelerations

IV

Conclusions and results

10

Conclusions

None of the currently available damping predictors adequately predicts damping of a building in the design phase. The complexity of damping mechanisms, the uniqueness of building structure design, and the lack of data from full scale measurements are the main reasons for this. Building characteristics such as soil-structure interactions, effects of non-structural elements, the building layout and the influence of higher modes of vibrations, are examples of factors that influence damping, but are not incorporated in current predictor models.

Damping in buildings can be assigned to structural damping, aerodynamic damping, intrinsic material damping, radiation damping, damping in non-structural elements and to additional dampers. Damping in floors both comprises intrinsic material damping and structural damping.

High damping values indicate that damping is significantly more influenced by structural damping than by material damping. In aerospace and mechanical engineering many studies are performed in which models are created to describe friction, viscous or hysteresis damping in joints. In civil engineering especially regarding concrete and concrete-steel connections conducted research regarding damping in joints is limited. No generic model for joints have been developed.

For materials the static properties of an element are well known, but studies of damping characteristics of construction members have not been performed frequently, providing uncertainties on damping for each individual member in constructions. Crack formation of concrete has been shown to increase damping and is assigned to local friction in the cracked parts. However, limited studies to model this behavior are presented in literature.

Conclusions regarding database study

A relation between natural frequency and slenderness is seen from full-scale measurements performed on fifteen dutch buildings. However, a clear relation between the damping ratio and slenderness is not obtained. Both higher and lower damping ratios are found compared with the prescribed values in the Eurocode. The lower damping plateau by Jeary is shown to be a very conservative limit for damping in the measured Dutch buildings.

For slender buildings in the Netherlands, deformation due to cantilever bending due to axial deformations is most common. Hollow slab floors, steel-concrete floors and wide slab floors are the most commonly used floor types. Such floors typically have a single spanning direction and are connected to a steel or concrete main structure with stiff main structure with floor-beam connections and medium stiff floor-slab to floor-beam connections.

Conclusions regarding the solution methods

No analytical exact solutions for the equation of motion describing the dynamic behavior of the 1D continuous model representing a floor in high-rise buildings can be determined for the natural frequencies or modes. For both the linear and non-linear problem, numerical calculation methods were needed. The method of Separation of Variables combined with numerical trial and error provided values for the natural frequencies and mode shapes which agreed strongly with solutions described in literature. However, for higher modes, the obtained frequencies encounter an error causing a slight increase of the frequencies. The natural frequencies depend mostly on the beam stiffness, but also on stiffness of rotational springs at the boundaries cause increases in the natural frequencies.

The Galerkin Method in combination with numerical integration following the Runge-Kutta integration scheme provided accurate solutions of the equation of motion for 1D continuous model with nonlinear boundary conditions. The use of ten modes was found to provide a sufficient solution. For very high viscous damping or friction damping forces at the boundaries, the mode shapes will differ strongly from the linear mode shapes, giving no good approximate solution using these linear mode shapes.

Numerical instability of the solution occurred using the Runge-Kutta numerical integration scheme for high viscous and high friction damping at the boundaries. The time step in the numerical integration should be sufficiently small to cope with high frequencies and depends on the number of modes incorporated.

Conclusions regarding experiment

In experiments odd modes of the 1D beam were found to be decisive. The first natural frequency of the system was found at a frequency of 13.5 Hz. The columns were found to vibrate in phase and only very small amplitudes were found in the center of the beam.

At higher modes, above 100 Hz, coupling of modes was present in the system. This coupling of modes only occurred during the very first seconds of vibrations. High modes damp out very fast and this coupling was only present at large amplitude of vibration. Due to this appearing amplitude dependency, these high coupled peaks might indicate a relation with cracking of the concrete, related with high local energy dissipation and reduction of the local stiffness of the beam.

Changes to the test set-up in the form of reducing the clamping moment and adding additional highly damped material caused increasing damping values. Changes in amplitude of excitation also caused changes in the damping. The biggest change was found in the first part of the measured signal.

Also, small changes in the natural frequencies of the system with time were detected. For the test set-up including highly-damped material and loosened bolts this reduction in natural frequencies was found larger, around 10%.

Conclusions regarding sensitivity study and model validation

Several combinations of damping parameters were found to fit the response of the in Matlab implemented analytical problem accurately with the obtained signal from the experiment.

Material damping was found to be decisive to the two boundary damping mechanisms. However, the possibility of changes in the material damping in a structure or building is limited. The presence of friction damping and viscous damping in the supports, resulted in the excitation of more modes. Friction damping was found to have a significant influence at small amplitudes of vibration.

11

RECOMMENDATIONS

In further studies full-scale measurements will be the key point for understanding damping in buildings. Measurements in real buildings during construction in different wind conditions will provide insight in the contribution of individual elements. Analytical and numerical models will help to achieve insight in the working of damping mechanisms. The model presented in this thesis is a starting point for the understanding of wind-induced vibrations and damping in floors.

Coupling between several modes in the floor were seen in this study. It is then expected that coupling of modes between the two lateral dimensions in plates and with the torsional mode is occurring as well. Extension of the 1D model presented to a model with two decisive lateral dimensions is recommended. Furthermore, torsional modes in building were not included in the model presented in this thesis. However, for buildings with a symmetric plan, the torsional mode is shown to be strongly present in the response of those buildings to wind.

Multiple variations on parameter combinations approximate the experimental results with the 1D model presented in this thesis. A calibration algorithm could be developed to study determine the optimal combination of parameters to fit the experimental results.

The measured signal exhibited a less smooth decay than the response calculated with the one-dimensional model. This indicates that other - non-linear - damping mechanisms were present which influenced the damping. Extension of the model in the form of for example displacement dependent friction implemented within the beam material or quadratic viscous damping at the boundaries, might improve the accuracy of the simulated response.

Also, experiments allowing more cracking of the concrete bar can be performed to study the coupling of modes. The representation of the nonlinear properties of the material can be studied in an extension to

current the Kelvin-Voight model.

Further experiments could also be conducted for several commonly used connections in building constructions. These experiments in combination with the developed model could provide for a classification of joints, listing the viscous and friction parameter combinations for different loading situations. Also, such studies can provide insight in possible adjustments to the structure's connections to obtain highly damped connections for a specific situation of loading.

An experimental validation with full-scale structures is recommended, for further development of this model. In this model, the rotations of the column were taken as known parameters of the model. For a full-scale building, the vertical accelerations in the floors should be measured together with the horizontal accelerations of the columns, which would allow the determination of damping parameters.

When the model is validated for different situations and loading cases, the next step would be understanding the contribution of floors to the total damping of the building. When the amount of energy dissipated within the entire building is known and knowledge is obtained of both the damping mechanisms that play a role and the dynamic behavior of floors, then the dissipated energy of each of those mechanisms can be determined.

The ultimate step would be the prediction of the contribution of the floor damping-mechanisms to the damping of the main structure, as a part of the prediction of the damping of the building based on values prescribed in the design phase of a building.

V

Appendices

A

DAMPING PREDICTORS

A.1. Predictor Formula by Jeary

Jeary developed an empirical formula based on observed damping values for the first natural frequency in sixteen buildings in Great Britain. Jeary's theorem is based on friction in combination with a stiction effect as physical mechanism for damping [82]. It was proposed that throughout the building, the level at which slip will occur, was randomly distributed with respect to the amplitude. Resulting in a response which behaves linear viscous at any amplitude but the damping increases with increasing amplitude. The main mechanism for energy dissipation is assumed to be friction between structural elements and friction in micro cracks in the material. All materials are assumed to behave linear elastic with micro-cracking due to higher amplitudes. The effect of plastic strain has not been included.

In Jeary's formula damping is defined as a percentage of the critical damping. The amplitude of response is stated as the lateral displacement at the top of the building normalized against the building height. Three regions are distinguished: the Low amplitude plateau region, the Non-linear region and the High amplitude region as can been seen in Figure A.1. In the Low amplitude region damping is caused by the friction

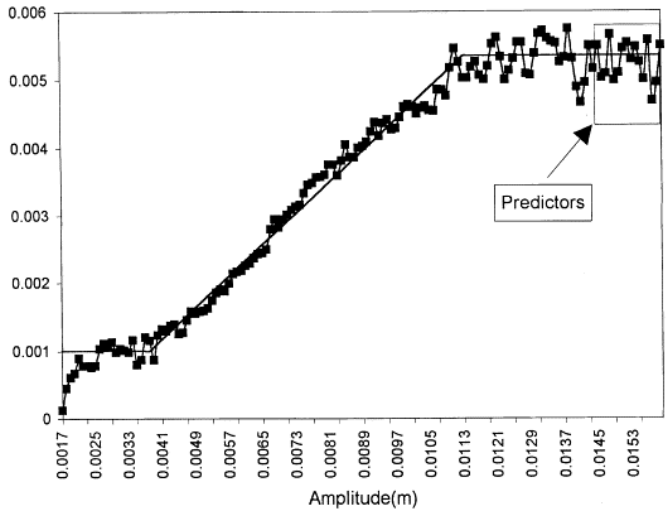

Figure A.1: Lower and higher amplitude plateau according to jeary

mechanisms between structural elements, all materials behave linear elastic. The structure dissipates very

little energy and moves quickly to an amplitude at which an energy balance is struck. The damping value is constant and governed by the structural form of the building only. This damping value in called the zero amplitude Value [40]. In the non-linear region the damping increases with amplitude. The energy is dissipated from the structure by the mechanisms of micro-cracking, providing the non-linear damping characteristics. Movements of joints and relative displacements of structural elements also contribute to non-linear energy dissipation and an increase in damping with vibrational amplitude. At high amplitudes the energy is large enough to mobilize all mechanisms and a new energy balance is struck, called the high-amplitude plateau damping.

The estimated absolute modal damping in the j^{th} mode according to Jeary:

$$\zeta_j = \zeta_{0j} + \zeta_{1j} \frac{x_H}{H} \tag{A.1}$$

with $Log_{10}\zeta_1 = \frac{\sqrt{D}}{2}$ and $\zeta_0 = f_0 = \frac{46}{H}$

It can be seen that the increase of damping is related to the dimension D at the base of the building. This relation is derived from the critical shear stress formula by Timoshenko, where the length of the crack and the friction force at both interfaces are related [40]: $S_{cr} = \frac{4ET}{l}$. Both bending and shear stresses are related with the width of the footprint. For larger stresses, at larger amplitudes of vibration, the damping increases.

A.2. Predictor Formula by Davenport and Hill-Carol

The main sources of damping in a building can be splitted into five parts according to Davenport [83]:

1. Intrinsic material damping, with a division between steel or concrete, of the building.
2. Foundation damping both due to radiation of energy and due to intrinsic damping in the soil.
3. Frictional damping between the components of the structure and architectural finishes.
4. Aerodynamic damping.
5. additional damping systems built into the structure

The instrinsic material damping is the result of the energy dissipation under dynamic stress. The viscous behaviour of materials is a part of the material damping, but also internal friction due to dislocation and movement between crystalline elements within the material and magneto-electric forces hereby contribute to the intrinsic damping. For intermediate, the critical damping is found to be proportional to the stress$^{0-1}$. For high stress levels a gradual increase up to the linear elastic limits of the main structure is expected [42]. In this point, Davenports model differs from other models, which assume a constant maximum damping value above a certain treshold. Friction damping origins at bolted joints, at bearing plates, in built-up members,

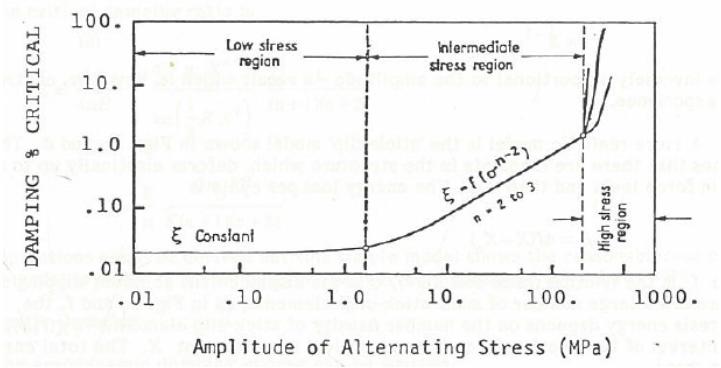

Figure A.2: Instrinsic material damping according to Davenport

between floors and beams, at in-fill panels in frames, between frame and cladding and between interfaces of other components within the building. Because the level of damping found for materials in much lower than

the measured damping in structures, Davenport assumes friction damping to be contribute significantly, which can be represented by stick-slip mechanisms.

No attempt was made by Davenport to include foundation damping to the empirical formula, because detailed knowlegde on soil characteristics are necessary. Aerodynamic damping is excepted to influence the damping, but is not taken into account for devellopingthe empirical formula.

DAMPING PROPERTIES OF BUILDINGS

Expected critical damping ratio : $\zeta = A(\Delta/H)^n$ mm/m
Coefficient of Variation: V

		A	n	V
5-20	Storey			
	Steel	0.03	0.075	0.40
	Concrete	0.03	0.11	0.40
> 20	Storey			
	Steel	0.02	0.11	0.40
	Concrete	0.025	0.11	0.40

Figure A.3: Empirical formula by Davenport

Besides a separation in building materials, also a division between buildings below and above 20 storeys is made. Based on mean values in data concluded Davenport that lower buildings experience 60% more damping. Also tall concrete buildings experience 30% more damping than their steel opponent. In Figure A.3 the empirical formula and characteristic for different building types as determined by Davenport can be seen.

A.3. Forecast model by Lagomarsino

Lagomarismo uses a similar division for different damping mechanisms following Davenport. With his attempt for a generic model for damping in building only the first two factors are taken into consideration for the development of the model. The other factor are assumed to be significant for only particular structures. Herewidth the frictional damping is of particular importance in buildings [84].

For ductile materials is the material damping seems to be principally due to viscous phenomena, but the contribution of material damping is two orders of magnitude less compared with the structural damping, so that material damping in ductile materials is negligible compared to structural damping. For brittle materials, which have a microstructure with cracks of variable shape and dimension, stresses cause both deformations and slidings between the crack faces of which the latter is limited by friction forces. Dissipation is also produced in the absence of damage or plastic phenomena and is larger than damping of ductile materials [84].

Damping due to friction between contacting elements in the structure is typical of steel structures with bolted joints; significant dissipation due to slippings between structural and non-structural elements such as partition walls, is present in any building [84]. Lagomarsino introduced different models for steel and reinforced concrete buildings. In steel buildings damping is solely caused by friction actions in the joints, neglecting the material damping. For reinforced concrete buildings, damping is caused by both to the slippings between structural and non-structural elements, macro-slipping, and to the dissipation in the material itself, due to microsliding, at high stresses.

The empirical model is based on multiple slipping models. There are many joints in a structure which become active at different levels of vibration, which are modeled as number of slip models in serier, where parameters activate slipping at certain thresholds, resulting in a behaviour in which the damping increases over the amplitude.

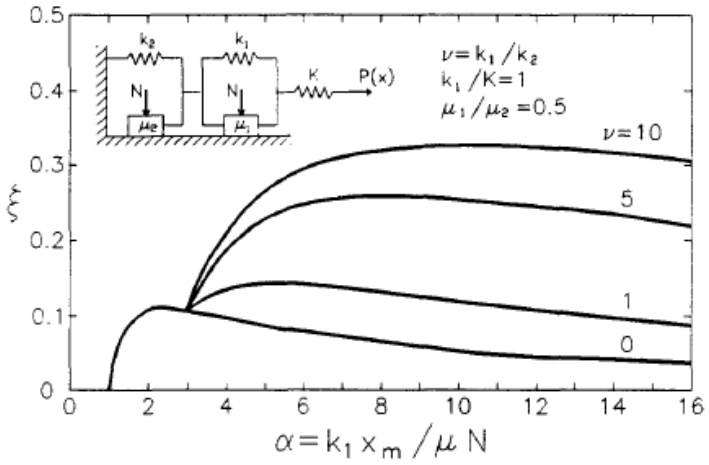

Figure A.4: Slip elements in series

A.4. Predictor Formula by Tamura et al.

In 2003 Sakate and Tamura et al. propose a damping predictor based on measurements in Japan in the small amplitude region. A significant increase in damping ratio for reinforced concrete and a steel-concrete combination are found as can be seen in Figure A.5a

Contrary to the other empirical formula's, Sakate and Tamura et al. looked the influence of Foundation type and depth on the damping ratio, Figure A.5b. Concluded is an decrease of damping with depth, but this develops simultaneously with the decrease in building height. Also a difference between the damping value for buildings with floor plans with many interior partions or buildings with open floor plans can be seen. The fitst have larger damping ratios. This increase is caused by the friction between non-structural elements.

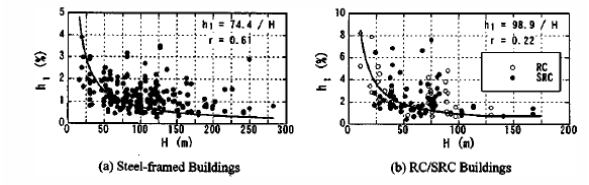

(a) Damping ratio in the first mode for steel and concrete buildings related to building height

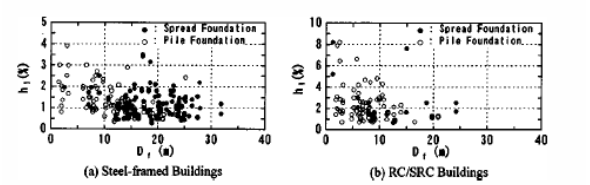

(b) Damping ratio in the first mode for steel and concrete buildings related to foundation depth

Figure A.5: Damping ratio's from full scale measurements in Japan

B

Calculation Methods Nonlinear Differential equations

Like linear systems can be described by sets of linear DE's, so can nonlinear sytems be described by sets of nonlinear DE's. However, there is no generally applicable method to solve nonlinear DE's. There are different methods and techniques developed which can be used to study the responds of nonlinear systems. However, all methods provide an approximate solution for the nonlinear system. An exact solution can only be derived for a small selection of nonlinear systems which are described with simple second-order differential equations [20]. Mainly due to the extended use of finite element methods is the direct time integration combined with decent integration methods for reaching equilibrium within each time increment the most used method to obtaining nonlinear responses in civil engineering practice [11]. In this section are besides the direct time integration methods some of the analytical approximate methods listed which can be used to solve weakly nonlinear systems.

The methods for studying the response of nonlinear differential equations can be subdivided into [18]:

1. Basic analytical methods
   - Direct integration method
   - Linearization of nonlinear system
2. Heuristic techniques
   - Galerkin Method
   - Harmonic Balance method
3. Asymptotic techniques
   - Ritz averaging method
   - Methods of averaging and multiple scales
4. Numerical methods
   - Direct numerical integration
   - Iterative solution methods
   - Incremental solution methods

B.1. Basic Analytical methods

The simple analytical methods are only valid for a small selection of dynamical systems which meet specific requirements. Only weak nonlinear system and systems containing uncoupled damping and a low order derivatives can be solved analytically by those methods.

Analytical direct integration method

In the analytical direct integration method the response is obtained by integrating both sides of the equation of motion. This is only analytically possible for simple uncoupled linear differential equations of the first order. However, the solution found can be seen as the exact solution to the system.

Linearization of a nonlinear system

Linearization of a small nonlinear system is the most frequent used method to cope with nonlinear systems. For the following cases a linear approximation of a system can be used for analyzing a system and will give solutions with sufficient accuracy [15]:

- In the case that only small displacements are present.
- In the case of low stresses and strains which do not exceed the linear limit of the material.
- When no inherently nonlinear elements are present or when nonlinear elements do not have any significant influence in the response amplitude and stability.
- In the case that no external inherently nonlinear mechanism influences the system.

Linearisation often is applied around a certain critical point. Using Taylor expansion of $f(x)$, the nonlinear part of the equation of motion, at x_0 the equation of motion can be approximated, assuming x_0 is an equilibrium position and $f(x_0) = 0$ is valid.

$$m\ddot{x} + f(x) = 0 \tag{B.1}$$

$$m\ddot{x} + (x - x_0)\left(\frac{\partial f}{\partial x}\right)_{x=x_0} + \frac{(x - x_0)^2}{2!}\left(\frac{\partial^2 f}{\partial x^2}\right)_{x=x_0} + \ldots \quad = 0 \tag{B.2}$$

For less weak nonlinear systems a linearization of the equations of motion can provide information of the behavior of the system at an equilibrium position. However, the behaviour of a nonlinear system can differ significantly from the linearized system on a very small time interval. Therefore, for strong nonlinear systems, this method will not produce reliable results.

B.2. Heuristic Techniques

With heuristic methods the solution is approximated with a periodic solution. The approximated solution is convergent with adding additional terms to the periodical solution [18]. However, the accuracy of a given number of terms within the periodic solution is unknown. These heuristic methods are therefore restricted to periodic solutions and the instability of the solution should taken into account.

Galerkin method

The Galerkin Method is widely used method for finding approximate solutions to partial differential equations [21]. The galerkin method is a method to approximate the solution with a sum of periodic function which consists of the product of the eigenfunction of the linear system and generalized time-dependent coordinates. The equations are projected on the linear space [22]. The problem is described with linear boundary conditions and an equation of motion where all nonlinear forces due to both internal and external effects are present.

The galerkin continuous projection consists out of two steps:

1. The first step is to give an approximation to the solution in the form of the sum of a product of a basis function and an unknown time coefficient. The base functions are determined by the linear space.

$$v(x,t) = \sum_{n=1}^{\infty} v_n(x,t) = \sum_{n=1}^{\infty} p_n(x)\, q_n(t) \tag{B.3}$$

2. The second step is to substitute the approximated function into the differential equation. Hereby a residual term $r(t)$ is obtained which contains all nonlinear contributions. The other term contains the orthogonal projecter to the linear space

$$v(x,t) = \sum_{n=1}^{\infty} p_n(x) q_n(t) + res \tag{B.4}$$

After the projection, the unknown coefficients can be found. By using the orthogonality property of the linear modes a set of N nonlinear equations and N unknown time dependent coordinates is obtained. By making the residual orthogonal to the assumed basis functions, the residual contributes to the set of N nonlinear equations by coupling of the nonlinear equations.

Mahmoodi [23] used the method of multiple scales together with the Galerkin projection on visco-elastic continuous beams with linear boundary conditions and found accurate results compared with experiments. Pesheck has used the method to model many coupled normal modes and showed that a wide variety of forms of nonlinearities at the boundaries are allowed within the solution procedure with little additional analytic work. Also the method significant promise for the development and understanding of reduced-order models for nonlinear systems according to Pesheck [24].

Kalashnikova used the Galerkin projection for continuous nonlinear equations with nonlinear boundary conditons. As the boundary conditions of the discretized system are not in general inherited by the reduced order model obtained after the projection, they should be implemented separately in the reduced order model [25]. Hereby the penalty method is used where the entire boundary value problem is rewrited in a single equation that is valid on both solid and boundary.

In finite elements the Bubnow-Galerkin method is used to find the best solution to a given collection of functions by taking the weak form of the governing equation which is multiplied by a weight function from the same finite dimensional space, dependent on the spatial boundaries due to Dirichlet boundary conditions, and integrating over the space [26], which is in principle equal to the method described above applied to a discrete problem. Several other variations on the Galerkin method exist for specific areas of practice, such as Petrov-Galerkin method where the weight functions come from a different space than the trial functions [26] or other nonlinear Galerkin Methods for Navier-Stokes equations [27], which are often used at fluid dynamics.

Harmonic Balance method

The technique of Harmonic Balance is a specialized application of the Galerkin method to find periodic solutions in vibration problems. In harmonic balance, there is a periodic solution with a convergent Fourrier series representation we wish to approximate [18]. All harmonics of the motion must then be so called balanced by substitution in the equation of motion and finding a set of nonlinear equations for the amplitudes of the various harmonics. HBM is based on finding linearized coefficients which depend on both the frequency and the amplitude of oscillations [28]. Not all harmonics can be balanced because for some harmonics the number of unknowns is larger than the number of equations [15]. Usually only a few harmonic terms are used to approximate the solutions. According to Genta, the harmomic balance technique is very good in the case of hardening or mildy nonlinear systems with softening and small amplitudes [15].

B.3. Asymptotic Techniques

Asymptotic techniques depend on some parameter in the problem being very small or very large. The solution is sought for the limit where this very small parameter goes towards zero or the large parameter goes to infinity [18].

Method of averaging

The asymptotic method of averaging can be applied to weakly nonlinear systems of the form.

$$\dot{x} = \epsilon f(x,t) \qquad \text{for} \epsilon << 1 \tag{B.5}$$

By averaging the original system a easier time-invariant system is obtained. The averaged system can be used to study the stability of the original system.

$$f(x,t) = f(x,t+T) \quad \rightarrow \quad \dot{x} = \epsilon f_0(x) \text{ with } f_0(x) = \frac{1}{T}\int_0^T f(x,t)\,dt \tag{B.6}$$

Ritz averaging technique or the method of Kirilov and Bogoljubov

Based on the substitution of some nonlinear functions with their average over one period [15]. The basis of the averaging technique is that the average energy of the virtual work done in a complete cycle of an undamped system must vanish. The solution is approximated with a linear combination of arbitrary time functions with a constant.

$$x(t) = \sum_{i=1}^{n} a_i \phi_i(t) \qquad \longrightarrow \qquad \delta x = \sum_{i=1}^{n} \delta a_i \phi_i(t) \tag{B.7}$$

Instead of substitution in the equation of motion, stating that the EM should be satisfied at each instant, the EM is only satisfied as an average over one period of motion. The average virtual work δxi n one cycle must be zero for each arbitraty constant a_i, giving a set of nonlinear differential equations that should be solved numerically.

$$\delta L = \sum_{i=1}^{n} \int_0^T \left[\ddot{x} + \frac{f(x)}{m}\right] \delta a_i \phi_i(t)\,dt = 0 \tag{B.8}$$

$$\longrightarrow \qquad \int_0^T \left[\ddot{x} + \frac{f(x)}{m}\right] \phi_i(t)\,dt = 0 \qquad \text{for} i = 1,2,...,n \tag{B.9}$$

Method of multiple scales

The method of multiple scales is an extension to the averaging method. It identifies and removes the secular terms within the system by introducing two time scales: an actual time and a reduced time scale [30]. Mahmoodi used the method of multiple scales to study the weakness of the nonlinear terms in the slow time scale [29] after discretizing the problem using Galerkin Methods.

B.4. Numerical methods

As mentioned above are numerical methods the most used methods in engineering practice, both direct integration of the equation of motion and numerical integration after several transformation steps. However, in nonlinear dynamics it is difficult to determine the quality of the found solution based on solely numerical simulations [18]. An analytical or theoretical study of simplified nonlinear systems is an essential contribution to all-numerical studies of large nonlinear systems.

Direct integration method

The response is obtained by integrating the equation of motion directly. Solutions to the system contain time histories and therefore a deterministic function for the excitations is needed to determine the amplitude at each time step [11]. The state of the system at time $t + \Delta t$ is computed from the known conditions at state t based on integration scheme's. The interval length should be small enough to eliminate large errors, but large enough to reduce the calculation effort.

Within the direct integration methods a distinction is made between implicit integration methods and ex-

plicit methods. Explicit methods are conditionally stable where implicit scheme's are unconditionally stable. Explicit methods are stable when the time step is smaller than the critical time step. With the need for a small time step, explicit methods are not suitable for long duration events. At implicit methods, the accuracy of the response is not garanteed and the calculation time at each step is longer than for explicit methods. Explicit methods are often used for systems with large deformations or nonlinearities, where implicit methods are used for linear systems with long duration events [11].

There are many integration schemes developed for initial value problems with ordinary differential equations. The most simple scheme is the Euler method. Closely related are the Trapezoidal method and the midpoint-method. They are easy to implement, but have a small maximum accuracy and are therefore not suited for nonlinear systems.

The implicit Euler method is described with:

$$y_{n+1} = y_n + h \cdot f(t_n, y_n) \tag{B.10}$$

Taylor methods look for higher order approximations following the Taylor polynomial approximation. However for computing higher order approximations, higher order derivatives of the true solution are needed which makes the method very time-consuming [31]

Runge-Kutta methods, and especially higher order RK-methods, provide a more accurate accuracy within reasonable computation time. The fourth-order Runge-Kutta method having a truncation error of $O(h^4)$ is one of the most widely used methods for solving differential equations [32] due to the relatively high accuracy compared with the calculation effort.

Runge-Kutta Method:

$$y_{n+1} = y_n + \frac{h}{6}(k_1 + 2\cot k_2 + 2 \cdot k_3 + k_4) \tag{B.11}$$

$$k_1 = f(t_n, y_n) \tag{B.12}$$

$$k_2 = f(t_n + h/2, y_n + k1 \cdot h/2) \tag{B.13}$$

$$k_3 = f(t_n + h/2, y_n + k2 \cdot h/2) \tag{B.14}$$

$$k_4 = f(t_n + h, y_n + k3 \cdot h) \tag{B.15}$$

In Figure B.1 the Runge-Kutta method is compared with the Euler method for a simple first order differential equation.

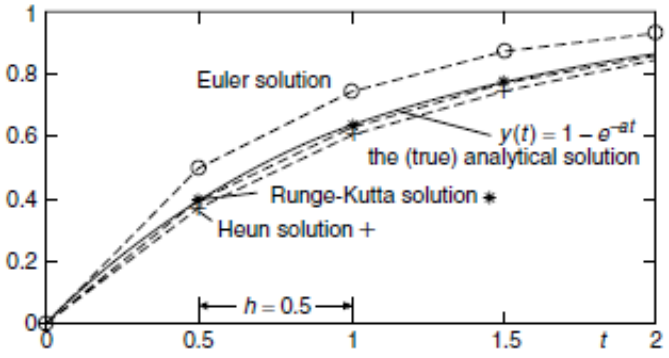

Figure B.1: Comparison numerical integration schemes [32]

Multi-step methods use solution values at several previous nodes to compute the numerical solution. Adams-bashforth methods and adams-moulton methods are the most used multiple-step methods [31]. They can cope with stiff differential equations, but the accuracy relative to computations time is low.

Iterative solution method

Iterative methods are restricted to weakly nonlinear and non-autonomous systems. It can be used at systems of which the equation of motion can be separated into a part containing only linear terms and a second relatively small part containing the nonlinear terms [15]. First a zero-order approximation solution is sought behaving equally to the harmonic behavior of the linearized system. Then this solution is introduced in the RHS of the EM to find a first-order solution.

C

FULL CALCULATIONS GALERKIN METHOD

C.1. Natural frequency and mode shape determination

The equation of motion and the boundary conditions that are using to find the linear natural frequencies and mode shapes of the beam are the following:

$$\rho A \frac{\partial^2 w}{\partial t^2} + EI \frac{\partial^4 w}{\partial x^4} = 0 \tag{C.1}$$

The boundary conditions are stated as:

$$EI \frac{\partial^2 w}{\partial x^2}|_{x=0} = kr_1 \frac{\partial w}{\partial x}|_{x=0} \tag{C.2}$$

$$w(0) = 0 \tag{C.3}$$

$$EI \frac{\partial^2 w}{\partial x^2}|_{x=L} = -kr_2 \frac{\partial w}{\partial x}|_{x=L} \tag{C.4}$$

$$w(L) = 0 \tag{C.5}$$

The method of separation of variables is used for solving this homogeneous equation of motion. A trial solution is used, containing both a space related and a time related part:

$$w(x,t) = W(x)\,\Psi(t) \tag{C.6}$$

Where $\Psi(t) = \sum \hat{\Psi} exp(i\omega t)$

$$\frac{\partial}{\partial t}(w(x,t)) = W(x)\, i\omega \Psi(t) \tag{C.7}$$

$$\frac{\partial^2}{\partial t^2}(w(x,t)) = -W(x)\,\omega^2 \Psi(t) \tag{C.8}$$

$$\frac{\partial}{\partial x}(w(x,t)) = \frac{\partial W(x)}{\partial x}\Psi(t) \tag{C.9}$$

$$\frac{\partial^2}{\partial x^2}(w(x,t)) = \frac{\partial^2 W(x)}{\partial x^2}\Psi(t) \tag{C.10}$$

$$\frac{\partial^3}{\partial x^3}(w(x,t)) = \frac{\partial^3 W(x)}{\partial x^3}\Psi(t) \tag{C.11}$$

$$\frac{\partial^4}{\partial x^4}(w(x,t)) = \frac{\partial^4 W(x)}{\partial x^4}\Psi(t) \tag{C.12}$$

(C.13)

Using substituting of the trial solution into the equation of motion, a time independent equation of motion can be derived which describes together with the boundary conditions the modes of vibration.

$$-\rho A W(x)\omega^2 \Psi(t) + EI\frac{\partial^4 W(x)}{\partial x^4}\Psi(t) = 0 \tag{C.14}$$

$$\left\{-\rho A\omega^2 W(x) + EI\frac{\partial^4 W(x)}{\partial x^4}\right\}\Psi(t) = 0 \tag{C.15}$$

$$EI\frac{\partial^4 W(x)}{\partial x^4} - \rho A\omega^2 W(x) = 0 \qquad \text{for all t} \tag{C.16}$$

$$\frac{\partial^4 W(x)}{\partial x^4} - \beta^4 W(x) = 0 \qquad \text{for all t} \tag{C.17}$$

where $\beta^4 = \frac{\rho A\omega^2}{EI}$.

The normal modes are assumed to be of the form:

$$W(x) = \sum^{4} C_k exp(\lambda_k x) \tag{C.18}$$

Inserting in Equation C.17 gives the roots of the lambda's in the assumed solution.

$$\lambda_1 = \beta, \lambda_2 = -\beta, \lambda_3 = i\beta, \lambda_4 = -i\beta \tag{C.19}$$

$$W(x) = C_1 exp(\beta x) + C_2 exp(-\beta x) + C_3 exp(i\beta x) + C_4 exp(-i\beta x) \tag{C.20}$$

$$W(x) = A\cosh(\beta x) + B\sinh(\beta x) + C\cos(\beta x) + D\sin(\beta x) \tag{C.21}$$

This is only space-related, so the differentials are:

$$\frac{d}{dx}W(x) = A\beta\sinh(\beta x) + B\beta\cosh(\beta x) - C\beta\sin(\beta x) + D\beta\cos(\beta x) \tag{C.22}$$

$$\frac{d^2}{dx^2}W(x) = A\beta^2\cosh(\beta x) + B\beta^2\sinh(\beta x) - C\beta^2\cos(\beta x) - D\beta^2\sin(\beta x) \tag{C.23}$$

For finding the modes the boundary conditions of C.2-C.5 should be met.

$$EI\frac{d^2W}{dx^2}|_{x=0} = kr_1\frac{dW}{dx}|_{x=0} \tag{C.24}$$

$$W(0) = 0 \tag{C.25}$$

$$EI\frac{d^2W}{dx^2}|_{x=L} = -kr_2\frac{dW}{dx}|_{x=L} \tag{C.26}$$

$$W(L) = 0 \tag{C.27}$$

Substitution of C.21,C.22,C.23 gives a system of equations:

$$EI\left\{A\beta^2\cosh(\beta x) + B\beta^2\sinh(\beta x) - C\beta^2\cos(\beta x) - D\beta^2\sin(\beta x)\right\}|_{x=0}$$
$$= kr_1\left\{A\beta\sinh(\beta x) + B\beta\cosh(\beta x) - C\beta\sin(\beta x) + D\beta\cos(\beta x)\right\}|_{x=0} \tag{C.28}$$

$$A\cosh(\beta x) + B\sinh(\beta x) + C\cos(\beta x) + D\sin(\beta x)|_{x=0} = 0 \tag{C.29}$$

$$EI\left\{A\beta^2\cosh(\beta x) + B\beta^2\sinh(\beta x) - C\beta^2\cos(\beta x) - D\beta^2\sin(\beta x)\right\}|_{x=L}$$
$$= -kr_2\left\{A\beta\sinh(\beta x) + B\beta\cosh(\beta x) - C\beta\sin(\beta x) + D\beta\cos(\beta x)\right\}|_{x=L} \tag{C.30}$$

$$A\cosh(\beta x) + B\sinh(\beta x) + C\cos(\beta x) + D\sin(\beta x)|_{x=L} = 0 \tag{C.31}$$

$$\tag{C.32}$$

Using values $x = 0$ and $x = L$ gives:

$$EI\left\{A\beta^2 - C\beta^2\right\} - kr_1\left\{B\beta + D\beta\right\} = 0 \tag{C.33}$$

$$A + C = 0 \tag{C.34}$$

$$\begin{aligned} EI\left\{A\beta^2\cosh(\beta L) + B\beta^2\sinh(\beta L) - \beta^2 C\cos(\beta L) - \beta^2 D\sin(\beta L)\right\} \\ + kr_2\left\{A\beta\sinh(\beta L) + B\beta\cosh(\beta L) - C\beta\sin(\beta L) + D\beta\cos(\beta L)\right\} = 0 \end{aligned} \tag{C.35}$$

$$A\cosh(\beta L) + B\sinh(\beta L) + C\cos(\beta L) + D\sin(\beta L) = 0 \tag{C.36}$$

Which can be written in the form of a matrix of coefficients:

$$\begin{bmatrix} EI\beta^2 & -kr_1\beta & -EI\beta^2 & -kr_1\beta \\ 1 & 0 & 1 & 0 \\ EI\beta^2\cosh(\beta L) + kr_2\beta\sinh(\beta L) & EI\beta^2\sinh(\beta L) + kr_2\beta\cosh(\beta L) & -EI\beta^2\cos(\beta L) - kr_2\beta\sin(\beta L) & -EI\beta^2\sin(\beta L) + kr_2\beta\cos(\beta L) \\ \cosh(\beta L) & \sinh(\beta L) & \cos(\beta L) & \sin(\beta L) \end{bmatrix} \begin{bmatrix} A \\ B \\ C \\ D \end{bmatrix} = 0 \tag{C.37}$$

C.1.0.1. Natural frequencies

The determinant of this matrix gives an equation dependent on β. Non-trivial solutions only exist when the determinant of the matrix above is equal to zero. So, only for specific β's there exist non-trivial solutions. These β's contain the natural frequencies of the system.

$$\begin{aligned} \text{Determinant} = \cos(\beta L)^2\beta^2 kr_1 kr_2 - 2(EI)^2\sinh(\beta L)\sin(\beta L)\beta^4 \\ - EI\sinh(\beta L)\cos(\beta L)\beta^3 kr_2 - EI\cosh(\beta L)\sin(\beta L)\beta^3 kr_2 \\ - 2EI^2\sinh(\beta L)\sin(\beta L)\beta^4 + 2EI\sinh(\beta L)\cos(\beta L)\beta^3 kr_1 \\ - EI\sinh(\beta L)\cos(\beta L)\beta^3 kr_2 - 2EI\cosh(\beta L)\sin(\beta L)\beta^3 kr_1 \\ - EI\cosh(\beta L)\sin(\beta L)\beta^3 kr_2 + \sinh(\beta L)^2\beta^2 kr_1 kr_2 \\ - \cosh(\beta L)^2\beta^2 kr_1 kr_2 - \sin(\beta L)^2\beta^2 kr_1 kr_2 = 0 \end{aligned}$$

C.1.0.2. Mode shapes

For each β or ω a corresponding space solution exists, which can be determined by solving the unknown constants A, B, C and D which dependend on the boundary conditions and the natural frequency. There are infinitly many solutions for these constants, because each solution can be multiplied by any constant. When a non-zero value is valid for constant D, this constant is set to 1 and all other constants are replaced by a ratio over D.

$$D(\beta) = 1 \tag{C.38}$$

$$\begin{bmatrix} EI\beta^2 & -kr_1\beta & -EI\beta^2 & -kr_1\beta \\ 1 & 0 & 1 & 0 \\ EI\beta^2\cosh(\beta L) + kr_2\beta\sinh(\beta L) & EI\beta^2\sinh(\beta L) + kr_2\beta\cosh(\beta L) & -EI\beta^2\cos(\beta L) - kr_2\beta\sin(\beta L) & -EI\beta^2\sin(\beta L) + kr_2\beta\cos(\beta L) \\ \cosh(\beta L) & \sinh(\beta L) & \cos(\beta L) & \sin(\beta L) \end{bmatrix} \begin{bmatrix} A/D \\ B/D \\ C/D \\ D/D \end{bmatrix} = 0 \tag{C.39}$$

$$\Longrightarrow \begin{bmatrix} EI\beta^2 & -kr_1\beta & -EI\beta^2 \\ 1 & 0 & 1 \\ EI\beta^2\cosh(\beta L) + kr_2\beta\sinh(\beta L) & EI\beta^2\sinh(\beta L) + kr_2\beta\cosh(\beta L) & -EI\beta^2\cos(\beta L) - kr_2\beta\sin(\beta L) \end{bmatrix} \begin{bmatrix} A/D \\ B/D \\ C/D \end{bmatrix} = \begin{bmatrix} +kr_1\beta \\ 0 \\ +EI\beta^2\sin(\beta L) - kr_2\beta\cos(\beta L) \end{bmatrix} \tag{C.40}$$

For each value β now a value for the unknown constants A,B and C can be determined and the mode shape for each natural frequency is determined.

$$\begin{bmatrix} A(\beta) \\ B(\beta) \\ C(\beta) \end{bmatrix} = \begin{bmatrix} EI\beta^2 & -kr_1\beta & -EI\beta^2 \\ 1 & 0 & 1 \\ EI\beta^2\cosh(\beta L) & EI\beta^2\sinh(\beta L) & -EI\beta^2\cos(\beta L) \\ +kr_2\beta\sinh(\beta L) & +kr_2\beta\cosh(\beta L) & -kr_2\beta\sin(\beta L) \end{bmatrix}^{-1} \begin{bmatrix} +kr_1\beta \\ 0 \\ +EI\beta^2\sin(\beta L) \\ -kr_2\beta\cos(\beta L) \end{bmatrix} \tag{C.41}$$

Using Maple, the following functions describe how A,B,C and D depend on β.

$$\begin{aligned} A(\beta) = {} & (EI\sinh(\beta L)\beta + \cosh(\beta L)kr_2)kr_1/(2EI^2\sinh(\beta L)\beta^2 + EI\cosh(\beta L)\beta kr_1 \\ & +2EI\cosh(\beta L)\beta kr_2 + EI\cos(\beta L)\beta kr_1 + \sinh(\beta L)kr_1kr_2 + \sin(\beta L)kr_1kr_2) + kr_1(EI\beta^2\sin(\beta L) \\ & -kr_2\beta\cos(\beta L))/(\beta(2EI^2\sinh(\beta L)\beta^2 + EI\cosh(\beta L)\beta kr_1 + 2EI\cosh(\beta L)\beta kr_2 + EI\cos(\beta L)\beta kr_1 \\ & +\sinh(\beta L)kr_1kr_2 + \sin(\beta L)kr_1kr_2)) \end{aligned} \tag{C.42}$$

$$\begin{aligned} B(\beta) = {} & -(EI\cosh(\beta L)\beta + EI\cos(\beta L)\beta + \sinh(\beta L)kr_2 + \sin(\beta L)kr_2)kr_1/(2EI^2\sinh(\beta L)\beta^2 \\ & +EI\cosh(\beta L)\beta kr_1 + 2EI\cosh(\beta L)\beta kr_2 + EI\cos(\beta L)\beta kr_1 + \sinh(\beta L)kr_1kr_2 \\ & +\sin(\beta L)kr_1kr_2) + 2EI(EI\beta^2\sin(\beta L) - kr_2\beta\cos(\beta L))/(2EI^2\sinh(\beta L)\beta^2 \\ & +EI\cosh(\beta L)\beta kr_1 + 2EI\cosh(\beta L)\beta kr_2 + EI\cos(\beta L)\beta kr_1 + \sinh(\beta L)kr_1kr_2 + \sin(\beta L)kr_1kr_2) \end{aligned} \tag{C.43}$$

$$\begin{aligned} C(\beta) = {} & -(EI\sinh(\beta L)\beta + \cosh(\beta L)kr_2)kr_1/(2EI^2\sinh(\beta L)\beta^2 + EI\cosh(\beta L)\beta kr_1 + 2EI\cosh(\beta L)\beta kr_2 \\ & +EI\cos(\beta L)\beta kr_1 + \sinh(\beta L)kr_1kr_2 + \sin(\beta L)kr_1kr_2) - kr_1(EI\beta^2\sin(\beta L) \\ & -kr_2\beta\cos(\beta L))/(\beta(2EI^2\sinh(\beta L)\beta^2 + EI\cosh(\beta L)\beta kr_1 + 2EI\cosh(\beta L)\beta kr_2 + EI\cos(\beta L)\beta kr_1 \\ & +\sinh(\beta L)kr_1kr_2 + \sin(\beta L)kr_1kr_2)) \end{aligned} \tag{C.44}$$

$$D(\beta) = 1 \tag{C.45}$$

This makes the mode shape:

$$w_n(x) = A_n\cosh(\beta_n x) + B_n\sinh(\beta_n x) + C_n\cos(\beta_n x) + D_n\sin(\beta_n x) \tag{C.46}$$

With derivatives:

$$\frac{dw_n}{dx} = \beta_n\left(A_n\sinh(\beta_n x) + B_n\cosh(\beta_n x) - C_n\sin(\beta_n x) + D_n\cos(\beta_n x)\right) \tag{C.47}$$

$$\frac{d^2w_n}{dx^2} = \beta_n^2\left(A_n\cosh(\beta_n x) + B_n\sinh(\beta_n x) - C_n\cos(\beta_n x) - D_n\sin(\beta_n x)\right) \tag{C.48}$$

$$\frac{d^3w_n}{dx^3} = \beta_n^3\left(A_n\sinh(\beta_n x) + B_n\cosh(\beta_n x) + C_n\sin(\beta_n x) - D_n\cos(\beta_n x)\right) \tag{C.49}$$

$$\frac{d^4w_n}{dx^4} = \beta_n^4\left(A_n\cosh(\beta_n x) + B_n\sinh(\beta_n x) + C_n\cos(\beta_n x) + D_n\sin(\beta_n x)\right) = \beta_n^4 w_n(x) \tag{C.50}$$

C.2. Galerkin approximation for nonlinear part

The equation of motion and the boundary conditions are the following:

$$\rho A\frac{\partial^2 w}{\partial t^2}+\left(E+E*\frac{\partial}{\partial t}\right)I\frac{\partial^4 w}{\partial x^4}=0 \tag{C.51}$$

(1) $$w(0)=0 \tag{C.52}$$

(2) $$EI\frac{\partial^2 w}{\partial x^2}|_{x=0}=kr_1\left(\frac{\partial w}{\partial x}|_{x=0}-\varphi_c(t)\right)+cr_1\left(\frac{\partial^2 w}{\partial t\partial x}|_{x=0}-\dot{\varphi}_c(t)\right)+\mu_1 sgn\left(\frac{\partial^2 w}{\partial t\partial x}|_{x=0}-\dot{\varphi}_c(t)\right) \tag{C.53}$$

(3) $$w(L)=0 \tag{C.54}$$

(4) $$EI\frac{\partial^2 w}{\partial x^2}|_{x=0}=-kr_2\left(\frac{\partial w}{\partial x}|_{x=L}-\varphi_c(t)\right)-cr_2\left(\frac{\partial^2 w}{\partial t\partial x}|_{x=L}-\dot{\varphi}_c(t)\right)-\mu_2 sgn\left(\frac{\partial^2 w}{\partial t\partial x}|_{x=L}-\dot{\varphi}_c(t)\right) \tag{C.55}$$

Here $\varphi(t)$ and $\dot{\varphi}(t)$ are the rotations of the MLBS.

For implementing the Galerkin approximation, the part of the boundary conditions which is not satisfied by the found mode shapes are introduced in the equation of motion. This are all conditions concerning damping and the external forces. Boundary conditions (1) and (3) are already met by the linear mode shapes $w_n(x)=A_n\cosh(\beta_n x)+B_n\sinh(\beta_n x)+C_n\cos(\beta_n x)+D_n\sin(\beta_n x)$. The springs are also already met by the modes.

Rewriting the equation of motion gives:

$$\begin{aligned}\rho A\frac{\partial^2 w}{\partial t^2}+EI\frac{\partial^4 w}{\partial x^4}+E^*I\frac{\partial}{\partial t}\frac{\partial^4 w}{\partial x^4}&\\ =\delta'(x)\left\{cr_1\left(\frac{\partial^2 w}{\partial t\partial x}-\dot{\varphi}_c(t)\right)+\mu_1 sgn\left(\frac{\partial^2 w_f}{\partial t\partial x}-\dot{\varphi}_c(t)\right)+kr_1\left(-\varphi_c(t)\right)\right\}&\\ -\delta'(x-L)\left\{-cr_2\left(\frac{\partial^2 w}{\partial t\partial x}-\dot{\varphi}_c(t)\right)-\mu_2 sgn\left(\frac{\partial^2 w_f}{\partial t\partial x}-\dot{\varphi}_c(t)\right)-kr_2\left(-\varphi_c(t)\right)\right\}&\end{aligned} \tag{C.56}$$

Following the Galerkin Method, the trial solution is described by Equation C.58, consisting of a summation of the product of a time related part and the mode shapes of the linear problem [29].

$$w(x,t)=\sum_{n=1}^{\infty}\psi_n(t)\,w_n(x) \tag{C.57}$$

Inserting this trial solution in the EM and solving the EM will give a approximated solution containing a part with uncoupled modes and a residual, which is including the nonlinear part of the solution ([30], [24]).

$$w(x,t)=\sum_{m=1}^{\infty}\psi_m(t)\,w_m(x)+\text{res} \tag{C.58}$$

LHS

Substitution the trial solution into the equation of motion and using the relation between $w_n(x)$ and $w_n''''(x)$ gives for the LHS:

$$\text{LHS} = \rho A \frac{\partial^2 w}{\partial t^2} + EI \frac{\partial^4 w}{\partial x^4} + E^* I \frac{\partial}{\partial t} \frac{\partial^4 w}{\partial x^4} \tag{C.59}$$

$$= \rho A \sum_{n=1}^{\infty} \ddot{\psi}_n(t) w_n(x) + EI \sum_{n=1}^{\infty} \psi_n(t) w_n''''(x) + E^* I \sum_{n=1}^{\infty} \dot{\psi}_n(t) w_n''''(x) \tag{C.60}$$

$$= \rho A \sum_{n=1}^{\infty} \ddot{\psi}_n(t) w_n(x) + EI \sum_{n=1}^{\infty} \psi_n(t) \beta_n^4 w_n(x) + E^* I \sum_{n=1}^{\infty} \dot{\psi}_n(t) \beta_n^4 w_n(x) \tag{C.61}$$

$$= \rho A \sum_{n=1}^{\infty} \ddot{\psi}_n(t) w_n(x) + EI \beta_n^4 \sum_{n=1}^{\infty} \psi_n(t) w_n(x) + E^* I \beta_n^4 \sum_{n=1}^{\infty} \dot{\psi}_n(t) w_n(x) \tag{C.62}$$

By multiplication with a base function $w_m(x)$ which fits the non-damped linear boundary conditions, the mode shapes, and by integration over the length of the beam Galerkin's projection is obtained [81]. Using the orthogonality conditions of the mode shapes, which gives that $\int w_n(x) w_m(x) dx = 0$ for $n \neq m$ [14].

$$\int_0^L \text{LHS} w_m^2(x) dx = \int_0^L \left(\rho A \sum_{n=1}^{\infty} \ddot{\psi}_n(t) w_n(x) \right) w_m(x) dx + \int_0^L \left(EI \beta_n^4 \sum_{n=1}^{\infty} \psi_n(t) w_n(x) \right) w_m(x) dx$$
$$+ \int_0^L \left(E^* I \beta_n^4 \sum_{n=1}^{\infty} \dot{\psi}_n(t) w_n(x) \right) w_m(x) dx \tag{C.63}$$

$$= \rho A \ddot{\psi}_m(t) \int_0^L w_m^2(x) dx + EI \beta_m^4 \psi_m(t) \int_0^L w_m^2(x) dx + E^* I \beta_m^4 \dot{\psi}_m(t) \int_0^L w_m^2(x) dx \tag{C.64}$$

where $\int_0^L w_m^2(x) dx$ is defined as:

$$\int_0^L w_m^2(x) dx = \int_0^L \left(A_m \cosh(\beta_m x) + B_m \sinh(\beta_m x) + C_m \cos(\beta_m x) + D_m \sin(\beta_m x) \right)^2 dx \tag{C.65}$$

$$\begin{aligned}
&= \frac{1}{8} \frac{1}{\beta_m} (-4 A_m \exp^{2\beta_m L} B_m + 2 A_m \exp^{4\beta_m L} B_m \\
&+ 8 A_m D_m \exp^{2\beta_m L} - 8 B_m C_m \exp^{2\beta_m L} + 8 C_m D_m \exp^{2\beta_m L} + B_m^2 \exp^{4\beta_m L} \\
&+ A_m^2 \exp^{4\beta_m L} + 4 A_m C_m \exp^{3\beta_m L} \cos(\beta_m L) + 4 A_m C_m \exp^{3\beta_m L} \sin(\beta_m L) \\
&- 4 A_m C_m \exp^{\beta_m L} \cos(\beta_m L) + 4 A_m C_m \exp^{\beta_m L} \sin(\beta_m L) - 4 A_m D_m \exp^{\beta_m L} \cos(\beta_m L) \\
&- 4 A_m D_m \exp^{\beta_m L} \sin(\beta_m L) + 4 B_m C_m \exp^{\beta_m L} \cos(\beta_m L) - 4 B_m C_m \exp^{\beta_m L} \sin(\beta_m L) \\
&+ 4 B_m D_m \exp^{\beta_m L} \cos(\beta_m L) + 4 B_m D_m \exp^{\beta_m L} \sin(\beta_m L) - 4 A_m D_m \exp^{3\beta_m L} \cos(\beta_m L) \\
&+ 4 A_m D_m \exp^{3\beta_m L} \sin(\beta_m L) - 4 B_m^2 \beta_m L \exp^{2\beta_m L} + 4 B_m C_m \exp^{3\beta_m L} \cos(\beta_m L) \\
&+ 4 B_m C_m \exp^{3\beta_m L} \sin(\beta_m L) - 4 B_m D_m \exp^{3\beta_m L} \cos(\beta_m L) + 4 B_m D_m \exp^{3\beta_m L} \sin(\beta_m L) \\
&+ 4 C_m^2 L \exp^{2\beta_m L} \beta_m + 4 C_m^2 \exp^{2\beta_m L} \cos(\beta_m L) \sin(\beta_m L) - 8 C_m D_m \cos(\beta_m L)^2 \exp^{2\beta_m L} \\
&+ 4 D_m^2 L \exp^{2\beta_m L} \beta_m - 4 D_m^2 \exp^{2\beta_m L} \cos(\beta_m L) \sin(\beta_m L) + 4 A_m^2 \beta_m L \exp^{2\beta_m L} \\
&+ 2 A_m B_m - A_m^2 - B_m^2) \exp^{-2\beta_m L}
\end{aligned} \tag{C.66}$$

$$\int_0^L w_m^2(x) dx = C_{w_m} \tag{C.67}$$

which gives a constant. As can be seen, all terms in the LHS contain fully uncoupled modes.

RHS

Substitution of the general solution into the equation of motion and expressing the approximate solution in linear mode shapes gives for the RHS:

$$\begin{aligned}\text{RHS} = \delta'(x)&\left\{cr_1\left(\frac{\partial^2 w}{\partial t\partial x}-\dot{\varphi}_c(t)\right)+\mu_1 sgn\left(\frac{\partial^2 w_f}{\partial t\partial x}-\dot{\varphi}_c(t)\right)+kr_1\left(-\varphi_c(t)\right)\right\}\\ &-\delta'(x-L)\left\{-cr_2\left(\frac{\partial^2 w}{\partial t\partial x}-\dot{\varphi}_c(t)\right)-\mu_2 sgn\left(\frac{\partial^2 w_f}{\partial t\partial x}-\dot{\varphi}_c(t)\right)-kr_2\left(-\varphi_c(t)\right)\right\} \qquad \text{(C.68)}\\ =\delta'(x)&\left\{M_{BC,l}\left(\frac{\partial^2 w}{\partial t\partial x},\dot{\varphi}_c(t),\varphi_c(t)\right)\right\}-\delta'(x-L)\left\{M_{BC,r}\left(\frac{\partial^2 w}{\partial t\partial x},\dot{\varphi}_c(t),\varphi_c(t)\right)\right\} \qquad \text{(C.69)}\\ =\delta'(x)&\left\{M_{BC,l}\left(\sum_{n=1}^{\infty}\dot{\psi}_n(t)w_n'(x),\dot{\varphi}_c(t),\varphi_c(t)\right)\right\}-\delta'(x-L)\left\{M_{BC,r}\left(\sum_{n=1}^{\infty}\dot{\psi}_n(t)w_n'(x),\dot{\varphi}_c(t),\varphi_c(t)\right)\right\} \qquad \text{(C.70)}\end{aligned}$$

Where

$$M_{BC,l}\left(\frac{\partial^2 w(x,t)}{\partial t\partial x},\dot{\varphi}_c(t),\varphi_c(t)\right)=cr_1\left(\frac{\partial^2 w(x,t)}{\partial t\partial x}-\dot{\varphi}_c(t)\right)+\mu_1 sgn\left(\frac{\partial^2 w(x,t)}{\partial t\partial x}-\dot{\varphi}_c(t)\right)+kr_1\left(-\varphi_c(t)\right) \qquad \text{(C.71)}$$

$$M_{BC,r}\left(\frac{\partial^2 w(x,t)}{\partial t\partial x},\dot{\varphi}_c(t),\varphi_c(t)\right)=-cr_2\left(\frac{\partial^2 w(x,t)}{\partial t\partial x}-\dot{\varphi}_c(t)\right)-\mu_2 sgn\left(\frac{\partial^2 w(x,t)}{\partial t\partial x}-\dot{\varphi}_c(t)\right)-kr_2\left(-\varphi_c(t)\right) \qquad \text{(C.72)}$$

By multiplication with a base function $w_m(x)$ which fits the non-damped linear boundary conditions, the mode shapes, and integration over the length of the beam Galerkin's projection is obtained.

$$\begin{aligned}\int_0^L \text{RHS}\, w_m(x)\,dx=&\int_0^L \delta'(x)\left\{M_{BC,l}\left(\sum_{n=1}^{\infty}\dot{\psi}_n(t)w_n'(x),\dot{\varphi}_c(t),\varphi_c(t)\right)\right\}w_m(x)\,dx\\ &-\int_0^L \delta'(x-L)\left\{M_{BC,r}\left(\sum_{n=1}^{\infty}\dot{\psi}_n(t)w_n'(x),\dot{\varphi}_c(t),\varphi_c(t)\right)\right\}w_m(x)\,dx \qquad \text{(C.73)}\end{aligned}$$

Using partial integration removes the derivative of the Delta Dirac function and gives us the following form:

$$\begin{aligned}\int_0^L \delta'(x-a)f(x)w_m(x)\,dx&=\left[f(x)w_m(x)\delta(x-a)\right]_0^L-\int_0^L \delta(x-a)\frac{d}{dx}\left(f(x)w_m(x)\right)dx \qquad \text{(C.74)}\\ &=\left[f(x)w_m(x)\delta(x-a)\right]_0^L-\int_0^L \delta(x-a)\left(f'(x)w_m(x)+f(x)w_m'(x)\right)dx \qquad \text{(C.75)}\end{aligned}$$

with

$$a_1=0 \qquad \text{(C.76)}$$

$$a_2=L \qquad \text{(C.77)}$$

$$f_1(x)=M_{BC,l}\left(\frac{\partial^2 w(x,t)}{\partial t\partial x},\dot{\varphi}_c(t),\varphi_c(t)\right) \qquad \text{(C.78)}$$

$$f_2(x)=M_{BC,r}\left(\frac{\partial^2 w(x,t)}{\partial t\partial x},\dot{\varphi}_c(t),\varphi_c(t)\right) \qquad \text{(C.79)}$$

Because $w_m(x)=0$ for $x=0$ and $x=L$, the first term falls out of equation C.75, only the integral remains.

$$\longrightarrow \quad =-\int_0^L \delta(x-a)\left(f'(x)w_m(x)+f(x)w_m'(x)\right)dx \qquad \text{(C.80)}$$

Using the properties of the Delta-Dirac function, Equation C.81, the integral can be rewritten is the following:

$$\int_{\infty} \delta(x-a) f(x) dx = f(a) \tag{C.81}$$

$$\rightarrow \quad = -f'(a) w_m(a) - f(a) w'_m(a) \tag{C.82}$$

Again because of the boundary conditions, $w_m(x) = 0$ for $x = 0$ and $x = L$, the first term falls out of the equation, leaving

$$\rightarrow \quad = -f(a) w'_m(a) \tag{C.83}$$

Now, using this relation in Equation C.73 gives:

$$\begin{aligned}
&\int_0^L \text{RHS} w_m(x) dx \\
&\quad = \int_0^L \delta'(x) \left\{ M_{BC,l} \left(\sum_{n=1}^{\infty} \dot{\psi}_n(t) w'_n(x), \dot{\varphi}_c(t), \varphi_c(t) \right) \right\} w_m(x) dx \\
&\qquad - \int_0^L \delta'(x-L) \left\{ M_{BC,r} \left(\sum_{n=1}^{\infty} \dot{\psi}_n(t) w'_n(x), \dot{\varphi}_c(t), \varphi_c(t) \right) \right\} w_m(x) dx \qquad \text{(C.84)} \\
&\quad = -M_{BC,l} \left(\sum_{n=1}^{\infty} \dot{\psi}_n(t) w'_n(0), \dot{\varphi}_c(t), \varphi_c(t) \right) w'_m(0) + M_{BC,r} \left(\sum_{n=1}^{\infty} \dot{\psi}_n(t) w'_n(L), \dot{\varphi}_c(t), \varphi_c(t) \right) w'_m(L) \qquad \text{(C.85)} \\
&\quad = -cr_1 \left(\sum_{n=1}^{\infty} \dot{\psi}_n(t) w'_n(0) - \dot{\varphi}_c(t) \right) w'_m(0) - \mu_1 sgn \left(\sum_{n=1}^{\infty} \dot{\psi}_n(t) w'_n(0) - \dot{\varphi}_c(t) \right) w'_m(0) \\
&\qquad - kr_1 \left(-\varphi_c(t) \right) w'_m(0) - cr_2 \left(\sum_{n=1}^{\infty} \dot{\psi}_n(t) w'_n(L) - \dot{\varphi}_c(t) \right) w'_m(L) \\
&\qquad - \mu_2 sgn \left(\sum_{n=1}^{\infty} \dot{\psi}_n(t) w'_n(L) - \dot{\varphi}_c(t) \right) w'_m(L) - kr_2 \left(-\varphi_c(t) \right) w'_m(L) \qquad \text{(C.86)}
\end{aligned}$$

LHS and RHS combined

The LHS is after the multiplication with a base function and integration over the beam length transformed into uncoupled terms independent of x, the right hand side, however, is still coupled and x-dependent with two Delta Dirac functions present. The complete equation becomes:

$$\begin{aligned}
&\rho A \ddot{\psi}_m(t) \int_0^L w_m^2(x) dx + EI\beta_m^4 \psi_m(t) \int_0^L w_m^2(x) dx + E^* I \beta_m^4 \dot{\psi}_m(t) \int_0^L w_m^2(x) dx \\
&\qquad = -cr_1 \left(\sum_{n=1}^{\infty} \dot{\psi}_n(t) w'_n(0) - \dot{\varphi}_c(t) \right) w'_m(0) - \mu_1 sgn \left(\sum_{n=1}^{\infty} \dot{\psi}_n(t) w'_n(0) - \dot{\varphi}_c(t) \right) w'_m(0) \\
&\qquad\quad - kr_1 \left(-\varphi_c(t) \right) w'_m(0) - cr_2 \left(\sum_{n=1}^{\infty} \dot{\psi}_n(t) w'_n(L) - \dot{\varphi}_c(t) \right) w'_m(L) \\
&\qquad\quad - \mu_2 sgn \left(\sum_{n=1}^{\infty} \dot{\psi}_n(t) w'_n(L) - \dot{\varphi}_c(t) \right) w'_m(L) - kr_2 \left(-\varphi_c(t) \right) w'_m(L) \qquad \text{(C.87)}
\end{aligned}$$

Shortened to:

$$\begin{aligned}
&\rho A\ddot{\psi}_m(t)C_{w_m} + EI\beta_m^4\psi_m(t)C_{w_m} + E^*I\beta_m^4\dot{\psi}_m(t)C_{w_m} \\
&\quad = -cr_1\left(\sum_{n=1}^{\infty}\dot{\psi}_n(t)w_n'(0) - \dot{\varphi}_c(t)\right)w_m'(0) - \mu_1 sgn\left(\sum_{n=1}^{\infty}\dot{\psi}_n(t)w_n'(0) - \dot{\varphi}_c(t)\right)w_m'(0) \\
&\qquad - kr_1\left(-\varphi_c(t)\right)w_m'(0) - cr_2\left(\sum_{n=1}^{\infty}\dot{\psi}_n(t)w_n'(L) - \dot{\varphi}_c(t)\right)w_m'(L) \\
&\qquad - \mu_2 sgn\left(\sum_{n=1}^{\infty}\dot{\psi}_n(t)w_n'(L) - \dot{\varphi}_c(t)\right)w_m'(L) - kr_2\left(-\varphi_c(t)\right)w_m'(L)
\end{aligned} \tag{C.88}$$

For solving it numerically, first the highest order derivative, ψ_n, is factored out.

$$\begin{aligned}
\ddot{\psi}_m(t) = &-\frac{cr_1\left(\sum_{n=1}^{\infty}\dot{\psi}_n(t)w_n'(0) - \dot{\varphi}_c(t)\right)w_m'(0)}{C_{w_m}\rho A} - \frac{\mu_1 sgn\left(\sum_{n=1}^{\infty}\dot{\psi}_n(t)w_n'(0) - \dot{\varphi}_c(t)\right)w_m'(0)}{C_{w_m}\rho A} \\
&- \frac{kr_1\left(-\varphi_c(t)\right)w_m'(0)}{C_{w_m}\rho A} - \frac{cr_2\left(\sum_{n=1}^{\infty}\dot{\psi}_n(t)w_n'(L) - \dot{\varphi}_c(t)\right)w_m'(L)}{C_{w_m}\rho A} \\
&- \frac{\mu_2 sgn\left(\sum_{n=1}^{\infty}\dot{\psi}_n(t)w_n'(L) - \dot{\varphi}_c(t)\right)w_m'(L)}{C_{w_m}\rho A} - \frac{kr_2\left(-\varphi_c(t)\right)w_m'(L)}{C_{w_m}\rho A} \\
&- \frac{EI}{\rho A}\beta_m^4\psi_m(t) - \frac{E^*I}{\rho A}\beta_m^4\dot{\psi}_m(t)
\end{aligned} \tag{C.89}$$

$$\begin{aligned}
\ddot{\psi}_m(t) = &-\frac{cr_1\left(\sum_{n=1}^{\infty}\dot{\psi}_n(t)w_n'(0) - \dot{\varphi}_c(t)\right)w_m'(0)}{C_{w_m}\rho A} - \frac{\mu_1 sgn\left(\sum_{n=1}^{\infty}\dot{\psi}_n(t)w_n'(0) - \dot{\varphi}_c(t)\right)w_m'(0)}{C_{w_m}\rho A} \\
&- \frac{kr_1\left(-\varphi_c(t)\right)w_m'(0)}{C_{w_m}\rho A} - \frac{cr_2\left(\sum_{n=1}^{\infty}\dot{\psi}_n(t)w_n'(L) - \dot{\varphi}_c(t)\right)w_m'(L)}{C_{w_m}\rho A} \\
&- \frac{\mu_2 sgn\left(\sum_{n=1}^{\infty}\dot{\psi}_n(t)w_n'(L) - \dot{\varphi}_c(t)\right)w_m'(L)}{C_{w_m}\rho A} - \frac{kr_2\left(-\varphi_c(t)\right)w_m'(L)}{C_{w_m}\rho A} \\
&- \omega_m^2\psi_m(t) - \frac{E^*I}{EI}\omega_m^2\dot{\psi}_m(t)
\end{aligned} \tag{C.90}$$

D

IMPLEMENTATION IN MATLAB

D.1. Implementation Galerkin Method in matlab

The implementation in Matlab R2013a consists out of four steps:

1. Determination of the natural frequencies
2. Determination of the mode shapes and related constants
3. Numerical integration using Runge-Kutta
4. Calculation total displacements

Here, a short description for each step is given. Full Matlab scripts can be found in Section D.2 of this Appendix.

D.1.1. Determination of the natural frequencies

The natural frequencies are determined by calculation of the determinant of the boundary condition matrix for a series of ω values, β below is a function of ω.

$$\begin{bmatrix} EI\beta^2 & -kr_1\beta & -EI\beta^2 & -kr_1\beta \\ 1 & 0 & 1 & 0 \\ EI\beta^2\cosh(\beta L) + kr_2\beta\sinh(\beta L) & EI\beta^2\sinh(\beta L) + kr_2\beta\cosh(\beta L) & -EI\beta^2\cos(\beta L) - kr_2\beta\sin(\beta L) & -EI\beta^2\sin(\beta L) + kr_2\beta\cos(\beta L) \\ \cosh(\beta L) & \sinh(\beta L) & \cos(\beta L) & \sin(\beta L) \end{bmatrix} \begin{bmatrix} A \\ B \\ C \\ D \end{bmatrix} = 0 \tag{D.1}$$

For each ω a value is found as can be seen in Figure D.1

When the determinant changes from negative to positive, a first guess for a natural frequency is taken, by linear interpolation between the two points. With the fzero function in Matlab R2013a, the zero value of the determinant function close at those points is found.

```
% First guess for the frequencies, random pick as power array:
nf_trial=1000;
for fgs=1:nf_trial
first_guess_small(fgs)=0.5+1.05^(fgs-1);
check(fgs)=isfinite(func_det4x4(first_guess_small(fgs)));
end
```

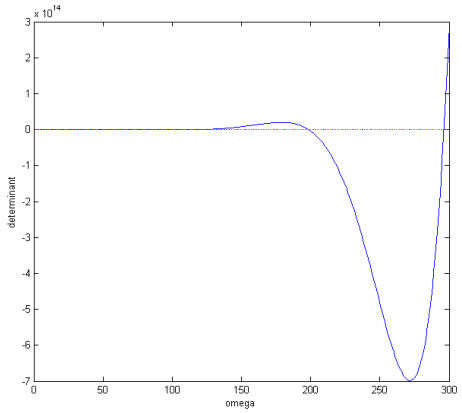

Figure D.1: Value for the determinant plotted against frequency (ω)

```
7
8  % Searching for zero values close at those n's:
9  second_guess=zeros(sum(check),1);
10 fun = @(omega) func_det4x4(omega);
11 for igs=1:sum(check)
12 second_guess(igs)=fzero(fun, first_guess_small(igs));
13 if second_guess(igs)<0
14     second_guess(igs)=0;
15 end
16 end
```

The determinant of the matrix is determined using Maple14 and given as a function of β, dependent on the natural frequency. e[ht]

```
1  function[determinant]=func_det4x4_v2(omega)
2  %calculation of the determinant of the matrix for the first model, where
3  %the determinant is given in the form of a function of omega.
4
5  %input parameters:
6  %omega is the natural frequency of the system
7
8  %output parameters:
9  %determinant for the matrix
10
11 %script:
12
13 %load and set parameters in this function script:
14 global p
15 EI=p.E*p.I;
16 beta=((p.rho*p.A*omega^2)/p.E*p.I)^(1/4);
17
18 determinant = -4*EI^2*sinh(beta*p.L)*sin(beta*p.L)*beta^4 ...
19 +2*EI*sinh(beta*p.L)*cos(beta*p.L)*beta^3*p.r1...
20     +2*EI*sinh(beta*p.L)*cos(beta*p.L)*beta^3*p.r2...
21     -2*EI*cosh(beta*p.L)*sin(beta*p.L)*beta^3*p.r1...
22     -2*EI*cosh(beta*p.L)*sin(beta*p.L)*beta^3*p.r2...
23     +sinh(beta*p.L)^2*beta^2*p.r1*p.r2-cosh(beta*p.L)^2*beta^2*p.r1*p.r2...
24     +2*cosh(beta*p.L)*cos(beta*p.L)*beta^2*p.r1*p.r2...
25     -sin(beta*p.L)^2*beta^2*p.r1*p.r2-cos(beta*p.L)^2*beta^2*p.r1*p.r2;
26 end
```

D.1.2. Determination of the mode shapes and related constants

The constants in the mode shapes are calculated by setting $D = 1$ and dividing the matrix by the 4th column of the original matrix, using Maple14, giving function for A,B and C depending on the natural frequency. The mode shapes and their first derivatives are determined with a short function of those constants and normalized such that the biggest value present equal is to 1.

```
for i=1:nf_number
omega=c.nf(i);
beta=((p.rho*p.A*(omega)^2)/p.E*p.I)^(1/4);
boundaryconditionmatrix;
c.C_D(i)=1;

%Finding amplitude constants
vectorB=-matrix4x4(1:3,4);
matrixA(1:3,1:3)=matrix4x4(1:3,1:3);
ABC=inv(matrixA)*vectorB;
c.C_A(i)=ABC(1);
```

```
function [ CA ] =func_CA( beta )
% Determination constant A in mode shape
global p
CA = (p.E*p.I*sinh(beta*p.L)*beta+cosh(beta*p.L)*p.r2)*p.r1/...
    (2*p.E*p.I^2*sinh(beta*p.L)*beta^2 +p.E*p.I*cosh(beta*p.L)...
    *beta*p.r1+2*p.E*p.I*cosh(beta*p.L)*beta*p.r2+p.E*p.I*cos(beta*p.L)...
    *beta*p.r1+sinh(beta*p.L)*p.r1*p.r2+sin(beta*p.L)*p.r1*p.r2)...
    +p.r1*(p.E*p.I*beta^2*sin(beta*p.L)-p.r2*beta*cos(beta*p.L))/...
    (beta*(2*p.E*p.I^2*sinh(beta*p.L)*beta^2+p.E*p.I*cosh(beta*p.L)...
    *beta*p.r1+2*p.E*p.I*cosh(beta*p.L)*beta*p.r2+p.E*p.I*cos(beta*p.L)...
    *beta*p.r1+sinh(beta*p.L)*p.r1*p.r2+sin(beta*p.L)*p.r1*p.r2));

end
```

Those numerical found constants are implemented in the analytical general solution for the space related part.

```
dx=0.01;
x_left=0;
x_right=p.L;
r.x=x_left:dx:x_right;

for ipp=1:nf_number
omega=c.nf(ipp);
beta=((p.rho*p.A*omega^2)/p.E*p.I)^(1/4);
for kxk=1:length(r.x);
xx=r.x(kxk);
w(ipp,kxk)=c.C_A(ipp)*cosh(beta*xx)+c.C_B(ipp)*sinh(beta*xx)+...
    c.C_C(ipp)*cos(beta*xx)+c.C_D(ipp)*sin(beta*xx);
w_diff(ipp,kxk)=c.C_A(ipp)*beta*sinh(beta*xx)+c.C_B(ipp)*beta*cosh(beta*xx)...
    -c.C_C(ipp)*beta*sin(beta*xx)+c.C_D(ipp)*beta*cos(beta*xx);
w_diff2(ipp,kxk)=c.C_A(ipp)*beta^2*cosh(beta*xx)+c.C_B(ipp)*beta^2*sinh(beta*xx)...
    -c.C_C(ipp)*beta^2*cos(beta*xx)-c.C_D(ipp)*beta^2*sin(beta*xx);
end
w(ipp,:)=w(ipp,:)/max(w(ipp,:));
```

C_{w_n} and values at the boundaries are determined for all modes. using analytical derivations. The first is calculated with Maple14 and its solution introduced as Matlab function, below, the latter is determined by hand, given above.

```
function [ cwm ] = func_cwm( nr_nf )
```

```
%UNTITLED Summary of this function goes here
%   Detaip.Led expp.Lanation goes here
global p
global c

beta=func_beta(nr_nf);
Am=c.C_A(nr_nf);
Bm=c.C_B(nr_nf);
Cm=c.C_C(nr_nf);
Dm=c.C_D(nr_nf);

cwm= 1/(8*beta)+ ( ( 2*Am*exp(4*beta*p.L)*Bm ...
    + 8*Am*Dm*exp(2*beta*p.L)-8*Bm*Cm*exp(2*beta*p.L)...
    + 8*Cm*Dm*exp(2*beta*p.L)-4*Am*exp(2*beta*p.L)*Bm ...
    + Bm^2*exp(4*beta*p.L)+ Am^2*exp(4*beta*p.L)...
    + 4*Am*Cm*exp(3*beta*p.L)*cos(beta*p.L)...
      + 4*Am*Cm*exp(3*beta*p.L)*sin(beta*p.L)...
 - 4*Am*Cm*exp(beta*p.L)*cos(beta*p.L)...
+ 4*Am*Cm*exp(beta*p.L)*sin(beta*p.L)...
- 4*Am*Dm*exp(beta*p.L)*cos(beta*p.L)...
 - 4*Am*Dm*exp(beta*p.L)*sin(beta*p.L)...
 + 4*Bm*Cm*exp(beta*p.L)*cos(beta*p.L)...
  - 4*Bm*Cm*exp(beta*p.L)*sin(beta*p.L)...
     + 4*Bm*Dm*exp(beta*p.L)*cos(beta*p.L)...
     + 4*Bm*Dm*exp(beta*p.L)*sin(beta*p.L)...
       - 4*Am*Dm*exp(3*beta*p.L)*cos(beta*p.L)...
 + 4*Am*Dm*exp(3*beta*p.L)*sin(beta*p.L)...
 - 4*Bm^2*beta*p.L*exp(2*beta*p.L)...
  + 4*Bm*Cm*exp(3*beta*p.L)*cos(beta*p.L)...
   + 4*Bm*Cm*exp(3*beta*p.L)*sin(beta*p.L)...
    - 4*Bm*Dm*exp(3*beta*p.L)*cos(beta*p.L)...
     + 4*Bm*Dm*exp(3*beta*p.L)*sin(beta*p.L)...
        + 4*Cm^2*p.L*exp(2*beta*p.L)*beta...
           + 4*Cm^2*exp(2*beta*p.L)*cos(beta*p.L)*sin(beta*p.L)...
           - 8*Cm*Dm*cos(beta*p.L)^2*exp(2*beta*p.L)...
              + 4*Dm^2*p.L*exp(2*beta*p.L)*beta...
      - 4*Dm^2*exp(2*beta*p.L)*cos(beta*p.L)*sin(beta*p.L)...
           + 4*Am^2*beta*p.L*exp(2*beta*p.L) ...
           + 2*Am*Bm - Am^2- Bm^2 )*exp(-2*beta*p.L) );
end
```

D.1.3. Numerical integration using Runge-Kutta

Matlab has several functions implemented which compute numerical solutions of ordinary differential equations:

ODE23 = second and third order Runga Kutta methods
ODE45 = fourth order Runga Kutta methods

In this script a fourth order Runge Kutta methods is used. Due to the large number of equations that have to be solved dependent on each other and the need to manually change the integration settings, it is chosen to use a selft-built script for the numerical integration.

```
r.a=zeros(2*c.n_modes,n-1);
yn=r.y0;

    for i1i=1:n-1
    t=r.ts(1)+(i1i-1)*r.h;
    indexnr=min(find(R.t(indexnr:indexnr+250)>t))+indexnr-1;
    phi=R.pos1F(indexnr)/p.H;
    phidot=R.velo1F(indexnr)/p.H;

    k1=func_q(t,yn,phi,phidot);
```

```
    k2=func_q(t+r.h/2,yn+k1*r.h/2,phi,phidot);
    k3=func_q(t+r.h/2,yn+k2*r.h/2,phi,phidot);
    k4=func_q(t+r.h,yn+k3*r.h,phi,phidot);

    yn=yn+(k1+2*k2+2*k3+k4)*r.h/6;
    r.q(:,i1i)=yn;
    r.a(:,i1i)=func_10(t,yn,phi,phidot);
    r.resp(i1i,1)=R.pos4F(indexnr);
```

D.1.3.1. Setting up functions for $\dot{q}_m(t)$ and $\dot{v}_m(t)$

For the derivatives, a single function is set-up, calling all modes needed for calculation. Several constants are set-up to reduce the number of parameters in the script.

```
function [ q_out ] = func_q( t,q,phi,phidot )
% Is this function, the set of first order derivatives is described which
% are needed for the numerical integration to find the time function.

global c

QQL=zeros(c.n_modes,1);
QQ0=zeros(c.n_modes,1);
VVL=zeros(c.n_modes,1);
VV0=zeros(c.n_modes,1);
for mm=1:c.n_modes
    VV0(mm)=q(mm*2)*c.accw0(mm);
    VVL(mm)=q(mm*2)*c.accwL(mm);
end
C1_q=sum(VV0)-phidot;
C2_q=abs(C1_q)/(C1_q);
C4_q=sum(VVL)-phidot;
C5_q=abs(C4_q)/(C4_q);

q_out=ones(c.n_modes*2,1);
for ll=1:c.n_modes;
q_out(ll*2-1)=q(ll*2);
q_out(ll*2)=-c.C1(ll)*(C1_q)...
    -c.C2(ll)*(C2_q)...
    +c.C3(ll)*(phi)...
    -c.C4(ll)*(C4_q)...
    -c.C5(ll)*(C5_q)...
    +c.C6(ll)*(phi)...
    -c.C7(ll)*q(ll*2-1)...
    -c.C8(ll)*q(ll*2);
end
end
```

```
global p
global c

for iii=1:nf_number
c.C1(iii)=p.cr1*c.accw0(iii)/(p.rho*p.A*p.L*c.Cwm(iii));  %cr 0
c.C2(iii)=p.mu1*c.accw0(iii)/(c.Cwm(iii)*p.rho*p.A);      %mu 0
c.C3(iii)=p.r1*c.accw0(iii)/(p.rho*p.A);                  %phi 0
c.C4(iii)=p.cr2*c.accwL(iii)/(p.rho*p.A*p.L*c.Cwm(iii));  %cr L
c.C5(iii)=p.mu2*c.accwL(iii)/(c.Cwm(iii)*p.rho*p.A);      %mu L
c.C6(iii)=p.r2*c.accwL(iii)/(p.rho*p.A);                  %phi L
c.C7(iii)=c.nf(iii)^2;              %E
c.C8(iii)=p.Estar*p.I/(p.E*p.I)*c.nf(iii)^2;          %Estar
end
```

D.1.4. Calculation total displacements

For each position of the beam the total displacements are calculated using the mode shape and the timedependent solution. m modes are taken into account for the calculation of the total response.

```
r.WWW=zeros(length(r.t),size(w,2));
for iti=1:length(r.t)
for izi=1:modes_m
r.WWW(iti,:)=r.WWW(iti,:)+r.q(izi*2-1,iti)*w(izi,:);
end
end
```

D.2. Full matlab codes Galerkin implementation

Mainfile.m

```
%% Main file
clear all; clc; %close all;

% Define the global parameters
parameters

% Damping parameters
p.Estar=0.004;
p.cr1=100;          %N(rad/s)^-1
p.cr2=p.cr1;          %Nm(rad/s)^-1
p.mu1=2;           %N
p.mu2=p.mu1;           %N

%% Determination mode shapes and natural frequencies
% Determine the natural frequencies
nf_number=20;
naturalfrequencies

% Define the space solution and it's constants
findingconstants
spacesolution

% Define derivative values at the boundaries.
for kk=1:nf_number
c.accw0(kk)=w_diff(kk,1);
if mod(kk,2)==0;
c.accwL(kk)=w_diff(kk,1);
else
c.accwL(kk)=w_diff(kk,1)*-1;
end
end

% Define Cwm. Stored in p.Cwm for different nf.
for kk=1:nf_number
c.Cwm(kk)=func_cwm(kk);
end

%% Loading data from experiment
% setting frequency range for filters
Low_range=5*2*pi;
High_range=1000*2*pi;

% setting test number for output
test_nr=87;

% Loading text files and filtering the data
global R
```

```
48  R=func_readingdata(test_nr,Low_range,High_range);
49
50  %% Numerical integration
51  % Numerical integration for finding time function.
52  % y0 are the guessed starting points, tx is the time domain.
53  % func_q contains the set of first order derivatives for i modes
54  global r
55
56  % c.n_modes = number of coupled modes
57  % Note that the maximum number can not overceed the
58  % amount of calculated natural frequencies, nf_number.
59  c.n_modes=10;
60
61  % Initial values
62  nr_phi=find(R.t==0);
63  indexnr=nr_phi;
64  r.y0=zeros(2*c.n_modes,1);
65
66  % Time steps
67  r.ts=[0 0.5];
68  tspan=(r.ts(2)-r.ts(1));
69  r.h=10^(-5);
70  r.t=r.ts(1):r.h:r.ts(2);
71  n=length(r.t);
72
73  % Define constants for integration function
74  constants_inRKfunction
75
76  % Runge-Kutta integration scheme (4th order RK)
77  RK4
78
79  %% Total response along beam
80  % Calculating the responds in time varying over x
81  modes_m=10;
82
83  r.WWW=zeros(length(r.t),size(w,2));
84  r.WWWa=zeros(length(r.t),size(w,2));
85  for iti=1:length(r.t)-1
86  for imi=1:modes_m
87      r.WWW(iti,:)=r.WWW(iti,:)+r.q(imi*2-1,iti)*w(imi,:);
88      r.WWWv(iti,30)=r.WWWa(iti,30)+r.q(imi*2,iti)*w_diff(imi,30);
89      r.WWWa(iti,:)=r.WWWa(iti,:)+r.a(imi*2,iti)*w_diff2(imi,:);
90  end
91  end
92
93  %% Plotting results
94  figure
95  hold on
96  xlim([0 r.ts(2)])
97  handlevector(1)=plot(R.t,R.pos4F,'k');
98  handlevector(2)=plot(r.t,r.WWW(:,30),'b');
99  % handlevector(3)=plot(r.t,outcome_w(:,2),'g');
100 % handlevector(4)=plot(r.t,outcome_w(:,3),'r');
101 % handlevector(5)=plot(r.t,outcome_w(:,4),'c');
102 % handlevector(6)=plot(r.t,outcome_w(:,5),'m');
103 % title(['influence change of friction damping for mu =' ,num2str(p.mu1),' cr1 =' ,num2str(p.cr1), 'and Es
104 % legend(handlevector([2,3,4,5,6]),{strcat('mu =',num2str(d.mu1(1)),'cr =',num2str(d.cr1(1))
    ) ,...
105 %     strcat('mu =',num2str(d.mu1(2)),'cr =',num2str(d.cr1(2))  ),...
106 %     strcat('mu =',num2str(d.mu1(3)) ,'cr =',num2str(d.cr1(3))  ),...
107 %     strcat('mu =',num2str(d.mu1(4)) ,'cr =',num2str(d.cr1(4))  ),...
108 %     strcat('mu =',num2str(d.mu1(5)),'cr =',num2str(d.cr1(5))  )},...
109 %     'Location','northeastoutside');
110 % xlabel('Time [s]')
111 % ylabel('Displacements [m]');
112 %
113 %
114 %
115 figure
```

```
hold on
xlim([0 r.ts(2)])
handlevector2(1)=plot(R.t,R.acc4F,'k');
handlevector2(2)=plot(r.t,r.WWWa(:,30),'b');
% handlevector2(3)=plot(r.t,outcome_a(:,2),'g');
% handlevector2(4)=plot(r.t,outcome_a(:,3),'r');
% handlevector2(5)=plot(r.t,outcome_a(:,4),'c');
% handlevector2(6)=plot(r.t,outcome_a(:,5),'m');
% title(['influence change of friction damping for mu =' ,num2str(p.mu1), ' cr1 =' ,num2str(p.cr1), 'and
% legend(handlevector2([2,3,4,5,6]),{strcat('mu =',num2str(d.mu1(1)),'cr =',num2str(d.cr1(1))
) ,...
%     strcat('mu =',num2str(d.mu1(2)),'cr =',num2str(d.cr1(2))  ),...
%     strcat('mu =',num2str(d.mu1(3)) ,'cr =',num2str(d.cr1(3))  ),...
%     strcat('mu =',num2str(d.mu1(4)) ,'cr =',num2str(d.cr1(4))  ),...
%     strcat('mu =',num2str(d.mu1(5)),'cr =',num2str(d.cr1(5))  )},...
%     'Location','northeastoutside');
% xlabel('Time [s]')
% ylabel('Accelerations [m/s2]');
```

parameters.m

```
%% parameters_1.m
%This scrcipt defines all global parameters 'p' that are used in the model.

global p

% General system parameters
p.r1=500;         %N/rad      574.4
p.r2=p.r1;          %N/rad
p.rho=2000;         %kg/m^2    2000
p.A=0.0098;         %m^2     0.0098
p.L=1.150;           %m    1.150
p.E=110.6;%184.8;          %Nm^2 or 110.6*10^6 Nmm^2       184
p.I=1;              %Not measured seperately from p.E
p.H=0.9;           %m
```

naturalfrequencies.m

```
% naturalfrequencies.m
% In this script the natural frequencies are sought by setting the
% determinant to zero and using a expolated function for finding the zeros.

%input:
%Determinant function func_det4x4_v2
%nf_number = numner of calculated natural frequencies at the first guess

%output:
%p.nf = a array with the natural frequencies

% First guess for the frequencies, random pick as power array:
nf_trial=1000;
for fgs=1:nf_trial
first_guess_small(fgs)=0.5+1.05^(fgs-1);
check(fgs)=isfinite(func_det4x4(first_guess_small(fgs)));
end

% Searching for zero values close at those n's:
second_guess=zeros(sum(check),1);
fun = @(omega) func_det4x4(omega);
for igs=1:sum(check)
second_guess(igs)=fzero(fun, first_guess_small(igs));
if second_guess(igs)<0
```

```
    second_guess(igs)=0;
end
end


% Found frequencies at second guess:
nfreq=unique(round(second_guess*10^5)/(10^5));

% Removing zeros from the guessed frequency array:
Nf=zeros(size(find(nfreq),1),1);
for ifr=1:size(find(nfreq),1)
Nf(ifr)=nfreq(ifr+1);
end

c.nf=Nf(1:nf_number);
c.nfHz=c.nf/(2*pi);
```

func_beta.m

```
function [ beta ] = func_beta(nr_nf)
%UNTITLED3 Summary of this function goes here
%   Detailed explanation goes here
global p
global c
omega=c.nfHz(nr_nf);
beta=((p.rho*p.A*omega^2)/p.E*p.I)^(1/4);
end
```

func_det4x4.m

```
% func_det4x4.m

function[determinant]=func_det4x4_v2(omega)
%calculation of the determinant of the matrix for the first model, where
%the determinant is given in the form of a function of omega.

%input parameters:
%omega is the natural frequency of the system

%output parameters:
%determinant for the matrix

%script:

%load and set parameters in this function script:
global p
EI=p.E*p.I;
beta=((p.rho*p.A*omega^2)/p.E*p.I)^(1/4);

determinant = -4*EI^2*sinh(beta*p.L)*sin(beta*p.L)*beta^4 ...
+2*EI*sinh(beta*p.L)*cos(beta*p.L)*beta^3*p.r1...
    +2*EI*sinh(beta*p.L)*cos(beta*p.L)*beta^3*p.r2...
    -2*EI*cosh(beta*p.L)*sin(beta*p.L)*beta^3*p.r1...
    -2*EI*cosh(beta*p.L)*sin(beta*p.L)*beta^3*p.r2...
    +sinh(beta*p.L)^2*beta^2*p.r1*p.r2-cosh(beta*p.L)^2*beta^2*p.r1*p.r2...
    +2*cosh(beta*p.L)*cos(beta*p.L)*beta^2*p.r1*p.r2...
    -sin(beta*p.L)^2*beta^2*p.r1*p.r2-cos(beta*p.L)^2*beta^2*p.r1*p.r2;
end
```

findingconstants.m

```
%% findingconstants.m
%Here the unknown constants A-D in the space solution are found.

%input parameters:
%nfreq = natural frequencies
%nf_number = number of natural frequencies
%matrix4x4 = boundaryconditionmatrix

%output parameters:
%constants (CA, CB,CC,CD) = the amplitude constants
global c

for i=1:nf_number
omega=c.nf(i);
beta=((p.rho*p.A*(omega)^2)/p.E*p.I)^(1/4);
boundaryconditionmatrix;
c.C_D(i)=1;

%Finding amplitude constants
vectorB=-matrix4x4(1:3,4);
matrixA(1:3,1:3)=matrix4x4(1:3,1:3);
ABC=inv(matrixA)*vectorB;
c.C_A(i)=ABC(1);
c.C_B(i)=ABC(2);
c.C_C(i)=ABC(3);
end
```

boundaryconditionmatrix.m

```
%% boundaryconditionmatrix.m
% matrix4x4 is the matrix which describes the system for the first model.
%set up from the boundary conditions of the system

matrix4x4=zeros(4);

%First BC in matrix:
matrix4x4(1,1)=p.E*p.I*beta^2;
matrix4x4(1,2)=-p.r1*beta;
matrix4x4(1,3)=-p.E*p.I*beta^2;
matrix4x4(1,4)=-p.r1*beta;
%Second BC in matrix:
matrix4x4(2,1)=1;
matrix4x4(2,2)=0;
matrix4x4(2,3)=1;
matrix4x4(2,4)=0;
%Third BC in matrix:
matrix4x4(3,1)=p.E*p.I*beta^2*cosh(beta*p.L)+p.r2*beta*sinh(beta*p.L);
matrix4x4(3,2)=p.E*p.I*beta^2*sinh(beta*p.L)+p.r2*beta*cosh(beta*p.L);
matrix4x4(3,3)=-p.E*p.I*beta^2*cos(beta*p.L)-p.r2*beta*sin(beta*p.L);
matrix4x4(3,4)=-p.E*p.I*beta^2*sin(beta*p.L)+p.r2*beta*cos(beta*p.L);
%Fourth BC in matrix:
matrix4x4(4,1)=cosh(beta*p.L);
matrix4x4(4,2)=sinh(beta*p.L);
matrix4x4(4,3)=cos(beta*p.L);
matrix4x4(4,4)=sin(beta*p.L);
```

spacesolution.m

```
%% spacesolution.m
% Here the space solution is described

%input parameters:
```

```
%nfreq = natural frequencies
%CA,CB,CC,CD = constants
%general parameters

%output parameters:
%w = is a matrix with the space solution
%for x (horizontal)
%and omega(vertical)
global r

dx=0.01;
x_left=0;
x_right=p.L;
r.x=x_left:dx:x_right;

for ipp=1:nf_number
omega=c.nf(ipp);
beta=((p.rho*p.A*omega^2)/p.E*p.I)^(1/4);
for kxk=1:length(r.x);
xx=r.x(kxk);
w(ipp,kxk)=c.C_A(ipp)*cosh(beta*xx)+c.C_B(ipp)*sinh(beta*xx)+...
    c.C_C(ipp)*cos(beta*xx)+c.C_D(ipp)*sin(beta*xx);
w_diff(ipp,kxk)=c.C_A(ipp)*beta*sinh(beta*xx)+c.C_B(ipp)*beta*cosh(beta*xx)...
    -c.C_C(ipp)*beta*sin(beta*xx)+c.C_D(ipp)*beta*cos(beta*xx);
w_diff2(ipp,kxk)=c.C_A(ipp)*beta^2*cosh(beta*xx)+c.C_B(ipp)*beta^2*sinh(beta*xx)...
    -c.C_C(ipp)*beta^2*cos(beta*xx)-c.C_D(ipp)*beta^2*sin(beta*xx);
end
w(ipp,:)=w(ipp,:)/max(w(ipp,:));
w(ipp,:)=round(w(ipp,:)*10^6)/(10^6);
w_diff(ipp,:)=w_diff(ipp,:)/max(w_diff(ipp,:));
w_diff(ipp,:)=round(w_diff(ipp,:)*10^6)/(10^6);
w_diff2(ipp,:)=w_diff2(ipp,:)/max(w_diff2(ipp,:));
w_diff2(ipp,:)=round(w_diff2(ipp,:)*10^6)/(10^6);
end
```

func_cwm.m

```
function [ cwm ] = func_cwm( nr_nf )
%UNTITLED Summary of this function goes here
%   Detaip.Led expp.Lanation goes here
global p
global c

beta=func_beta(nr_nf);
Am=c.C_A(nr_nf);
Bm=c.C_B(nr_nf);
Cm=c.C_C(nr_nf);
Dm=c.C_D(nr_nf);

cwm= 1/(8*beta)+ ( ( 2*Am*exp(4*beta*p.L)*Bm ...
    + 8*Am*Dm*exp(2*beta*p.L)-8*Bm*Cm*exp(2*beta*p.L)...
    + 8*Cm*Dm*exp(2*beta*p.L)-4*Am*exp(2*beta*p.L)*Bm ...
    + Bm^2*exp(4*beta*p.L)+ Am^2*exp(4*beta*p.L)...
    + 4*Am*Cm*exp(3*beta*p.L)*cos(beta*p.L)...
      + 4*Am*Cm*exp(3*beta*p.L)*sin(beta*p.L)...
 - 4*Am*Cm*exp(beta*p.L)*cos(beta*p.L)...
+ 4*Am*Cm*exp(beta*p.L)*sin(beta*p.L)...
- 4*Am*Dm*exp(beta*p.L)*cos(beta*p.L)...
 - 4*Am*Dm*exp(beta*p.L)*sin(beta*p.L)...
 + 4*Bm*Cm*exp(beta*p.L)*cos(beta*p.L)...
  - 4*Bm*Cm*exp(beta*p.L)*sin(beta*p.L)...
     + 4*Bm*Dm*exp(beta*p.L)*cos(beta*p.L)...
     + 4*Bm*Dm*exp(beta*p.L)*sin(beta*p.L)...
       - 4*Am*Dm*exp(3*beta*p.L)*cos(beta*p.L)...
 + 4*Am*Dm*exp(3*beta*p.L)*sin(beta*p.L)...
 - 4*Bm^2*beta*p.L*exp(2*beta*p.L)...
```

```
  + 4*Bm*Cm*exp(3*beta*p.L)*cos(beta*p.L)...
   + 4*Bm*Cm*exp(3*beta*p.L)*sin(beta*p.L)...
    - 4*Bm*Dm*exp(3*beta*p.L)*cos(beta*p.L)...
     + 4*Bm*Dm*exp(3*beta*p.L)*sin(beta*p.L)...
        + 4*Cm^2*p.L*exp(2*beta*p.L)*beta...
           + 4*Cm^2*exp(2*beta*p.L)*cos(beta*p.L)*sin(beta*p.L)...
           - 8*Cm*Dm*cos(beta*p.L)^2*exp(2*beta*p.L)...
              + 4*Dm^2*p.L*exp(2*beta*p.L)*beta...
      - 4*Dm^2*exp(2*beta*p.L)*cos(beta*p.L)*sin(beta*p.L)...
           + 4*Am^2*beta*p.L*exp(2*beta*p.L) ...
           + 2*Am*Bm - Am^2- Bm^2 )*exp(-2*beta*p.L) );
end
```

RK4.m

```
% RK4.m
% Runge-Kutta integration scheme

r.q=zeros(2*c.n_modes,n-1);
r.a=zeros(2*c.n_modes,n-1);
yn=r.y0;

    for i1i=1:n-1
    t=r.ts(1)+(i1i-1)*r.h;
    indexnr=min(find(R.t(indexnr:indexnr+250)>t))+indexnr-1;
    phi=R.pos1F(indexnr)/p.H;
    phidot=R.velo1F(indexnr)/p.H;

    k1=func_q(t,yn,phi,phidot);
    k2=func_q(t+r.h/2,yn+k1*r.h/2,phi,phidot);
    k3=func_q(t+r.h/2,yn+k2*r.h/2,phi,phidot);
    k4=func_q(t+r.h,yn+k3*r.h,phi,phidot);

    yn=yn+(k1+2*k2+2*k3+k4)*r.h/6;
    r.q(:,i1i)=yn;
    r.a(:,i1i)=func_10(t,yn,phi,phidot);
    r.resp(i1i,1)=R.pos4F(indexnr);
    end
```

func_q.m

```
function [ q_out ] = func_q( t,q,phi,phidot )
% Is this function, the set of first order derivatives is described which
% are needed for the numerical integration to find the time function.

global c

QQL=zeros(c.n_modes,1);
QQ0=zeros(c.n_modes,1);
VVL=zeros(c.n_modes,1);
VV0=zeros(c.n_modes,1);
for mm=1:c.n_modes
    VV0(mm)=q(mm*2)*c.accw0(mm);
    VVL(mm)=q(mm*2)*c.accwL(mm);
end
C1_q=sum(VV0)-phidot;
C2_q=abs(C1_q)/(C1_q);
C4_q=sum(VVL)-phidot;
C5_q=abs(C4_q)/(C4_q);

q_out=ones(c.n_modes*2,1);
for ll=1:c.n_modes;
```

```
q_out(ll*2-1)=q(ll*2);
q_out(ll*2)=-c.C1(ll)*(C1_q)...
    -c.C2(ll)*(C2_q)...
    +c.C3(ll)*(phi)...
    -c.C4(ll)*(C4_q)...
    -c.C5(ll)*(C5_q)...
    +c.C6(ll)*(phi)...
    -c.C7(ll)*q(ll*2-1)...
    -c.C8(ll)*q(ll*2);
end
end
```

constants_inRKfunction.m

```
%% Constants in the func_1 function

global p
global c

for iii=1:nf_number
c.C1(iii)=p.cr1*c.accw0(iii)/(p.rho*p.A*p.L*c.Cwm(iii));  %cr 0
c.C2(iii)=p.mu1*c.accw0(iii)/(c.Cwm(iii)*p.rho*p.A);      %mu 0
c.C3(iii)=p.r1*c.accw0(iii)/(p.rho*p.A);                  %phi 0
c.C4(iii)=p.cr2*c.accwL(iii)/(p.rho*p.A*p.L*c.Cwm(iii));  %cr L
c.C5(iii)=p.mu2*c.accwL(iii)/(c.Cwm(iii)*p.rho*p.A);      %mu L
c.C6(iii)=p.r2*c.accwL(iii)/(p.rho*p.A);                  %phi L
c.C7(iii)=c.nf(iii)^2;                %E
c.C8(iii)=p.Estar*p.I/(p.E*p.I)*c.nf(iii)^2;          %Estar
end
```

func_readingdata.m

```
function R = func_readingdata(test_nr,Low_range,High_range)
% Importing data from output.txt files

% The unfiltered signal
last_test_nr=100;              %121 is last experiment number
AC=zeros(32768,(121-64)*5);
FC=zeros(32768,57);
for kk=65:last_test_nr
if kk == 67
% Output time response file experiment
[ time,accel ]=func_resp(kk,5,750);
AC(:,(kk-65)*5+1)=accel(:,1);
AC(:,(kk-65)*5+2)=accel(:,2);
AC(:,(kk-65)*5+3)=accel(:,3);
AC(:,(kk-65)*5+4)=accel(:,4);
AC(:,(kk-65)*5+5)=accel(:,5);
elseif kk == 87
% Output time response file experiment
[ time,accel ]=func_resp(kk,5,750);
AC(:,(kk-65)*5+1)=accel(:,1);
AC(:,(kk-65)*5+2)=accel(:,2);
AC(:,(kk-65)*5+3)=accel(:,3);
AC(:,(kk-65)*5+4)=accel(:,4);
AC(:,(kk-65)*5+5)=accel(:,5);
else
AC(:,(kk-65)*5+1:(kk-65)*5+5)=0;
end
end

%% Filtered accelerations, velocities and displacements
```

```
% calculation of the accelerations and velocities and displacements using
% integration and a bandpassfilter
R.t=time;
Final_time=time(end,1);Time_steps=size(time,1);

% Accelerations
% Obtained directly from measurent data files in AC
nr=test_nr-64;
acc1=AC(:,(nr-1)*5+1);
acc2=AC(:,(nr-1)*5+2);
acc3=AC(:,(nr-1)*5+3);
acc4=AC(:,(nr-1)*5+4);
acc5=AC(:,(nr-1)*5+5);
% Filter
% Using bandpass function to filter out frequencies
[acc1F] = sergio_bandpass(time,acc1,Low_range,High_range,0);
[acc2F] = sergio_bandpass(time,acc2,Low_range,High_range,0);
[acc3F] = sergio_bandpass(time,acc3,Low_range,High_range,0);
[acc4F] = sergio_bandpass(time,acc4,Low_range,High_range,0);
[acc5F] = sergio_bandpass(time,acc5,Low_range,High_range,0);
% Mean: removing the present offset from data
R.acc1F=acc1F-mean(acc1F);
R.acc2F=acc2F-mean(acc2F);
R.acc3F=acc3F-mean(acc3F);
R.acc4F=acc4F-mean(acc4F);
R.acc5F=acc5F-mean(acc5F);

% Velocities
% Integration of filtered acceleration signal
[velo1]=trapezoidal_integration(Final_time,Time_steps,R.acc1F);
[velo2]=trapezoidal_integration(Final_time,Time_steps,R.acc2F);
[velo3]=trapezoidal_integration(Final_time,Time_steps,R.acc3F);
[velo4]=trapezoidal_integration(Final_time,Time_steps,R.acc4F);
[velo5]=trapezoidal_integration(Final_time,Time_steps,R.acc5F);
% Mean: removing the present offset from data
velo1=velo1-mean(velo1);
velo2=velo2-mean(velo2);
velo3=velo3-mean(velo3);
velo4=velo4-mean(velo4);
velo5=velo5-mean(velo5);
% Filter
% Using bandpass function to filter out frequencies
[velo1F] = sergio_bandpass(time,velo1,Low_range,High_range,0);
[velo2F] = sergio_bandpass(time,velo2,Low_range,High_range,0);
[velo3F] = sergio_bandpass(time,velo3,Low_range,High_range,0);
[velo4F] = sergio_bandpass(time,velo4,Low_range,High_range,0);
[velo5F] = sergio_bandpass(time,velo5,Low_range,High_range,0);
% Mean: removing the present offset from data
R.velo1F=velo1F-mean(velo1F);
R.velo2F=velo2F-mean(velo2F);
R.velo3F=velo3F-mean(velo3F);
R.velo4F=velo4F-mean(velo4F);
R.velo5F=velo5F-mean(velo5F);

% Displacements
% By integration of filtered velocity signal
[posi1]=trapezoidal_integration(Final_time,Time_steps,R.velo1F);
[posi2]=trapezoidal_integration(Final_time,Time_steps,R.velo2F);
[posi3]=trapezoidal_integration(Final_time,Time_steps,R.velo3F);
[posi4]=trapezoidal_integration(Final_time,Time_steps,R.velo4F);
[posi5]=trapezoidal_integration(Final_time,Time_steps,R.velo5F);
% Mean: removing the present offset from data
posi1=posi1-mean(posi1);
posi2=posi2-mean(posi2);
posi3=posi3-mean(posi3);
posi4=posi4-mean(posi4);
posi5=posi5-mean(posi5);
% Filter
% Using bandpass function to filter out frequencies
```

```
[pos1F] = sergio_bandpass(time,posi1,Low_range,High_range,0);
[pos2F] = sergio_bandpass(time,posi2,Low_range,High_range,0);
[pos3F] = sergio_bandpass(time,posi3,Low_range,High_range,0);
[pos4F] = sergio_bandpass(time,posi4,Low_range,High_range,0);
[pos5F] = sergio_bandpass(time,posi5,Low_range,High_range,0);
% Mean: removing the present offset from data
R.pos1F=pos1F-mean(pos1F);
R.pos2F=pos2F-mean(pos2F);
R.pos3F=pos3F-mean(pos3F);
R.pos4F=pos4F-mean(pos4F);
R.pos5F=pos5F-mean(pos5F);


% phi value
acc1=AC(:,(nr-1)*5+1);
acc2=AC(:,(nr-1)*5+2);
acc3=AC(:,(nr-1)*5+3);
acc4=AC(:,(nr-1)*5+4);
acc5=AC(:,(nr-1)*5+5);
% Filter
% Using bandpass function to filter out frequencies
[acc1F] = sergio_bandpass(time,acc1,Low_range,High_range,0);
[acc2F] = sergio_bandpass(time,acc2,Low_range,High_range,0);
[acc3F] = sergio_bandpass(time,acc3,Low_range,High_range,0);
[acc4F] = sergio_bandpass(time,acc4,Low_range,High_range,0);
[acc5F] = sergio_bandpass(time,acc5,Low_range,High_range,0);
% Mean: removing the present offset from data
R.acc1F=acc1F-mean(acc1F);
R.acc2F=acc2F-mean(acc2F);
R.acc3F=acc3F-mean(acc3F);
R.acc4F=acc4F-mean(acc4F);
R.acc5F=acc5F-mean(acc5F);

% Velocities
% Integration of filtered acceleration signal
[velo1]=trapezoidal_integration(Final_time,Time_steps,R.acc1F);
[velo2]=trapezoidal_integration(Final_time,Time_steps,R.acc2F);
[velo3]=trapezoidal_integration(Final_time,Time_steps,R.acc3F);
[velo4]=trapezoidal_integration(Final_time,Time_steps,R.acc4F);
[velo5]=trapezoidal_integration(Final_time,Time_steps,R.acc5F);
% Mean: removing the present offset from data
velo1=velo1-mean(velo1);
velo2=velo2-mean(velo2);
velo3=velo3-mean(velo3);
velo4=velo4-mean(velo4);
velo5=velo5-mean(velo5);
% Filter
% Using bandpass function to filter out frequencies
[velo1F] = sergio_bandpass(time,velo1,Low_range,High_range,0);
[velo2F] = sergio_bandpass(time,velo2,Low_range,High_range,0);
[velo3F] = sergio_bandpass(time,velo3,Low_range,High_range,0);
[velo4F] = sergio_bandpass(time,velo4,Low_range,High_range,0);
[velo5F] = sergio_bandpass(time,velo5,Low_range,High_range,0);
% Mean: removing the present offset from data
R.velo1F=velo1F-mean(velo1F);
R.velo2F=velo2F-mean(velo2F);
R.velo3F=velo3F-mean(velo3F);
R.velo4F=velo4F-mean(velo4F);
R.velo5F=velo5F-mean(velo5F);

% Displacements
% By integration of filtered velocity signal
[posi1]=trapezoidal_integration(Final_time,Time_steps,R.velo1F);
[posi2]=trapezoidal_integration(Final_time,Time_steps,R.velo2F);
[posi3]=trapezoidal_integration(Final_time,Time_steps,R.velo3F);
[posi4]=trapezoidal_integration(Final_time,Time_steps,R.velo4F);
[posi5]=trapezoidal_integration(Final_time,Time_steps,R.velo5F);
% Mean: removing the present offset from data
posi1=posi1-mean(posi1);
```

```
posi2=posi2-mean(posi2);
posi3=posi3-mean(posi3);
posi4=posi4-mean(posi4);
posi5=posi5-mean(posi5);
% Filter
% Using bandpass function to filter out frequencies
[pos1F] = sergio_bandpass(time,posi1,Low_range,High_range,0);
[pos2F] = sergio_bandpass(time,posi2,Low_range,High_range,0);
[pos3F] = sergio_bandpass(time,posi3,Low_range,High_range,0);
[pos4F] = sergio_bandpass(time,posi4,Low_range,High_range,0);
[pos5F] = sergio_bandpass(time,posi5,Low_range,High_range,0);
% Mean: removing the present offset from data
R.pos1F=pos1F-mean(pos1F);
R.pos2F=pos2F-mean(pos2F);
R.pos3F=pos3F-mean(pos3F);
R.pos4F=pos4F-mean(pos4F);
R.pos5F=pos5F-mean(pos5F);


end
```

func_dampingratio.m

```
function [Amplitude,damp_ratio,peaks,time_peaks]=func_dampingratio(signal,t,Wn)
%%
% Wn is the damping ratio in radians
% If Wn=1, then the damping ratio has to be divided by =2*pi*f(hz);
%peaks,damp_ratio
find_signal=find(signal==max(signal));
signal=signal(find_signal:end);
t=t(1:end-find_signal+1);
%% Bookkeeping
ii=1;jj=1;
for i1=1:length(signal)-1
    if isequal(sign(signal(i1)),1)
        T(ii,jj)=signal(i1);
        Time_pos(ii,jj)=i1;
        ii=ii+1;
    end
    if ~isequal(sign(signal(i1)),sign(signal(i1+1))) && isequal(sign(signal(i1)),1)
        jj=jj+1;
        ii=1;
    end
end

for i1=1:size(T,2)
    idx_time=find(T(:,i1)==max(T(:,i1)));
    idx_time_peaks=Time_pos(idx_time,i1);
    time_peaks(i1,1)=t(idx_time_peaks);
end
for i1=1:size(T,2)
    peaks(i1,1)=max(T(:,i1));
end
%% Damping
f=fit(time_peaks,peaks,'exp1');
exp_coef=coeffvalues(f);
damp_ratio=-exp_coef(1,2)/Wn;
Amplitude=max(signal);
x=max(signal)*exp(-Wn*damp_ratio*t);
% figure;
% hold on
% plot(t,signal)
% plot(t,x,'k')
```

FFT.m

```
%% Script that performs the discrete Fourier transform

Data=r.WWW(:,30);

NFFT=2^nextpow2(length(Data));

% Fast Fourrier transform
FFTx=fft(Data,NFFT)/NFFT;
ABS_FFTx=2*abs(FFTx(1:NFFT/2+1));

f=(1/r.h)/2*linspace(0,1,NFFT/2+1);

% Plotting
figure
plot(f,ABS_FFTx,'r')  %f/(2*pi) for rad/s
box off
xlabel('Frequency [Hz]')
ylabel('|Y(f)|');
set(gca);
set(gcf,'Color',[1 1 1]);
grid('on');
xlim([0 300]);
axis tight
```

E

Fourier Transform

Application of Fourier Transform

The Fourier Series theory states that any periodical function $\partial(t)$ in the time domain, not necessarily harmonic, has an equivalent counterpart in the frequency domain, which can be represented by a convergent series of independent harmonic functions as a Fourier series [11]. Fourrier transform is based on the same assumption:

$$F(\omega) = \int_{-\inf}^{\inf} f(t) e^{-i\omega t} dt \tag{E.1}$$

Fourrier series and Fourrier transformation are based on the superposition phenomenom and are therefore suited for linear systems. A restriction is the applicability to only stationary processes or periodic function [11]:

1. The mean of the process is constant over time
2. The variance of the process is constant over time
3. The probability of the process is a function of time difference $(t_2 - t_1)$ and does not depend on individual times $t2$ and $t1$
4. The joint probability of the process at any time is identical to the joint probability of the same variable displaced with an arbitrary amount of periods.

When Fourier transform is used on the set of equations describing the problem, the equations are transformed into many sinusoidal functions so that the time-dependent function is changed into a complex-valued functions of frequency. These new equations can be solved for several frequencies giving a solution described with frequency and position. The complex modulus represents the amplitude of vibration and the complex argument represents the phase offset of the basic sinusoid [85].

Definition and use

According to Beerends [86], the Fourier transform of a function, referred to as Fourier transform or spectrum, is defined as follow for a given function $f : R \longrightarrow C$ the function $F(\omega)$for$\omega \in \Re$ is :

$$F(\omega) = \int_{-\inf}^{\inf} f(t) e^{-i\omega t} dt \tag{E.2}$$

Provided the integral exists as an improper Riemann integral. Here, function $F(\omega)$ is called the Fourier transform or spectrum of funxction $f(t)$. In inverse Fourier Transform can be used to convert the spectral density

of $f(t)$, $F(\omega)$, back to the time domain and is defined by:

$$f(t) = \frac{1}{2\pi}\int_{-\inf}^{\inf} F(\omega)e^{i\omega t}d\omega \tag{E.3}$$

One of the most important properties of Fourier Transform is the linearity property. When linear combination of functions are transformed using Fourier Transform, the transforms of these functions have the same linear combination.

Differentiation in time:

When derivatives to the time domain are present, in the case a Fourier Transform is performed from the time to the frequency domain, a imaginary factor times the Fourier transformed function represents the Fourier transform of the derivative.

$$\int_{-\inf}^{\inf} \frac{\partial}{\partial t} f(t)e^{-i\omega t}dt \tag{E.4}$$

$$\overset{integration\ by\ parts}{\rightarrow} \left[F(t)e^{-i\omega t}\right]_{-\infty}^{\infty} - \int_{-\inf}^{\inf} -i\omega F(t)e^{-i\omega t}dt \tag{E.5}$$

$$= F(\infty)... - F(-)... + i\omega\int_{-\inf}^{\inf} F(t)e^{-i\omega t}dt \tag{E.6}$$

$$= 0 + i\omega\int_{-\inf}^{\inf} F(t)e^{-i\omega t}dt \tag{E.7}$$

$$= i\omega F(\omega) \tag{E.8}$$

For higher derivatives in time Equation E.9 is valid:

$$(Ff(t)^n)(\omega) = (i\omega)^n F(\omega) \tag{E.9}$$

Which gives $(F\frac{\partial}{\partial t}f(t))(\omega) = i\omega F(\omega)$ and $(F\frac{\partial^2}{\partial^2 t}f(t))(\omega) = -\omega^2 F(\omega)$.

Time history

Instead of a transfer to the frequency domain, a transfer to the Laplace domain can be used to solve a dynamical problem. A advantage with the Laplace transform compared with Fourrier is that time histories can be taken into account, where using in Fourrier information due to initial displacements or velocities are not present in the transformed form. However, with making use of the relation between Laplace and Fourrier, such as shown in Equation E.10, this time history information can be taken into account when using Fourrier as wel [85].

$$i\omega = s \tag{E.10}$$

For Laplace transformed functions, the time history is taken into account when transforming to the Laplace domain, following the following rule:

$$L\{\frac{\partial^n f}{\partial^n t}\}(s) = s^n * F(s) - s^{n-1}f(0) - s^{n-2}f'(0) - ... - sf^{(n-2)}(0) - f^{(n-1)}(0) \tag{E.11}$$

At all positions where a derivative in time domain is present, time history information has to be added:

$$L\{\frac{\partial f}{\partial t}\}(s) = (i\omega) * F(s) - f(0) \tag{E.12}$$

$$L\{\frac{\partial^n f}{\partial^n t}\}(s) = (i\omega)^n * F(s) - (i\omega)^{n-1} f(0) - (i\omega)^{n-2} f'(0) - \ldots - (i\omega) f^{(n-2)}(0) - f^{(n-1)}(0) \tag{E.13}$$

F

FULL CALCULATIONS FREQUENCY DOMAIN

F.1. Without friction at the boundaries

For solving in the frequency domain without the presence of friction, the equation of motion and boundary conditions are described with Equation F.1 to F.5. The displacement and rotations present in the equations below represent the relative displacement of the floor with respect to the main structure. The external moment, M, represents the internal forces of the structure which act as loading on the described floor model.

$$\rho A \frac{\partial^2 w}{\partial t^2} + \left(E + E^* \frac{\partial}{\partial t}\right) I \frac{\partial^4 w}{\partial x^4} = 0 \tag{F.1}$$

$$\left(E + E^* \frac{\partial}{\partial t}\right) I \frac{\partial^2 w}{\partial x^2}|_{x=0} - kr_1 \frac{\partial w}{\partial x}|_{x=0} - cr_1 \frac{\partial^2 w}{\partial t \partial x}|_{x=0} = M \tag{F.2}$$

$$w(0) = 0 \tag{F.3}$$

$$\left(E + E^* \frac{\partial}{\partial t}\right) I \frac{\partial^2 w}{\partial x^2}|_{x=L} + kr_2 \frac{\partial w}{\partial x}|_{x=L} + cr_2 \frac{\partial^2 w}{\partial t \partial x}|_{x=L} = -M \tag{F.4}$$

$$w(L) = 0 \tag{F.5}$$

Using Fourier transform we obtain the EM in the Frequency domain. The initial conditions are introduced in the equation, following the rules for the relation of Laplace and Fourier, see Appendix E, and using the Laplace transform for a function with a first and second derivative to time.

$$\rho A \frac{\partial^2 w}{\partial t^2} + \left(E + E^* \frac{\partial}{\partial t}\right) I \frac{\partial^4 w}{\partial x^4} = 0 \tag{F.6}$$

$$\rightarrow \int_{-\infty}^{\infty} \left[\rho A \frac{\partial^2 w}{\partial t^2} + EI \frac{\partial^4 w}{\partial x^4} + E^* I \frac{\partial^5 w}{\partial t \partial x^4}\right] e^{-i\omega t} dt = 0 \tag{F.7}$$

$$\rightarrow \rho A \left\{(i\omega)^2 W(x,\omega) - (i\omega) w(x,0) - \dot{w}(x,0)\right\} + EI \frac{d^4 W(x,\omega)}{dx^4} + E^* I \left\{(i\omega) \frac{d^4 W(x,\omega)}{dx^4} - w(x,0)\right\} = 0 \tag{F.8}$$

$$\rightarrow \rho A (i\omega)^2 W(x,\omega) + EI \frac{d^4 W(x,\omega)}{dx^4} + E^* I (i\omega) \frac{d^4 W(x,\omega)}{dx^4} = \left\{\rho A (i\omega) + E^* I\right\} w(x,0) + \rho A \dot{w}(x,0) \tag{F.9}$$

Setting $w(x,0) = w_0$ and $\dot{w}(x,0) = v_0$ gives

$$\frac{\partial^4 W(x,\omega)}{\partial x^4} - \frac{\omega^2 \rho A}{EI + i\omega E^* I} W(x,\omega) = \frac{\left\{\rho A (i\omega) + E^* I\right\} w_0 + \rho A v_0}{EI + i\omega E^* I} \tag{F.10}$$

$$\rightarrow \frac{\partial^4 W(x,\omega)}{\partial x^4} - \beta^4 W(x,\omega) = \frac{\left\{\rho A (i\omega) + E^* I\right\} w_0 + \rho A v_0}{EI + i\omega E^* I} \qquad \text{with} \qquad \beta^4 = \frac{\omega^2 \rho A}{EI + i\omega E^* I} \tag{F.11}$$

When setting the RHS to zero, the homogeneous solution can we sought in the form of $W(x,\omega) = \sum^4 C_k exp(\lambda_k x)$ by substitution in the equation of motion. This gives the homogenous solution:

$$W(x)_{hom} = C1\cosh(\beta x) + C2\sinh(\beta x) + C3\cos(\beta x) + C4\sin(\beta x) \tag{F.12}$$

$$\text{where} \qquad \beta^4 = \frac{\omega^2 \rho A}{EI + i\omega E^* I} \tag{F.13}$$

The particular solution can be sought in the form of:

$$W(x)_{part} = C5\, w_0 + C6\, v_0 \tag{F.14}$$

$$\text{with} \qquad C5 = \frac{1}{i\omega} - \frac{E*I}{\rho A \omega^2} \qquad \text{and} \qquad C6 = -\frac{1}{\omega^2} \tag{F.15}$$

Which makes the general solution:

$$W(x)_{gen} = C1\cosh(\beta x) + C2\sinh(\beta x) + C3\cos(\beta x) + C4\sin(\beta x) + C5\, w_0(x) + C6\, v_0(x) \tag{F.16}$$

With derivatives to space give:

$$\frac{dW}{dx} = C1\beta\sinh(\beta x) + C2\beta\cosh(\beta x) - C3\beta\sin(\beta x) + C4\beta\cos(\beta x) C5\, w_0' + C6\, v_0' \tag{F.17}$$

$$\frac{d^2 W}{dx^2} = C1\beta^2\cosh(\beta x) + C2\beta^2\sinh(\beta x) - C3\beta^2\cos(\beta x) - C4\beta^2\sin(\beta x) + C5\, w_0'' + C6\, v_0'' \tag{F.18}$$

For the boundary conditions, the following Fourrier transformed set of equations is found:

$$(1) \qquad \int_{-\infty}^{\infty} \left[\left(E + E^* \frac{\partial}{\partial t} \right) I \frac{\partial^2 w(x,t)}{\partial x^2}|_{x=0} \right] e^{-i\omega t} dt - \int_{-\infty}^{\infty} \left[kr_1 \frac{\partial W(x,t)}{\partial x}|_{x=0} \right] e^{-i\omega t} dt$$
$$- \int_{-\infty}^{\infty} \left[cr_1 \frac{\partial^2 W(x,t)}{\partial t \partial x}|_{x=0} \right] e^{-i\omega t} dt = \int_{-\infty}^{\infty} [M(t)]\, e^{-i\omega t} dt \tag{F.19}$$

$$\longrightarrow \qquad EI \frac{d^2 W(x,\omega)}{dx^2}|_{x=0} + i\omega E^* I \frac{d^2 W(x,\omega)}{dx^2}|_{x=0} - kr_1 \frac{dW(x,\omega)}{dx}|_{x=0} - i\omega cr_1 \frac{dW(x,t)}{dx}|_{x=0} = M(\omega) \tag{F.20}$$

$$\longrightarrow \qquad \left(EI + i\omega E^* I\right) \frac{d^2 W(x,\omega)}{dx^2}|_{x=0} - kr_1 \frac{dW(x,\omega)}{dx}|_{x=0} - i\omega cr_1 \frac{dW(x,\omega)}{dx}|_{x=0} = M(\omega) \tag{F.21}$$

$$(2) \qquad \int_{-\infty}^{\infty} [w(x,t)|_{x=0}]\, e^{-i\omega t} dt = 0 \tag{F.22}$$

$$\longrightarrow \qquad W(0,\omega) = 0 \tag{F.23}$$

$$(3)\qquad \int_{-\infty}^{\infty}\left[\left(E+E^*\frac{\partial}{\partial t}\right)I\frac{\partial^2 w(x,t)}{\partial x^2}|_{x=L}\right]e^{-i\omega t}dt+\int_{-\infty}^{\infty}\left[kr_2\frac{\partial W(x,t)}{\partial x}|_{x=L}\right]e^{-i\omega t}dt$$
$$+\int_{-\infty}^{\infty}\left[cr_2\frac{\partial^2 W(x,t)}{\partial t\partial x}|_{x=L}\right]e^{-i\omega t}dt=0 \tag{F.24}$$

$$\longrightarrow\qquad EI\frac{d^2W(x,\omega)}{dx^2}|_{x=0}+i\omega E^*I\frac{d^2W(x,\omega)}{dx^2}|_{x=0}+kr_2\frac{dW(x,\omega)}{dx}|_{x=L}+i\omega cr_2\frac{dW(x,t)}{dx}|_{x=L}=0 \tag{F.25}$$

$$\longrightarrow\qquad \left(EI+i\omega E^*I\right)\frac{d^2W(x,\omega)}{dx^2}|_{x=L}+kr_2\frac{dW(x,\omega)}{dx}|_{x=L}+i\omega cr_1\frac{dW(x,\omega)}{dx}|_{x=L}=0 \tag{F.26}$$

$$(4)\qquad \int_{-\infty}^{\infty}[w(x,l)|_{x=L}]\,e^{-i\omega t}dt=0 \tag{F.27}$$

$$\longrightarrow\qquad W(L,\omega)=0 \tag{F.28}$$

For solving the unknowns in Equation F.16, the general solution is substituted in the boundary conditions.

$$(1)\qquad \left(EI+i\omega E^*I\right)\frac{d^2W(x,\omega)}{dx^2}|_{x=0}-kr_1\frac{dW(x,\omega)}{dx}|_{x=0}-i\omega cr_1\frac{dW(x,\omega)}{dx}|_{x=0}=M(\omega) \tag{F.29}$$

$$\longrightarrow\qquad \left(EI+i\omega E^*I\right)\left\{C1\beta^2\cosh(0)+C2\beta^2\sinh(0)-C3\beta^2\cos(0)-C4\beta^2\sin(0)+C5w_0''+C6v_0''\right\}$$
$$-kr_1\left\{C1\beta\sinh(0)+C2\beta\cosh(0)-C3\beta\sin(0)+C4\beta\cos(0)+C5w_0'+C6v_0'\right\}$$
$$-i\omega cr_1\left\{C1\beta\sinh(0)+C2\beta\cosh(0)-C3\beta\sin(0)+C4\beta\cos(0)+C5w_0'+C6v_0'\right\}=M(\omega) \tag{F.30}$$

$$\longrightarrow\qquad \left(EI+i\omega E^*I\right)\left\{C1\beta^2-C3\beta^2+C5w_0''+C6v_0''\right\}-kr_1\left\{C2\beta+C4\beta+C5w_0'+C6v_0'\right\} \tag{F.31}$$
$$-i\omega cr_1\left\{C2\beta+C4\beta+C5w_0'+C6v_0'\right\}=M(\omega) \tag{F.32}$$

$$\longrightarrow\qquad C1\left(EI+i\omega E^*I\right)\beta^2+C2\beta\left(-kr_1-i\omega cr_1\right)-C3\left(EI+i\omega E^*I\right)\beta^2$$
$$+C4\beta\left(-kr_1-i\omega cr_1\right)+C5\left\{EIw_0''+i\omega E^*Iw_0''-kr_1w_0'-i\omega cr_1w_0\right\} \tag{F.33}$$
$$+C6\left\{EIw_0''+i\omega E^*Iw_0''-kr_1w_0'-i\omega cr_1w_0\right\}=M(\omega) \tag{F.34}$$

$$(2)\qquad W(0,\omega)=0 \tag{F.35}$$

$$\longrightarrow\qquad C1\cosh(0)+C2\sinh(0)+C3\cos(0)+C4\sin(0)+C5w_0+C6v_0=0 \tag{F.36}$$

$$\longrightarrow\qquad C1+C3+C5w_0+C6v_0=0 \tag{F.37}$$

$$\longrightarrow\qquad C1+C3=-C5w_0-C6v_0 \tag{F.38}$$

$$(3)\qquad \left(EI+i\omega E^*I\right)\frac{d^2W(x,\omega)}{dx^2}|_{x=L}+kr_2\frac{dW(x,\omega)}{dx}|_{x=L}+i\omega cr_1\frac{dW(x,\omega)}{dx}|_{x=L}=0 \tag{F.39}$$

$$\longrightarrow\qquad \left(EI+i\omega E^*I\right)\left\{C1\beta^2\cosh(\beta L)+C2\beta^2\sinh(\beta L)-C3\beta^2\cos(\beta L)-C4\beta^2\sin(\beta L)+C5w_0''+C6v_0''\right\}$$
$$+kr_2\left\{C1\beta\sinh(\beta L)+C2\beta\cosh(\beta L)-C3\beta\sin(\beta L)+C4\beta\cos(\beta L)+C5w_0'+C6v_0'\right\}$$
$$+i\omega cr_1\left\{C1\beta\sinh(\beta L)+C2\beta\cosh(\beta L)-C3\beta\sin(\beta L)+C4\beta\cos(\beta L)+C5w_0'+C6v_0'\right\}=M(\omega) \tag{F.40}$$

$$\longrightarrow\qquad C1\beta^2\cosh(\beta L)\left(EI+i\omega E^*I\right)+C1\beta\sinh(\beta L)kr_2+C1\beta\sinh(\beta L)i\omega cr_1$$
$$+C2\beta^2\sinh(\beta L)\left(EI+i\omega E^*I\right)+C2\beta\cosh(\beta L)kr_2+C2\beta\cosh(\beta L)i\omega cr_1$$
$$-C3\beta^2\cos(\beta L)\left(EI+i\omega E^*I\right)-C3\beta\sin(\beta L)kr_2-C3\beta\sin(\beta L)i\omega cr_1$$
$$-C4\beta^2\sin(\beta L)\left(EI+i\omega E^*I\right)+C4\beta\cos(\beta L)kr_2+C4\beta\cos(\beta L)i\omega cr_1 \tag{F.41}$$
$$+C5\left\{EIw_0''+i\omega E^*Iw_0''+kr_1w_0'+i\omega cr_1w_0\right\} \tag{F.42}$$
$$+C6\left\{EIw_0''+i\omega E^*Iw_0''+kr_1w_0'+i\omega cr_1w_0\right\}=M(\omega) \tag{F.43}$$

$$\begin{aligned}
\longrightarrow \quad & C1\left\{\beta^2\cosh(\beta L)\left(EI+i\omega E^*I\right)+\beta\sinh(\beta L)\left(kr_2+\beta i\omega cr_1\right\}\right. \\
& +C2\left\{\beta^2\sinh(\beta L)\left(EI+i\omega E^*I\right)+\beta\cosh(\beta L)\left(kr_2+i\omega cr_1\right)\right\} \\
& +C3\left\{-\beta^2\cos(\beta L)\left(EI+i\omega E^*I\right)-\beta\sin(\beta L)\left(kr_2-i\omega cr_1\right)\right\} \\
& +C4\left\{-\beta^2\sin(\beta L)\left(EI+i\omega E^*I\right)+\beta\cos(\beta L)\left(kr_2+i\omega cr_1\right)\right\} && \text{(F.44)} \\
& +C5\left\{EIw_0''+i\omega E^*Iw_0''+kr_1w_0'+i\omega cr_1w_0\right\} && \text{(F.45)} \\
& +C6\left\{EIw_0''+i\omega E^*Iw_0''+kr_1w_0'+i\omega cr_1w_0\right\}=M(\omega) && \text{(F.46)}
\end{aligned}$$

$$(4) \qquad W(L,\omega)=0 \tag{F.47}$$

$$\longrightarrow \quad C1\cosh(\beta L)+C2\sinh(\beta L)+C3\cos(\beta L)+C4\sin(\beta L)+C5w_0+C6v_0=0 \tag{F.48}$$

$$\longrightarrow \quad C1\cosh(\beta L)+C2\sinh(\beta L)+C3\cos(\beta L)+C4\sin(\beta L)=-C5w_0-C6v_0 \tag{F.49}$$

This can be written as a resulting matrix of coefficients which can be solved for every ω.

$$\begin{bmatrix}
\left(E+i\omega E^*\right)I\beta^2 & -(kr_1+i\omega cr_1)\beta & -\left(E+i\omega E^*\right)I\beta^2 & -(kr_1+i\omega cr_1)\beta \\
1 & 0 & 1 & 0 \\
\left(E+i\omega E^*\right)I\beta^2\cosh(\beta L) & \left(E+i\omega E^*\right)I\beta^2\sinh(\beta L) & -\left(E+i\omega E^*\right)I\beta^2\cos(\beta L) & -\left(E+i\omega E^*\right)I\beta^2\sin(\beta L) \\
\quad +(kr_2+i\omega cr_2)\beta\sinh(\beta L) & \quad +(kr_2+i\omega cr_2)\beta\cosh(\beta L) & \quad -(kr_2+i\omega cr_2)\beta\sin(\beta L) & \quad +(kr_2+i\omega cr_2)\beta\cos(\beta L) \\
\cosh(\beta L) & \sinh(\beta L) & \cos(\beta L) & \sin(\beta L)
\end{bmatrix}\cdots$$

$$\begin{bmatrix} C1 \\ C2 \\ C3 \\ C4 \end{bmatrix} = \begin{bmatrix}
M(\omega)-C5\left\{EIw_0''+i\omega E^*Iw_0''+kr_1w_0'+i\omega cr_1w_0\right\}-C6\left\{EIw_0''+i\omega E^*Iw_0''+kr_1w_0'+i\omega cr_1w_0\right\} \\
\qquad -C5w_0-C6v_0 \\
-M(\omega)-C5\left\{EIw_0''+i\omega E^*Iw_0''+kr_1w_0'+i\omega cr_1w_0\right\}-C6\left\{EIw_0''+i\omega E^*Iw_0''+kr_1w_0'+i\omega cr_1w_0\right\} \\
\qquad -C5w_0-C6v_0
\end{bmatrix}$$

Where

$$\beta^4=\frac{\omega^2\rho A}{EI+i\omega E^*I} \qquad \text{and} \tag{F.50}$$

$$C5=\frac{1}{i\omega}-\frac{E*I}{\rho A\omega^2} \qquad \text{and} \tag{F.51}$$

$$C6=-\frac{1}{\omega^2} \tag{F.52}$$

With using a white noise spectrum for the external Moment $M(\omega)$, the transfer function $T(x,\omega)$ can be calculated. Here, the initial conditions and therewith w_0 and v_0 are set to zero.

$$M(\omega)=1 \tag{F.53}$$

$$W(x,\omega)=T\left(x,C1(\omega),C2(\omega),C3(\omega),C4(\omega)\right)\cdot M(\omega) \tag{F.54}$$

Values for constants C1, C2, C3 and C4 can then be determined.

$$\begin{bmatrix}
\left(E+i\omega E^*\right)I\beta^2 & -(kr_1+i\omega cr_1)\beta & -\left(E+i\omega E^*\right)I\beta^2 & -(kr_1+i\omega cr_1)\beta & 0 & 0 \\
1 & 0 & 1 & 0 & w_0 & v_0 \\
\left(E+i\omega E^*\right)I\beta^2\cosh(\beta L) & \left(E+i\omega E^*\right)I\beta^2\sinh(\beta L) & -\left(E+i\omega E^*\right)I\beta^2\cos(\beta L) & -\left(E+i\omega E^*\right)I\beta^2\sin(\beta L) & 0 & 0 \\
\quad +(kr_2+i\omega cr_2)\beta\sinh(\beta L) & \quad +(kr_2+i\omega cr_2)\beta\cosh(\beta L) & \quad -(kr_2+i\omega cr_2)\beta\sin(\beta L) & \quad +(kr_2+i\omega cr_2)\beta\cos(\beta L) & & \\
\cosh(\beta L) & \sinh(\beta L) & \cos(\beta L) & \sin(\beta L) & w_0 & v_0
\end{bmatrix}\cdots$$

$$\begin{bmatrix} C1 \\ C2 \\ C3 \\ C4 \\ C5 \\ C6 \end{bmatrix} = \begin{bmatrix} 1 \\ 0 \\ -1 \\ 0 \end{bmatrix} M(\omega)$$

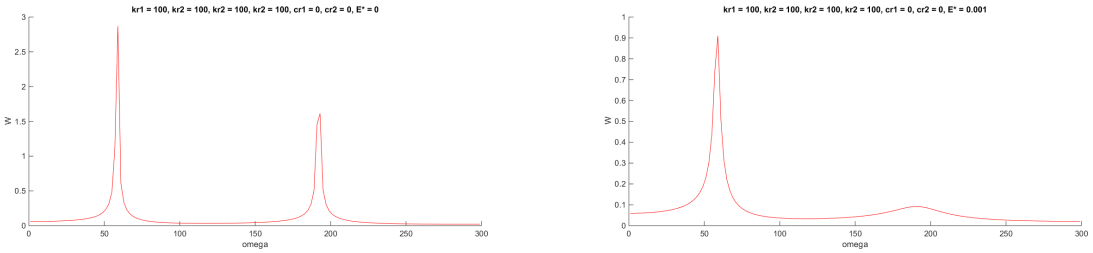

(a) No material damping

(b) Small material damping

Figure F.1: Influence material damping

This gives transfer functions that depend on the different boundary conditions. With increasing material-damping a strong decrease of the higher frequency peaks is found.

With a white noise spectrum the Output spectra has the same shape as the Transferfuction. A pulse load, such as a impulse load due to a hammer, has an identical spectrum as the white noise. The applied external moment is transferred to the frequency domain by the fft function in Matlab. After a multiplication with the transferfunction, the output in the frequency domain is obtained. Using $ifft$ in Matlab, the function is transferred back to the time domain. In Figure F.2 the response along the beam can be seen for a beam with viscous damping at the boundaries and material damping. Before applying the moment-pulse, the response should be zero. However, some small amplitudes are present due to the transfer between frequency and time domain.

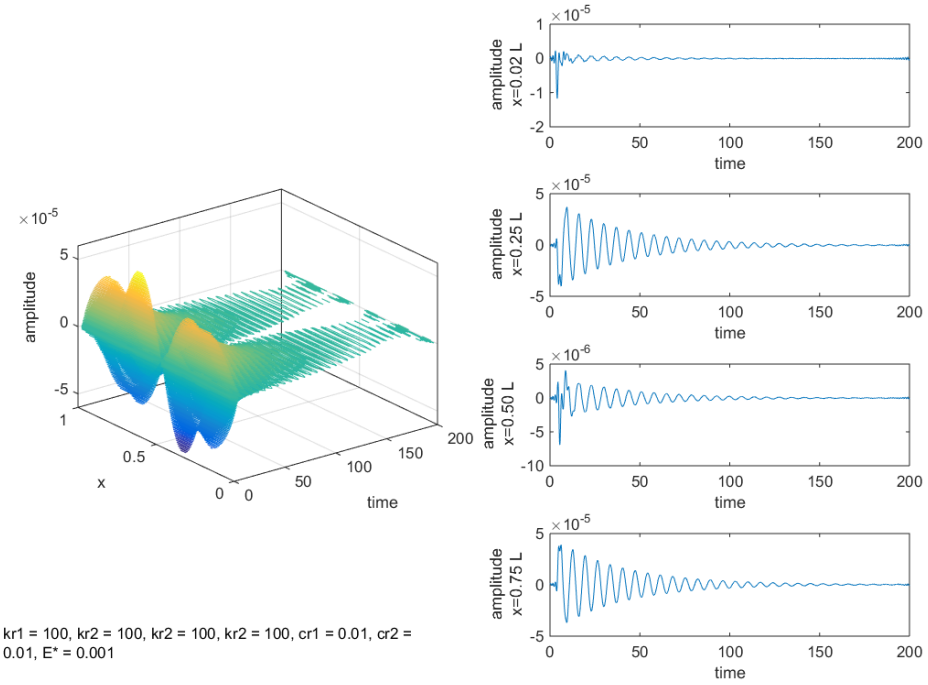

Figure F.2: Response along beam for model with small material damping and viscous damping at the boundaries.

F.2. Including friction damping at the boundaries

When friction is present at the boundaries, the system is described with the following equations:

$$\rho A \frac{\partial^2 w}{\partial t^2} + \frac{\partial^2}{\partial x^2}\left(EI \frac{\partial^2 w}{\partial x^2}\right) = 0 \tag{F.55}$$

(1) $$w(0) = 0 \tag{F.56}$$

(2) $$\left(E + E^* \frac{\partial}{\partial t}\right) I \frac{\partial^2 w}{\partial x^2}|_{x=0} = kr_1 \frac{\partial w}{\partial x}|_{x=0} - kr_1 \varphi_c + cr_1 \frac{\partial^2 w}{\partial t \partial x}|_{x=0} - cr_1 \dot{\varphi}_c + F_c sgn\left(\frac{\partial^2 w_f}{\partial t \partial x}\right)_{x=0} - F_c sgn\left(\dot{\varphi}_c\right) = M_{ext} \tag{F.57}$$

(3) $$w(L) = 0 \tag{F.58}$$

(4) $$\left(E + E^* \frac{\partial}{\partial t}\right) I \frac{\partial^2 w}{\partial x^2}|_{x=0} = -kr_2 \frac{\partial w}{\partial x}|_{x=L} + kr_2 \varphi_c - cr_2 \frac{\partial^2 w}{\partial t \partial x}|_{x=L} + cr_2 \dot{\varphi}_c - F_c sgn\left(\frac{\partial^2 w_f}{\partial t \partial x}\right)_{x=L} + F_c sgn\left(\dot{\varphi}_c\right) = -M_{ext} \tag{F.59}$$

Due to the friction, the system is nonlinear and Fourier transform can not be applied by principle. However, when the total signal is cut into intervals with a continuous friction force, the system is linear and solvable in the frequency domain for each interval. In Figure F.3 this method is shown.

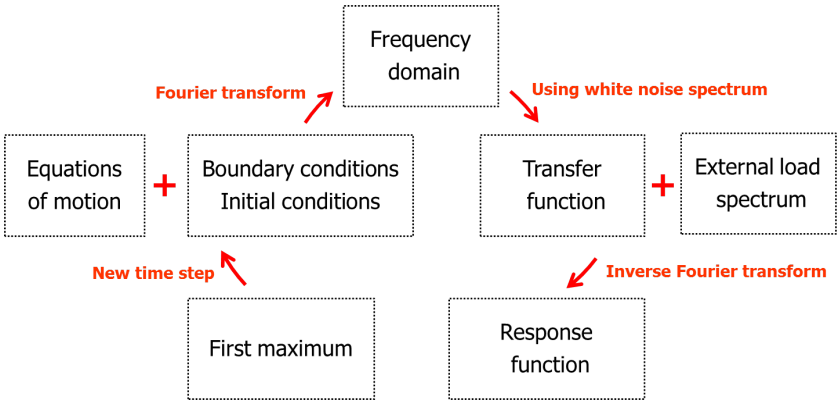

Figure F.3: Solution method with Fourier transform

The new system of equations :

$$\rho A \frac{\partial^2 w}{\partial t^2} + \frac{\partial^2}{\partial x^2}\left(EI \frac{\partial^2 w}{\partial x^2}\right) = 0 \tag{F.60}$$

(1) $$w(0) = 0 \tag{F.61}$$

(2) $$\left(E + E^* \frac{\partial}{\partial t}\right) I \frac{\partial^2 w}{\partial x^2}|_{x=0} = kr_1 \frac{\partial w}{\partial x}|_{x=0} - kr_1 \varphi_c + cr_1 \frac{\partial^2 w}{\partial t \partial x}|_{x=0} - cr_1 \dot{\varphi}_c + F_c sgn\left(\frac{\partial^2 w_f}{\partial t \partial x}\right)_{x=0} \pm F_c = M_{ext} \tag{F.62}$$

(3) $$w(L) = 0 \tag{F.63}$$

(4) $$\left(E + E^* \frac{\partial}{\partial t}\right) I \frac{\partial^2 w}{\partial x^2}|_{x=0} = -kr_2 \frac{\partial w}{\partial x}|_{x=L} + kr_2 \varphi_c - cr_2 \frac{\partial^2 w}{\partial t \partial x}|_{x=L} + cr_2 \dot{\varphi}_c - F_c sgn\left(\frac{\partial^2 w_f}{\partial t \partial x}\right)_{x=L} \pm F_c = -M_{ext} \tag{F.64}$$

Results in:

$$\begin{bmatrix} \left(E+i\omega E^*\right)I\beta^2 & -(kr_1+i\omega cr_1)\beta & -\left(E+i\omega E^*\right)I\beta^2 & -(kr_1+i\omega cr_1)\beta \\ 1 & 0 & 1 & 0 \\ \left(E+i\omega E^*\right)I\beta^2\cosh(\beta L) & \left(E+i\omega E^*\right)I\beta^2\sinh(\beta L) & -\left(E+i\omega E^*\right)I\beta^2\cos(\beta L) & -\left(E+i\omega E^*\right)I\beta^2\sin(\beta L) \\ +(kr_2+i\omega cr_2)\beta\sinh(\beta L) & +(kr_2+i\omega cr_2)\beta\cosh(\beta L) & -(kr_2+i\omega cr_2)\beta\sin(\beta L) & +(kr_2+i\omega cr_2)\beta\cos(\beta L) \\ \cosh(\beta L) & \sinh(\beta L) & \cos(\beta L) & \sin(\beta L) \end{bmatrix} \cdots$$

$$\begin{bmatrix} C1 \\ C2 \\ C3 \\ C4 \end{bmatrix} = \begin{bmatrix} M(\omega) - C5\left\{EIw_0'' + i\omega E^* Iw_0'' + kr_1 w_0' + i\omega cr_1 w_0\right\} - C6\left\{EIw_0'' + i\omega E^* Iw_0'' + kr_1 w_0' + i\omega cr_1 w_0\right\} \\ -C5\,w_0 - C6\,v_0 \\ -M(\omega) - C5\left\{EIw_0'' + i\omega E^* Iw_0'' + kr_1 w_0' + i\omega cr_1 w_0\right\} - C6\left\{EIw_0'' + i\omega E^* Iw_0'' + kr_1 w_0' + i\omega cr_1 w_0\right\} \\ -C5\,w_0 - C6\,v_0 \end{bmatrix} \pm \begin{bmatrix} Fc \\ 0 \\ -Fc \\ 0 \end{bmatrix}$$

The end of each interval should be determined by evaluating the friction forces at each time step. At zero-rotational-velocity timesteps, the initial conditions should be determined and used when calculating the new transfer functions. This process takes large computation time and is not very accurate due to numerical error at the beginning of each time interval.

G

EXPERIMENT

G.1. Experimental set-up

G.2. Measurement positions

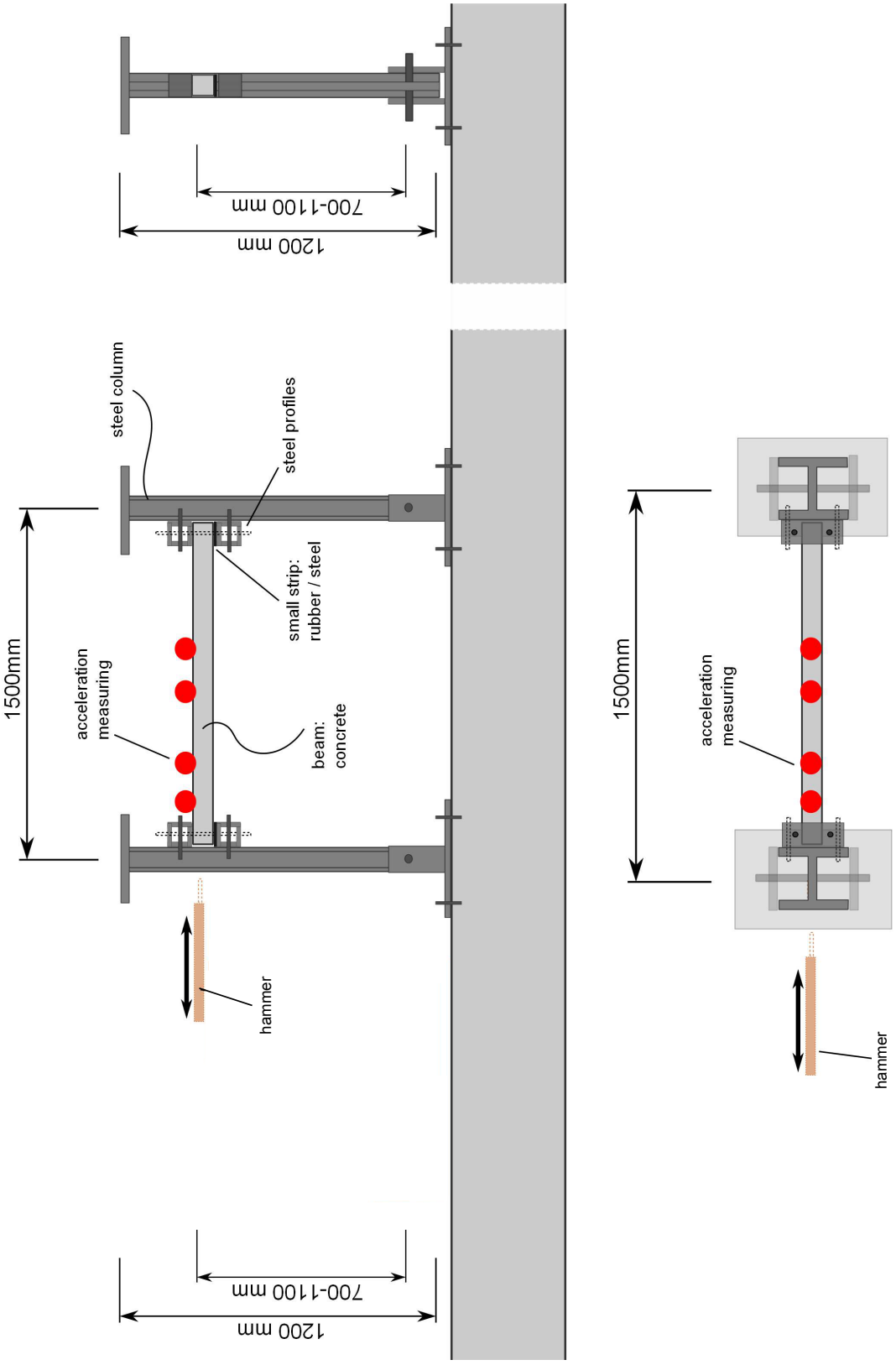

Figure G.1: The experimental set-up, a) front view, b) side view, c) top view

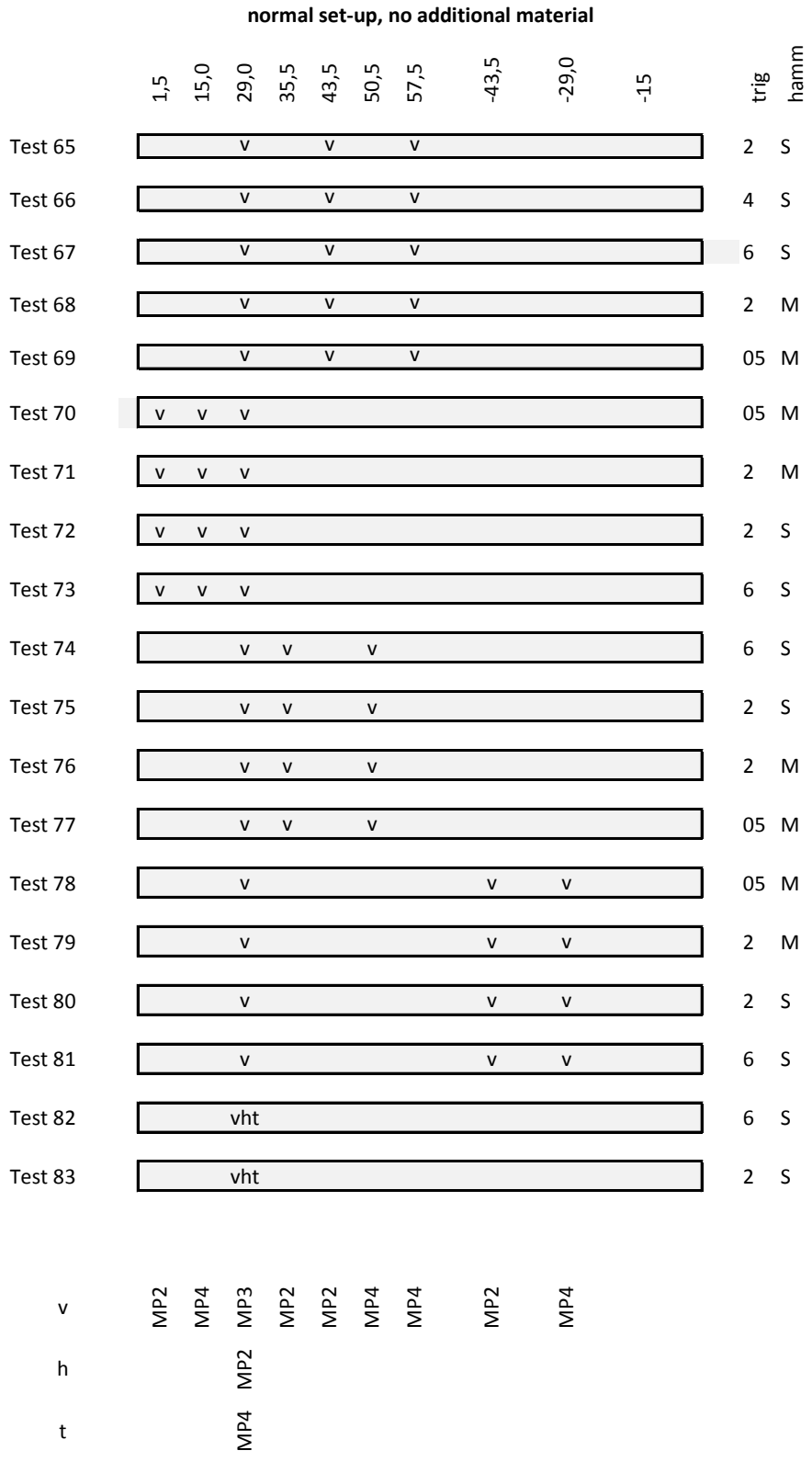

Figure G.2: The position of the accelo measurement devices several the tests.

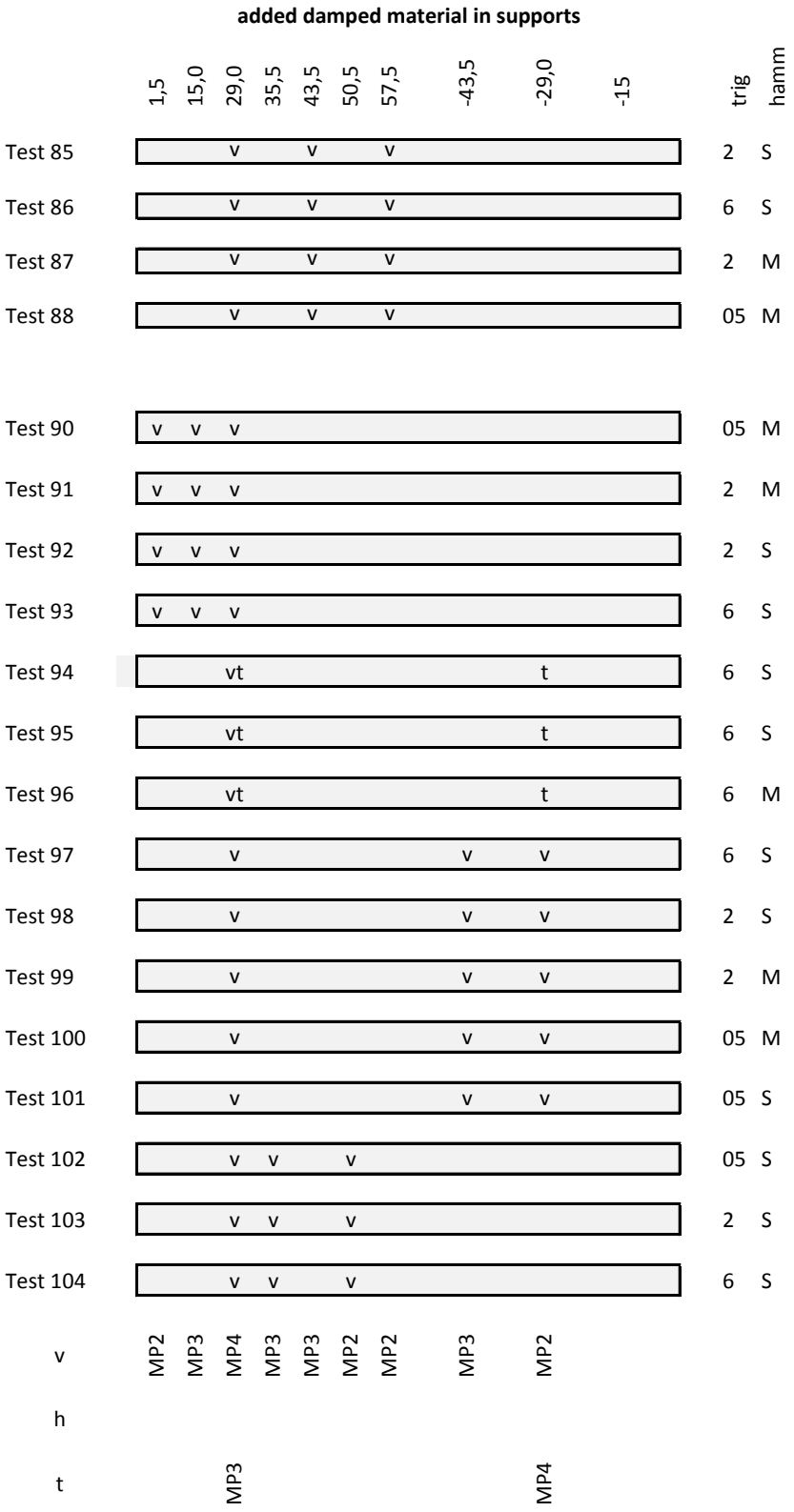

Figure G.3: The position of the accelo measurement devices for several tests with added damped material.

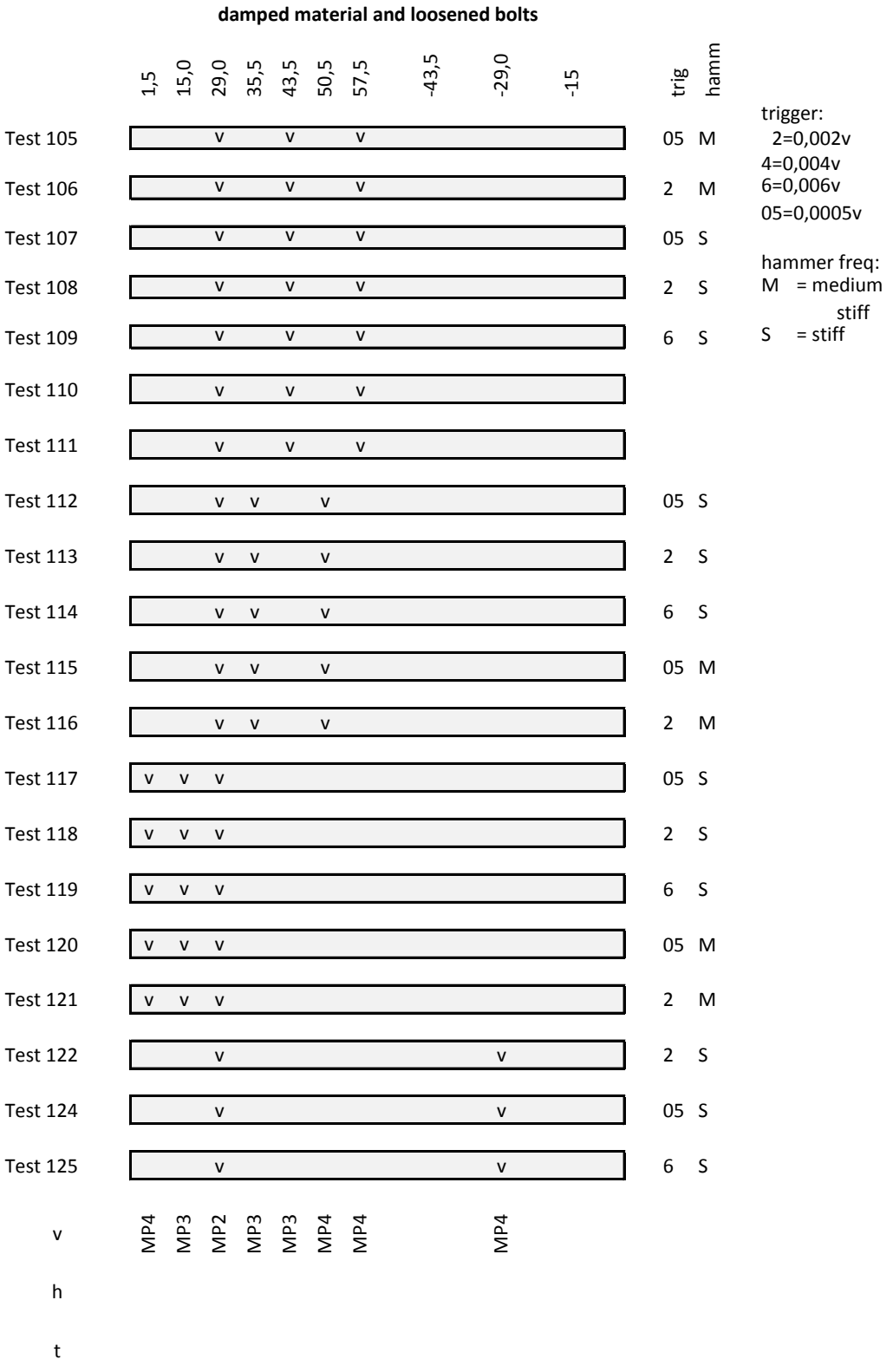

Figure G.4: The position of the accelo measurement devices for several tests with loosened botls.

G.3. Matlab codes data processing

mainfile_experiment.m

```
%% Mainfile.m
clear all; close all;
clc;

global AC
global time
global FC
global FRF_real
global FRF_img
global FREQ

%% Importing data from output.txt files
% The unfiltered signal
last_test_nr=121;
AC=zeros(32768,(121-64)*5);
FC=zeros(32768,57);

for kk=65:last_test_nr
if kk==84
AC(:,(kk-65)*5+1:(kk-65)*5+5)=0;
FRF_real(:,(kk-65)*5+111)=0;
FRF_img(:,(kk-65)*5+111)=0;
FC(:,(kk-65)+1)=0;
elseif kk==89
AC(:,(kk-65)*5+1:(kk-65)*5+5)=0;
FRF_real(:,(kk-65)*5+111)=0;
FRF_img(:,(kk-65)*5+111)=0;
FC(:,(kk-65)+1)=0;
elseif kk==95
AC(:,(kk-65)*5+1:(kk-65)*5+5)=0;
FRF_real(:,(kk-65)*5+111)=0;
FRF_img(:,(kk-65)*5+111)=0;
FC(:,(kk-65)+1)=0;
elseif kk==104
AC(:,(kk-65)*5+1:(kk-65)*5+5)=0;
FRF_real(:,(kk-65)*5+111)=0;
FRF_img(:,(kk-65)*5+111)=0;
FC(:,(kk-65)+1)=0;
elseif kk==115
AC(:,(kk-65)*5+1:(kk-65)*5+5)=0;
FRF_real(:,(kk-65)*5+111)=0;
FRF_img(:,(kk-65)*5+111)=0;
FC(:,(kk-65)+1)=0;
elseif kk==118
AC(:,(kk-65)*5+1:(kk-65)*5+5)=0;
FRF_real(:,(kk-65)*5+111)=0;
FRF_img(:,(kk-65)*5+111)=0;
FC(:,(kk-65)+1)=0;
else

% Output time response file experiment
[ time,accel ]=func_resp(kk,5,750);
AC(:,(kk-65)*5+1)=accel(:,1);
AC(:,(kk-65)*5+2)=accel(:,2);
AC(:,(kk-65)*5+3)=accel(:,3);
AC(:,(kk-65)*5+4)=accel(:,4);
AC(:,(kk-65)*5+5)=accel(:,5);

[ timeF,force ]=func_force(kk,750);
FC(:,(kk-65)+1)=force;

% Ouput FRF file experiment
[ frf ]=func_frf(kk,5,750);
```

```
for lll=1:5
FRF_real(:,(kk-65)*5+lll)=frf(:,2+3*(lll-1));
FRF_img(:,(kk-65)*5+lll)=frf(:,3+3*(lll-1));
end

FREQ(:,1)=frf(:,1);

end
end


%% Filtered accelerations, velocities and displacements
% calculation of the accelerations and velocities and displacements using
% integration and a bandpassfilter

% setting test number for data processing
test_nr=67;

global R
R.t=time;
% setting frequency range for filters
Low_range=2*2*pi;
High_range=250*2*pi;
Final_time=time(end,1);Time_steps=size(time,1);

% filter original signal
dataprocess

%% Fourrier transform
% Script that performs fast fourrier transform
FFT

%% Plotting filtered signal
%setting position acceleration measurement devices for plots
% MP1=0;MP2=0;MP3=0;MP4=1;MP5=0;
% MPis=[MP1, MP2, MP3, MP4, MP5];
% % plot_positions(test_nr,MPis)
% plot_accelerations(test_nr,MPis)
```

func_resp.m

```
function [ time,accel ] = func_resp( ii,jj,ff )
% ff is filter frequency e.g. 750Hz
% jj is number of cahneels -- so 5 for res.txt
% ii is the directory number

Fs=4096;

file='\res';
input=['data\',num2str(ii),file,'.txt'];
eval(['[header,data]=hdrload(input);']);

time=data(1:end,1);
accel=data(1:end,2:2:jj*2);
offset=mean(accel(1:100,:));

for kk=1:jj
    accel(:,kk)=accel(:,kk)-offset(kk);
end

% % Filtering the signal old method
% [B,A] = butter(6,ff/(Fs/2),'low');
% accel=filtfilt(B,A,accel);
end
```

hdrload.m

```
function [header, data] = hdrload(file)


% HDRLOAD Load data from an ASCII file containing a text header.
%     [header, data] = HDRLOAD('filename.ext') reads a data file
%     called 'filename.ext', which contains a text header.  There
%     is no default extension; any extensions must be explicitly
%     supplied.
%
%     The first output, HEADER, is the header information,
%     returned as a text array.
%     The second output, DATA, is the data matrix.  This data
%     matrix has the same dimensions as the data in the file, one
%     row per line of ASCII data in the file.  If the data is not
%     regularly spaced (i.e., each line of ASCII data does not
%     contain the same number of points), the data is returned as
%     a column vector.
%
%     Limitations:  No line of the text header can begin with
%     a number.  Only one header and data set will be read,
%     and the header must come before the data.
%
%     See also LOAD, SAVE, SPCONVERT, FSCANF, FPRINTF, STR2MAT.
%     See also the IOFUN directory.


% check number and type of arguments
if nargin < 1
  error('Function requires one input argument');
elseif ~isstr(file)
  error('Input must be a string representing a filename');
end


% Open the file.  If this returns a -1, we did not open the file
% successfully.
fid = fopen(file);
if fid==-1
  error('File not found or permission denied');
  end


% Initialize loop variables
% We store the number of lines in the header, and the maximum
% length of any one line in the header.  These are used later
% in assigning the 'header' output variable.
no_lines = 0;
max_line = 0;


% We also store the number of columns in the data we read.  This
% way we can compute the size of the output based on the number
% of columns and the total number of data points.
ncols = 0;


% Finally, we initialize the data to [].
data = [];


% Start processing.
line = fgetl(fid);
if ~isstr(line)
  disp('Warning: file contains no header and no data')
  end;
[data, ncols, errmsg, nxtindex] = sscanf(line, '%f');
```

```
67
68
69  % One slight problem, pointed out by Peter vanderWal: If the
70  % first character of the line is 'e', then this will scan as
71  % 0.00e+00. We can trap this case specifically by using the
72  % 'next index' output: in the case of a stripped 'e' the next
73  % index is one, indicating zero characters read.  See the help
74  % entry for 'sscanf' for more information on this output
75  % parameter. We loop through the file one line at a time until
76  % we find some data.  After that point we stop checking for
77  % header information. This part of the program takes most of the
78  % processing time, because fgetl is relatively slow (compared to
79  % fscanf, which we will use later).
80  while isempty(data)|(nxtindex==1)
81    no_lines = no_lines+1;
82    max_line = max([max_line, length(line)]);
83    % Create unique variable to hold this line of text information.
84    % Store the last-read line in this variable.
85    eval(['line', num2str(no_lines), '=line;']);
86    line = fgetl(fid);
87    if ~isstr(line)
88      disp('Warning: file contains no data')
89      break
90      end;
91    [data, ncols, errmsg, nxtindex] = sscanf(line, '%f');
92    end % while
93
94
95  % Now that we have read in the first line of data, we can skip
96  % the processing that stores header information, and just read
97  % in the rest of the data.
98  data = [data; fscanf(fid, '%f')];
99  fclose(fid);
100
101
102 % Create header output from line information. The number of lines
103 % and the maximum line length are stored explicitly, and each
104 % line is stored in a unique variable using the 'eval' statement
105 % within the loop. Note that, if we knew a priori that the
106 % headers were 10 lines or less, we could use the STR2MAT
107 % function and save some work. First, initialize the header to an
108 % array of spaces.
109 header = setstr(' '*ones(no_lines, max_line));
110 for i = 1:no_lines
111   varname = ['line' num2str(i)];
112   % Note that we only assign this line variable to a subset of
113   % this row of the header array.  We thus ensure that the matrix
114   % sizes in the assignment are equal.
115   eval(['header(i, 1:length(' varname ')) = ' varname ';']);
116   end
117
118
119 % Resize output data, based on the number of columns (as returned
120 % from the sscanf of the first line of data) and the total number
121 % of data elements. Since the data was read in row-wise, and
122 % MATLAB stores data in columnwise format, we have to reverse the
123 % size arguments and then transpose the data.  If we read in
124 % irregularly spaced data, then the division we are about to do
125 % will not work. Therefore, we will trap the error with an EVAL
126 % call; if the reshape fails, we will just return the data as is.
127 eval('data = reshape(data, ncols, length(data)/ncols)'';', '');
```

dataprocess.m

```
1  %% dataprocess.m
2  % Filter signal en find velocities and displacements:
```

```
3
4  % Accelerations
5  % Obtained directly from measurent data files in AC
6  nr=test_nr-64;
7  acc1=AC(:,(nr-1)*5+1);
8  acc2=AC(:,(nr-1)*5+2);
9  acc3=AC(:,(nr-1)*5+3);
10 acc4=AC(:,(nr-1)*5+4);
11 acc5=AC(:,(nr-1)*5+5);
12 % Filter
13 % Using bandpass function to filter out frequencies
14 [acc1F] = sergio_bandpass(time,acc1,Low_range,High_range,0);
15 [acc2F] = sergio_bandpass(time,acc2,Low_range,High_range,0);
16 [acc3F] = sergio_bandpass(time,acc3,Low_range,High_range,0);
17 [acc4F] = sergio_bandpass(time,acc4,Low_range,High_range,0);
18 [acc5F] = sergio_bandpass(time,acc5,Low_range,High_range,0);
19 % Mean: removing the present offset from data
20 R.acc1F=acc1F-mean(acc1F);
21 R.acc2F=acc2F-mean(acc2F);
22 R.acc3F=acc3F-mean(acc3F);
23 R.acc4F=acc4F-mean(acc4F);
24 R.acc5F=acc5F-mean(acc5F);
25
26 % Velocities
27 % Integration of filtered acceleration signal
28 [velo1]=trapezoidal_integration(Final_time,Time_steps,R.acc1F);
29 [velo2]=trapezoidal_integration(Final_time,Time_steps,R.acc2F);
30 [velo3]=trapezoidal_integration(Final_time,Time_steps,R.acc3F);
31 [velo4]=trapezoidal_integration(Final_time,Time_steps,R.acc4F);
32 [velo5]=trapezoidal_integration(Final_time,Time_steps,R.acc5F);
33 % Mean: removing the present offset from data
34 velo1=velo1-mean(velo1);
35 velo2=velo2-mean(velo2);
36 velo3=velo3-mean(velo3);
37 velo4=velo4-mean(velo4);
38 velo5=velo5-mean(velo5);
39 % Filter
40 % Using bandpass function to filter out frequencies
41 [velo1F] = sergio_bandpass(time,velo1,Low_range,High_range,0);
42 [velo2F] = sergio_bandpass(time,velo2,Low_range,High_range,0);
43 [velo3F] = sergio_bandpass(time,velo3,Low_range,High_range,0);
44 [velo4F] = sergio_bandpass(time,velo4,Low_range,High_range,0);
45 [velo5F] = sergio_bandpass(time,velo5,Low_range,High_range,0);
46 % Mean: removing the present offset from data
47 R.velo1F=velo1F-mean(velo1F);
48 R.velo2F=velo2F-mean(velo2F);
49 R.velo3F=velo3F-mean(velo3F);
50 R.velo4F=velo4F-mean(velo4F);
51 R.velo5F=velo5F-mean(velo5F);
52
53 % Displacements
54 % By integration of filtered velocity signal
55 [posi1]=trapezoidal_integration(Final_time,Time_steps,R.velo1F);
56 [posi2]=trapezoidal_integration(Final_time,Time_steps,R.velo2F);
57 [posi3]=trapezoidal_integration(Final_time,Time_steps,R.velo3F);
58 [posi4]=trapezoidal_integration(Final_time,Time_steps,R.velo4F);
59 [posi5]=trapezoidal_integration(Final_time,Time_steps,R.velo5F);
60 % Mean: removing the present offset from data
61 posi1=posi1-mean(posi1);
62 posi2=posi2-mean(posi2);
63 posi3=posi3-mean(posi3);
64 posi4=posi4-mean(posi4);
65 posi5=posi5-mean(posi5);
66 % Filter
67 % Using bandpass function to filter out frequencies
68 [pos1F] = sergio_bandpass(time,posi1,Low_range,High_range,0);
69 [pos2F] = sergio_bandpass(time,posi2,Low_range,High_range,0);
70 [pos3F] = sergio_bandpass(time,posi3,Low_range,High_range,0);
71 [pos4F] = sergio_bandpass(time,posi4,Low_range,High_range,0);
```

```
[pos5F] = sergio_bandpass(time,posi5,Low_range,High_range,0);
% Mean: removing the present offset from data
R.pos1F=pos1F-mean(pos1F);
R.pos2F=pos2F-mean(pos2F);
R.pos3F=pos3F-mean(pos3F);
R.pos4F=pos4F-mean(pos4F);
R.pos5F=pos5F-mean(pos5F);
```

sergio_bandpass.m

```
function [Y] = sergio_bandpass(t,X,wfiltlo,wfiltup,plotswitch);
% BANDPASS.M
%
% Band pass filter: Y = bandpass(t,X,wfiltlo,wfiltup)
%
% Input:  time base 't'
%         signal 'X'
%         filter frequency 'wfiltlo' [rad/s]: lower boundary (high pass filter)
%         filter frequency 'wfiltup' [rad/s]: upper boundary (low pass filter)
%
% Output: filtered signal 'Y'
%
%
% 10-jul-2006: modified to check on consistent length of t & X
%
% 11-sep-2006: modified to avoid spurious oscillations at ends of timetrace

t = t(:); X = X(:);

if nargin < 5,
    plotswitch = 0;
end
%
if length(t) ~= length(X), error('Vectors t & X must be the same lengths'), end
%
t = t-t(1);
%
N    = length(X);
dt   = (t(N) - t(1))/(N-1);
wNyq = pi/dt;   % Nyquist frequency = 1/2 sampling frequency
if wfiltup > wNyq,
   wfilt = wNyq;
   disp('warning: lowpass filter frequency > Nyquist frequency')
   disp('         lowpass filter frequency set to Nyquist frequency')
end
if wfiltlo >= wfiltup,
   wfiltlo = 0;
   disp('warning: highass filter frequency > lowpass filter frequency')
   disp('         highpass filter frequency set to zero')
end
% houtje-touwtje
tt=0:dt:(3*N-1)*dt;
N    = length(tt);
XX=[-X(end:-1:1)+2*X(1); X; -X(end:-1:1)+2*X(end)];
FX = fft(XX);
FY = FX;
dom= 2*pi/tt(N);
om = 0:dom:(N-1)*dom;
y1 = find(om > wfiltup);
y2 = find(om < wfiltlo);
FY(y1) = 0;
FY(y2) = 0;
N2 = sergio_rnd(N/2,0);
i  = 0:N2;
FY(N-i) = conj(FY(i+2));
YY  = real(ifft(FY));
```

```
Y=YY(end/3+1:end/3*2);
%
if plotswitch == 1,
    plot(om,abs(FX),om,abs(FY),'r')
    pause
    close
end
return
% official method
 w1    = wfilt/wNyq;
 B     = fir1(n,w1);
 Y     = filtfilt(B,1,X);
return
```

trapezoidal_integration.m

```
function [acc_trapz_int]=trapezoidal_integration(Final_time,Time_steps,acc)
tk=Final_time/(Time_steps-1);
t=[0:tk:Final_time];
acc_trapz_int=zeros(size(t,2),1);
trapz_rule=zeros(size(t,2),1);
engine_vector=0;
N_intervals=size(t,2)-1;
ii=1;
for i1=1:N_intervals
    trapz_rule(i1,1)=(tk/2)*(acc(i1)+acc(i1+1));
    acc_trapz_int(ii+1,1)=acc_trapz_int(ii,1)+engine_vector+trapz_rule(i1,1);
    ii=ii+1;
end
```

sergio_rnd.m

```
function [y] = rnd(x,N);
%
% function rounds with N-digits
%
n = 10^N;
y = round(n*x)/n;
```

FFT.m

```
%% Script that performs the discrete Fourier transform

Data=r.acc3F(:,30);

% % Including window
% window = hanning(length(R.acc3F(1:10000)))
% Data=R.acc3F(1:10000).*hanning(length(R.acc3F(1:10000)));

NFFT=2^nextpow2(length(Data));

% Fast Fourrier transform
FFTx=fft(Data,NFFT)/NFFT;
ABS_FFTx=2*abs(FFTx(1:NFFT/2+1));

f=(1/r.h)/2*linspace(0,1,NFFT/2+1);

% Plotting
figure
```

```
plot(f,ABS_FFTx,'r')  %f/(2*pi) for rad/s
box off
xlabel('Frequency [Hz]')
ylabel('|Y(f)|');
set(gca);
set(gcf,'Color',[1 1 1]);
grid('on');
xlim([0 300]);
axis tight
```

plot_accelerations.m

```
function plot_accelerations(test_nr,MPi )
%UNTITLED2 Summary of this function goes here
%   Detailed explanation goes here

global R

zeroline=zeros(size(R.t,1),1);

acc1F=R.acc1F.*MPi(1);
acc2F=R.acc2F.*MPi(2);
acc3F=R.acc3F.*MPi(3);
acc4F=R.acc4F.*MPi(4);
acc5F=R.acc5F.*MPi(5);

fig3a=figure;
hold on
plot(R.t,zeroline,'k')
plot(R.t,acc1F,'b')
plot(R.t,acc2F,'k')
plot(R.t,acc3F,'r')
plot(R.t,acc4F,'b')
plot(R.t,acc5F,'r')
ylabel('acceleration (m/2)')
xlabel('time (s)')
title(['Horizontal and vertical accelerations at height of the beam, test ',num2str(test_nr)])
legend('','MP1','MP2','MP3','MP4','MP5')
xlim([-0.02 R.t(end,1)])
axis tight
% saveas(fig3a,['figures\accel_test' num2str(test_nr)  'MP1toMP4'],'fig')

end
```

plot_positions.m

```
function plot_positions(test_nr,MPi )
%UNTITLED2 Summary of this function goes here
%   Detailed explanation goes here

global R

zeroline=zeros(size(R.t,1),1);

pos1F=R.pos1F.*MPi(1);
pos2F=R.pos2F.*MPi(2);
pos3F=R.pos3F.*MPi(3);
pos4F=R.pos4F.*MPi(4);
pos5F=R.pos5F.*MPi(5);

fig3a=figure;
hold on
```

```
17 plot(R.t,zeroline,'k')
18 plot(R.t,pos1F,'g')
19 plot(R.t,pos2F,'k')
20 plot(R.t,pos3F,'b')
21 plot(R.t,pos4F,'r')
22 plot(R.t,pos5F,'y')
23 ylabel('amplitude (mm)')
24 xlabel('time (s)')
25 title(['Horizontal and vertical displacements columns at height of the beam, test ',num2str(test_nr)])
26 legend('','MP1','MP2','MP3','MP4','MP5')
27 axis tight
28 xlim([-0.02 R.t(end,1)])
29 saveas(fig3a,['figures\pos_test' num2str(test_nr)  'MP1toMP4'],'fig')
30
31 end
```

H

STATICAL CALCULATION BEAM

H.1. Stiffness beam

Beam consists out of 3 parts: left part (I), right part (III) and loaded middle part(II) where an uniformly distributed load is assumed.

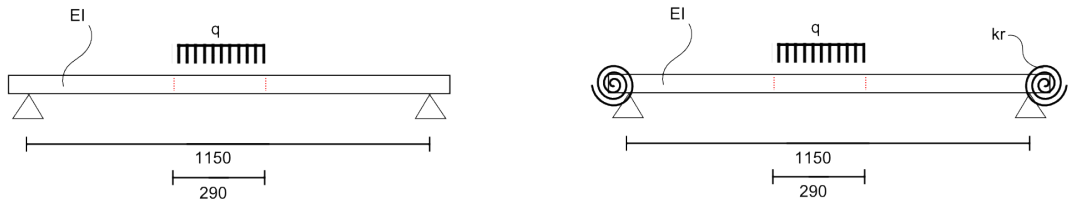

(a) Reference model beam stiffness calculations

(b) Reference model spring stiffness calculations

Figure H.1: Reference models for beam stiffness and spring stiffness calculations

The differential equations describing the beam parts are given by:

$$EI\frac{d^4 w_I}{dx^4} = 0 \tag{H.1}$$

$$EI\frac{d^4 w_{II}}{dx^4} = q \tag{H.2}$$

$$EI\frac{d^4 w_{III}}{dx^4} = 0 \tag{H.3}$$

where

$$q = \frac{M \cdot g}{l} = \frac{130 \cdot 9.81}{0.29} = 4144.48\text{N/m} \tag{H.4}$$

M, the dead weight during measurement is 130 kg, loaded on 29.0cm. The total length of the beam and is 1440 mm, the distance between the two supports is 1250 mm, noted as L.

For the deflection the 4th integral is needed, giving:

$$w_I = \frac{1}{EI}\left(\frac{1}{6}C1x^3 + \frac{1}{2}C2x^2 + C3x + C4\right) \tag{H.5}$$

$$w_{II} = \frac{1}{EI}\left(\frac{1}{24}qx^4 + \frac{1}{6}C5x^3 + \frac{1}{2}C6x^2 + C7x + C8\right) \tag{H.6}$$

$$w_{III} = \frac{1}{EI}\left(\frac{1}{6}C9x^3 + \frac{1}{2}C10x^2 + C11x + C12\right) \tag{H.7}$$

The boundary and interface conditions are the following: $x = 0$:

$$w_I = 0 \tag{H.8}$$

$$EIw_I'' = 0 \tag{H.9}$$

$x = 480$:

$$w_I = w_{II} \tag{H.10}$$

$$w_I' = w_{II}' \tag{H.11}$$

$$EIw_I'' = EIw_{II}'' \tag{H.12}$$

$$EIw_I''' = EIw_{II}''' \tag{H.13}$$

$x = 770$:

$$w_{II} = w_{III} \tag{H.14}$$

$$w_{II}' = w_{III}' \tag{H.15}$$

$$EIw_{II}'' = EIw_{III}'' \tag{H.16}$$

$$EIw_{II}''' = EIw_{III}''' \tag{H.17}$$

$x = L = 1250$:

$$w_{III} = 0 \tag{H.18}$$

$$EIw_{III}'' = 0 \tag{H.19}$$

Substitution of Equations H.5, H.6 and H.7 in these conditions gives a set of 12 equations, which gives the 12 unknown constants.

$$C1 = -145 * q \tag{H.20}$$

$$C2 = 0 \tag{H.21}$$

$$C3 = (83436625/3) * q \tag{H.22}$$

$$C4 = 0 \tag{H.23}$$

$$C5 = -625 * q \tag{H.24}$$

$$C6 = 115200 * q \tag{H.25}$$

$$C7 = (28140625/3) * q \tag{H.26}$$

$$C8 = 2211840000 * q \tag{H.27}$$

$$C9 = 145 * q \tag{H.28}$$

$$C10 = -181250 * q \tag{H.29}$$

$$C11 = (256407125/3) * q \tag{H.30}$$

$$C12 = -(37305781250/3) * q \tag{H.31}$$

Now, the deflection of the beam element due to a distributed load is determined.

$$w = \begin{cases} \frac{1}{EI}\left(-\frac{145}{6}qx^3 + \frac{83436625}{3}qx\right) & \text{x<480} \\ \frac{1}{EI}\left(\frac{1}{24}qx^4 - \frac{625}{6}qx^3 + 57600qx^2 + \frac{28140625}{3}qx + 2211840000q\right) & \text{480<x<770} \\ \frac{1}{EI}\left(\frac{145}{6}qx^3 - 90625qx^2 + \frac{256407125}{3}qx - \frac{37305781250}{3}q\right) & \text{x>770} \end{cases} \tag{H.32}$$

A deflection of $w_{mid} = w_{II}(625) = \frac{0.882406095e-2*q}{EI} = 0.02$ mm was measured after loading with $q = \frac{130*9.81*10^{-3}}{290*10^{-3}} = 4.398N/m$, resulting in a beam stiffness of $EI = 2.528828404 * 10^{13}$ Nmm^2.

H.2. Spring stiffness - bare connection

For the calculation of the spring stiffness, slightly different Boundary conditions are valid for similar equations. Assumed is that the both sides have the same magnitude of spring stiffness. $x = 0$:

$$w_I = 0 \tag{H.33}$$
$$EIw_I'' = krw_I' \tag{H.34}$$

$x = 480$:

$$w_I = w_{II} \tag{H.35}$$
$$w_I' = w_{II}' \tag{H.36}$$
$$EIw_I'' = EIw_{II}'' \tag{H.37}$$
$$EIw_I''' = EIw_{II}''' \tag{H.38}$$

$x = 770$:

$$w_{II} = w_{III} \tag{H.39}$$
$$w_{II}' = w_{III}' \tag{H.40}$$
$$EIw_{II}'' = EIw_{III}'' \tag{H.41}$$
$$EIw_{II}''' = EIw_{III}''' \tag{H.42}$$

$x = L = 1250$:

$$w_{III} = 0 \tag{H.43}$$
$$EIw_{III}'' = -krw_I II' \tag{H.44}$$

Substitution in the boundary conditions give the unknown constants.

$$C1 = -145 * q \tag{H.45}$$
$$C2 = (83436625/3) * kr * q/(EI + 625 * kr) \tag{H.46}$$
$$C3 = (83436625/3) * EI * q/(EI + 625 * kr) \tag{H.47}$$
$$C4 = 0, C5b = -625 * q \tag{H.48}$$
$$C6 = (25/3) * q * (13824 * EI + 11977465 * kr)/(EI + 625 * kr) \tag{H.49}$$
$$C7 = (15625/3) * q * (1801 * EI - 2211840 * kr)/(EI + 625 * kr) \tag{H.50}$$
$$C8 = 2211840000 * q \tag{H.51}$$
$$C9 = 145 * q \tag{H.52}$$
$$C10 = -(3625/3) * q * (150 * EI + 70733 * kr)/(EI + 625 * kr) \tag{H.53}$$
$$C11 = (3625/3) * q * (70733 * EI + 29822500 * kr)/(EI + 625 * kr) \tag{H.54}$$
$$C12 = -(37305781250/3) * q \tag{H.55}$$

in

$$w_I = \frac{1}{EI}\left(\frac{1}{6}C1x^3 + \frac{1}{2}C2x^2 + C3x + C4\right) \tag{H.56}$$
$$w_{II} = \frac{1}{EI}\left(\frac{1}{24}qx^4 + \frac{1}{6}C5x^3 + \frac{1}{2}C6x^2 + C7x + C8\right) \tag{H.57}$$
$$w_{III} = \frac{1}{EI}\left(\frac{1}{6}C9x^3 + \frac{1}{2}C10x^2 + C11x + C12\right) \tag{H.58}$$

This gives for the total deflection:

$$w = \begin{cases} \frac{1}{EI}\left(-\frac{145}{6}qx^3 + \frac{83436625}{6}\frac{krqx^2}{EI+625kr} + 83436625/3\frac{EIqx}{EI+625kr}\right) & \text{x<480} \\ \frac{1}{EI}\left(\frac{1}{24}qx^4 - \frac{625}{6}qx^3 + \frac{25}{6}\frac{q(13824EI+11977465kr)x^2}{EI+625kr} + \frac{15625}{3}\frac{(q(1801EI-2211840kr)x}{EI+625kr} + 2211840000q\right) & \text{480<x and x<770} \\ \frac{1}{EI}\left(\frac{145}{6}qx^3 - \frac{3625}{6}\frac{q(150EI+70733kr)x^2}{EI+625kr} + \frac{3625}{3}\frac{q(70733EI+29822500kr)x}{EI+625kr} - \frac{37305781250}{3}q\right) & \text{770<x} \end{cases} \tag{H.59}$$

For deflection at midspan this gives:

$$w_{mid} = \frac{1}{EI}\left(-\frac{134893170625}{8} * q + \frac{9765625}{6}\frac{q * (13824 * EI + 11977465 * kr}{EI + 625 * kr} + \frac{9765625}{3}\frac{q * (1801 * EI - 2211840 * kr}{EI + 625 * kr}\right) \tag{H.60}$$

Using q and EI as calculated above and the measured displacement after loading gives us the spring stiffness of the connections.

$$w_{mid,m} = ??? \tag{H.61}$$
$$\longrightarrow k_r = ??? \tag{H.62}$$

H.3. Spring stiffness - connection including highly damped material

When additional highly damped material is added in the connections, the rotational stiffness of this connection changes. Using Equation H.60, the spring stiffness of the adjusted joint can be calculated. Here also the assumption is made for equal rotaional stiffnesses at both joints.

$$w_{mid,m} = ??? \tag{H.63}$$
$$\longrightarrow k_r = ??? \tag{H.64}$$

VI

References and List of Figures

BIBLIOGRAPHY

[1] J. Hoenderkamp, *High-rise structures, preliminary design for lateral load,* (TU Eindhoven, 2007) Chap. Sway structures for lateral load, pp. 12–25.

[2] R. van den Berg, *Investigation of damping in high-rise buildings. Identification and prediction of damping in the serviceability limit state for wind-induced vibrations*, Master's thesis, Delft University of Technology (2012).

[3] R. Steenbergen, A. Vrouwenvelder, and C. Geurts, *The use of eurocode en1991-1-4 procedures 1 and 2 for building dynamics, a comparative study,* Journal of Wind Engineering and Industrial Aerodynamics **107-108**, 299 (2012).

[4] D. Walton, S. Lamb, and K. Kwok, *A review of two theories of motion sickness and their implications for tall building motion sway,* Wind and Structures **14**, 499 (2011).

[5] S. Lamb, K. Kwok, and D. Walton, *Occupant comfort in wind-excited tall buildings: Motion sickness, compensatory behaviours and complaint,* journal of Wind Engineering and Industrial Aerodynamics **119**, 1 (2013).

[6] K. Kwok, P. Hitchcock, and M. Burton, *Perception of vibration and occupant comfort in wind-excited tall buildings,* Journal of Wind Engineering and Industrial Aerodynamics **97**, 368 (2009).

[7] C. Geurts, S. Sanchez, S. van Dijk, and C. van Bentum, *Demping in hoogbouwconstructies - trilling voorspellen en dempen,* Bouwen met Staal **243**, 52 (2015).

[8] C. Geurts, C. van Bentum, S. Sanchez, and S. van Dijk, *Demping hoogbouw voorspeld,* Cement **3** (2015).

[9] *En 1991-1-4 (2005), eurocode 1:actions on structures part 1-4: General actions - wind actions,* (2005).

[10] A. Jeary, *Damping in tall buildings - a mechanism and a predictor,* Earthquake engineering and structural dynamics **14**, 733 (1986).

[11] J. Jia, *Essentials of Applied Dynamic Analysis*, edited by D. Proske, Risk Engineering (Springer-Verlag Berlin Heidelberg, Vienne, Austria, 2014).

[12] L. Meirovitch, *Fundamentals of Vibrations*, international edition 2001 ed., edited by M.-H. H. Education, Mechanical Engineering Series (McGraw-Hill, 2001).

[13] A. Metrikine, *Dynamics, Slender Structures and an Introduction to Continuum Mechanics (CT 4145)*, edited by F. o. C. E. Section of Structural Mechanics and Geoscience (Delft University of Technology, 2005).

[14] J. Spijkers, A. Vrouwenvelder, and E. Klaver, *Lecture Notes on Structural Dynamics, part 1 - Structural Vibrations*, edited by F. of Civil Engineering (Delft University of Technology, 2005).

[15] G. Genta, *Vibration Dynamics and Control*, edited by F. Ling, Mechanical Engineering Series (Springer Science, Torino, 2009).

[16] A. Falati, *The contribution of non-structural components to the overall dynamic behaviour of concrete slabs*, Ph.D. thesis, University of Oxford (1999).

[17] F. van Keulen, *Collegedictaat Stijfheid en Sterkte III*, edited by S. T. Mechanica (Faculteit Ontwerp, Constructie en Productie Werktuigbouwkunde, 2000).

[18] A. Chatterjee, *A brief introduction to nonlinear vibrations,* (2009), mechanical Engineering, Indian Institute of Science, Bangalore.

[19] J. Jia, *The load sequence effects on structures - ultimate limit strength evaluation,* Journal of Constructional Steel Research **67**, 255 (2011).

[20] A. A. Rao, *Mechanical Vibrations*, 5th ed., edited by M. Horton, S. Disanno, and S. Parthasaranthy (Prentice Hall - Pearson, 2011).

[21] S. Rao, *Vibration of Continuous Systems*, edited by S. Rao (John Wiley & Sons, INC, Coral Gables, Florida, 2007) department of Mechanical and Aerospace Engineering, University of Miami.

[22] C. Devulder, M. Marion, and S. Edriss, *On the rate of convergence of the nonlinear galerkin methods,* MATHEMATICSO F COMPUTATION **60**, 495 (1993).

[23] S. Mahmoodi, N. Jalili, and S. Khadem, *An experimental investigation of nonlinear vibration and frequency response analysis of cantilever viscoelastic beams,* Journal of Sound and Vibration **311**, 1409 (2008).

[24] E. Pesheck, C. Pierre, and S. Shaw, *A new galerkin-based approach for accurate non-linear normal modes through invariant manifolds,* Journal of Sound and Vibration **249**, 971 (2002).

[25] I. Kalashnikova and M. Barone, *Efficient non-linear proper orthogonal decomposition/galerkin reduced order models with stable penalty enforcement of boundary conditions,* International Journal for Numerical Methods in Engineering (2012), 10.1002/nme.3366.

[26] G. Wells, *The finite element method: an introduction,* edited by G. Wells (University of Cambridge and University of Delft, 2009).

[27] M. Marion and R. Temam, *Nonlinear galerkin methods,* SIAM Journal on numerical analysis **26**, 1139 (1989).

[28] Z. Erisen and E. Cigeroglu, *Frequency domain optimazation of dry friction dampers on buildings under harmonic excitation,* in *Topics on the Dynamics of Civil Structures, Volume 1*, Proceedings of the 30th IMAC, A Conference on Structural Dynamics, Vol. 1, edited by J. Caicedo, F. Catbas, A. Cunha, V. Racic, P. Reynolds, and K. Salyards (Springer, 2012) pp. 113–125.

[29] A. Mahmoodi, S. Khadem, and M. Kokabi, *Non-linear free vibrations of kelvin-voigt visco-elastic beams,* International Journal of Mechanical Sciences **49**, 722 (2007).

[30] A. Nayfeh, J. Nayfeh, and D. Mook, *On mmethod for continuous systems with quadratic and cubic nonlinearities,* Nonlinear Dynamics **3**, 145 (1992).

[31] K. Atkinson, W. Han, and D. Stewart, *Numerical solution of ordinary differential equations*, edited by F. Ling, Pure and Applied Mathematics: A Wiley Series of Texts, Monographs, and Tracts (John Wiley & Sons, New Jersey, 2009).

[32] W. Yang, E. Cao, T. Chung, and J. Morris, *Applied numerical mmethod using matlab*, edited by W. Yang (John Wiley & Sons, New Jersey, 2005).

[33] *Ordinary differential equations using matlab2014,* `http://web.archive.org/web/20080207010024/http://www.808multimedia.com/winnt/kernel.htm` (2015), accessed: 2015-04-05.

[34] *ode45,* `http://nl.mathworks.com/help/matlab/ref/ode45.html` (2015), accessed: 2015-04-05.

[35] J. Reddy and N. Phan, *Stability and vibration of isotropic, orthotropic and laminated plates according to a higher-order shear deformation theory,* Journal of Sound and Vibration **98**, 157 (1985).

[36] A. PREUMONT, *Twelve lectures on structural dynamics,* (2013).

[37] D. Dawe and O. Roufaeil, *Rayleigh-ritz vibration analysis of mindlin plates,* Journal of Sound and Vibration **69**, 345 (1980).

[38] K. Liew, Y. Xiang, and S. Kitipornachai, *Research on thick plate vibration: A literature survey,* Journal of Sound and Vibration **180**, 163 (1995).

[39] *Human induced vibrations, vibration design of floors - guidelines,* (2008).

[40] A. Jeary, *Designer's guide to the dynamic response of structures*, edited by T. S. . Professional (E&FN Spon, 1997).

[41] R. Steenberger and C. Geurts, *Praktische handvatten voor eigenfrequentie,* Bouwen met Staal **219**, 46 (2011).

[42] R. Aquino and Y. Tamura, *Framework for structural damping predictor models based on stick-slip mechanism for use in wind-resistant design of buildings,* Journal of Wind Engineering and Industrial Aerodynamics **117**, 25 (2013).

[43] A. Devin and P. Fanning, *Impact of nonstructural components on modal response and structural damping,* in *Topics on the Dynamics of Civil Structures*, Conference Proceedings of the Society for Experimental Mechanics Series, Vol. 1, edited by F. Caicedo, J.M.and Catbas, A. Cunha, V. Racic, P. Reynolds, and K. Salyards, Society for Experimental Mechanics Series (Springer, 2012).

[44] Y. Tamura, *Advanced structural wind engineering,* (Springer Japan, 2013) Chap. Chapter 13: Damping in Buildings and Estimation Techniques, pp. 347–376.

[45] L. Gaul, *The influence of damping on waves and vibrations,* Mechanical Systems and Signal Processing **13**, 1 (1999).

[46] S. Chowdhury, *Damping Characteristics of Reinforced and Partially Prestressed Concrete Beams*, Ph.D. thesis, Griffith University (1999).

[47] A. Metrikine, *Dynamics, Slender Structures and an Introduction to Continuum Mechanics CT 4145*, edited by F. of Civil Engineering and G. S. of Structural Mechanics (Delft University of Technology, 2005).

[48] unknown, *unknown*, Master's thesis, unknown (0000).

[49] E. Ungar and E. Kerwin, *Loss factors of viscoelastic systems in terms of energy concepts,* THE JOURNAL OF THE ACOUSTICAL SOCIETY OF AMERICA **34** (1962), 10.1121/1.1918227.

[50] F. Orban, *Damping of materials and members in structures,* in *5th International Workshop on Multi-Rate Processes and Hysteresis (MURPHYS 2010)*, Journal of Physics: Conference Series, Vol. 268 (2011).

[51] J. Bouchaala, N.and Dion, N. Peyret, and M. Haddar, *Micro-slip induced damping in the contact of nominally flat surfaces,* International Journal of Applied Mechanics **5** (2013), DOI: 10.1142/S1758825113500051.

[52] L. Gaul and J. Lenz, *Nonlinear dynamics of structures assembled by bolted joints,* Acta Mechanica **125**, 169 (1997).

[53] J. Oden and J. Martin, *Models and computational methods for dynamic friction phenomena,* Computer Methods in applied Mechanics and Engineering **52**, 527 (1985).

[54] A. Abolmaali, A. Kukreti, A. Motahari, and M. Ghassemiehc, *Energy dissipation characteristics of semi-rigid connections,* Journal of Constructional Steel Research **65**, 1187 (2009).

[55] K. Astrom and C. Canudas-de Wit, *Revisiting the lugre model. stick-slip motion and rate dependence,* IEEE Control Systems Magazine **28**, 101 (2008).

[56] H. Olsson, K. Astrom, C. Canudas de Wit, M. Gafvert, and P. Lischinsky, *Friction models and friction compensation,* European Journal of Control **4**, 176 (1998).

[57] R. Ibrahim and C. Pettit, *Uncertainties and dynamic problems of bolted jointsand other fasteners,* Journal of Sound and Vibration **279**, 857 (2005).

[58] K. Popp, L. Panning, and W. Sextro, *Vibration damping by friction forces: theory and applications,* Journal of Vibration and Control **9**, 419 (2003).

[59] W. Whiteman and A. Ferri, *Displacement-dependent dry friction damping of a beam-like structure,* Journal of Sound and Vibration **198**, 313 (1996).

[60] S. Andersson, A. Soderberg, and S. Bjorklund, *Friction models for sliding dry, boundary and mixed lubricated contacts,* Tribology International **40**, 580 (2007).

[61] M. Badila, *Modeling frictional elements using the LuGre mechanism for a better evaluation of damping in structures,* Master's thesis, Delft University of Technology (2014).

[62] N. Bouchaala, N. Peyret, I. Tawfiq, J. Dion, and M. Haddar, *Compact model and identification process for friction induced damping in a rotational joint with flawed surfaces,* International Journal of Solids and Structures **51**, 3570 (2011).

[63] M. Maane, *Study of Modified Friction Device for the Control of Civil Structures*, Master's thesis, Massachusetts Institure of Technology (2010).

[64] L. Goodman, *Material damping and slip damping,* (McGraw-Hill, 2002) Chap. 36, pp. 36.1–36.30, 5th ed.

[65] R. Gibson, *Damping characteristics of composite materials and structures,* Journal of Materials Engineering and Performance **1**, 11 (1992).

[66] C. Bert, *Material dampin: an introductory review of mathematic measures and experimental techniques,* Journal of Sound and Vibration **29**, 129 (1973).

[67] P. Franchetti, C. Modena, and M. Feng, *Nonlinear damping identification in precast prestressen reinforced concrete beams,* computer-aided civil and infrastructure engineering **24**, 577 (2009).

[68] C. Carpinteri, A.and BernarCar and K. Nemati, *Complex fracture energy dissipation in concrete under different loaload conditions,* Mechanics of Materials **26**, 93 (1997).

[69] J. Berthelot, M. Assarar, Y. Sefrani, and A. El Mahi, *Damping analysis of composite materials and structures,* Composite Structures **85**, 189 (2008).

[70] N. Labonnote, A. Ronnquist, and K. Malo, *Prediction of material damp ing in timber ffloor, and subsequent evaluatin of structural damp ing,* Materials and Structures (2014).

[71] F. van Duin, *Dempingsmetingen in vier gebouwen die in hoogte varieren tussen 22 en 54 meter*, Technical report (TNO, 2000) opdrachtgever: Nederlands Normalisatie Instituut.

[72] F. Galanti and J. Oostvogels, *Metingen van de beweging van twee hoge gebouwen bij wind*, Technical Report (TNO Bouw en Ondergrond, 2006).

[73] H. van Koten, *The comparison of measured and calculated aamplitude of some buildings and determination of the damping effects of the buildings.*, Tech. Rep. (Institute of Building Materials and Building Structures TNO Delft, 1971).

[74] R. Steenbergen, F. Galanti, and S. Lentzen, *Dynamische eigenschappen Kennedy Toren Eindhoven*, Technical Report (TNO Bouw en Ondergrond, 2010) opdrachtgever: Ingenieursbureau Zonneveld.

[75] R. Steenbergen and S. Lentzen, *Dynamische eigenschappen MontevideoToren Rotterdam*, Technical Report (TNO Bouw en Ondergrond, 2010) opdrachtgever: Ingenieursbureau Zonneveld.

[76] M. den Boon and P. Fraanje, *V(l)oer voor Vernieuwing - 19 moderne vloersystemen voor de bouw*, Tech. Rep. (Stichting Research Rationalisatie Bouw (RRBouw), 2007).

[77] S. van Hellenberg Hubar, *Duurzaamheid, flexibiliteit en kosten van hoogbouw*, Master's thesis, Delft University of Technology (2009).

[78] S. Zegers, *Lightweight floor system for vibration comfort*, Ph.D. thesis, Eindhoven Technical University (2011).

[79] J. Proakis and D. Manolakis, *Digital Signal Processing - Principles, Algorithms, and Applications*, edited by M. Horton, Pearson Education (Pearson Prentice Hall, 2007).

[80] A. Simone, *An Introduction to the Analysis of Slender Structures*, edited by F. o. C. E. Computational Mechanics Group Structural Mechanics Section and Geosciences (Delft University of Technology, 2011).

[81] H. Vu, A. Ordonez, and B. Karnopp, *Vibration of a double-beam system,* Journal of Sound and Vibration **229**, 807 (2000).

[82] A. Jeary, *Damping in structures,* Journal of Wind Engineering and Industrial Aerodynamics **72**, 345 (1997).

[83] A. Davenport and P. Hill-Caroll, *Damping in tall buildings: its variability and treatment in design*, in *Building motion in wind: proceedings of a session, in conjunction with the ASCE convention in Seattle*, 1, edited by N. Isyumov (American Society of Civil Engineers (ASCE), 1986).

[84] S. Lagomarsino, *Forecast models for damping and vibration periods of buildings,* Journal of Wind Engineering and Industrial Aerodynamics **48**, 221 (1993).

[85] J. Ratzkin, *The fourier transform and related topics - lecture notes,* (2003), department of Mathematics, University of Utah.

[86] R. Beerends, H. ter Morsche, J. van den Berg, and E. van de Vrie, *Fourier and Laplace Transforms*, edited by C. U. Press (Cambridge University Press, The Edinburgh Building, Cambridge CB2 8RU, UK, 2003).

List of Figures

List of Tables